

Mechanisms of Degradation of Concrete by External Sulfate Ions under Laboratory and Field Conditions

THÈSE N° 4597 (2010)

PRÉSENTÉE LE 19 FÉVRIER 2010

À LA FACULTÉ SCIENCES ET TECHNIQUES DE L'INGÉNIEUR
LABORATOIRE DES MATÉRIAUX DE CONSTRUCTION
PROGRAMME DOCTORAL EN SCIENCE ET GÉNIE DES MATÉRIAUX

ÉCOLE POLYTECHNIQUE FÉDÉRALE DE LAUSANNE

POUR L'OBTENTION DU GRADE DE DOCTEUR ÈS SCIENCES

PAR

Aude CHABRELIE

acceptée sur proposition du jury:

Prof. N. Baluc, présidente du jury
Prof. K. Scrivener, Dr U. Müller, directeurs de thèse
Dr R. Beddoe, rapporteur
Prof. H. Hofmann, rapporteur
Dr R. Härdtl, rapporteur



ÉCOLE POLYTECHNIQUE
FÉDÉRALE DE LAUSANNE

Suisse
2010

Mechanisms of Degradation of Concrete

by External Sulfate Ions

under Laboratory and Field Conditions

Aude Chabrelie

sous la co-direction du Prof. Karen Scrivener (EPFL)

unter der Co-Betreuung vom Dr. Urs Müller (BAM)

Ce travail a été réalisé dans le cadre de NanoCem, consortium européen de la recherche dans le domaine cimentaire alliant industriels et universitaires -

Financement par la communauté européenne via le Marie-Curie Research Training Network -

Différents partenaires ont participé à ce projet :

Ecole Polytechnique Fédérale de Lausanne (EPFL, Suisse)
Bundesanstalt für Materialforschung und -prüfung (BAM, Allemagne)
University of Surrey (U. Surrey, Royaume Uni)
Verein Deutscher Zement (VDZ, Allemagne)

Le paradoxe du béton -

omniprésent et si peu compris

Je garde le rêve de continuer à explorer ce matériau sous tous ses angles...

scientifique, sociétal, artistique...

Abstract

The durability of concrete is a major challenge for the construction, which devotes one third to one half of its annual investment to building maintenance. The lack of field data regarding concrete durability, especially in the case of exposure to sulfate ions (“sulfate attack”) makes it difficult to determine the appropriate test methods and performance criteria. Additionally, the increased use of blended concretes (cement with mineral admixtures) suffers from a lack of experience regarding their long-term performance. Most results for sulfate resistance are derived from accelerated laboratory tests where performance criteria are based only on macroscopic properties, especially expansion.

To fill this gap and better understand the mechanisms of sulfate attack under real conditions, a parallel study of laboratory micro-concrete and field concrete samples under sulfate exposure was undertaken, focussing on microstructural changes in addition to the typical macroscopic characterisation.

Four exposure regimes were designed in the laboratory: full immersion (traditional test in “ponding”), pH-control, semi-immersion and wet/dry cycles. Pure Portland blends and slag blends with high level of slag replacement (70 wt.-%) were investigated. The exposure regime has been found to play a main role in the damage process. In ponding conditions, the damage process takes place three stages characterised by a first period of induction, followed by surface damage that finally extends to the bulk of the material. Paradoxically, the w/c-ratio does not seem to have much impact on the ionic transport phenomena but might be more decisive in the microstructure mechanical strength against local stresses. The slag blends, considered as sulfate resistant in ponding exposure, revealed bad performance under wet/dry cycles. This behaviour was attributed to poor proper physical resistance of the slag hydrates to the applied drying.

Field observations tend to confirm the laboratory results and validate the test settings.

It has been underlined that a direct relationship between the damage (e.g.; cracking/expansion) and the phase assemblage was not evident. However, the study highlights that sulfate combination with the hydrates of cement (e.g.; C-S-H) and to those of slag was found to play a role in the initiation of expansion, which would be initiated either by a swelling of the hydrates or by the precipitation of fine ettringite when the saturation level in sulfate of the hydrates has been reached.

Keywords: sulfate attack, exposure conditions, concrete, laboratory test, field, phase assemblage, microstructure, XRD, SEM, SCM, slag

Zusammenfassung

Die Dauerhaftigkeit von Betonbauwerken steht für eine der wichtigsten Herausforderung im Bausektors dar, in welchem ein Drittel zur Hälfte der jährlichen Unterhaltsinvestitionen aufgebracht werden. Das Fehlen von Daten aus Feldstudien bezüglich der Dauerhaftigkeit von Beton, insbesondere im Hinblick auf den Einfluss von Sulfat-Ionen („Sulfatangriff“) erschwert die Ausarbeitung von geeigneten Tests und die Festlegung von Leistungskriterien. Außerdem werden immer mehr Portlandkompositzemente Mischungen (Zement mit Mineralzusatzstoff) eingesetzt, jedoch gibt es keine fundierten langfristigen Erkenntnisse über den Eigenschaften. Die meisten Ergebnisse zum Sulfatwiderstand kommen aus beschleunigten Labortesten, deren Leistungskriterien nur auf makroskopischen Eigenschaften basieren, besonders hinsichtlich Expansion.

Um diese Lücken zu schließen und die Sulfatangriffmechanismen in realen Bedingungen besser zu verstehen, wurde eine parallele Studie an Labor Mikro-Betonen und anFeldbetonen durchgeführt. Der Schwerpunkt lag dabei auf mikrostrukturellen Änderrungen, zusätzlich zur klassischen makroskopischen Charakterisierung.

Vier Expositionssysteme wurden im Labor erarbeitet: völliges Eintauchen (herkömmliches Verfahren in „Ponding“), pH-Überwachung, halbes Eintauchen und nass/trocken Zyklen. Die Expositionen wurden an reinen Portlandzementmischungen Systemen so wie an Hochofenzemente, mit hohem Schlackeanteil (70 M.-%), angewandt. Die durchgeführten Tests zeigen, dass es einen direkten Einfluss auf dem Schädigungsvorgang gibt. Bei völligem Eintauchen folgte der Schädigungsprozess einem dreistufigen Verhalten, das gekennzeichnet wird durch eine erste Induktionsperiode, gefolgt durch eine Oberflächenschädigung, welche sich letztlich bei bis in den Kern des Materials ausdehnt. Es konnte gezeigt werden, dass der W/Z-Wert keinen großen Einfluss auf die ionischen Transportsphänomene hat, aber den mechanischen Widerstand der Mikrostruktur gegenüber im Material vorhandenen lokalen Spannungen beeinflusst. Die Hochofenzemente, welche bei völligem Eintauchen als sulfatbeständig anzusehen sind, geben ein vermindertes Leistungsvermögen bei nass/trocken Zyklen, dem ein geringer Eigenwiderstand der Hydratphasen beim Trocknen zuzuschreiben ist. Die Beobachtung der Feldproben zielen darauf die Laborergebnisse zu bekräftigen und die vorgelegten Testparameter zu bestätigen.

Es wurde betont, dass sich eine direkte Beziehung zwischen der Schädigung (e.g; Rissbildung/Expansion) und des Phasenverbunds nicht so einfach feststellen lässt. Die Studie zeigt weiterhin, dass die Schwefeladsorption in den Hydratphasen des Zements (e.g.; C-S-H Phase), als auch der Schlacke, eine Rolle zu Beginn der Expansion spielt. Die Ursache ist eine Expansion der Hydratphasen oder die Feinnettringit ausfällung bei Erreichen der Schwefelsättigung in der C-S-H Phasen.

Schlüsselwörter: Sulfatangriff, Expositionsbedingungen, Beton, Laborverfahren, Feld, Phasenverbund, Mikrostruktur, XRD, REM, SCM, Schlacke

Version abrégée

La durabilité des ouvrages en béton est un défi important pour le domaine de la construction qui alloue du tiers à la moitié de ses investissements annuels à la maintenance. Le manque de données concernant la durabilité des bétons sur le terrain, en particulier en cas d'exposition aux ions sulfate (« attaque sulfatique »), complexifie l'élaboration de tests et la définition de critères de performance appropriés. Par ailleurs, les bétons composés (ciment avec ajout minéral) sont de plus en plus utilisés tandis que leurs formulations souffrent d'un manque de recul vis-à-vis de leur comportement sur le long terme. La plupart des résultats concernant la résistance aux sulfates sont issus de tests accélérés en laboratoire où les critères de performance sont basés uniquement sur des propriétés macroscopiques telles que l'expansion. Afin de combler ce fossé et de mieux comprendre les mécanismes d'attaque sulfatique en conditions réelles, une étude parallèle menée sur des micro-bétons exposés en laboratoire et sur des bétons de terrain a été entreprise, agrémentant la caractérisation macroscopique classique d'une recherche approfondie des évolutions microstructurales.

Quatre régimes d'exposition ont été élaborés en laboratoire : en immersion totale (test traditionnel en « ponding »), à pH contrôlé, en semi-immersion et suivant des cycles sec/humide. Les expositions ont été appliquées à des systèmes de ciment Portland pur et à des liants composés avec laitier à taux de substitution élevé (70 pds.-%). Il apparaît que le régime d'exposition considéré influence directement le processus de dégradation. En immersion totale, le processus de dégradation suit un comportement en trois étapes caractérisé par une première période d'induction, suivie d'une période de dégradation de surface qui est finalement étendue à une dégradation au cœur du matériau. Le ratio e/c n'apparaît paradoxalement pas avoir un impact majeur sur les phénomènes de transport ionique mais semble être décisif dans la résistance mécanique de la microstructure aux contraintes développées localement dans le matériau. Les systèmes avec laitier, considérés comme résistants aux sulfates lorsqu'exposés en immersion totale, révèlent une performance réduite lors de cycles sec/humide, attribuée à une faible résistance physique propre des hydrates au séchage appliqué.

Les observations des échantillons de terrain tendent à confirmer les résultats obtenus en laboratoire et valident les paramètres des tests proposés.

Il a été souligné qu'une relation directe entre dégradation (e.g. ; fissuration/expansion) et assemblage de phases ne peut être si simplement établie. L'étude permet de mettre en évidence que la combinaison du soufre aux hydrates du ciment (e.g. ; C-S-H), ainsi qu'à ceux du laitier, semble jouer un rôle dans l'initiation de l'expansion, laquelle serait amorcée soit par un gonflement des hydrates soit par la précipitation d'ettringite fine lorsque le niveau de saturation en soufre des hydrates est atteint.

Mots clefs : attaque sulfatique, conditions d'exposition, béton, test de laboratoire, terrain, assemblage de phases, microstructure, DX, MEB, SCM, laitier

Remerciements – Danksagung – Acknowledgments

Mes premiers mots s'adressent à la Professeure Karen Scrivener, véritable « phénomène » dans le domaine, qui m'a finalement ouvert la voie d'une thèse à expériences multiples.

Une thèse dont j'ai pu relever les défis notamment grâce au cadre idéal dans lequel elle s'est inscrite, à savoir le réseau NanoCem et ses flexibilités qui ont permis de façonner un projet entre deux laboratoires tout en alliant au mieux les compétences de part et d'autre.

Je remercie les principaux acteurs de cette aventure / ich danke den meinsten Akteuren dieses Abenteuers : le laboratoire LMC de l'EPFL où l'étude microstructurale a pu être menée en profondeur, und die Arbeitsgruppe VII.1 der BAM in Berlin mit Birgit Meng und meinem Co-Betreuer, dem Dr. Urs Müller, wo die Sulfatwiderstandsversuche hergestellt und durchgeführt wurden.

Je remercie également les partenaires directs du projet / I thank the direct partners of the project / ich danke auch den direkten Partnern des Projekts: the University of Surrey, thanks to Prof. Tony Clough and to Salah for having introduced me to the secrets of the proton-induced X-ray emission, and VDZ für das Willkommen in Düsseldorf und den Kenntnissenaustausch.

Les différentes réunions au sein de NanoCem et via le réseau Marie-Curie, à qui je dois le financement de ma thèse, ont stimulé ma recherche et m'ont apportée une vision large mais précise de la recherche dans le domaine cimentaire, que ce soit au cours de transferts de connaissance ou en foulant le béton de des villes d'Europe / The various meetings in the frame of NanoCem and the Marie-Curie Research Network, acknowledged for the financial support, stimulated my research and brought me a large and precise view of the research in the field of cementitious materials, both along transfers of knowledge or while walking on the concrete of European cities.

Une pensée particulière à ceux dont les projets ont été en lien direct avec le mien et avec qui les échanges se sont maintenus en marge de la thèse / Ein besonders Denken an die, denen Projekten in direkter Bindung mit meinem waren und mit denen die Austäuche sich am Rand der Doktorarbeit: Andrés, Victor, Wolfgang, Wolfram.

Un grand merci au Dr. Irassar pour les échantillons de terrains et les données précises quant à leur historique / A big thank to Dr. Irassar for the field samples supply and the complete data providing to track their history.

Je remercie / ich danke: Robin Beddoe, Rainer Härdtl et les Professeurs / und den Professoren Heinrich Hofmann et Nadine Baluc, qui ont accepté de faire partie du jury de thèse / die damit einverstanden waren, der Doktorarbeitsjury teilzunehmen.

Thanks to Aditya and Cyrille for reviewing the English of the thesis / Danke Silke, Uwe und Thomas für die deutschen Korrekturen auf der Zusammenfassung.

Ce qui m'a réellement attirée dans le béton c'est sa tridimensionnalité, au sens propre comme au figuré. Car si en anglais le béton se traduit par « concrete », il n'en demeure pas moins le centre moteur de trois fondements principaux de l'esprit humain : la société, la science, l'art.

Aussi, mes premiers remerciements plus personnels vont à ceux qui ont, en prémices de la thèse, initiés mes premiers pas dans le béton... où je suis restée bien prise !! : Emmanuel Gallucci, « Manu » ; mais aussi les incontournables du laboratoire de l'époque : Julien, Vanessa, Rodrigo, Patrick, Shashank, Xixi, Cyrille, Mercedes, Carolina, Mohsen, Lionel ; et les passagers américains : Jason, Kevin, Christophe, Kyle.

Un clin d'œil à certains de mes collègues de travail à Lausanne comme à Berlin / A wink to some of my colleagues in Lausanne and in Berlin / Ein Augenzwinkern manchen meiner Kollegen in Lausanne und in Berlin: Vanessa pour nos échanges enrichissants tant scientifiquement que personnellement, Carolina et sa force sous un masque tranquille, Delphine pour sa fée-raclette, Cyrille et son « English touch », Aditya and our philosophic discussions, Urs für das menschliches Verständnis, André für den Betonaquarium, Martin mit seiner Freude an der Arbeit, Mathias für die große Hilfe trotz der großen Beanspruchung, Théo pour les cheveux, Alexandra pour les desserts partagés, Philip für das Schweizerdeutsch!

Je souhaite particulièrement remercier certaines personnes pour qui distance ni rime pas avec absence : Nadja et nos vies « synchro », Isabelle avec qui je partage le double amour du théâtre et de l'allemand - langue de la philosophie -, Emmanuelle et nos discussions qui reprennent comme si elles ne s'interrompaient jamais, Juliette pour les retrouvailles toujours insolites, Arnaud dont la porte ouverte à la découverte de l'Asie a été une bouffée exotique durant la thèse.

Papa

- souvenir des cours de physique racontés le soir... voilà où ça m'a menée !
- tu m'as transmis, je crois, ce caractère à trouver de l'intérêt dans tout... j'ai peut-être poussé le bouchon un peu loin à en venir à me découvrir une passion du... béton !

Maman

- souvenir de ces (longues) discussions sur mes doutes et mes choix... j'ai choisi une voie où le doute est un moteur...
- c'est sûrement à toi que je dois cette vision transversale de la vie et de ce qui la compose... et c'est bien la transversalité du béton qui m'a conquise !

P'tit frère

- souvenir de ces heures passées à bricoler ensemble... bon entraînement à vrai dire pour toutes ces manips !
- tu as toujours su garder ce calme tranquille qui est quelque part l'encrage stable de ma confiance en moi... confiance qui doit rester le cap bienveillant d'un travail de recherche...

Julien

- rencontre en même temps que ma thèse... placée sous le signe du béton !
- tu as su être là, même à distance, dans tous les moments qui ont bercé ce travail... des petites choses pratiques aux grandes remises en question, tu sais donner un souffle léger à tout instant... merci !

Table of contents

Abstract	i
Zusammenfassung	iii
Version abrégée	v
Remerciements – Danksagung – Acknowledgments	vii
Table of contents	xi
List of figures	xvii
List of tables	xxv
Glossary and nomenclature	xxvii
Chapter I – Introduction	1
I.1. BACKGROUND	2
I.1.1. DURABILITY OF CONCRETE STRUCTURES.....	2
I.1.2. DEGRADATION OF CONCRETE BY EXTERNAL SULFATE IONS	3
I.2. MOTIVATIONS OF THE THESIS.....	4
I.3. OBJECTIVES AND INNOVATIONS OF THE THESIS	5
I.3.1. OBJECTIVES	5
I.3.2. INNOVATIONS.....	5
I.4. SYNOPSIS OF THE THESIS.....	6
I.5. PRELIMINARY NOTIONS: CEMENT CHEMISTRY AND SULFATE PHASES	7
I.5.1. CHEMICAL AND PHYSICAL ASPECTS IN CEMENT CHEMISTRY	7
I.5.1.A. SULFATE-BEARING PHASES	7
I.5.1.B. PORE NETWORK.....	8
I.5.2. IMPLICATIONS IN PRESENCE OF ADDITIONAL SULFATE SOURCE.....	9
Chapter II – State-of-the-Art	11
II.1. CHEMICAL AND PHYSICAL ASPECTS OF EXTERNAL SULFATE ATTACK	12
II.1.1. CHEMICAL ASPECTS: REACTIONS	12
II.1.2. PHYSICAL ASPECTS: TRANSPORT PROCESSES.....	14
II.1.2.A. POSSIBLE TRANSPORT PROCESSES	14
II.1.2.B. THE ROLE OF W/C-RATIO	16

II.2.	APPROACHES TO AVOID SULFATE ATTACK	17
II.2.1.	THE PRESCRIPTIVE APPROACH.....	17
II.2.1.A.	CHEMICAL CHANGES	17
II.2.1.B.	PHYSICAL CHANGES	18
II.2.1.C.	NEEDS FOR ANOTHER APPROACH	18
II.2.2.	THE PERFORMANCE APPROACH	19
II.2.2.A.	ACCELERATION METHODS	19
II.2.2.B.	SIMPLE SETTING	19
II.2.3.	LIMITATIONS OF THE PERFORMANCE APPROACH	20
II.2.3.A.	CHEMICAL ASPECTS	20
II.2.3.B.	PHYSICAL ASPECTS	24
II.3.	DAMAGE MECHANISMS	25
II.3.1.	EXPANSION	25
II.3.1.A.	INCREASE IN SOLID VOLUME	26
II.3.1.B.	TOPOCHEMICAL REACTION	26
II.3.1.C.	SWELLING.....	26
II.3.1.D.	CRYSTAL GROWTH PRESSURE.....	27
II.3.2.	SOFTENING	28
II.3.3.	DECOHESION	28
II.3.4.	KEY OPEN QUESTIONS	29
Chapter III – Research strategy.....		31
III.1.	MATERIALS AND EXPOSURE CONDITIONS.....	32
III.1.1.	LABORATORY	32
III.1.1.A.	MICRO-CONCRETES	32
III.1.1.B.	LOW Na ₂ SO ₄ CONCENTRATION AND VARIOUS EXPOSURE SETTINGS.....	35
III.1.2.	FIELD	37
III.1.2.A.	CONCRETES	37
III.1.2.B.	EXPOSURE CONDITIONS	39
III.2.	ANALYSIS METHODS FOR A “MACRO-TO -MICRO” APPROACH	40
III.2.1.	IONIC TRANSPORT CHARACTERIZATION METHODS	40
III.2.1.A.	TITRIMETRIC ANALYSES.....	40
III.2.1.B.	ATOMIC ABSORPTION SPECTROSCOPY (AAS)	40

III.2.1.C.	PH-METRY	40
III.2.2.	PHYSICAL CHANGES CHARACTERIZATION METHODS	41
III.2.2.A.	EXPANSION.....	41
III.2.2.B.	MASS.....	41
III.2.2.C.	COMPRESSIVE STRENGTH.....	41
III.2.2.D.	DYNAMIC ELASTIC MODULUS	42
III.2.3.	MICROSTRUCTURAL ANALYSIS METHODS.....	44
III.2.3.A.	SEM AND CEMENT CHEMISTRY	44
III.2.3.B.	SEM MAPPINGS AND IMAGE ANALYSIS	45
III.2.3.C.	MICRO-XRF MAPPINGS.....	48
III.2.3.D.	XRD	49
III.2.3.E.	SEM-EDS.....	49
III.3.	MATURE CEMENT MICROSTRUCTURE.....	51
Chapter IV – Ponding.....		57
IV.1.	MACROSCOPIC BEHAVIOUR.....	58
IV.1.1.	IONIC TRANSPORT	58
IV.1.1.A.	CALCIUM LEACHING.....	58
IV.1.1.B.	SULFATE INGRESS	60
IV.1.2.	PHYSICAL CHANGES	61
IV.1.2.A.	MASS CHANGE	61
IV.1.2.B.	EXPANSION.....	63
IV.1.2.C.	COMPRESSIVE STRENGTH.....	64
IV.1.2.D.	ELASTIC MODULUS	67
IV.1.3.	EXTERNAL APPEARANCE	71
IV.1.4.	SUMMARY	72
IV.1.4.A.	A THREE-STAGE PROCESS (P-0.55)	72
IV.1.4.B.	EFFECT OF REDUCTION OF W/C-RATIO (P-0.38).....	74
IV.1.4.C.	EFFECT OF SLAG ADDITION (S-0.55 AND S-0.38).....	74
IV.2.	DAMAGE PROCESS AND LINK TO PHASE ASSEMBLAGE.....	76
IV.2.1.	P-0.55	76
IV.2.1.A.	MICRO-CRACKING	76
IV.2.1.B.	IONIC PROFILE.....	78

IV.2.1.C.	PHASE ASSEMBLAGE ZONATION	80
IV.2.1.D.	SUMMARY	88
IV.2.2.	EFFECT OF REDUCTION OF W/C-RATIO (P-0.38)	89
IV.2.2.A.	MICRO-CRACKING	89
IV.2.2.B.	IONIC PROFILE	89
IV.2.2.C.	PHASE ASSEMBLAGE ZONATION	90
IV.2.3.	EFFECT OF SLAG ADDITION (S-0.55 AND S-0.38)	91
IV.2.3.A.	MICRO-CRACKING	91
IV.2.3.B.	IONIC PROFILE	92
IV.2.3.C.	PHASE ASSEMBLAGE ZONATION	93
IV.2.4.	SUMMARY	94
IV.2.4.A.	SULFATE INGRESS	94
IV.2.4.B.	GYPSUM FORMATION	95
IV.2.4.C.	ETTRINGITE FORMATION	96
IV.3.	IMPACTS ON THE MICROSTRUCTURE	99
IV.3.1.	LOCAL EFFECTS ON THE MICROSTRUCTURE	99
IV.3.1.A.	LEACHING OF THE HYDRATES	99
IV.3.1.B.	SULFATE INGRESS IN THE HYDRATES	101
IV.3.1.C.	CRACKING OF THE HYDRATES	107
IV.3.1.D.	SUMMARY	110
IV.4.	SUMMARY	110
IV.4.1.	RELEVANCE OF TECHNIQUES	110
IV.4.2.	PROPOSED MECHANISM OF DAMAGE	111
IV.4.3.	EFFECT OF W/B-RATIO	113
IV.4.4.	EFFECT OF SLAG ADDITION	113
Chapter V – Effect of different testing conditions		115
V.1.	pH-CONTROL	116
V.1.1.	MACROSCOPIC BEHAVIOUR	116
V.1.1.A.	IONIC TRANSPORT	116
V.1.1.B.	PHYSICAL CHANGES	118
V.1.2.	DAMAGE AND CRACKING	122
V.1.2.A.	EXTERNAL APPEARANCE	122

V.1.2.B.	MICRO-CRACKING	123
V.1.3.	STUDY OF THE MICROSTRUCTURE	124
V.1.3.A.	IONIC PROFILE	124
V.1.3.B.	PHASE ASSEMBLAGE ZONATION AND IMPACTS ON THE MICROSTRUCTURE	126
V.2.	SEMI-IMMERSION	127
V.2.1.	MACROSCOPIC BEHAVIOUR	127
V.2.1.A.	IONIC TRANSPORT	127
V.2.1.B.	PHYSICAL CHANGES	128
V.2.2.	DAMAGE AND CRACKING	131
V.2.2.A.	EXTERNAL APPEARANCE	131
V.2.2.B.	MICRO-CRACKING	132
V.2.3.	STUDY OF THE MICROSTRUCTURE	133
V.2.3.A.	IONIC PROFILE	133
V.2.3.B.	PHASE ASSEMBLAGE ZONATION AND IMPACTS ON THE MICROSTRUCTURE	137
V.3.	WET/DRY CYCLES	138
V.3.1.	MACROSCOPIC BEHAVIOUR	138
V.3.1.A.	IONIC TRANSPORT	138
V.3.1.B.	PHYSICAL CHANGES	140
V.3.2.	DAMAGE AND CRACKING	146
V.3.2.A.	EXTERNAL APPEARANCE	146
V.3.2.B.	MICRO-CRACKING	146
V.3.3.	STUDY OF THE MICROSTRUCTURE	148
V.3.3.A.	IONIC PROFILE	148
V.3.3.B.	PHASE ASSEMBLAGE ZONATION	150
V.3.3.C.	IMPACTS ON THE MICROSTRUCTURE	154
V.4.	SUMMARY	158
Chapter VI – Field exposures		161
VI.1.	PARTIAL IMMERSION IN SULFATE ENRICHED GROUND (ARGENTINA)	162
VI.1.1.	STATE OF DAMAGE	162
VI.1.1.A.	MASS CHANGE	162
VI.1.1.B.	DYNAMIC ELASTIC MODULUS	163
VI.1.1.C.	VISUAL APPEARANCE	164

VI.1.1.D. MICRO-CRACKING	165
VI.1.2. STUDY OF THE MICROSTRUCTURE	167
VI.1.2.A. IONIC PROFILE	167
VI.1.2.B. PHASE ASSEMBLAGE ZONATION	170
VI.1.2.C. LOCAL EFFECTS ON THE MICROSTRUCTURE	171
VI.2. COMPARISON BETWEEN FIELD AND LABORATORY	174
Chapter VII – Discussion, conclusions and perspectives.....	177
VII.1. MAIN RESULTS	178
VII.1.1. IMPROVEMENTS OF UNDERSTANDING OF DAMAGE UNDER PONDING EXPOSURE.....	178
VII.1.1.A. DAMAGE PROCESS	178
VII.1.1.B. INFLUENCE OF W/C-RATIO	179
VII.1.1.C. INFLUENCE OF SLAG ADDITION.....	179
VII.1.2. INFLUENCE OF THE TYPE OF EXPOSURE	180
VII.1.2.A. pH-CONTROL.....	180
VII.1.2.B. SEMI-IMMERSION	180
VII.1.2.C. WET/DRY CYCLES.....	181
VII.2. DISCUSSION	181
VII.2.1. COMPARISON BETWEEN LABORATORY AND FIELD	181
VII.2.2. EVALUATION OF THE DEVELOPED TESTS	183
VII.2.3. RELEVANCE OF THE TECHNIQUES INVOLVED.....	184
VII.3. PERSPECTIVES.....	185
VII.3.1. INPUTS FOR MODELLING.....	185
VII.3.2. RECOMMENDATIONS FOR FUTURE RESEARCH	185
Appendices.....	I
Appendix A – Thin and Polished Sections Preparation	III
Appendix B – Carbonation of the laboratory samples.....	V
Appendix C – Comparison of Methods for Ion Profiling	IX
References.....	XIII
Curriculum vitae	XIX

List of figures

Fig. I-1. Evidence of a two-stage process in expansion phenomenon of sulfate attack in the case of sodium sulfate exposure, after Santhanam <i>et al.</i> (2002).	4
Fig. I-2. Schematic view of cement hydrates formation, after Young <i>et al.</i> (1998).....	7
Fig. I-3. Pores types in concrete, after Setzer (1977).....	8
Fig. II-1. Scheme of the reactions between sulfate ions and cement hydrates.	12
Fig. II-2. Sulfate attack reaction products in the $C_3A-CaSO_4-CaCO_3$ three components system.....	13
Fig. II-3. Zonation through leaching as of OPC in pure, after Kamali <i>et al.</i>	15
Fig. II-4. Zonation through combined sulfate attack and leaching as exposed for OPC in Na_2SO_4 solution at 20°C, after Gollop and Taylor (1992).	15
Fig. II-5. Competition between capillary rise and evaporation from concrete in semi-immersion, after Scherer (2004).	16
Fig. II-6. Time to failure as a function of w/c-ratio, after Monteiro and Kurtis (2003).....	17
Fig. II-7. Influence of C_3A content on sulfate resistance of CEM I, after [2].	17
Fig. II-8. Robin tests expansion results, after [24].	20
Fig. II-9. Phases equilibrium in the $SO_4-Ca-Al$ ternary system at 25°C, after Damidot and Glasser (1992).	21
Fig. II-10. Effect of temperature on sulfate-bearing phases stability, after Damidot and Glasser (1992-1993).	21
Fig. II-11. pH cycles along solution renewal cycles, after Moir.	23
Fig. III-1. Aggregate granulometry of the laboratory micro-concretes.	33
Fig. III-2. Scheme of the laboratory setting.....	35
Fig. III-3. Exposure setting of the Argentinean concretes.....	39
Fig. III-4. Method of ion profile quantification from SEM-mapping;	47
Fig. III-5. Method of C-S-H point cloud isolation from SEM-EDS analyses;	50
Fig. III-6. SEM-micrographs of a PC micro-concrete (w/c = 0.55) after 28 days of hydration.....	52
Fig. III-7. SEM-micrographs of a PC micro-concrete (w/c = 0.55) after 1 year of hydration.....	53
Fig. III-8. EDS plots of S/Ca versus Al/Ca atomic ratios from the outer C-S-H,	55

Fig. III-9. EDS plots of Fe/Ca versus Al/Ca atomic ratios from the ferrite and its hydration product;	55
Fig. IV-1. pH evolution of the Na₂SO₄ exposure solutions.	58
Fig. IV-2. Evolution of calcium leaching from the laboratory micro-concretes under ponding (bottom) versus reference (top) exposure.	59
Fig. IV-3. Evolution of sulfate combination from exposure solution to the laboratory micro-concretes under ponding (bottom) versus reference exposure (top).	60
Fig. IV-4. Mass evolution of the laboratory micro-concretes under ponding versus reference exposure.	61
Fig. IV-5. Relationship between mass balance of ions exchange and mass changes of P-0.55 under ponding versus reference exposure.	62
Fig. IV-6. Length evolution of the laboratory micro-concretes under ponding versus reference exposure.	63
Fig. IV-7. Compressive strength evolution of the laboratory micro-concretes under ponding versus reference exposure.	65
Fig. IV-8. Normalised compressive strength evolution of the laboratory micro-concretes under ponding.	65
Fig. IV-9. Dynamic elastic and shear modulus evolution of the laboratory micro-concretes under ponding versus reference exposure.	68
Fig. IV-10. Normalised dynamic elastic and shear modulus evolution of the laboratory micro-concretes under ponding exposure.	69
Fig. IV-11. Relationships between the normalised dynamic elastic or shear moduli and the expansion of the laboratory micro-concretes under ponding.	70
Fig. IV-12. Visual appearance of the laboratory micro-concretes after 575 days of exposure in ponding.	71
Fig. IV-13. Relationship between length and mass changes of the laboratory micro-concretes under ponding versus reference exposure.	73
Fig. IV-14. Crack patterns from BSE micrographs with corresponding quantified S-mapping of P-0.55 under ponding in Na₂SO₄ solution.	77
Fig. IV-15. Evolution of calcium (left) and sulfur (right) profiles of the cementitious matrix of P-0.55 under ponding in Na₂SO₄ solution.	78

Fig. IV-16. XRD patterns at low angles of the first millimetres of P-0.55 after 28, 119, 245 and 357 days under ponding in Na ₂ SO ₄ solution; Ett.: ettringite, G.: gypsum, Ms.: monosulfoaluminate, P.: portlandite.	81
Fig. IV-17. Typical double ettringite peak observable in some samples exposed to sulfate and in the reference samples exposed to lime water; Ett.: ettringite.	82
Fig. IV-18. SEM-EDS plots of S/Ca versus Al/Ca atomic ratios from the outer (left) and inner C-S-H (right) of P-0.55 under ponding in Na ₂ SO ₄ solution; Ett.: ettringite, G.: gypsum, Mc./Hc.: mono- or hemicarboaluminate, Ms.: monosulfoaluminate.	83
Fig. IV-19. Evolution in depth of phase assemblage in the binder of P-0.55 after various exposure times under ponding in Na ₂ SO ₄ solution.	86
Fig. IV-20. SEM-EDS plots of S/Ca versus Al/Ca atomic ratios from the outer (left) and inner C-S-H (right) after refinement of P-0.55 under ponding in Na ₂ SO ₄ solution; Ett.: ettringite, G.: gypsum, Mc./Hc.: mono- or hemicarboaluminate, Ms.: monosulfoaluminate.	87
Fig. IV-21. Crack patterns from BSE micrographs with corresponding quantified S-mapping of P-0.38 after 357 days of exposure under ponding in Na ₂ SO ₄ solution.	89
Fig. IV-22. Evolution of calcium (left) and sulfur (right) profiles of the cementitious matrix of P-0.38 under ponding in Na ₂ SO ₄ solution.	90
Fig. IV-23. Phase assemblage in the binder of P-0.38 after 357 days under ponding in Na ₂ SO ₄ solution.	91
Fig. IV-24. Crack patterns from BSE micrographs with corresponding quantified S-mapping of S-0.55 and S-0.38 after 357 days of exposure under ponding in Na ₂ SO ₄ solution.	91
Fig. IV-25. Evolution of calcium (left) and sulfur (right) profiles of the cementitious matrix of S-0.55 and S-0.38 under ponding in Na ₂ SO ₄ solution.	92
Fig. IV-26. Phase assemblage in the binder of S-0.55 and S-0.38 after 357 days under ponding in Na ₂ SO ₄ solution.	93
Fig. IV-27. Relationship between the sulfur combined in the solution and the sulfur combined in the binder of the laboratory micro-concretes along exposure time in ponding in Na ₂ SO ₄ solution.	94
Fig. IV-28. Relationship between the expansion and the sulfur combination in the solution (right) and in the binder (left) of the laboratory micro-concretes under ponding in Na ₂ SO ₄ solution.	95
Fig. IV-29. BSE micrographs (left) with corresponding EDS plots of S/Ca versus Al/Ca of P-0.38 at 0.5 mm depth after 357 days under ponding in Na ₂ SO ₄ solution.	96
Fig. IV-30. Relationship between the cumulative semi-quantified ettringite from XRD and the expansion of the laboratory micro-concretes under ponding in Na ₂ SO ₄ solution.	97

Fig. IV-31. Relationship between the cumulative S/Si atomic ratio of the outer and inner C-S-H and the cumulative semi-quantified ettringite from XRD of P-0.55 under ponding in Na ₂ SO ₄ solution.	98
Fig. IV-32. BSE micrographs of the bulk (left) and the surface (right) of S-0.55 after 357 days of exposure in ponding in Na ₂ SO ₄ solution.	98
Fig. IV-33. Leaching of the outer (top) and inner C-S-H (bottom); case of P-0.38 after 245 days under ponding in Na ₂ SO ₄ solution.....	99
Fig. IV-34. Leaching of the inner C-S-H with precipitation of portlandite rim; case of P-0.38 after 357 days under ponding in Na ₂ SO ₄ solution.....	99
Fig. IV-35. EDS Ca/Si-ratio evolution from the outer (left) and inner C-S-H (right) of the laboratory micro-concretes after 357 days under ponding in Na ₂ SO ₄ solution.....	100
Fig. IV-36. EDS S/Si atomic ratio evolution from the outer (left) and inner C-S-H (right) of P-0.55 under ponding in Na ₂ SO ₄ solution.....	102
Fig. IV-37. EDS S/Si atomic ratio evolution from the outer (left) and inner C-S-H (right) of P-0.38 under ponding in Na ₂ SO ₄ solution.....	102
Fig. IV-38. BSE micrograph and corresponding quantified S-and Ca-mappings of inner C-S-H from P-0.55 under ponding in Na ₂ SO ₄ solution at different times of exposure and depths.....	103
Fig. IV-39. EDS S/Si atomic ratio evolution from the outer (left) and inner C-S-H (right) of S-0.55 under ponding in Na ₂ SO ₄ solution.....	104
Fig. IV-40. EDS S/Si atomic ratio evolution from the outer (left) and inner C-S-H (right) of S-0.38 under ponding in Na ₂ SO ₄ solution.....	104
Fig. IV-41. Relationship between the cumulative S/Si atomic ratio of the outer (top) and inner C-S-H (bottom) and the expansion of the laboratory micro-concretes under ponding in Na ₂ SO ₄ solution. ..	105
Fig. IV-42. BSE-micrograph (left) and corresponding quantified S-mapping (right) of a slag grain with hydration rim at 0.5 mm depth of S-0.55 after 357 days under ponding in Na ₂ SO ₄ solution.....	106
Fig. IV-43. Relationship between the cumulative S/Si atomic ratio of the slag hydration rim and the expansion of S-0.55 and S-0.38 under ponding in Na ₂ SO ₄ solution.	107
Fig. IV-44. BSE micrographs of inner C-S-H at the surface of P-0.55 after 119 (top) and 357 days (bottom) under ponding in Na ₂ SO ₄ solution.....	108
Fig. IV-45. BSE micrographs of inner C-S-H of P-0.38 after 357 days under ponding in Na ₂ SO ₄ solution.....	109
Fig. IV-46. BSE micrographs of slag grain with hydration rim at 0.5 mm depth in S-0.55 (right) and S-0.38 (left) after 357 days under ponding in Na ₂ SO ₄ solution.	109

Fig. IV-47. Proposed mechanism of expansion in three stages as depicted for P-0.55 under ponding exposure.....	112
Fig. V-1. pH evolution of the pH-control exposure solutions.....	116
Fig. V-2. Evolution of calcium leaching from the laboratory micro-concretes under pH-control.....	117
Fig. V-3. Length evolution of the laboratory micro-concretes under pH-control exposure.....	118
Fig. V-4. Expansion under pH-control versus expansion under ponding for the laboratory micro-concretes.....	119
Fig. V-5. Mass evolution of the laboratory micro-concretes under pH-control.....	120
Fig. V-6. Normalised compressive strength evolution of the laboratory micro-concretes under pH-control.....	121
Fig. V-7. Normalised flexural dynamic elastic modulus evolution of the laboratory micro-concretes under pH-control.....	122
Fig. V-8. Relationship between the normalised flexural dynamic elastic modulus and the expansion of the laboratory micro-concretes under pH-control.....	122
Fig. V-9. Visual appearance of P-0.55 after 386 days of exposure under pH-control.....	122
Fig. V-10. Crack patterns from BSE micrographs of the laboratory micro-concretes after 112 days of exposure under pH-control.....	123
Fig. V-11. Evolution of calcium leaching from the cementitious matrix of the laboratory micro-concretes under pH-control.....	124
Fig. V-12. Evolution of sulfate ingress in the cementitious matrix of the laboratory micro-concretes under pH-control.....	125
Fig. V-13. Phase assemblage zonation of P-0.55 after 386 days of exposure under pH-control.....	126
Fig. V-14. Evolution of calcium leaching from the laboratory micro-concretes under semi-immersion.....	127
Fig. V-15. Evolution of sulfate combination from exposure solution to the laboratory micro-concretes under semi-immersion.....	128
Fig. V-16. Length evolution of the laboratory micro-concretes under semi-immersion.....	129
Fig. V-17. Mass evolution of the laboratory micro-concretes under semi-immersion.....	130
Fig. V-18. Normalised flexural dynamic elastic modulus evolution of the laboratory micro-concretes under semi-immersion.....	131

Fig. V-19. Typical visual appearance of the laboratory micro-concretes after 175 days of exposure in semi-immersion.....	131
Fig. V-20. Crack patterns from BSE micrographs of the laboratory micro-concretes after 357 days of exposure under semi-immersion.....	132
Fig. V-21. Evolution of calcium leaching from the cementitious matrix of the laboratory micro-concretes under semi-immersion exposure; submerged part (left) and emerged part (right)..	134
Fig. V-22. Qualitative SEM sulfur mapping of P-0.55 in semi-immersion.	135
Fig. V-23. Evolution of sulfur profiles in the cementitious matrix of the laboratory micro-concretes under semi-immersion; submerged part (left) and emerged part (right).	136
Fig. V-24. Phase assemblage zonation of the submerged part (left) and the air emerged (right) of P-0.55 after 357 days under semi-immersion; submerged part (left) and emerged part (right).....	137
Fig. V-25. Evolution of calcium leaching from the laboratory micro-concretes under wet/dry cycles exposure.....	138
Fig. V-26. Evolution of sulfate combination from exposure solution to the laboratory micro-concretes under wet/dry cycles exposure.....	139
Fig. V-27. Length evolution of the laboratory micro-concretes under wet/dry cycles.....	140
Fig. V-28. Expansion under wet/dry cycles versus expansion under ponding for the laboratory micro-concretes.	141
Fig. V-29. Mass evolution of the laboratory micro-concretes under wet/dry cycles.	142
Fig. V-30. Relationship between length and mass changes of the laboratory micro-concretes under wet/dry cycles.....	143
Fig. V-31. Normalised compressive strength evolution of the laboratory micro-concretes under wet/dry cycles.	143
Fig. V-32. Normalised flexural dynamic elastic modulus evolution of the laboratory micro-concretes under wet/dry cycles.....	144
Fig. V-33. Relationship between the normalised flexural dynamic elastic modulus and the expansion of the laboratory micro-concretes under wet/dry cycles.....	145
Fig. V-34. Visual appearance of the laboratory micro-concretes after 577 days of exposure in wet/dry cycles.	146
Fig. V-35. Crack patterns from BSE micrographs of P-0.55 and S-0.55 after 28, 119, 245 and 357 days of exposure in wet-dry cycles	147

Fig. V-36. Evolution of calcium leaching from the cementitious matrix of the laboratory micro-concretes under wet/dry exposure.....	148
Fig. V-37. Evolution of sulfur profiles in the cementitious matrix of the laboratory micro-concretes under wet/dry cycles.....	149
Fig. V-38. Evolution in depth of phase assemblage in the binder of P-0.55 and S-0.55 after various exposure times under wet/dry cycles.....	151
Fig. V-39. Evolution in depth of phase assemblage in the binder of P-0.38 and S-0.38 after 357 days of exposure under wet/dry cycles.....	152
Fig. V-40. Relationship between expansion and ettringite formation	152
Fig. V-41. SEM-EDS plots of S/Ca versus Al/Ca atomic ratios from the outer C-S-H of P-0.55 after 357 days under ponding (left) and wet/dry cycles (right); Ett.: ettringite, G.: gypsum, Mc./Hc.: mono- or hemicarboaluminate, Ms.: monosulfoaluminate..	153
Fig. V-42. Relationship between the cumulative S/Si atomic ratio of the outer and inner C-S-H and the expansion of P-0.55 (top) and S-0.55 (bottom) under wet/dry cycles.	154
Fig. V-43. SEM-BSE micrograph (left) and corresponding quantified S-mapping (right) of a slag grain with hydration rim at 0.5 mm depth of S-0.55 after 357 days under ponding.	155
Fig. V-44. Relationship between the cumulative S/Si atomic ratio of the slag hydration rim and the expansion of S-0.55 under wet/dry cycles.	155
Fig. V-45. SEM-BSE micrographs of the inner C-S-H of the micro-concretes	156
Fig. V-46. SEM-BSE micrographs of the slag with hydration rim at 0.5 mm depth	157
Fig. VI-1. Mass evolution of the field concretes under partial immersion in sulfate enriched ground, after Irassar.....	162
Fig. VI-2. Dynamic elastic and shear modulus evolution of the field concretes under partial immersion in sulfate enriched ground, after Irassar.	163
Fig. VI-3. Visual appearance of the field concretes after 19 years under partial immersion (submerged part: bottom of the concrete blocks – exposed part: top of the concrete blocks) in sulfate enriched ground.....	164
Fig. VI-4. Visual appearance of the field blended concretes after 15 years under semi- immersion in sulfate enriched ground, after Irassar.	165
Fig. VI-5. Crack patterns from BSE micrographs of the field concretes after 19 years under full immersion in sulfate enriched ground.	166

Fig. VI-6. Calcium profiles of the cementitious matrix of the field concretes after 19 years under partial immersion in sulfate enriched ground; submerged part.....	167
Fig. VI-7. Calcium profiles of the cementitious matrix of the field concretes after 19 years under partial immersion in sulfate enriched ground; exposed part.....	167
Fig. VI-8. Sulfate profiles of the cementitious matrix of the field concretes after 19 years under partial immersion in sulfate enriched ground; submerged part.....	168
Fig. VI-9. Sulfate profiles of the cementitious matrix of the field concretes after 19 years under partial immersion in sulfate enriched ground; exposed part.	168
Fig. VI-10. Micro-XRF quantitative sulfate mapping of S-0.53 after 19 years under partial immersion; submerged part (top) and exposed part (bottom).	169
Fig. VI-11. Phase assemblage zonations as determined from XRD and SEM-EDS analyses of the field concretes after 19 years under partial immersion in sulfate enriched ground (submerged part: left – exposed part: right).	170
Fig. VI-12. EDS S/Si atomic ratio of the outer (left) and inner C-S-H (right) of P-0.53 after 19 years under partial immersion in sulfate enriched ground; submerged part.	171
Fig. VI-13. EDS S/Si atomic ratio from the outer (left) and inner C-S-H (right) of P-0.53 after 19 years under partial immersion in sulfate enriched ground; exposed part.....	171
Fig. VI-14. SEM-BSE micrograph of a slag with hydration rim with corresponding quantitative S-mapping for S-0.53 after 19 years under partial immersion in sulfate enriched ground; submerged part.....	172
Fig. VI-15. SEM-BSE micrograph of a slag with hydration rim with corresponding quantitative S-mapping for S-0.53 after 19 years under partial immersion in sulfate enriched ground; exposed part.....	173

List of tables

Table II-1. Thermodynamic properties at 25 °C of the main phases involved in sulfate attack, after Matschei <i>et al.</i> (2007) and Schmidt <i>et al.</i> (2008).	13
Table III-1. Binder mix-design of the laboratory micro-concretes.	32
Table III-2. Phase composition of the cement used in the laboratory micro-concretes.....	33
Table III-3. Oxide composition of the cement and slag used in the laboratory micro-concretes.....	34
Table III-4. Density and porosity of binders of the laboratory micro-concretes.....	34
Table III-5. Binder mix-design of the Argentinean concretes.....	38
Table III-6. Phase composition of the cement used in the Argentinean concretes.....	38
Table III-7. Oxide composition of the cement and slag	38
Table III-8. Chemical characteristics of the Argentinean soil.	39
Table III-9. EDS Ca/Si-ratio of C-S-H phases after 28 days and 1 year of saturated hydration.....	54
Table IV-1. Characteristics of the three-stage behaviour of the physical changes of P-0.55 under ponding exposure;.....	72
Table IV-2. EDS S/Si atomic ratio from slag hydration rim of S-0.55 at 0.5 mm depth: evolution along ponding in Na₂SO₄ solution.....	106
Table V-1. Sulfate concentration evolution of the solutions of the ponding and pH-control tests.....	118

Glossary and nomenclature

GLOSSARY

CEMENT NOTATIONS

C	CaO, free lime
c	CO ₂
A	Al ₂ O ₃
F	Fe ₂ O ₃
S	SiO ₂
\$	SO ₃
H	H ₂ O
M	MgO
K	K ₂ O
C₃S	Tricalcium silicate (3CaO.SiO ₂) <i>alite, impure form of C₃S found in commercial Portland clinker</i>
C₂S	Dicalcium silicate (2CaO.SiO ₂) <i>belite, impure form of C₂S found in commercial Portland clinker</i>
C₃A	Tricalcium aluminate (3CaO.Al ₂ O ₃)
C₄AF	Ferrite (4CaO.Al ₂ O ₃ .Fe ₂ O ₃) <i>solid solution between C₂F and C₂A</i>
C-S-H	Calcium silicate hydrate <i>XRD-amorphous phase of non-stoichiometric composition, close to jennite and tobermorite structures major hydration product of Portland cement</i>
C-S-H_d	Decalcified C-S-H
CH	Calcium hydroxide (Ca(OH) ₂) <i>portlandite, hexagonal phase, second major hydration product of Portland cement</i>
C/S-ratio	Atomic (molar) ratio of Ca/Si (CaO/SiO ₂)

CEMENT ABBREVIATIONS

AFm	Alumino ferrite monosubstituted - monosulfoaluminate ($C_3A.C\$.12H = Ca_4Al_2(SO_4)(OH)_{12}\cdot 5(H_2O)$) <i>usually with substitution of Al by Fe</i>
AFt	Alumino ferrite trisubstituted - ettringite ($C_3A.3C\$.H_{32} = Ca_6Al_2(SO_4)_3(OH)_{12}\cdot 26(H_2O)$) <i>usually with some substitution of Al by Fe</i> <i>typical product of sulfate attack</i>
ASR	Alkali-silica reaction of the aggregates <i>one of the main durability problem on concrete</i> <i>“cancer” of concrete</i>
FA	Fly ash
ITZ	Interfacial transition zone <i>In concrete, zone around aggregates characterized by a packing discontinuity at the surface of aggregate particles, “wall effect”</i>
PC	Portland cement <i>commercial cement of type I (§ below) of 95-100 wt.-% clinker;</i> <i>often abusively described as OPC – ordinary Portland cement –</i> <i>which is of a specific pure composition of 100 wt.-% clinker</i>
SCM	Supplementary cementitious material <i>see “mineral admixture”</i>
SF	Silica fume
SRPC	Sulfate Resisting Portland Cement <i>with reduced C_3A content compared to PC</i>
w/c- or w/b-ratio	Mass ratio of water to cement or water to binder

CEMENT VOCABULARY

Binder	Paste possessing binding capacities as cement alone does <i>cement plus mineral admixtures</i>
Brucite	Magnesium hydroxide ($MH = Mg(OH)_2$) <i>typical product of sulfate attack in magnesium environment</i>
Cement	Pulverized clinker with sulfate added during grinding
Clinker	Partially fused nodular product from cement manufacturing kiln <i>consisting essentially of hydraulic calcium silicates</i>
Concrete	Mix of sand, aggregates ($\emptyset > 2$ mm), cement and water
Ettringite	See “AFt”
Fly ash	Fine residue from the combustion of ground or powdered coal
Friedel’s salts	Hydrocalumite ($C_3A.CaCl_2.10H_2O$) <i>chloride-bearing AFm</i>
Gypsum	Calcium sulfate hydrate ($C\$H_2 = CaSO_4.2H_2O$) <i>typical product of sulfate attack</i>
Hemicarboaluminate	Calcium aluminate carbonate hydrate ($Ca_4Al_2(CO_3)_{0.5}(OH)_{13}.5.5(H_2O)$) <i>carbonate-bearing AFm</i>
Hydrotalcite	Magnesium aluminate carbonate hydrate ($Mg_6Al_2(CO_3)(OH)_{16}.4(H_2O)$) <i>magnesium-bearing hydration product of slag</i>
Limestone	Calcium carbonate ($CaCO_3$)
Mineral admixture	Ground mineral added to cement <i>used to reduce the clinker factor (CO_2 reduction)</i>
Monocarboaluminate	Calcium aluminate carbonate hydrate ($C_3A.Cc.12H = Ca_4Al_2(CO_3)(OH)_{12}.5(H_2O)$) <i>carbonate-bearing AFm</i>
Monosulfoaluminate	See “AFm”

Mortar	Mix of sand ($\text{Ø} \leq 2 \text{ mm}$), cement and water
Paste	Mix of cement and water
Portland	Standard cement of colour of the stone of the Portland Isle <i>see "PC"</i>
Pozzolan	Natural/industrial siliceous or siliceous and aluminous material <i>of little cementitious value but able to react with portlandite to form compounds with cementitious properties (e.g.; C-S-H)</i>
Quintinite	Hydrotalcite type with $\text{Mg/Al} = 2$ <i>magnesium-bearing hydration product of slag</i>
Slag	Glassy granular material from quenching of blast-furnace slag <i>by-product of the iron manufacture</i> <i>chemical composition close to that of cement</i>
Thaumasite	Calcium sulfate carbonate hydrate $(\text{C}_3\text{Sc}\text{H}_{15} = \text{Ca}_3[\text{Si}(\text{OH})_6]\text{CO}_3 \cdot \text{SO}_4 \cdot 12\text{H}_2\text{O})$ <i>typical product of sulfate attack</i>
U-phase	Calcium aluminate sodium sulfate hydrate $(4\text{CaO} \cdot 0.9\text{Al}_2\text{O}_3 \cdot 1.1\text{SO}_3 \cdot 0.5\text{Na}_2\text{O} \cdot 16\text{H}_2\text{O})$ <i>sodium-substituted AFm</i> <i>product of sulfate attack</i>

INVESTIGATION TECHNIQUES

AAS	Atomic absorption spectroscopy
BSE	Back scattered electron
EDS	Energy dispersive spectroscopy
Micro-XRF	Micro X-ray fluorescence
MIP	Mercury intrusion porosimetry
PIXE	Proton induced X-ray emission
RH	Relative humidity
SEM	Scanning electron microscopy
XRD	X-ray diffraction
XRF	X-ray fluorescence

NOMENCLATURE OF CEMENT TYPES

Cement types and primary compositions, after the European standard EN 197-1

Cement type	Designation	Notation	Clinker (wt.-%)	Mineral addition (wt.-%)	
CEM I	Portland cement	I	95-100	-	
	Portland slag cement	II/A-S	80-94	6-20	
		II/B-S	65-79	21-35	
	Portland silica fume cement	II/A-D	90-94	6-10	
	Portland pozzolans cement	II/A-P	80-94	6-20	
		II/B-P	65-79	21-35	
		II/A-Q	80-94	6-20	
		II/B-Q	65-79	21-35	
	CEM II	Portland fly ash cement	II/A-V	80-94	6-20
			II/B-V	65-79	21-35
II/A-W			80-94	6-20	
Portland burnt shale cement		II/B-W	65-79	21-35	
		II/A-T	80-94	6-20	
Portland limestone cement		II/B-T	65-79	21-35	
		II/A-L	80-94	6-20	
		II/B-L	65-79	21-35	
		II/A-LL	80-94	6-20	
Portland composite cement		II/B-LL	65-79	21-35	
	II/A-M	80-94	6-20		
CEM III	Blastfurnace cement	II/B-M	65-79	21-35	
		III/A	35-94	35-65	
		III/B	20-34	66-80	
CEM IV	Pozzolanic cement	III/C	5-19	81-95	
		IV/A	65-89	11-36	
CEM V	Composite cement	IV/B	45-64	36-55	
		V/A	40-64	36-60	
		V/B	20-38	61-80	



Chapter I – Introduction

The penetration of sulfate ions into hardened cement can lead to expansion and cracking resulting in a reduced service life of the concrete structure.

The durability problem for construction in the frame of the development of new blended cements is exposed. Degradation of concrete by external sulfate ions is introduced. Motivations, objectives and innovations of the thesis are explained.

Preliminary notions on cement chemistry in relation to additional sulfate source are introduced.

I.1. BACKGROUND

I.1.1. DURABILITY OF CONCRETE STRUCTURES

Cement industry is facing the challenges of society in terms of environment, economy and technical development.

One third to one half of the annual investments of construction are devoted to maintenance. Concrete durability issues are, therefore, a key problematic for cement industry.

Durability problems are made more complex by the increased use of blended cements which suffer from a lack of experience concerning their long-term performance on the field, especially in sulfate environment. The motivation for using more blended cements is the challenge of sustainability to reduce CO₂ emissions from clinker production. Among others, this can be done employing supplementary cementitious materials (SCMs) to reduce the clinker factor. SCMs must be either hydraulic or react with cement hydrates to contribute to the binding properties (pozzolanic reaction). They can be by-products from other industries (e.g.; slag from iron industry, fly ashes from coal burning), raw minerals (e.g.; limestone, silica fume) or industrial or natural minerals with pozzolanic activity (e.g.; pozzolans, activated clays). Over the past decades, cement types have been diversified from the original PC to 27 possible primary cement compositions (§ Glossary and nomenclature). But in practice, the CEM I (PC) and CEM II cover 80 % of the market. However, slag is particularly interesting for cement producers, primarily due to its chemical composition very close to that of Portland cement. It has a latent hydraulicity allowing high levels of replacement. Slag replacement in cement has a great CO₂ reduction potential, and is cost-saving regarding clinker production. Mixing of slag with cement is simple due to the close chemistries of both materials. Slag replacement in cement presents however the advantage of valorising industrial wastes. This makes of CEM III a high value perspective for cement producers both in terms of environment and technical development but also in terms of costs. Durability studies are, hence, an essential step to validate such blends over the long-term.

1.1.2. DEGRADATION OF CONCRETE BY EXTERNAL SULFATE IONS

Loss of strength of concrete structures in a wet sulfate-bearing environment, such as ground water, rivers and seawater, has been widely reported [1]. Sulfate concentrations typically reach $0.02\text{-}3.0\text{ g.l}^{-1}$ ($0.2\text{-}30\text{ mmol.l}^{-1}$) and pH 7-8. The loss of mechanical performance has been attributed to the formation of secondary sulfate-bearing phases from sulfate penetration at the surface of the cementitious materials. “Sulfate attack” can be defined as a set of mineralogical changes with physical effects. “Sulfate attack” is generally attributed to the formation of ettringite from the interaction between sulfate and alumina-bearing phases in the cement.

Different approaches were developed by engineers and researchers over the past century to overcome and understand the mechanisms behind the degradation of concrete by external sulfate sources. In a first time, owing to different usages and raw materials availability, most countries have established national prescription standards (§ II.2.1) concerning the type of cement to be used and the w/c-ratio according to the type of exposure [2]. But with the increased use of SCMs, there was a drive towards a much analytical approach ground on the idea to set tests to evaluate the sulfate resistance of such new blends. The parameters of such a performance approach have found to be neither realistic, nor repeatable (§ II.2.2) and no EU standard for sulfate resistance testing could be drawn up to now.

Degradation of concrete by external sulfate ions involves both chemical and physical aspects that remain unclear and highly controversial. Moreover, the chemical and physical changes implied by the SCMs on the binder are still matter of open questions and, as a result, their relative chemical and physical influences on the sulfate resistance of the binder are far to be understood.

I.2. MOTIVATIONS OF THE THESIS

The non-representative conditions in the laboratory are for a large part at the origin of the development of the large panel of theories concerning the mechanisms of sulfate attack and especially the mechanisms of expansion.

Despite the extensive studies carried out on the question of external sulfate attack, there is no clear understanding of the mechanisms involved and most of the researchers do not come to a general agreement. This is due mainly to:

- a highly fragmentation of data on field cases;
- non-representative chemical (especially high sulfate concentration) and physical (exposure setting influence underestimated) testing conditions;
- a lack of data at the microstructural level.

In particular, laboratory data report that expansion phenomenon under sodium sulfate exposure attack follows a two-stage process [3] (Fig. I-1). To understand sulfate attack, the mechanisms occurring in the first stage and the transition between the stages need to be elucidated. This can only be done considering a microstructural approach.

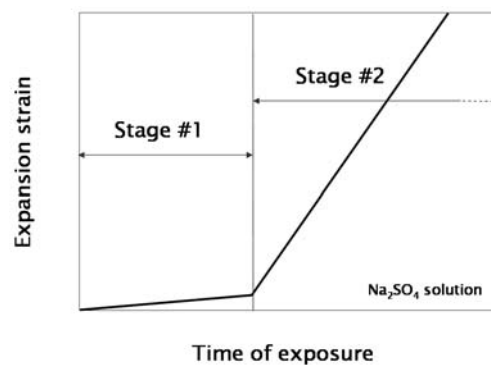


Fig. I-1. Evidence of a two-stage process in expansion phenomenon of sulfate attack in the case of sodium sulfate exposure, after Santhanam *et al.* (2002).

Regarding what authors previously did, it is evident that there is a lack of laboratory investigation on concrete and with a w/c-ratio below 0.40. There are also only separate studies focussed on the different exposure conditions and parameters: there is a need for a unique study comparing the different transport processes that may be involved in external sulfate attack. Additionally, other macroscopic control of the damage must be implemented since sulfate attack cannot only be described and evaluated through expansion.

1.3. OBJECTIVES AND INNOVATIONS OF THE THESIS

1.3.1. OBJECTIVES

Considering the lack of field data on sulfate attack cases, the fact that there is no reliable EU test for sulfate resistance and the gap between the field and the laboratory, the objective of the present work is multiple:

- defining phase assemblages and deterioration mechanisms in field concrete under different environmental regimes;
- developing a testing reference for sulfate induced damage as a function of the environmental exposure conditions;
- evaluating the laboratory tests with comparison to the field results.

A subsidiary objective is also to be considered regarding the increased used of SCMs in cement mix-design without having any retrospect of their durability:

- understanding the influence of SCMs, notably slag at high replacement level, over long-term sulfate exposure.

1.3.2. INNOVATIONS

To better understand the mechanisms of sulfate attack under real conditions, the present thesis proposes:

- a parallel study of field and laboratory concretes under sulfate exposure;
- a transversal study from the macro to the micro (damage, ion ingress, microstructure);
- a monitoring of the macroscopic damage using different methods;
- a focus on microstructural changes;

A subsidiary innovation is to be considered:

- the implementation of low w/c and w/b-ratio below the percolation threshold (0.40).

I.4. SYNOPSIS OF THE THESIS

In order to answer the defined objectives, the thesis is organised around seven chapters.

- **Chapter I – Introduction**
presents the durability framework in relation with the development of new cements and introduces preliminary notions on cement chemistry and additional sulfate.
- **Chapter II – State-of-the-Art**
exposes the duality of sulfate attack in terms of chemical and physical effects, develops the different approaches to the problem over the twenty past years and reviews the main mechanisms of degradation proposed.
- **Chapter III – Research strategy**
presents the materials, describes the methodology and details the analysis parameters adopted.
- **Chapter IV – Ponding**
makes the link with the situation most commonly studied in the literature and proposes a mechanism of degradation of concrete under ponding exposure.
- **Chapter V – Effect of different testing conditions**
investigates the influence of the exposure setting on the sulfate attack mechanism compared to the ponding exposure.
- **Chapter VI – Field exposures**
analyses the damage process on available representative field concretes.
- **Chapter VII – Discussion, conclusions and perspectives**
concludes on the possible mechanisms of external sulfate attack on concrete according to the exposure type with an emphasis on the influence of high level slag replacement, evaluates the test settings proposed regarding the field results and introduces direct perspectives of the work and future investigations.

I.5. PRELIMINARY NOTIONS: CEMENT CHEMISTRY AND SULFATE PHASES

I.5.1. CHEMICAL AND PHYSICAL ASPECTS IN CEMENT CHEMISTRY

I.5.1.A. SULFATE-BEARING PHASES

Portland cement (PC) can be simply described as powder composed of calcium silicate (C_2S and C_3S) and calcium aluminate phases (C_3A) with calcium aluminate ferrite (C_4AF) present in smaller amount, also called clinker, that reacts in presence of water and sets. The so-called binder possesses both good cohesive and compressive strength properties. Cement hydration has been widely studied [4]. If some points are still under research, several statements can be made concerning the hydrates formed.

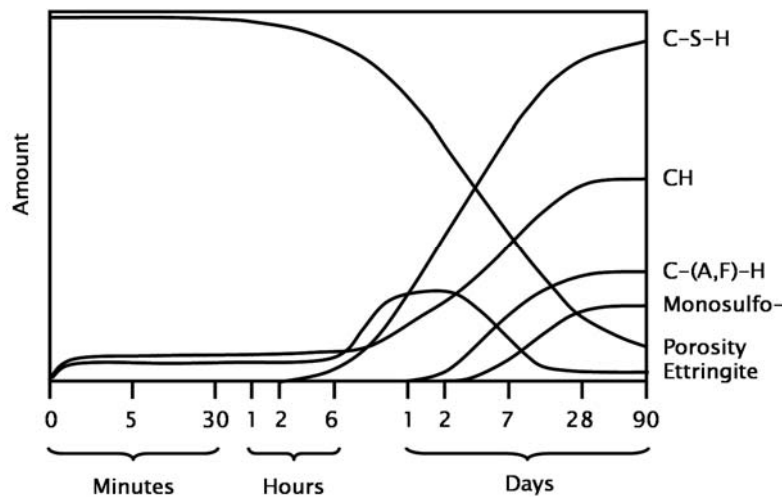


Fig. I-2. Schematic view of cement hydrates formation, after Young *et al.* (1998).

Hardened cementitious matrix is largely constituted of the hydration products of the main phases C_3S (alite) and C_2S (belite): ~ 15 vol.-% of the crystalline calcium hydroxide (CH – portlandite –) and ~ 50 vol.-% of the XRD-amorphous calcium silicate hydrate (C-S-H). The minor C_3A (aluminate) and C_4AF (ferrite) phases are interstitial between alite and belite grains. Ferrite phases are very slow in terms of reactivity, whereas aluminate is, on the contrary, a highly reactive phase (~ 10 min). The drawbacks of C_3A flash set are that the calcium hydroaluminate (C_2AH_8 , C_4AH_{13} , C_3AH_6) massively formed possesses neither the binding nor the compressive strength qualities required but also spatially prevents the development of other essential hydrates (e.g.; portlandite and C-S-H). Traditionally, calcium sulfate additions ($CaSO_4 \cdot xH_2O$, $C\$H_x$; $x = 0, 0.5, 2$: respectively anhydrite, hemihydrate, gypsum) are used by cement producers as C_3A set retarder. Indeed, sulfate

can be substituted in the calcium hydroaluminate phases, as well as iron from the C_4AF dissolution. This results in a two-stage reaction forming first (after ~ 18 h) a hydrated calcium aluminium sulfate hydroxide ($Ca_6(Al,Fe)_2(SO_4)_3(OH)_{12} \cdot 26H_2O$ – Alumino ferrite trisubstituted (AFt) – ettringite –) which, due to sulfate depletion, then reacts with the remaining anhydrous C_3A to form a calcium monosulfoaluminate hydrate ($3CaO \cdot (Al,Fe)_2O_3 \cdot CaSO_4 \cdot 12H_2O$ – Alumino ferrite monosubstituted (AFm) – monosulfoaluminate –). The sulfate introduced is therefore shared in hardened cement between these two main sulfate-bearing hydrates: ettringite and monosulfoaluminate. Nevertheless, these two hydrates are present in minor quantities (Fig. I-2). Ettringite may dissolve over the long term. The two phases are finely intermixed to the C-S-H.

I.5.1.B. PORE NETWORK

Cement hydration is accompanied by the formation of a pore network of different scales (Fig. I-3): disconnected macro-pores, connected capillary pores and structural gel pores between C-S-H foils.

The overall porosity represents ~ 15 vol.-%.

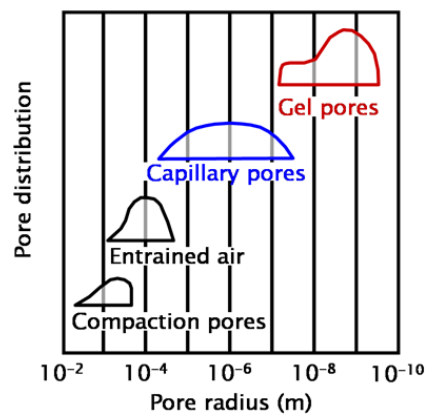


Fig. I-3. Pores types in concrete, after Setzer (1977).

1.5.2. IMPLICATIONS IN PRESENCE OF ADDITIONAL SULFATE SOURCE

The capillary pore network represents a connection with the surrounding environment and it serves as network for transport processes between the cementitious microstructure and the outside.

Sulfate from the surrounding environment can diffuse through the pore network, provided saturated conditions. As known from the hydration mechanisms, some phases from the cementitious microstructures are very sensitive to sulfate: monosulfoaluminate especially can easily be destabilised and transform back to ettringite in presence of sulfate. Ettringite molar volume ($707 \text{ cm}^3 \cdot \text{mol}^{-1}$) is more than twice molar volume of monosulfoaluminate ($309 \text{ cm}^3 \cdot \text{mol}^{-1}$) [5]. Thus, the secondary formation of ettringite from monosulfoaluminate can develop stresses in the set microstructure. This provides a first approach on the possible consequences of sulfate ingress in cement.

However, in aged microstructures additional phases are accessible (e.g.; ferrite) and could react with additional sulfate.

These first simplistic considerations point out the necessary condition for possible interactions between an additional source of sulfate and an aged cementitious microstructure, which is the presence of water as support for the transport process.

Two types of sulfate attack are distinguished: internal and external, depending on whether the sulfate ions are provided respectively from the concrete itself (aggregates with case of pyrite inclusions leading to sulfides liberation) or cement paste (mineral additions, SO_3 from clinker with the typical case of delayed ettringite formation – DEF – in presence of thermal activation) or from the surrounding environment. This thesis concerns the external type of sulfate attack.



Chapter II – State-of-the-Art

The literature with regards to the chemical and physical aspects of sulfate attack is reviewed. Then, an overview is given on the different approaches to avoid external sulfate attack on concrete that have been developed by engineers and researchers over the twenty past years. The failures of these approaches introduced. Finally, the mechanisms of damage proposed in the literature are described.

II.1. CHEMICAL AND PHYSICAL ASPECTS OF EXTERNAL SULFATE ATTACK

II.1.1. CHEMICAL ASPECTS: REACTIONS

Sulfate attack can be studied as a reaction between sulfate ions and cement hydrates (Fig. II-1). The reaction products are crystalline and mainly of three types:

- ettringite ($\text{Ca}_6(\text{Al,Fe})_2(\text{SO}_4)_3(\text{OH})_{12} \cdot 26\text{H}_2\text{O}$; hexagonal);
- gypsum ($\text{CaSO}_4 \cdot 2\text{H}_2\text{O}$; monoclinic);
- thaumasite ($3\text{CaO} \cdot \text{SiO}_2 \cdot \text{SO}_4 \cdot \text{CO}_3 \cdot 15\text{H}_2\text{O}$; hexagonal).

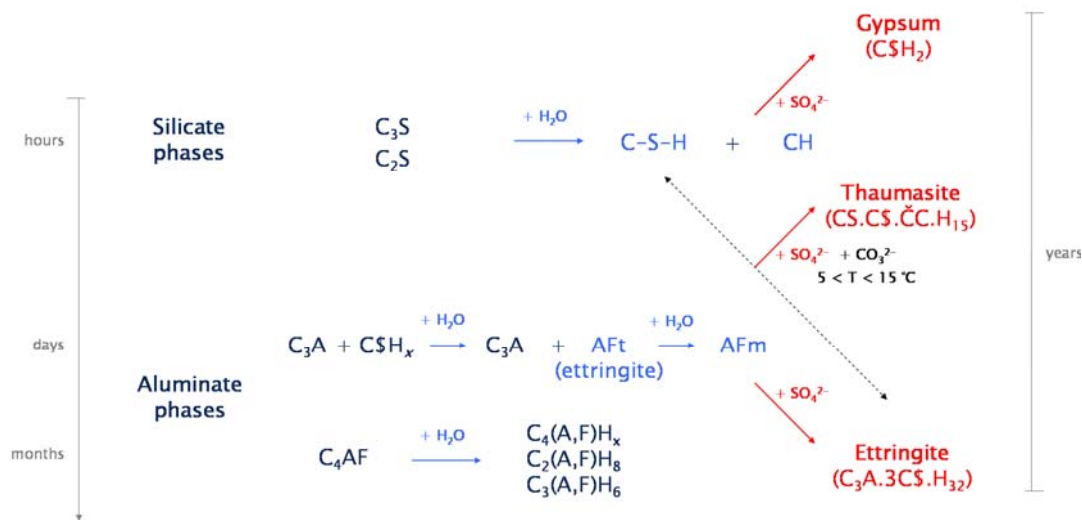


Fig. II-1. Scheme of the reactions between sulfate ions and cement hydrates.

Ettringite formation is the subject of most papers because of its supposed expansive behaviour. This compound forms from aluminate-bearing sources in the cement paste for instance, C_3A and its hydration products (monosulfoaluminate - AFm) or even aluminate-bearing glass in fly ash. Gypsum can form from CH while thaumasite needs more specific conditions to form C-S-H and at low temperature and in presence of carbonate. However, carbonate presence in cement among other causes the formation of monocarboaluminate ($3\text{CaO} \cdot (\text{Al,Fe})_2\text{O}_3 \cdot \text{CaCO}_3 \cdot 11-12\text{H}_2\text{O}$) from monosulfoaluminate.

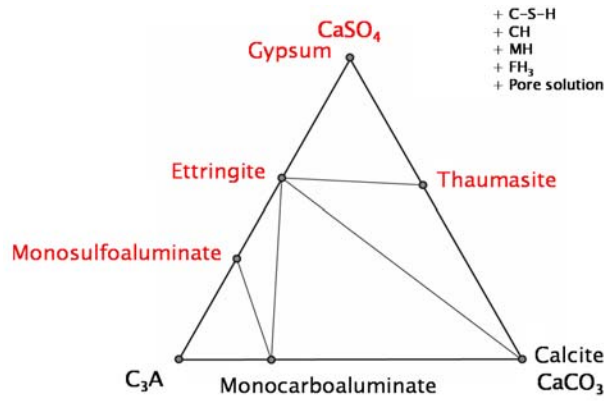


Fig. II-2. Sulfate attack reaction products in the C_3A - $CaSO_4$ - $CaCO_3$ three components system.

The whole of these phases can be represented in the same three components system with respect to cement hydrates and pore solution (Fig. II-2).

At this stage, it is worth noting that sulfate attack can be approached from thermodynamic perspective. Thermodynamic modelling describes phases stability (Table II-1) according to the phase rule based on Gibb's energy minimisation [6-9]. The main problem is the choice of the more realistic system; field data are therefore a considerable input for such theoretical approaches.

Table II-1. Thermodynamic properties at 25 °C of the main phases involved in sulfate attack, after Matschei *et al.* (2007) and Schmidt *et al.* (2008).

Phase	Solubility constant ⁽¹⁾ $-\log K_{sp}$	Gibbs formation energy $\Delta_f G^\circ$ (kJ.mol ⁻¹)	Molar volume V° (cm ³ .mol ⁻¹)
Portlandite	5.2	- 897.01	33
C_3A	-	- 3382.3	89
C-S-H Jennite $C_{1.67}SH_{2.1}$	13.2	- 2480.81	78
Tobermorite $C_{0.83}SH_{1.3}$	8.0	- 1744.36	59
Monocarboaluminate	32.5	- 7337.50	262
Monosulfoaluminate	29.3	- 7778.5	309
Ettringite	44.9	- 15205.94	707
Thaumassite	49.4	- 15128.46	663
Gypsum	4.6	- 1797.76	75

⁽¹⁾: with respect to the species $Al(OH)_4^-$, $Si(OH)_3^-$, OH^- , H_2O , Ca^{2+} , Mg^{2+} , CO_3^{2-} , SO_4^{2-} .

II.1.2. PHYSICAL ASPECTS: TRANSPORT PROCESSES

External sulfate attack on concrete is supposed to be based on transport processes implying mineralogical changes between the surface and the core regions that can be directly related to the uptake of sulfate combined with leaching [10, 11]. Most studies are nevertheless carried out in saturated conditions while in the field there may exist different types of exposure to a wet sulfate source involved in different transport processes. Aside from the water saturated conditions, other settings can be envisaged: wetting and drying cycles, wet and dry sides for instance.

II.1.2.A. POSSIBLE TRANSPORT PROCESSES

Water saturated conditions: diffusion-based transport

In full immersion the concrete structure is water saturated. Ions may diffuse either inwards the cementitious system (case of SO_4^{2-}) or outwards (case of OH^- and Ca^{2+}) [10]. Before interaction with the environment, the pore solution of concrete predominantly consists of K^+ , Na^+ and OH^- ions and is saturated with respect to $\text{Ca}(\text{OH})_2$; its pH is therefore buffered to the value of portlandite pK_a of 12.6. The presence of alkali rises the pH up to higher values in the range of 13. Relative to cement paste, any natural environment is acid. As a consequence, alkali ions are quickly leached out. When K^+ , Na^+ have leached, portlandite plays its role of pH buffer: $\text{Ca}(\text{OH})_2$ dissolves and Ca^{2+} ions are in turn leached out. In similar fashion, C-S-H may decalcify and form a C-S-H_d poor in calcium up to leave eventually its silicate skeleton (“SiO₂ gel”) that does not possess any binding capacity. Ettringite and monosulfoaluminate are unstable below pH 10-11 and therefore very sensitive to CH and C-S-H decomposition. Cements hydrates decompose along the pH gradient from the surface to the bulk of the material (Fig. II-3). This simple zonation through leaching, whose modelling has been developed by Kamali *et al.* [12, 13], is however superposed with the ingress of ions and subsequent interactions with the cement paste. The works of Gollop and Taylor using a Na_2SO_4 exposure solution summarize well the different effects due to SO_4^{2-} supply combined with leaching effect [14]. Successive changes were observed from the unaltered bulk material to the damaged surface: replacement of monosulfoaluminate by ettringite, dissolution of portlandite, partial decalcification of C-S-H, precipitation of gypsum in veins sub-parallel to the surface associated to cracks, and further decalcification and leaching (Fig. II-4).

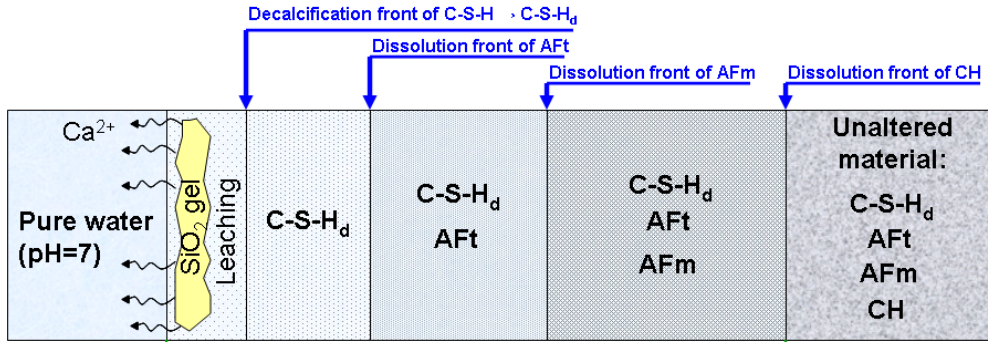


Fig. II-3. Zonation through leaching as of OPC in pure, after Kamali *et al.*

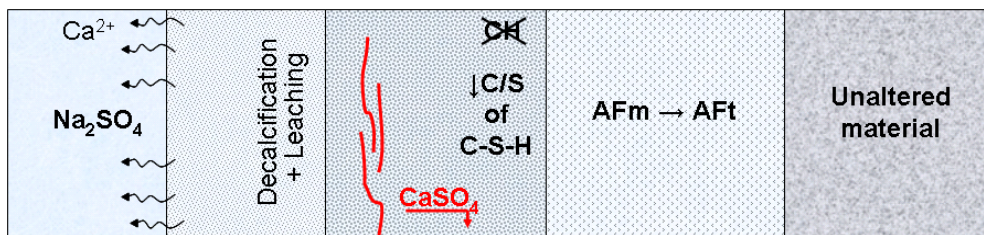
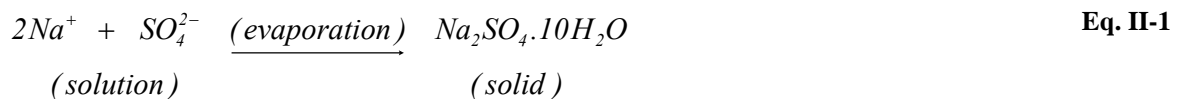


Fig. II-4. Zonation through combined sulfate attack and leaching as exposed for OPC in Na_2SO_4 solution at 20°C , after Gollop and Taylor (1992).

Wetting and drying cycles: absorption-based transport

Weathering in the field, among others, is characterised by wetting and drying cycles. A porous material such as concrete can absorb liquid during the wet phase, which may evaporate during the dry phase, allowing the precipitation of the salts it contains. A case of particular interest is the damage caused by sodium sulfate (Eq. II-1). This salt exists as an anhydrate called thenardite, Na_2SO_4 , or as a decahydrate called mirabilite, $\text{Na}_2\text{SO}_4 \cdot 10\text{H}_2\text{O}$. At room temperature and at relative humidity $\text{RH} < 75\%$, mirabilite decomposes to thenardite. In presence of wetting and drying cycles this implies repeated thenardite recrystallization (Eq. II-2) [15]. This temperature and humidity dependent process causes repeated increase in volume leading to fatigue of the cement paste causing a cohesion loss.



Wet and dry sides (semi-immersion): “wick” action

At foundation level or at tidal zone level, concrete structures are respectively semi-buried in the soil or semi-immersed in the water. In such semi-immersion case, rates of capillary rise and evaporation are in competition (Fig. II-5) and at a specific height h_s the rate of evaporation equals the rate of capillary rise. As a result the solution that has diffused through the concrete may become supersaturated, so that crystal efflorescence occurs, characterised by crystal growth in the external water film. Above that location, the water evaporates inside the material, resulting in subflorescence, characterised by crystal growth below the material surface. Subflorescence may be critical if the crystallization pressure exceeds the tensile strength of the material [16].

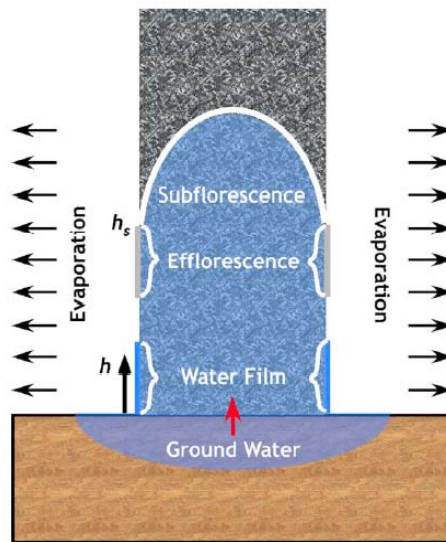


Fig. II-5. Competition between capillary rise and evaporation from concrete in semi-immersion, after Scherer (2004).

II.1.2.B. THE ROLE OF W/C-RATIO

The w/c-ratio controls the capillary porosity of cement [17]. Monteiro and Kurtis [18] pointed out a “safe region” in terms of time to failure for mixtures with w/c-ratio below 0.45 (Fig. II-6). It appears that the relationship between the time to failure and the w/c-ratio follows a step function. This tends to controvert the hypothesis owing to which sulfate attack would be controlled by diffusion mechanisms. The value of w/c-ratio of 0.45 may be related to percolation threshold.

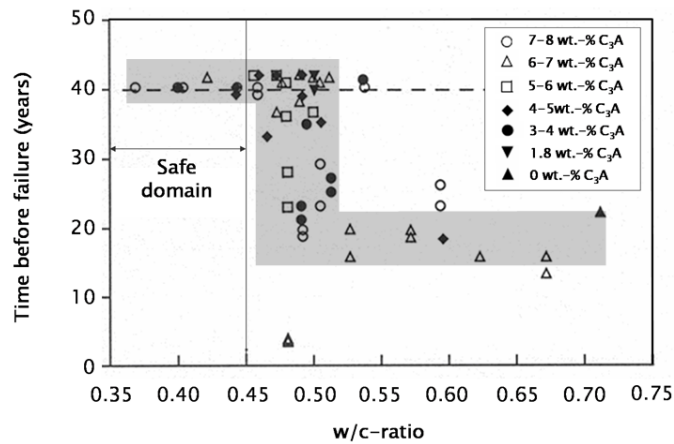


Fig. II-6. Time to failure as a function of w/c-ratio, after Monteiro and Kurtis (2003).

II.2. APPROACHES TO AVOID SULFATE ATTACK

II.2.1. THE PRESCRIPTIVE APPROACH

II.2.1.A. CHEMICAL CHANGES

Sulfate attack is often commonly defined by secondary ettringite formation leading to expansion. Therefore, from the 1930s, the availability of C₃A in cement has been limited to prevent from secondary ettringite formation. C₃A content of cements were reduced and sulfate resisting Portland cements (SRPCs) were introduced on the market. According to the country, the C₃A content determined by Bogue calculation was reduced to down to 5 wt.-% (ASTM C 1157-03), 3 wt.-% (EN 196, 197) and even 0 wt.-% for some countries. But the result of Monteiro and Kurtis (Fig. II-6) and studies of other authors [18, 19] point out that that expansion and failure can occur with low C₃A contents (Fig. II-7).

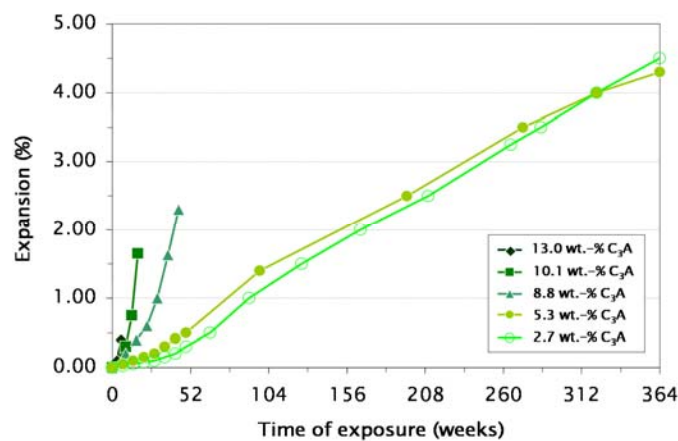


Fig. II-7. Influence of C₃A content on sulfate resistance of CEM I, after [2].

II.2.1.B. PHYSICAL CHANGES

Physical effects, especially reduction of permeability, are more and more considered to be important in addition to chemical effects.

For the most used cements a w/c or w/b-ratio lower than 0.45 is traditionally recommended to decrease permeability and limit the transport phenomena.

From the 1980s, with the appearance on the market of new blended cements, new prescriptions were developed.

Especially, fly ash and slag blends were considered to be sulfate resistant providing replacement levels exceeding respectively 20 and 65 wt.-% [2].

However, Irassar pointed out that concretes containing high volume of mineral admixtures can be more susceptible to the so-called “physical attack” where evaporation is believed to be involved with subsequent salt precipitation without much change in the cementitious matrix (typically related to semi-immersion case) than to so-called “chemical attack” where changes strictly concern the chemistry stability of the system with any physical effect (thought to be dominant in full immersion case) [20, 21]. Most severe deterioration occurred for slag concrete specimen with a replacement level of 80 wt.-%. Slag seems to enhance C-S-H decalcification and some works showed that slag blends fail rather through disintegration and softening than through expansion and cracking [14, 22, 23].

II.2.1.C. NEEDS FOR ANOTHER APPROACH

Prescriptions are not necessary a reliable answer to sulfate attack issues. Sulfate attack mechanism is not simple and may not exclusively be attributed to ettringite formation while prescriptions are typically based upon this hypothesis. The physical and chemical aspects of sulfate attack cannot be so simply dissociated and may feed each other.

Prescriptions clash against the increased use of diverse cements. The mechanisms of degradation of blended cements in sulfate environments are still a subject of debate: what is the relative importance of chemical versus physical effects of SCMs?

There is therefore there is a drive towards performance approach with the idea of elaborating an EU standard for sulfate resistance.

II.2.2. THE PERFORMANCE APPROACH

The performance approach is based on the need to develop fast, realistic and repeatable tests to evaluate sulfate resistance of concrete.

II.2.2.A. ACCELERATION METHODS

Sulfate attack is a slow process occurring in the field within decades. The main problem is to simulate this at the laboratory scale within a few months. Traditional methods to accelerate the tests for sulfate resistance consist of:

- using high sulfate concentrations (e.g.; 30 g.l^{-1} which corresponds to about 10 times the maximum values found in the field) to increase the ionic strength and thus accelerate the transport process;
- storing at high temperatures (e.g.; $> 25 \text{ }^\circ\text{C}$ while typical water temperature in the field reaches $10\text{-}20 \text{ }^\circ\text{C}$) to promote the reaction kinetics;
- reduced curing time (e.g.; few days) before the exposure start to have a more porous material that increases the transport flow (and this reduces the time of pre-exposure).

II.2.2.B. SIMPLE SETTING

To enhance the test reproducibility and let it assessable to most people, its set-up must be simple. Common sulfate resistance tests implement the following simplified conditions:

- liquid exposure because it is easier to control in terms of chemical composition and transport process while in the field exposure often implies contact with a soil;
- full immersion because easier to set up but in the field most of the structures are partially immersed in the sulfate environment;
- Na_2SO_4 solution because it is of the limited interactions of the counter cation Na^+ and therefore a better isolation of the SO_4^{2-} effect while various species are present in the field;
- no control of the pH because it is easier to set up while the pH is in the range of 7-8 in the field but regular renewal of the solution (monthly after ASTM C1012) to lower the pH and simulate the continuous ionic supply as it is the case in the field;
- mortar or cement paste to simplify the diffusion process and the analysis (quantitative XRD easy implementable) while concrete structure are exposed in the field;
- high w/c or w/b-ratios (e.g.; in the range of 0.60 while < 0.50 for field concrete) to have a more porous microstructure and thus increase the diffusion flow.

II.2.3. LIMITATIONS OF THE PERFORMANCE APPROACH

Nevertheless, there is at this time no harmonized CEN standard (i.e.; no reliable laboratory test for sulfate resistance): the draft for establishing an EN test method failed because of a too large dispersion of results between the participating laboratories (Fig. II-8).

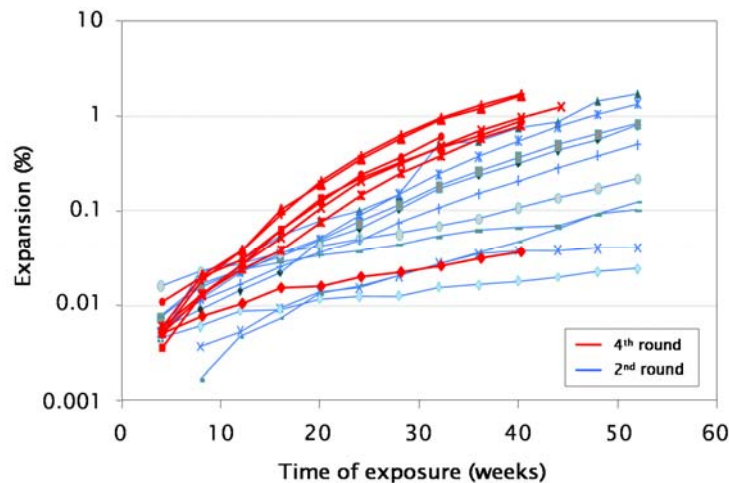


Fig. II-8. Robin tests expansion results, after [24].

Such dispersion in the results is essentially due to non-reproducible testing conditions.

II.2.3.A. CHEMICAL ASPECTS

Sulfate concentration

According to the phases equilibrium at 25 °C [25], the high sulfate concentrations commonly employed in tests (in the range of 300 mmol.l⁻¹) may lead to gypsum formation in addition to ettringite while the sulfate concentration in the field (0.2-30 mmol.l⁻¹) would hardly stabilise gypsum and the attack should be dominated by ettringite formation (Fig. II-9). Indeed, gypsum is rarely observed under typical field conditions [14, 26, 27].

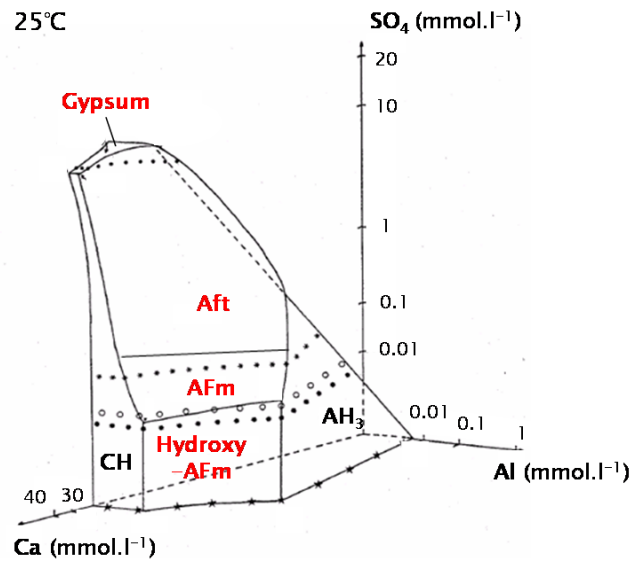


Fig. II-9. Phases equilibrium in the SO_4 -Ca-Al ternary system at 25°C , after Damidot and Glasser (1992).

Temperature

The stability of sulfate-bearing phases with temperature [28, 29] reveals that gypsum becomes stable at lower sulfate concentrations with increasing temperature (Fig. II-10). Within the range of 10 to 25°C this effect is not great: it starts to be significant above 50°C .

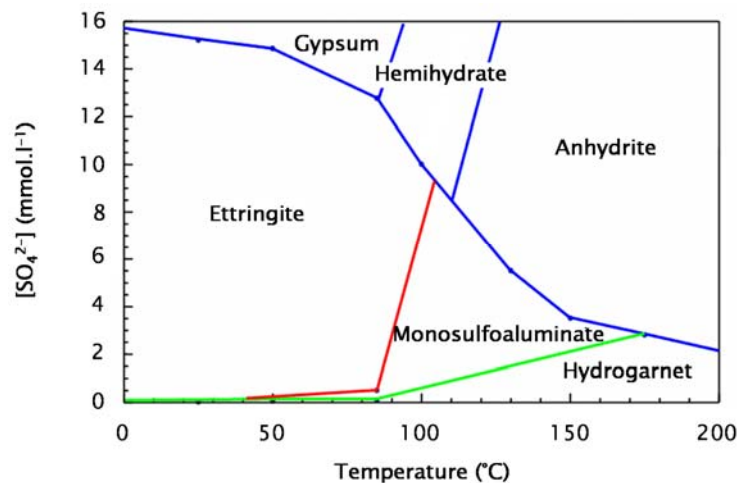


Fig. II-10. Effect of temperature on sulfate-bearing phases stability, after Damidot and Glasser (1992-1993).

However, if temperature is low enough (i.e.; below 15°C) thaumasite can form from C-S-H and the incoming sulfate in presence of calcite [30].

Counter ions and other species

“Pure” sulfate attack never happens since SO_4^{2-} anions are always associated to a counter cation. The nature of the associated cation (e.g.; Mg^{2+} , Ca^{2+} Na^+), has a direct influence on the type of products formed and on the attack process. Magnesium is present in non negligible amount in most waters and a typical consequence is the formation of a layer of brucite (magnesium hydroxide, $\text{Mg}(\text{OH})_2$) at the concrete surface as well as the formation of a magnesia rich silica gel at the edge of the exposed sample [14]. CaSO_4 exposure causes a reduction of leaching compared to Na_2SO_4 exposure since calcium ions from the pore solution are counterbalanced by calcium ions from the surrounding solution. Leaching is claimed to accelerate sulfate attack since it provides a more porous microstructure where sulfate can ingress more easily.

Some studies also focus on the combined effects of SO_4^{2-} and Cl^- to simulate marine environment [31]. But in most cases, sulfate and chloride penetration into cement are treated separately, chloride attack being directly connected with corrosion problems [32]. From a chemical point of view, Cl^- ions are partially absorbed by the C-S-H and can be bound to monosulfoaluminate as revealed by ^{35}Cl NMR in the study of Yu and Kirkpatrick [33] to form Friedel's salts (chloride-bearing AFm phase also named hydrocalumite) and tend to limit the stability of ettringite [34].

Another species that can influence sulfate attack is carbonate, in the case of external sulfate attack coming from the surrounding air, water or soil. Carbonate causes carbonation which is generally characterised by the transformation of portlandite into calcite. The calcium from the C-S-H can also form calcite. The basic pH of the cementitious matrix is controlled by portlandite and alkali ions at ~ 12.5 -13. When CO_2 dissolves, it leads to the formation of H_2CO_3 , whose pK_a is 6.35. The pH of pore solution inside the carbonated zone is thus reduced. Carbonated concrete has a $\text{pH} < 9$ [35], which is below the stability range of ettringite ($\text{pH} 10.5$ -13). In the case of sulfate exposure, sulfate and carbonate ions may be in solution in the carbonated zone. Carbonate is more likely to react than sulfate due to the higher electronegativity of carbon compared to sulfur. Consequently, carbonate compounds will be more stable than sulfate compounds, which explains the better stability of monocarboaluminate over monosulfoaluminate in presence of carbonate. It has indeed been observed that monocarboaluminate is formed from monosulfoaluminate and can further breakdown into calcite and gypsum.

An important effect of carbonation is that the carbonated zone is characterised by a higher density than the rest of the cementitious material. This higher density external layer might play a role of a barrier to transport-based processes such as sulfate attack. Although carbonation occurs in field concretes, in the laboratory an effort is made to minimize the potential for carbonation so as to not limit sulfate attack from occurring.

pH

The pH plays a major role in sulfate attack since it controls the leaching effect and the phases solubility. It should therefore be as close to field conditions as possible. But in the laboratory, even if the solution is regularly renewed according to ASTM C1012 prescription, there is a cycling pH rise from 7 to 12-13 owing to the solution renewal frequency (Fig. II-11). Moir suggested making a test at constant pH 7.5. Few authors have worked at a constant pH but in the case of limestone-blends [36], adding a titration solution which did not ensure a constant concentration in sulfate.

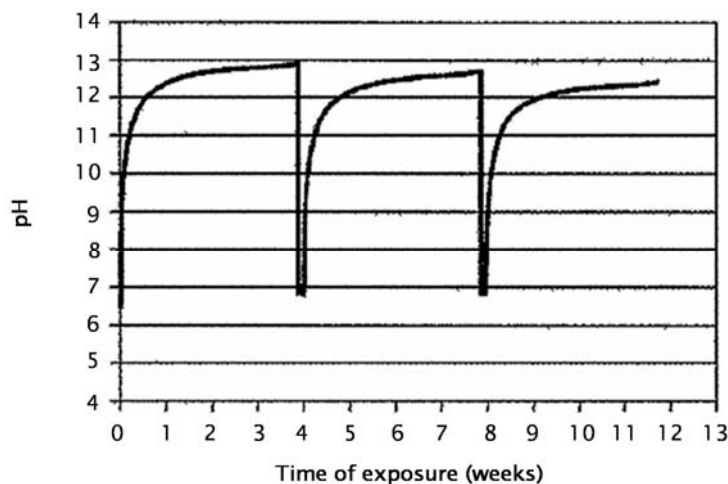


Fig. II-11. pH cycles along solution renewal cycles, after Moir.

The renewal of the solution prescribed in ASTM C1012 is bad to control the pH but good to renew the ionic species and simulate the unlimited sulfate source from the field.

II.2.3.B. PHYSICAL ASPECTS

Curing time and conditions

A too short curing (in saturated lime water) implies that the samples present a low degree of hydration when placed in a sulfate environment. In the field, due to its slow reactivity, sulfate attack concerns mature materials. A young microstructure differs from a mature microstructure in terms of hydrate development. The further reactions with sulfate ions might be influenced, notably in terms of available space.

Full immersion

In lab models a pure diffusion process (i.e.; full immersion) is assumed while in the field semi-immersion and/or to wetting and drying cycles may occur. In such more complex exposures, the diffusion process may be more controlled by capillary forces that can play a major role in the field that might be underestimated in the laboratory.

w/c and w/b

The increased w/c and w/b-ratios implemented in most tests compared to field cases leads to a change in the microstructure especially in terms of porosity and density.

There is little literature on tests using a low w/c or w/b-ratio especially below the percolation threshold (0.40), while prescriptions in the field encourage the use of such low values.

Interfacial transition zone (ITZ)

Tests involving cement paste or mortar are not comparable to field cases involving concrete structures in terms of transport process.

The interface between the aggregates and the cement paste, the so-called ITZ, shows a higher porosity due to the “wall” effect of packing of cement grains [37]. The ITZ thus plays a role in any transport process involved in concrete. Nevertheless, all of these impacts seem to be counteracted by other factors which generally lead to a reduction of transport rates with increasing aggregate contents (i.e.; increasing ITZ proportion) if all other variables are held constant [38].

II.3. DAMAGE MECHANISMS

Three kinds of macroscopic damage due to sulfate ion interaction with the cementitious matrix have been reported: expansion (cracking, spalling), softening and decohesion [39].

II.3.1. EXPANSION

Sulfate attack is generally associated with, and even defined, in the literature as the formation of sulfate-bearing products within the cement paste leading to macroscopic expansion [40]. Expansion is generally attributed to ettringite formation.

Ettringite forms from cement hydrates when SO_4^{2-} is supplied. However, even in the absence of external sulfate, ettringite tends to recrystallize according to an Ostwald ripening process in any available cavities, when water is present for transport. Thus, the presence of ettringite in a distressed concrete observed by petrography, SEM or XRD does not necessarily mean that the ettringite has caused the distress. Nevertheless, ettringite is believed to be the first cause of sulfate induced macroscopic damages and especially of cracking [23]. Due to its formation from the dispersed monosulfoaluminate, ettringite formed during sulfate attack is also finely intermixed to the cement hydrates. This type of ettringite present as very small crystals within the paste may be more likely responsible of distress in cement paste than the most obviously detectable large crystals precipitated in cavities [41].

Cement is known to perform very well in compression but very badly under tension with a failure criterion in the range of few MPa (e.g.; in the order of 4 MPa). Hence, any microstructural effects responsible of macroscopic expansion should be able to generate stresses in such a range. Various different theories exist regarding the mechanism of expansion:

- increase in solid volume;
- topochemical reaction;
- swelling;
- crystal growth pressure.

II.3.1.A. INCREASE IN SOLID VOLUME

The increase in solid volume [42] is based on the idea that the solid volume of the secondary sulfate-bearing phases is higher than that of their respective reactants. In particular, owing to this theory, the formation of such phases would put the surrounding set microstructure in tension. Nevertheless, such differences between the solid volume of the products and the reactants is common in cement chemistry in the case of other reactions (e.g.; C-S-H and CH formation from C_3S) that are not accompanied by any expansion. Indeed, such reactions only proceed to the extent that sufficient space is available. Therefore, ettringite formation does not necessarily lead to primary expansion owing to the theory of the increase in solid volume since pores and voids in the microstructure provide space for ettringite precipitation especially in the beginning of sulfate exposure. The amount of porosity available stands therefore for the critical criterion for expansion to occur following the increase in solid volume theory.

II.3.1.B. TOPOCHEMICAL REACTION

Some authors [43] support the idea owing to which expansive ettringite forms *in-situ* from C_3A . Nevertheless, C_3A and ettringite possess two different crystalline structures (respectively cubic or orthorhombic and hexagonal) and such a process without any intervening layer and any passage of ions in solution cannot be envisaged.

II.3.1.C. SWELLING

Swelling theory of expansion considers ettringite as colloid. Owing to Mehta [44], the agglomeration of ettringite crystals of colloidal size would imbibe water and would thereby cause expansion. In over sulfated cement systems at early ages, interparticular forces can generate swelling pressure. But this is unlikely in hardened cement systems since ettringite is not colloidal but a fine dispersed phase. Ettringite is not a gel-like material that could be able to expand without breaking, ettringite is on the contrary a highly crystalline phase.

II.3.1.D. CRYSTAL GROWTH PRESSURE

Crystal growth theory requires two conditions: supersaturation and confinement. Considering a crystal growth from solution inside a cylindrical pore [45], the crystallization pressure is related to the supersaturation and the size of the pore according to the Laplace's equation (Eq. II-3). For the typical liquid and crystal characteristics expected of a crystal such as ettringite [46], in order to exert a pressure of 3 MPa, which corresponds to the range of tensile strength of concrete, a pore radius smaller than 50 nm is necessary. This underlines, that large ettringite crystals observed ins cracks and pores have probably recrystallised inside pre-existing cracks because of the space available with little constraint and do not therefore generate any significant expansive pressure.

$$p_c - p_l = -\frac{2\gamma_{cl} \cos(\theta)}{r_p} = \frac{R_g T}{v_c} \ln\left(\frac{C}{C_0}\right) \quad \text{Eq. II-3}$$

$p_c - p_l$ represents the difference between the crystal and the liquid pressure, corresponding to the crystallization pressure exerted on the surrounding pore wall;

γ_{cl} is the crystal surface energy at the crystal/liquid interface;

$-\frac{2\cos(\theta)}{r_p}$ is the optimal (crystal energy minimization) curvature κ_{cl} of the advancing surface of a crystal growing inside a cylindrical pore of radius r_p with a contact angle θ ;

R_g, T, v_c are the specific invariant parameters of the system, respectively gas constant, absolute temperature and molar volume of the crystal;

C, C_0 concentration of the solute and equilibrium solubility, their quotient defines the supersaturation magnitude (if activity coefficients are ignored).

II.3.2. SOFTENING

Gypsum is mainly found as precipitates in macroscopic cracks. Nevertheless, it may also be found intermixed in the cement matrix. This suggests that gypsum can form from portlandite and also from calcium in C-S-H which becomes decalcified. Monosulfoaluminate is usually assumed to be the source of aluminium for ettringite formation but a source of calcium is also needed. In ordinary Portland cement paste, the experimentally determined Ca/Si-ratio is around 1.7-1.8 [47] compared to the upper limit of synthetic C-S-H of 1.5. This implies that in real cement matrix the C-S-H has an excess of calcium, which become available for gypsum and ettringite formation.

Both gypsum and ettringite formation therefore lead to a relative decalcification of C-S-H, which is the main hydrate of cement matrix and stands for its cohesive property. This would result in a softening of this phase.

II.3.3. DECOHESION

Decohesion mainly occurs when thaumasite formation is observed. Thaumasite is indeed a very brittle material whose fracture produces small conchoidal fragments: it does not possess the cohesive properties proper to the cementitious matrix.

Thaumasite forms in presence of carbonate from a sulfate source and drawing silicon from the C-S-H, the consumption of the silica of the C-S-H can lead to a loss of its binding properties.

There is no evidence that ettringite is theoretically required as a precursor to thaumasite formation, but thermodynamically as sulfate concentration increases, ettringite forms first [48]. Ettringite and thaumasite can also enter into partial solid solution [49].

II.3.4. KEY OPEN QUESTIONS

Softening and decohesion occurrence is understood and their mechanisms are agreed by the scientific community.

On the contrary, the mechanism(s) of expansion is still a subject of controversy. The crystal growth pressure theory appears to be the most possible one but there is still no evidence that supersaturation initiates the expansion.

In addition, there is a lack of relationship between the chemical changes and the macroscopic consequences. No link between the phase assemblage and the damage has been clearly done and especially the combined effects of different phases (e.g.; ettringite and gypsum) are widely discussed [3, 14, 22, 23].

Moreover, the absence of linear relationship between the amount of secondary sulfate-bearing phases and the expansion rises up the fact that sulfate attack can actually not be only and directly related to ettringite formation: different physical and chemical effects often overlap [50] and are hardly identified. Physical and chemical effects are often considered separately while they might not be so simply divided.



Chapter III – Research strategy

The methodology adopted in this thesis involves a parallel study of laboratory and field concrete samples subjected to various conditions of degradation by external sulfate ions.

Concretes made of pure Portland and with slag substitution of 70 wt.-% or more were exposed. In the laboratory, a low Na₂SO₄ concentration is used similar to levels in the field. In the field, exposures involve other ions in addition to SO₄²⁻. Various exposure conditions were studied: ponding, pH-control, semi-immersion and wet/dry cycles.

The analysis of the concrete samples covers the macro to the micro scale. A first approach to the ion ingress and leaching comes from the measurement of the exposure solutions using AAS. Evaluation of the damage of the concrete samples is assessed by visual control and measurement of the physical properties such as expansion, mass loss, compressive strength and dynamic elastic modulus. To study the microstructure, specimens must be sacrificed at specific ages. Quantitative ion profiles were determined by image analysis of SEM elemental mappings and by micro-XRF for the field samples. The evolution with depth of the phase assemblages zonation was made combining XRD and statistical SEM-EDS analyses. Further local microstructural details were studied mainly by SEM-BSE images and local EDS analysis.

After describing these analytical techniques, the reference microstructures are introduced.

III.1. MATERIALS AND EXPOSURE CONDITIONS

III.1.1. LABORATORY

III.1.1.A. MICRO-CONCRETES

The laboratory samples were standard $4 \times 4 \times 16 \text{ cm}^3$ prisms, which allow easily comparison with existing data. In order to be as comparable as possible to the field conditions, these prisms are micro-concretes and not mortars. According to the geometry of the samples, the maximum aggregate size is 8 mm. The quartz aggregate grinding follows a sieving curve type AB8 from the German normalisation (Fig. III-1).

Four binders were designed (Table III-1) according to three characteristics:

- PC to be representative of one of the field most used binder;
- high slag replacement level to evaluate the durability perspectives of such mixes;
- $w/b > 0.40 > w/b$ to check the influence of the connectivity of capillary porosity, which is generally shown to be connected above 0.40 and disconnected below.

Sample preparation (mixing, demoulding and curing) was done according to the European standard EN 196-1. For the slag blends, slag and cement were premixed in a turbula shaker-mixer with three-dimensional movement during 5 hours. The micro-concrete prisms were prepared using a standard mixer. The water was first introduced, then the cement or the cement-slag mix and mixing started at low speed ($145 \pm 5 \text{ rpm}$) during 30'', after which the aggregates were added from the bigger to the smaller sieve size and the mixing speed increased ($285 \pm 10 \text{ rpm}$) during 30''. Mixing was stopped during 1'30'' to homogenize the mix by hand. Mixing was started again at high speed during 60''.

The mixes with highest w/b-ratio (of 0.55) and that ones with lowest w/b-ratio (of 0.38) were made using respectively 400 kg.m^{-3} and 480 kg.m^{-3} of cement or cement-slag mix.

Table III-1. Binder mix-design of the laboratory micro-concretes.

Mix label	Equivalent binder type	28 days compressive strength (MPa)	w/b	Mineral addition	
				Substitution level (wt.-%)	Type
P-0.55	CEM I	42.5	0.55	0	-
P-0.38	CEM I	52.5	0.38	0	-
S-0.55	CEM III/B	32.5	0.55	70	Slag
S-0.38	CEM III/B	52.5	0.38	70	Slag

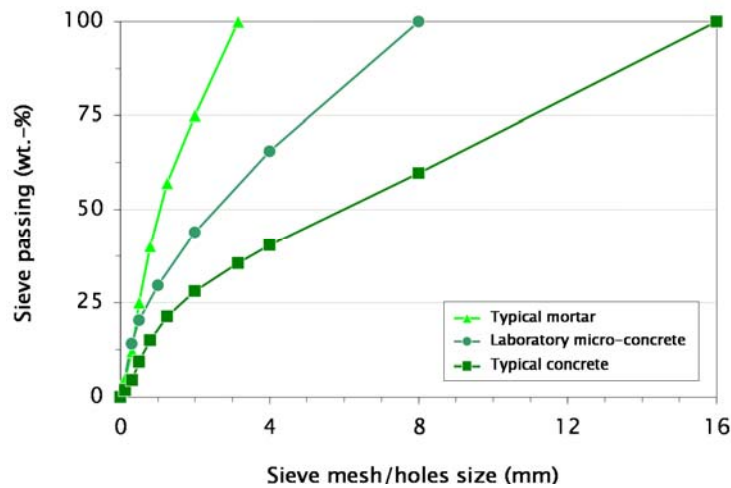


Fig. III-1. Aggregate granulometry of the laboratory micro-concretes.

This project was undertaken under the umbrella of the NanoCem research network, the raw materials were the same as used in the thesis core project of Kocaba [51]. The cement used is a CEM I with high C_3S , and high alkali content (Table III-2), designated as “cement C” by Kocaba. The C_3A content is about the average for commercial PCs. The slag employed is a slag of normal reactivity with an amorphous content exceeding 99 wt.-% (Table III-3), designated as “slag 01” by Kocaba. All mixes were made without any superplasticizer. The XRD-Rietveld and XRF analyses were supplied by Kocaba.

Table III-2. Phase composition of the cement used in the laboratory micro-concretes.

Phases	Formula	Content (wt.-%)
Alite	C_3S (M3)	61.5
Belite	β - C_2S	17.3
	α h- C_2S	-
Aluminate	C_3A -cubic	5.6
	C_3A -orthorhombic	1.7
Ferrite	C_4AF	8.6
Lime	C	0
Periclase	M	0.3
Gypsum	$C\$H_2$	0
Hemihydrate	$C\$H_{0.5}$	1.3
Anhydrite	C\$	1.4
Quartz	S	0
Portlandite	CH	0.8
Calcite	Cc	0
Arcanite	K\$	1.5

Table III-3. Oxide composition of the cement and slag used in the laboratory micro-concretes.

Oxides	Content (wt.-%)	
	Cement	Slag
SiO ₂	21.01	36.61
Al ₂ O ₃	4.626	12.21
Fe ₂ O ₃	2.603	0.8503
CaO	64.18	41.59
SO ₃	2.78	0.6304
MgO	1.823	7.177
Na ₂ O	0.197	0.184
K ₂ O	0.939	0.275
P ₂ O ₅	0.4	0.0065
TiO ₂	0.143	0.3532
Mn ₂ O ₃	0.029	0.1439
LOI	1.26	-0.03

Table III-4. Density and porosity of binders of the laboratory micro-concretes after 28 days of hydration.

Binder	Density (g.cm ⁻³)		Total porosity (vol.-%)	
	Apparent	Bulk	$(1 - \frac{\rho_{bulk}}{\rho_{apparent}}) \cdot 100$	MIP
P-0.55	2.5506	2.2924	10.1260	7.6912
P-0.38	2.5447	2.3553	7.4421	5.5438
S-0.55	2.4920	2.2636	9.1661	7.7936
S-0.38	2.4711	2.3065	6.6624	5.9069

The apparent and bulk densities of the binders after 28 days of hydration were determined by helium pycnometry (Micromeritics Accu Pyc 1330) and their global porosity, excluding the aggregates, was assessed by MIP (Porotec CE Instruments Pascal 140/240 series) (Table III-4).

III.1.1.B. LOW Na_2SO_4 CONCENTRATION AND VARIOUS EXPOSURE SETTINGS

All laboratory studies were carried out at $20.5\text{ }^\circ\text{C} \pm 0.5$. The exposure environment was a low ion concentrated Na_2SO_4 solution of 3 g.l^{-1} (i.e.; 0.021 mol.l^{-1} or 3000 ppm), renewed every month except pH-control. The ratio between the volume of the solution and the volume of the cementitious material was 20 (i.e.; 5 times higher than that prescribed in the ASTM C1012) to avoid limitations due to sulfate availability and to be closer to field conditions where sulfate is usually present in an unlimited reservoir. The solution was prepared at $20.5\text{ }^\circ\text{C} \pm 0.5$ mixing 165 g of anhydrous Na_2SO_4 with 55 l of deionised water under cover with a paddle at the bottom of the container and rotating at low speed (120 rpm) to limit CO_2 entrainment into the solution. The pH of the initial solution is close to neutral.

Samples are exposed after a curing period of 28 days in sealed conditions in lime saturated water at $20.5\text{ }^\circ\text{C} \pm 0.5$. Samples of same chemistry (i.e.; same mix-design) were exposed in a common container: for each exposure setting, four containers were in use, one for the P-0.55, one for the P-0.38, one for the S-0.55 and one for the S-0.38 micro-concretes. The containers are filled up to the top and covered to limit contact with the air and thus avoid CO_2 dissolution and further carbonation.

Four tests were designed (Fig. III-2) to evaluate the influence of the exposure setting on the interaction between sulfates and the cementitious material. The exposure settings were ponding, pH-control, semi-immersion and wet/dry cycles. A sample holder maintains the prisms vertically in the baths.

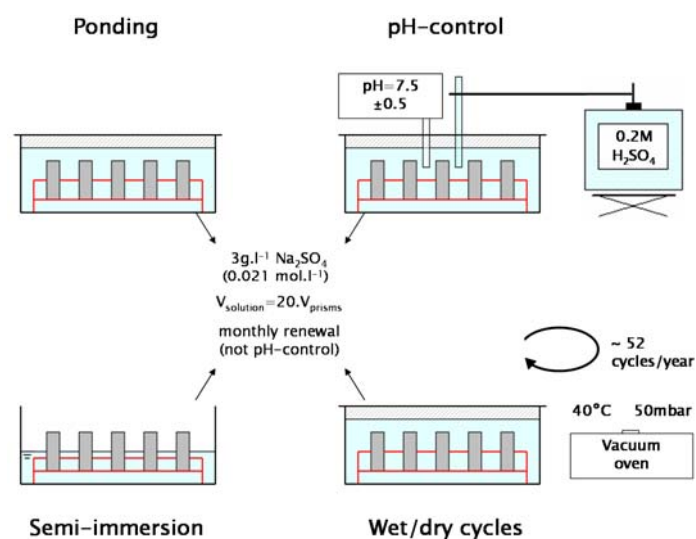


Fig. III-2. Scheme of the laboratory setting.

Ponding

The simplest test setting consists in a continuous full immersion of the samples in the exposure solution. This is the test adopted in most sulfate resistance studies. Its representativity of field cases is nevertheless questionable. The aim of conducting such a test is first to have a basis comparable to most literature data and second to evaluate it compared to other exposure settings and field data.

pH-control

One of the questions raised about the ponding exposure is the unrepresentative pH value compared to field conditions. The pH in ponding tests is found to rise rapidly to 11-13 despite the regular renewal of the solution while the pH in the ground, fresh or sea waters in the field is usually in the range of 6-8. Therefore, a pH-control test was designed. The test applies a titration system initially destined for aquarium use from AQUA MEDIC to maintain the pH at 7.5 ± 0.5 by the use of an H_2SO_4 titration solution. To simplify the setting, two baths containing samples of similar chemistry (PC on the one hand, slag blends on the other hand) were connected to the same central intermediate bath where the titration took place. A pump working at 200 l.h^{-1} situated in the intermediate bath permits a rapid mixing of the solution in the two exposure baths without neither concentration gradient, nor flow effect. The concentration of the titration solution has been adjusted to disturb as little as possible the nature of the exposure solutions in terms of Na_2SO_4 concentration. The best compromise between low volume addition (highly concentrated titration solution) and constant sulfate concentration (low concentrated titration solution) has been found using a 0.2 M H_2SO_4 solution. A first test was done using a 0.01 M H_2SO_4 titration solution. But this was found to be of low titration efficiency. Only results for the pH-control test involving the 0.2 M H_2SO_4 solution are presented, which are limited to shorter exposure times compared to the other tests because of the delayed test start.

No renewal of the solution was carried out for the pH-control tests.

Semi-immersion

Cases of structures damaged by external sulfate sources may involve tidal zones or foundations. The ponding test does not take into account the effects of relative humidity changes that can strongly influence salt crystallisation processes [16]. The semi-immersion test aims to investigate such effects on the cementitious material damage. No steps were taken either to limit evaporation, or to avoid carbonation.

Wet/dry cycles

To examine normal weathering effects, controlled wet/dry cycles were applied on samples, alternating 4 days of full immersion in ponding conditions with 3 days of drying at 40 °C in a vacuum oven to prevent from carbonation; a total of 52 cycles.year⁻¹. Relative humidity (RH) measurements revealed that the samples RH oscillated between 90 % and 20 % respectively after the wetting and drying periods.

References

Reference samples were stored at 20.5 °C ±0.5 in tap water under sealed conditions (RH 100 %). The tap water revealed a sulfate concentration of 0.02 g.l⁻¹ corresponding to an equivalent Na₂SO₄ concentration of 0.03 g.l⁻¹, which is 100 times less than the Na₂SO₄ solution implemented in the tests. The solution of the reference test is not renewed and quickly reaches portlandite saturation and is therefore commonly called “lime water” as designated in the study.

III.1.2. FIELD

A large panel of field samples from real structures and trial sites was catalogued for the study. A selection of the most interesting samples was made according to the availability and completeness of data on their mix-design and on their exposure conditions. Some supplied samples were found to suffer from other degradation mechanisms (e.g.; alkali silica reaction (ASR)) overlapping with the sulfate induced damage and were not examined in detail. The field concretes were selected to be the most comparable to the laboratory samples.

III.1.2.A. CONCRETES

A Portland cement with 8.5 wt.-% C₃A was used to make concretes with 80 wt.-% of slag (Table III-5). The analyses of the anhydrous materials (Table III-6 and Table III-7) were provided by Irassar [21].

The samples were exposed as concrete blocks of 7×10×40 cm³.

Table III-5. Binder mix-design of the Argentinean concretes.

Mix label	Equivalent binder type	28 days compressive strength (MPa)	w/b	Mineral addition	
				Substitution level (wt.-%)	Type
P-0.53	CEM I	32.5	0.53	0	-
S-0.53	CEM III/B	32.5	0.53	80	Slag

Table III-6. Phase composition of the cement used in the Argentinean concretes.

Phases	Formula	Content (wt.-%)
Alite	C ₃ S	40.0
Belite	C ₂ S	31.0
Aluminate	C ₃ A	8.5
Ferrite	C ₄ AF	8.2

Table III-7. Oxide composition of the cement and slag used in the Argentinean concretes.

Oxides	Content (wt.-%)	
	Cement	Slag
SiO ₂	21.35	33.20
Al ₂ O ₃	4.94	13.30
Fe ₂ O ₃	2.71	4.10
CaO	60.16	39.30
SO ₃	1.96	-
MgO	0.46	6.20
Na ₂ O	1.00	0.28
K ₂ O	0.48	0.80
LOI	5.57	-

III.1.2.B. EXPOSURE CONDITIONS

The samples were partially buried (Fig. III-3) for 19 years in a muddy soil enriched in sulfate [21] (Table III-8). The upper layer of the samples was exposed to weathering with a wet/dry cycles frequency of 15-20 cycles.year⁻¹ and with temperatures varying from 0 to 34 °C. The sulfate amount in the soil was 0.97 wt.-%, which would correspond to an equivalent Na₂SO₄ concentration of 14.34 g.l⁻¹ assuming that the entire sulfate in the soil is available as ionic species in the ground water. The pH of the soil is of 7.8 ±0.5.

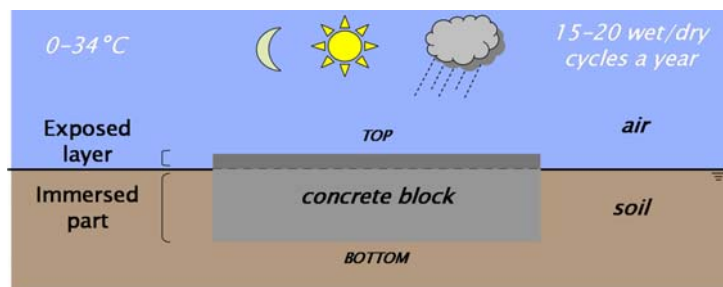


Fig. III-3. Exposure setting of the Argentinean concretes.

Table III-8. Chemical characteristics of the Argentinean soil.

Content of the main species (wt.-%)				pH
SO ₄ ²⁻	Na ⁺	Mg ²⁺	Cl ⁻	
0.97	0.32	0.23	0.05	7.8
±0.04	±.003	±0.02	±0.02	±0.5

III.2. ANALYSIS METHODS FOR A “MACRO-TO -MICRO” APPROACH

III.2.1. IONIC TRANSPORT CHARACTERIZATION METHODS

Representative samples of 100 ml of the exposure solutions were collected for analyses at each renewal.

III.2.1.A. TITRIMETRIC ANALYSES

The concentrations of SO_4^{2-} and Ca^{2+} ions were titrated with an accuracy of $\pm 5 \text{ g.l}^{-1}$. SO_4^{2-} was measured in acid solution (methylorange as indicator) from its precipitation in presence of BaCl_2 in BaSO_4 . Ca^{2+} was measured in basic solution (calconcarbon acid as indicator) from its reaction with disodium salt, which after full reaction with calcium reacts with the calconcarbon acid that becomes blue.

III.2.1.B. ATOMIC ABSORPTION SPECTROSCOPY (AAS)

The concentration of Na^+ ions was determined by atomic absorption spectroscopy with a Perkin Ellmer 4100 device, with an accuracy of $\pm 5 \text{ g.l}^{-1}$. The AAS method is based upon flame atomization. The energy from the heat of the flame brings the atoms to an excited state which relax to a ground state giving up their energy as photons of visible or ultraviolet radiation. The absorption spectrum thus collected is specific for a given element. The wavelength of sodium is $\lambda_{\text{Na}} = 589 \text{ nm}$. 1 ml of the exposure solution is mixed to 10 ml of buffer solution to make sure that all the sodium will be excited. The solution is spread in the flame and a chromator measures the change of the flame intensity.

III.2.1.C. PH-METRY

The pH of the exposure solutions was controlled with glass KCl electrodes with an accuracy of ± 0.5 . From the pH, the OH^- content in the exposure solution could be assessed.

The titration system employed for the pH-control test is monitored by an acquisition software (AT-Control from AQUA MEDIC) to allow a continuous control of the pH of the exposure solution. Plastic electrodes from AQUA MEDIC with an electronic connexion and measure the pH with an accuracy of ± 0.5 .

III.2.2. PHYSICAL CHANGES CHARACTERIZATION METHODS

III.2.2.A. EXPANSION

The expansion of the laboratory prisms was regularly measured on a LVDT device in the horizontal position to avoid the effect of sample weight compared to the traditional vertical setting from ASTM C 1012. For a given mix, three prisms were measured. Steel plug gages were directly cast in the prisms reserved for length measurement. Invar references were used.

III.2.2.B. MASS

The mass of the laboratory samples was regularly controlled on three prisms for each mix. A laboratory balance with a precision of ± 0.01 g was used. The samples were surface dried up before weighting to avoid measurements artefacts due to surface water.

III.2.2.C. COMPRESSIVE STRENGTH

The compression measurements were carried out to follow the strength evolution of the laboratory micro-concretes, according to the European standard EN 196-1. The test carried on a Walter + Bai AG D 501/200 press consists of applying a load with a linear increase ($0.5 \text{ MPa}\cdot\text{s}^{-1}$) on a $4\times 4 \text{ cm}^2$ contact surface with the rhomb and in measuring the load every 100 ms up to the breaking load.

Compressive strengths were measured on pieces remaining after cutting the samples for SEM and XRD measurements, providing they were large enough for the test. The testing was not initially planned and was done only as an indication of the change in mechanical properties. The accuracy of the measurements was not checked since only one piece of sample was tested at each sampling time for each sample type. Considering the low Na_2SO_4 concentration applied strengths of the samples after 28 days of exposure should not be much affected by the sulfate. Therefore the differences in compressive strengths measured for a same mix after 28 days of exposure in the different exposure settings were taken as a representative standard deviation. This value is in the range of 5 MPa, which appears to be consistent with the standard deviation of experimental data carried out by Kocaba on mortars made from the same binders [51]. But standard deviation is likely to increase with exposure time due to the statistical uncertainty of damage process. Results from this test should be considered with caution and remain indicative.

No strength measurement was done on the field concretes.

III.2.2.D. DYNAMIC ELASTIC MODULUS

The elastic modulus or Young modulus E describes the stress-strain relationship for a given material under load, and is generally assessed by a traction test. The dynamic elastic modulus E_{dyn} can be reliably assessed by non-destructive methods. The empiric relationship between static and dynamic elastic moduli follows a law of type $E = E_{dyn}(1 - ae^{-bE_{dyn}})$, $a, b \in [0, 1]$ dependant on material and environment parameters.

Impulse excitation method

The principle of the impulse excitation method is to make the sample excitation frequency vary up to reaching resonance. A grindosonic device from Lemmers was used to assess the fundamental frequency by means of a frequencemeter with a precision of 0.5 %. A transducer-emitter characterized by a natural resonant frequency of at least two times the supposed one of the sample is put directly in contact with the sample. The period $2T$ is recorded. From $2T$ the fundamental frequency can be calculated (Eq. III-1). Three measure modes are possible: leongitudinal L , flexural F and in torsion T . The fundamental longitudinal and flexural frequencies allow the dynamic elastic modulus to be calculated in two ways (Eq. III-2 and Eq. III-3), while the torsion mode permits the calculation of the dynamic shear modulus G_{dyn} (Eq. III-4).

This method was applied to the laboratory micro-concretes, measuring three prisms each time, according to the procedure for normalised $4 \times 4 \times 16 \text{ cm}^3$ prisms from ASTM C 215.

$$f = \frac{2.10^6}{2.T} \quad \text{Eq. III-1}$$

$$E_{dyn}^L = 4.10^{-6} L^2 \cdot f_L^2 \cdot \rho \cdot k_1 \quad \text{Eq. III-2}$$

k_1 corrective factor dependant on geometry and Poisson coefficient

$k_1 = 1$ for prismatic samples with square basis and $L = 4d$ (standard prismatic samples)

$$E_{dyn}^F = 4.10^{-6} \frac{\Pi^2}{4.73^4} \cdot \frac{L^4}{i^2} \cdot f_F^2 \cdot \rho \cdot k_2 \quad \text{Eq. III-3}$$

$\Rightarrow E_{dyn}^F = 15.136.10^{-6} L^2 \cdot f_F^2 \cdot \rho \cdot k_2$ for standard prismatic samples

k_2 corrective factor dependant on geometry and Poisson coefficient

$k_2 \in [1.435, 1.450]$ for prismatic samples with square basis and $\nu \in [0.25, 0.30]$ (concrete)

$$G_{dyn}^T = 4.10^{-6} L^2 \cdot f_T^2 \cdot \rho \cdot k_3 \quad \text{Eq. III-4}$$

k_3 corrective factor dependant on geometry

$k_3 = 1.183$ for standard prismatic samples

Impulse velocity method

The principle of the impulse velocity method is based on the fact that waves propagate with a higher velocity in a denser material. If the material contains cracks, waves will propagate slower in the spaces opened by the cracks. The method can thus potentially measure the damage state of a piece of concrete that has been subjected to destructive conditions such as sulfate attack. This method does not require a specific geometry of the samples, but the length should not be less than 10 cm to avoid interference due to reflection waves. The ultra sound impulse velocity measured can be related to the dynamic elastic modulus knowing the apparent density of the material (Eq. III-5) [52].

The impulse velocity method was used to study the field concrete cores, making three measurements on each core. Measurements were carried out in the direction of the core length, according to EN 13296, using transducers for longitudinal waves of 50 kHz.

$$E_{dyn} = \frac{l_s^2}{(t_s - t_k)^2} \cdot \rho_s \cdot k \quad \text{Eq. III-5}$$

E_{dyn} dynamic elastic modulus ($N \cdot mm^{-2}$ # MPa)

l_s sample length (mm)

t_s ultra sound impulse delay time in the sample (μs)

t_k correction factor: intrinsic delay time of the transducers (μs)

ρ_s sample apparent density ($kg \cdot m^{-3}$)

c_l correction factor considering the hindrance of lateral strain (= 0.9)

III.2.3. MICROSTRUCTURAL ANALYSIS METHODS

III.2.3.A. SEM AND CEMENT CHEMISTRY

Scanning electron microscopy (SEM) has proven to be a valuable tool in the study of cement chemistry and microstructure over the past 20 years [53].

SEM was used in the investigation methodology at different levels:

- elemental mapping at low magnification level ($\times 100$) for the study of the ions profiles in the microstructure (§ III.2.3.B) and at higher magnification level ($> \times 1500$) for local ions repartition analysis;
- energy dispersive spectroscopy (EDS) for local phase assemblage determination and local chemistry quantification (§ III.2.3.E);
- back-scattered electron (BSE) imaging for local study of damage and phase formation.

The elemental mapping consists of EDS analyses carried out at each pixel location. EDS analysis is based on the ability of X-ray (generated from the electron-mater interaction) to excite the surrounding atoms, which in turn emit a characteristic fluorescence radiation.

Qualitative elemental mappings were done with a spot size allowing at least 100 kcps to reach the detector and with an analysis time of $1.5 \text{ ms}\cdot\text{pixel}^{-1}$ running 30 cycles on $512 \times 384 \text{ pixel}^2$ areas (i.e.; 15 min for one qualitative mapping). A quantification method based on image analysis was developed for the ions profile (§ III.2.3.B).

The local EDS analyses have been conducted at relative high magnification ($> \times 1500$) with a spot size enabling at least 50 kcps to reach the detector and with a single quantitative analysis run of 2 s. Phase assemblage could be assessed plotting atomic ratios, providing a good statistic of the local quantitative EDS analyses (§ III.2.3.E).

BSE imaging is based on the fact that emission rate of back-scattered electrons from the primary electron beam is an increasing function of the atomic number Z_i of the irradiated atoms. The resulting micrographs are in grey levels. The grey level of a given phase is directly related to its back-scatter coefficient η (Eq. III-6). In consequence the heavier the atoms of a phase are the brighter the phase contrast appears in BSE imaging.

$$\eta = \sum_i \eta_i C_i \quad \text{Eq. III-6}$$

$$\eta_i = -0.0254 + 0.016Z_i - 1.86 \cdot 10^{-4} Z_i + 8.3 \cdot 10^{-7} Z_i^3 \quad \text{empirical relation}$$

C_i mass fraction of the phase i

The SEM used was a Quanta 200 from FEI (Philips) where electrons are thermionically emitted from a tungsten cathode, accelerated under high vacuum (10^{-4} - 10^{-5} mbar) and focused up to a spot size of 1 to 5 nm. The acquisition software is Esprit version 1.8.2.2089. The EDS detector is an Si(Li) Brucker 133 eV. An accelerating voltage E_0 of 15 kV has been found to be the best compromise between a representative spatial resolution (low voltage) and a representative chemical signal (excitation of the highest K_α peak: $E_0 \sim 2.E_{FeK\alpha}$).

SEM applications require flat polished surfaces for reliable analyses. The long preparation time of the polished sections (Appendix A) is the main disadvantage of the use of SEM in this study and limits the possibility to make repeatability measurements.

III.2.3.B. SEM MAPPINGS AND IMAGE ANALYSIS

Quantitative profiles of elements were obtained from SEM-mappings at low magnification ($\times 100$) through a calibration and rescaling technique. A code for image analysis has been developed with the support of Gallucci to extract quantitative profiles from the qualitative mappings. Considering the relative large area investigated ($2500 \times 1870 \mu\text{m}$) and their high resolution (512×384 pixels) compared to the phenomenon studied, the treatment of a single mapping is representative of the ion profile in the material and no further statistical measurements are necessary.

The qualitative elemental mappings measured are scaled according to the pixel of major intensity and cannot be compared to each others. The method of quantitative profiles extraction consists in two stages: rescaling and calibration (Fig. III-4). Prior to these stages, the acquired mappings A are transformed to grey scale mappings A^{grey} in order to further get rid from the influence of the RGB colour factor (for an element x a specific colour in RGB notation has been attributed). From the grey scale mapping A^{grey} of an element x a rescaled mapping A^{resc} is calculated by dividing each intensity value of a pixel p by the mean intensity value of pixels of the concerned element x from a selected bulk area B . The bulk area B is the same for each element of a given sample and is selected according to two criteria:

- homogeneous sulfur intensity in order to get rid from the influence of sulfate ingress;
- as large as possible and with as few aggregates as possible in order to be as representative as possible of cementitious matrix composition.

During the rescaling stage, a factor is applied for each element (e.g.; Ca and S) to make the resulting mappings visible on a 256 grey level image. This factor is arbitrary chosen and different for each element. For a given element mappings of different samples are comparable, but for a given sample mappings of different elements are not; this is the role of the calibration stage. Since the object of interest is the cementitious matrix in terms of ions ingresses, a criterion is defined to exclusively quantify the ions in the cementitious matrix. The laboratory and field samples selected have siliceous aggregates (e.g.; quartz sand). Calcium is the element present in higher quantities and distributed the most homogeneously in the cementitious matrix without taking part to the aggregates: it is the element whose mapping is the most representative of the cementitious matrix. Therefore, the criterion for calculation of ions profiles in the cementitious matrix is based on the rescaled Ca-mapping histogram. The initial Ca-mapping has been converted to an image in grey levels ranking from 0 (black) to 255 (white), corresponding respectively to pixels of lowest to highest Ca intensity (i.e.; content). Zones with absence of Ca possess pixels values close to 0 and can be isolated through a segmentation made from the histogram: the threshold grey scale value g_t corresponds to the first minimum of the histogram curve after the first peak closest to 0. To pixels verifying $g(p) < g_t$ the value $b(p) = 255$ is attributed, while to pixels verifying $g(p) \geq g_t$ the value $b(p) = 0$ is attributed. The resulting segmented binary image reveals in black the cementitious matrix constituted of pixels where Ca is present independently of the amount of Ca in each pixel (i.e.; influence due to leaching phenomena taken out). Considering an element x : for pixels verifying $b(p) = 0$ in the segmented Ca-mapping, their values in the corresponding rescaled x -mapping are maintained; while for pixels verifying $b(p) = 255$ in the segmented Ca-mapping, their values in the corresponding rescaled x -mapping are fixed to 0. The new matrix A^{CEM} is thus the matrix A^{resc} without the aggregates pixel values. Pixels values are added along each column (i.e.; along the penetration depth) and divided by the pixels amount for which $b(p) = 0$ in the considered column of the segmented Ca-mapping (i.e.; calibrated according to the cementitious matrix amount in each depth). The obtained profile is calibrated according to the bulk content of the concerned element x measured by EDS spots quantitative analyses: the mean value in of the profile bulk plateau is assumed to correspond to the amount of the concerned element x measured in the bulk by hundreds EDS spots quantitative analyses at high magnification ($\geq \times 1000$), then each value of the profile is calibrated by the cross-product. The resulting quantitative profiles are expressed in the value of EDS measurement, that can be at.-%, wt.-%, oxide-%.

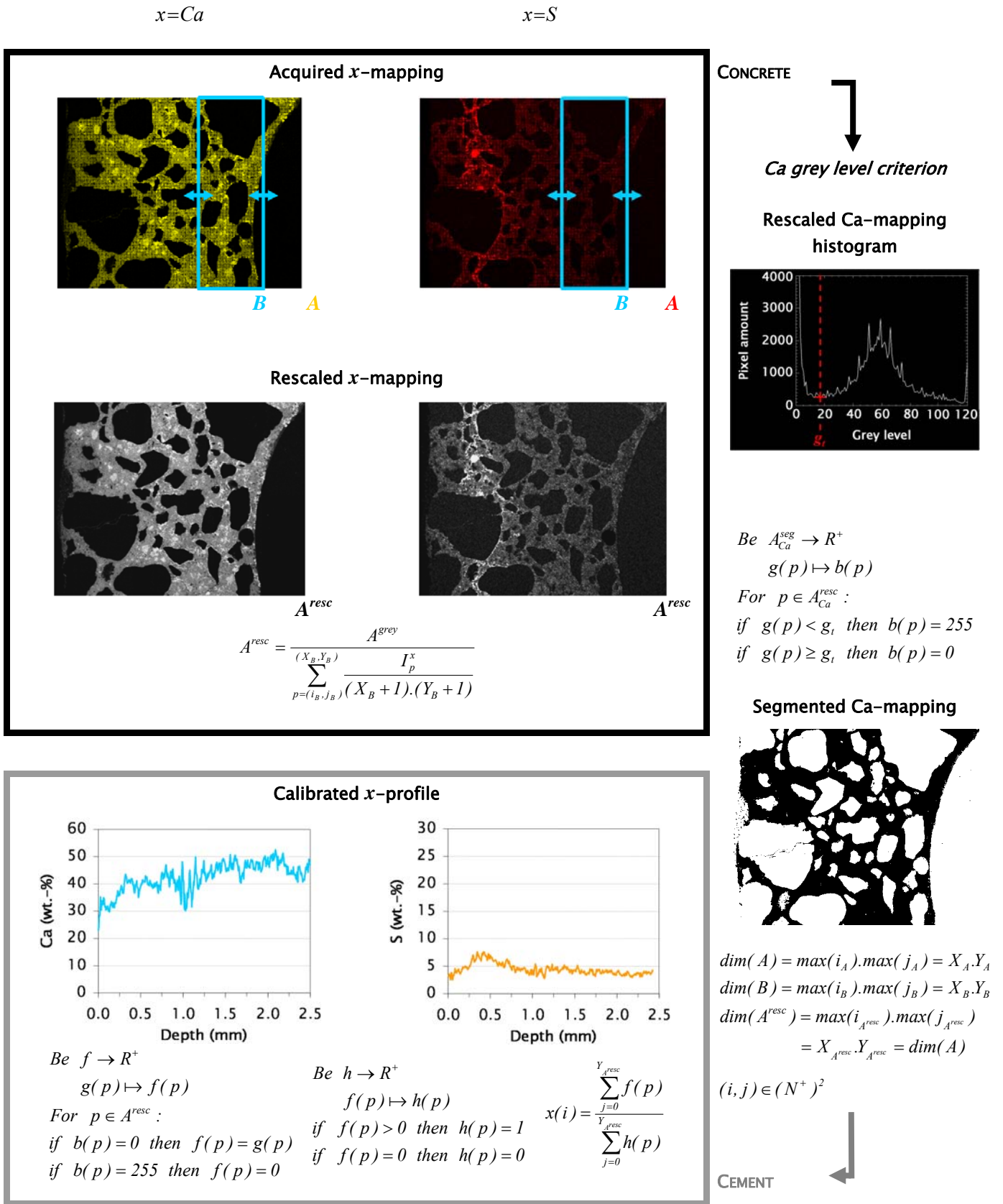


Fig. III-4. Method of ion profile quantification from SEM-mapping; case of P-0.55 after 119 days of exposure in ponding.

The resulting profiles are quasi-continuous and relate directly to the cementitious matrix, the aggregates being extracted from the calculation.

The full completion of the quantification of the mappings and the profile extraction only takes few minutes while an automated quantification of the mappings by the Esprit software would last for 5 to 10 h. and the step of aggregate exclusion should be still to do. Such quantitative mappings were only acquired for local ions repartition analyses.

III.2.3.C. MICRO-XRF MAPPINGS

With micro X-ray fluorescence (micro-XRF) analysis the chemical composition of an inorganic material can be determined in an easy way. As mentioned in the previous section, X-ray fluorescence analysis is based on the ability of X-ray to excite elements, which in turn emit a characteristic fluorescence radiation that can be registered by a semi-conductor detector. The equipment used is an Eagle III micro-XRF from EDAX operated by the two software programmes Vison32 and Eagle Image. The incident X-rays are emitted from a rhodium anode and the X-ray fluorescence is registered on a Si(Li) detector. A low vacuum of 0.5-1 mbar is sufficient due to the high energy of the X-rays.

The equipment can work in elemental mapping mode, which consists in the analysis of multiple equidistant spots along a dot matrix. Areas of $70 \times 60 \text{ mm}^2$ can be measured in a single run of 24 h but twice the time is required for quantitative analysis. The mappings were conducted under an accelerating voltage of 40 kV and with a spot size of $150 \mu\text{m}$. The resulting profiles are quasi-continuous and quantitative.

Such measurements were carried out on some field samples, as comparative method to the quantification of the profiles from SEM mappings.

Advantage of micro-XRF over SEM is that the requirement for specimen preparation are much less arduous. Considering the low possible magnification, the surface does not need to be as flat as for SEM purpose: a macroscopic flat cut surface is enough for reliable measurements. Neither impregnation nor conductive surface is necessary. The main disadvantage of the method is its long acquisition time, especially for quantitative measurements. Additionally, the aggregates could not be extracted from the measurements.

III.2.3.D. XRD

X-ray diffraction (XRD) analysis is based on the ability of crystalline phases to diffract rays of wavelength λ in the range of their d -spacing (interplanar space). Diffraction occurs when the Bragg's law (Eq. III-7) is satisfied. For a given wavelength, a specific crystalline phase possesses a specific diffraction pattern (counts versus 2θ). The amorphous C-S-H cannot be detected.

Laboratory and field samples were reduced to powder mm by mm from the contact surface using an electrical hand abraser. The aggregates are harder than the cementitious matrix and their powder is less fine. Each powdered layer was separately sieved down to 100 μm to exclude the largest aggregate particles. Further grinding of the remaining powder down to the optimal 5-10 μm did not show any influence on the diffraction pattern compared to the 100 μm sieved powder. XRD patterns were collected using a PANalytical X'Pert Pro MPD diffractometer in a θ - θ Bragg Brentano configuration employing the $\text{CuK}\alpha$ radiation ($\lambda_{\text{CuK}\alpha} = 1.54 \text{ \AA}$) and operating at 40 kV and 50 mA. The samples were scanned with the X'Celerator detector at a step size of 0.02° with a scan speed of $0.05^\circ \cdot \text{s}^{-1}$ between 7 and 70° and the same step size of 0.02° with a scan speed of $0.01^\circ \cdot \text{s}^{-1}$ between 6 and 20.5° . No quantification could be run due to the too much overlap between the cementitious hydrates and the aggregates patterns.

$$n\lambda = 2d \cdot \sin(\theta)$$

Eq. III-7

n integer corresponding to the harmonic number;

λ wavelength of the X-ray radiation;

d d-spacing (space between atomic planes);

θ angle between the incident X-ray and the crystal plane.

III.2.3.E. SEM-EDS

Due to the fine intermixing of the hydrates phases in cementitious systems relatively to the $1 \mu\text{m}^3$ electron-matter interaction volume, information on several compounds is combined in the EDS spectra. The problem can be got around considering elemental ratios rather than absolute element contents. Plotting elemental ratios (e.g.; S/Ca versus Al/Ca) and knowing the stoichiometry of usual phases (e.g.; CH, gypsum, mono- or hemicarboaluminate, monosulfoaluminate, ettringite), phases and phase intermixes can be identified. In order to refine the phase assemblage as determined from XRD

measurements, such EDS analyses were conducted at specific depths in the outer and the inner C-S-H of chosen laboratory and field samples. At least 100 analyses were carried out in each phase in each region..

Another interest of such statistical analyses is the measurement of chemical change of a given phase. The present study looks closely at the chemical changes encountered by the outer and inner C-S-H phases, especially concerning their calcium leaching and their sulfate combination levels. Both phenomena are respectively assessed measuring the evolution of the Ca/Si and S/Si atomic ratios. Nevertheless, a pre-treatment of the acquired EDS analyses is required to isolate the C-S-H, which consists in a graphical selection of the C-S-H point cloud from the Al/Ca versus Si/Ca plot (Fig. III-5). Thus large crystals of monosulfoaluminate, mono- or hemicarboaluminate, ettringite or portlandite are excluded and only very fine intermixes of C-S-H are considered. Enrichment of the C-S-H in sulfate or depletion in calcium can be statistically followed. The standard deviation σ between measurements is taken as representative of the error in measuring the Ca/Si ratio since calcium and silicon are elements representative of the C-S-H chemistry. Sulfate is in turn very unequally combined in the C-S-H. A way to take into account this intrinsic heterogeneity of the material in the measurement error is to consider the standard error ε instead of the standard deviation for the S/Si atomic ratio (Eq. III-8). The outer and the inner C-S-H chemistry of some laboratory and field samples was thus followed.

$$\varepsilon = \frac{\sigma}{\sqrt{N}}$$

Eq. III-8

ε standard error

σ standard deviation

N number of measures

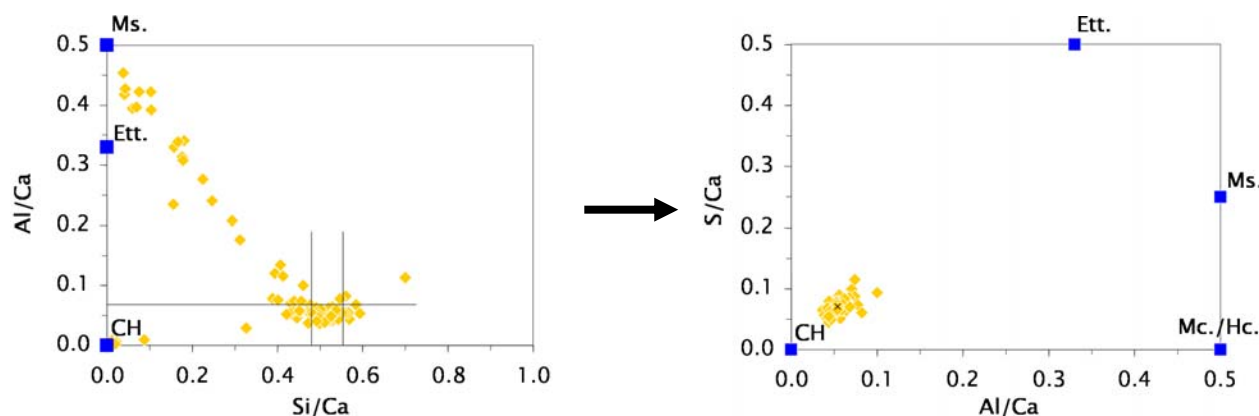


Fig. III-5. Method of C-S-H point cloud isolation from SEM-EDS analyses; case of the outer C-S-H at 2 mm depth of P-0.55 after 119 days of exposure in ponding; Ett.: ettringite, Mc./Hc.: Mono- or hemicarboaluminate, Ms.: Monosulfoaluminate.

III.3. MATURE CEMENT MICROSTRUCTURE

The thesis concerns field and matured laboratory samples. The microstructure of such mature binders is not commonly known.

Preliminary notions about the cement microstructure studied may be required and are developed below, comparing microstructures after 28 days and 1 year of hydration.

Civil engineers usually assess concretes and cementitious materials according to their performance at 28 days, which is considered to be a representative measure of 90% of the long term strength. Research in the chemistry of cementitious materials is therefore mainly focused on the first 28 days of cement hydration. Hence, microstructures of young cement pastes (< 28 days of hydration) are more known than microstructures of aged cement pastes.

Nevertheless, with the greater prevalence of durability questions, civil engineers are becoming more interested in later age evolution of the performances of cement. Consequently, there is an increased need for researchers to acquire knowledge on aged microstructures.

Hydration is not restricted to the early ages but also continues at later ages in even more complex conditions because of the effects of weathering.

Comparing the microstructures of PC micro-concretes ($w/c = 0.5$) stored in lime saturated water at $20.5\text{ }^{\circ}\text{C} \pm 0.5$ after 28 days (Fig. III-6) and after 1 year (Fig. III-7), it appears that hydrates develop, filling the capillary porosity. This is evident from the SEM-micrographs of the outer C-S-H which shows less empty spaces after 1 year. The extent of hydration can be assessed using the SEM-micrographs of alite grains: the hydration rim (inner C-S-H) around the alite grain after 28 days extends until the disappearance of the anhydrous grain after 1 year. Also, only isolated, and easy accessible belite, grains are hydrated after 28 days while all of belite, even those in clinker clusters are hydrated after 1 year (note the hydration owing to preferential planes). Ferrites start to show differences in grey levels on their edges after 1 year, which suggests the beginning of hydration. AFm may show longer and thinner layer structures after 1 year, but overall, no apparent change is seen from the morphological point of view of the AFm, and portlandite either.

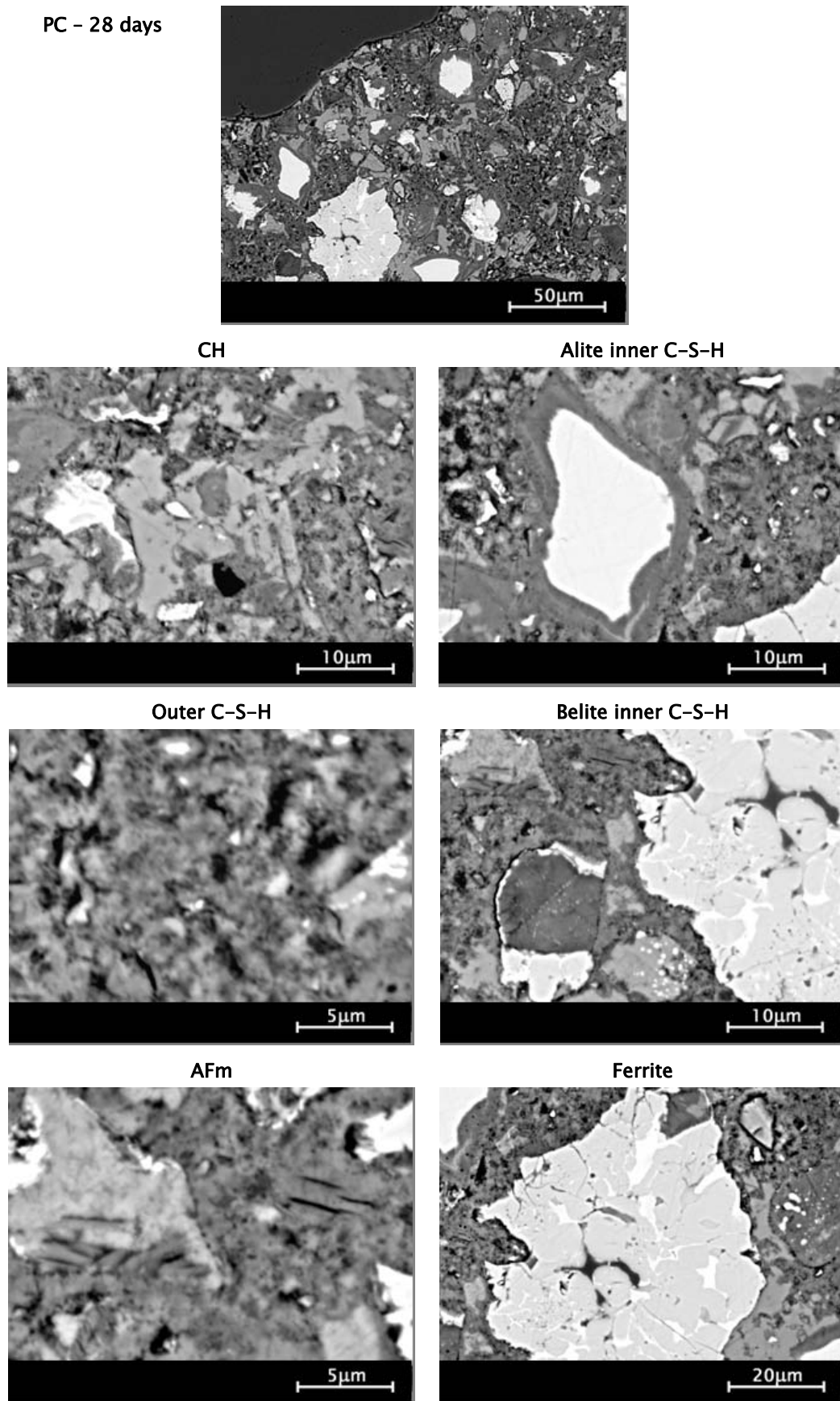


Fig. III-6. SEM-micrographs of a PC micro-concrete ($w/c = 0.55$) after 28 days of hydration.

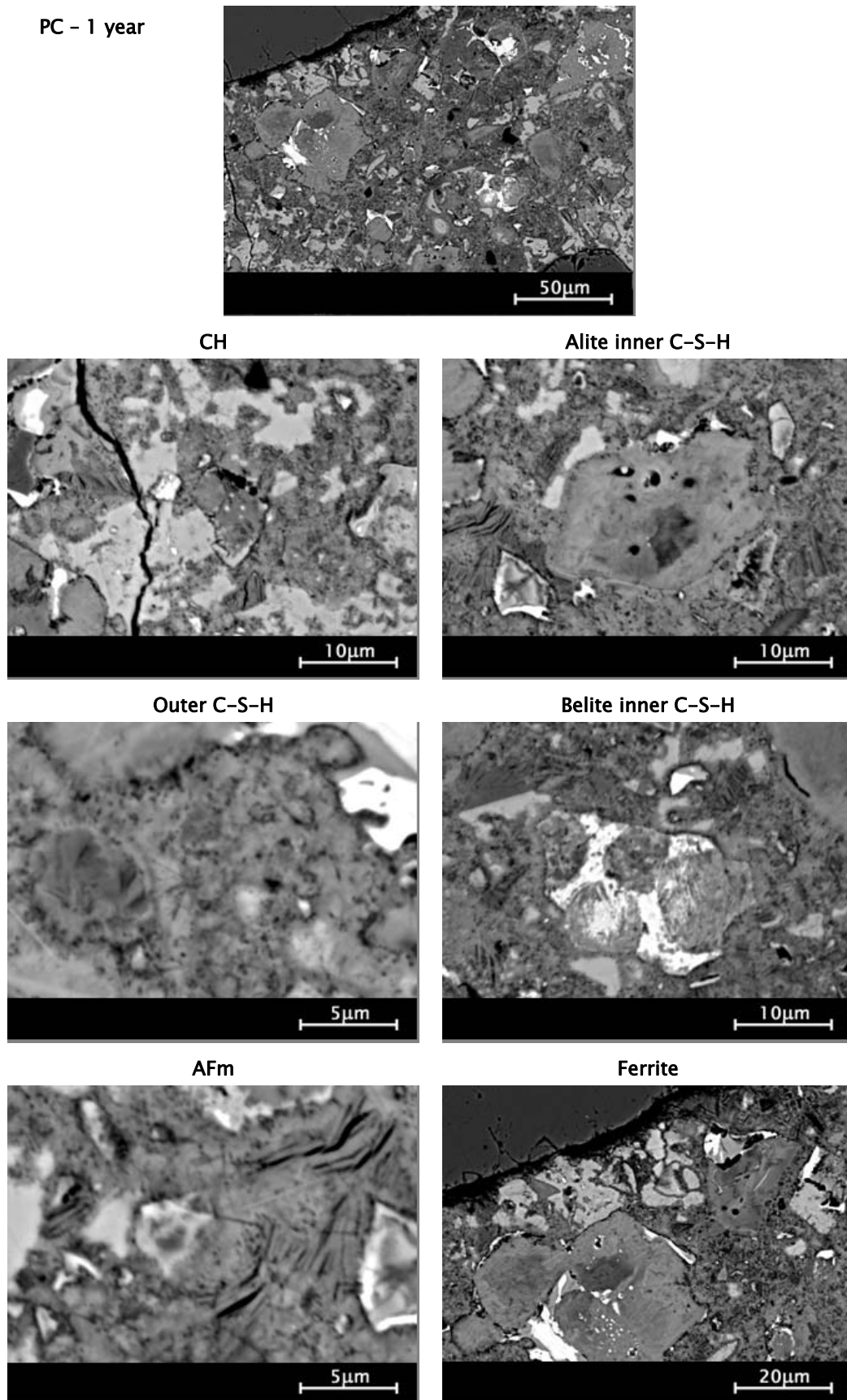


Fig. III-7. SEM-micrographs of a PC micro-concrete ($w/c = 0.55$) after 1 year of hydration.

Comparing the EDS Ca/Si-ratios of the different C-S-H phases after 28 days and 1 year (Table III-9), information on the chemical stability of the C-S-H can be extracted. The outer and inner C-S-H layer of alite decalcify with time and is characterised by a stabilisation their chemistry. The released (or leached) calcium may activate the hydration of secondary phases, belite and ferrite. The belite inner C-S-H seems to be chemically less stable marked by the higher dispersion of its chemistry, over time as a result of its hydration. Ageing is accompanied by a chemical equilibrium.

Table III-9. EDS Ca/Si-ratio of C-S-H phases after 28 days and 1 year of saturated hydration.

	Ca/Si (normalised at.-% ratio)	
	28 days	1 year
Outer C-S-H	1.90 ±0.10	1.69 ±0.08
Inner C-S-H (alite)	1.80 ±0.12	1.67 ±0.05
Inner C-S-H (belite)	1.86 ±0.04	1.88 ±0.07

EDS plots of S/Ca versus Al/Ca atomic ratios (Fig. III-8) allow the phases intermixes in the different hydrates to be studied. The outer C-S-H appears to be more stable in its chemistry after 1 year, the cloud of points exhibits less dispersion, than after 28 days of hydration. After 28 days, the AFm is finely intermixed to the outer C-S-H but becomes unstable with time and seems to turn into mono- or hemicarboaluminate. The inner C-S-H from alite and particularly from belite fuses with AFm with time. AFm in the outer C-S-H is destabilised by the slow reacting carbonate-bearing phases in mono- or hemicarboaluminate and the remaining sulfate probably dissolves in the pore solution. The late hydration of belite makes C₃A and C₄AF interstitial phases accessible. Hence, hydration of belite is accompanied by AFm formation intermixed to the belite inner C-S-H.

EDS plots of Fe/Ca versus Al/Ca atomic ratios of ferrite (Fig. III-9) points out its late hydration. After 28 days the anhydrous ferrite starts to dissolve, freeing iron and aluminium ions in solution. After 1 year ferrite hydrates in an Fe-enriched type of very stable hydrogarnet C₄(A,F)H₆ with up to 20 at.-% of aluminium substitution by iron. A part of the iron from the original ferrite probably enriches monosulfoaluminates with a substitution level up to 60 at.-%.

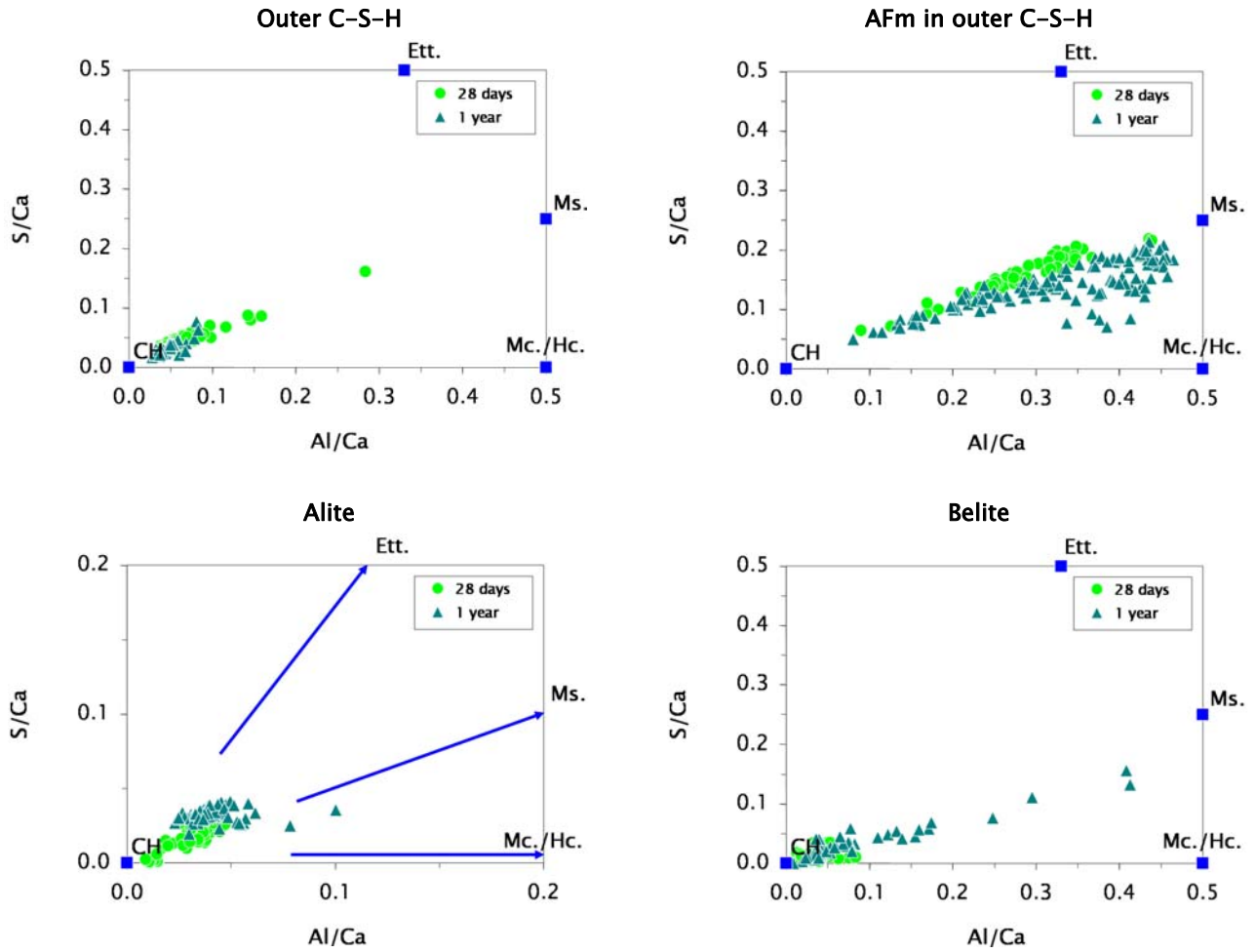


Fig. III-8. EDS plots of S/Ca versus Al/Ca atomic ratios from the outer C-S-H, the AFm in the outer C-S-H, the alite and belite with their inner C-S-H; Ett.: ettringite, Mc./Hc.: Mono- or hemihydrate, Ms.: Monosulfoaluminate.

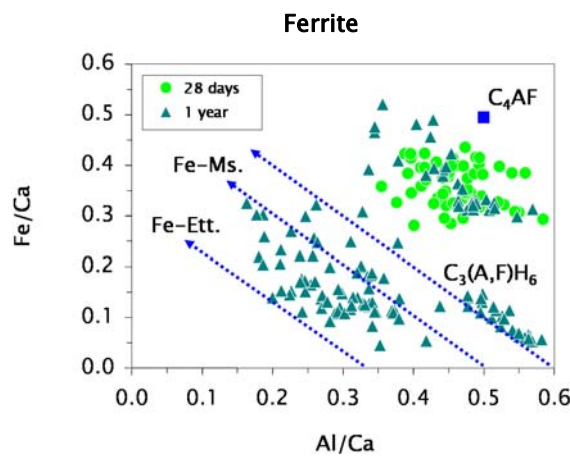


Fig. III-9. EDS plots of Fe/Ca versus Al/Ca atomic ratios from the ferrite and its hydration product; Fe-Ett.: Fe-enriched ettringite, Fe-Ms.: Fe-enriched monosulfoaluminate.



Chapter IV – Ponding

The purpose of this chapter is to describe the results of the laboratory exposure in sulfate solution comparable to most literature data (i.e.; full immersion/ponding) and to identify the mechanisms of degradation under such conditions.

Traditional macro characterization was carried out and extended with a detailed microstructural analysis along the sulfate profile.

As described in the previous chapter, four mixes were studied. Two made with pure Portland cement with water-to-cement ratio of 0.55 and 0.38 (P-0.55 and P-0.38) and two mixes with 70 wt.-% slag replacement (S-0.55 and S-0.38). Additionally, some results of the reference samples stored in lime saturated water are presented for comparison.

IV.1. MACROSCOPIC BEHAVIOUR

IV.1.1. IONIC TRANSPORT

IV.1.1.A. CALCIUM LEACHING

The pH of concrete is buffered by portlandite whose pK_a is 12.6. But in reality the pH of concrete is known to be above 12.6 due to the presence in the pore solution of alkalis (e.g.; Na^+ and K^+). The pH of the surrounding solution of the reference samples in lime water remained constant at 12.5 ± 0.5 .

The initial pH of the Na_2SO_4 solution used in ponding test was of 7.5 ± 0.5 . The relatively acid pH stimulates dissolution of portlandite providing OH^- ions to raise the pH and freeing Ca^{2+} ions in solution. This phenomenon is called leaching. The Na_2SO_4 solution was renewed every month. Na_2SO_4 exposure results in cyclic changes in pH (Fig. IV-1) accompanied by leaching. The pH rises 11-12 within about one week.

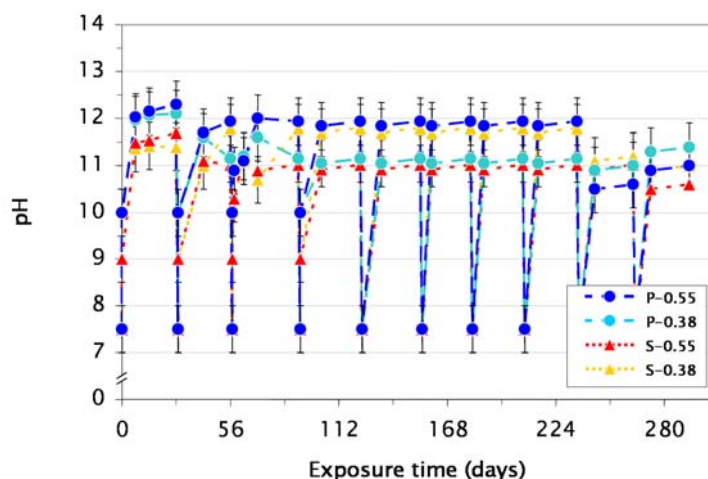


Fig. IV-1. pH evolution of the Na_2SO_4 exposure solutions.

Consequently, the leaching can be monitored by regular measurement of the Ca^{2+} content in the exposure solution before each renewal (Fig. IV-2). It has been observed that after 84 days of exposure in reference conditions, the non renewed solution reaches values of calcium concentration in the range of 0.4 g.l^{-1} which corresponds to a concentration in $\text{Ca}(\text{OH})_2$ of 0.7 g.l^{-1} . Such values are close to the values of portlandite solubility estimated to be of 1.1 g.l^{-1} at 18°C but which is known to decrease with temperature increase [2]. In Na_2SO_4 solutions, where the solution is monthly renewed, saturation is never reached and calcium is continuously leached out. The calcium leaching evolves for the sulfate exposed

samples at a quasi constant rate. There seems to be no effect of the w/c-ratio on the leaching rate of the pure PCs, while a lower w/b-ratio results in a lower leaching rate for the slag blends. The leaching rate of the PCs increases with exposure time, which could be a sign of increasing deterioration of the concretes that leads to greater surface exposed. The leaching rate of the slag blends is 1.7 to 2.6 times lower than that of the pure PCs. The hydraulic reaction of the slag does not produce calcium hydroxide. Additionally, the extra calcium needed for slag reaction comes from the C-S-H rather than from portlandite [51]. Therefore, if the leaching would only concern the portlandite phase, it would be expected to be 30 % that of the Portland blends. The fact that it is greater indicates that other hydrates contribute to the leaching (e.g.; C-S-H phases and slag hydration products).

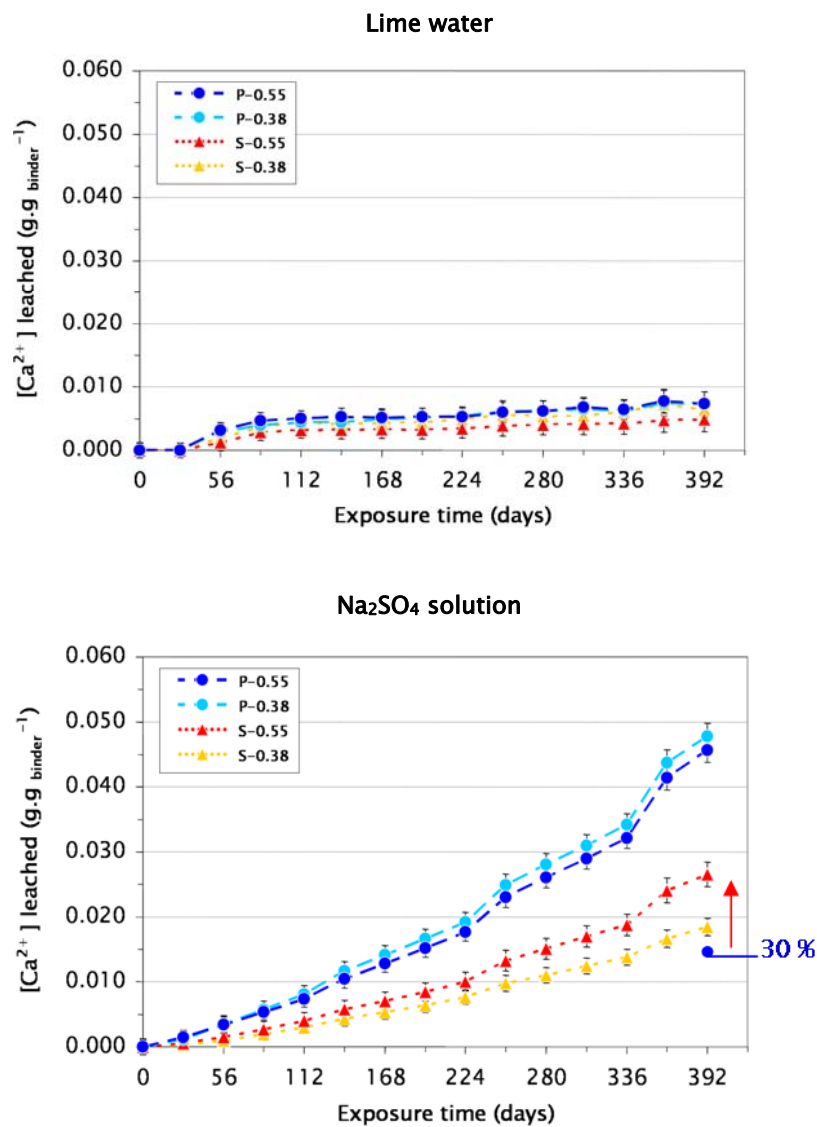


Fig. IV-2. Evolution of calcium leaching from the laboratory micro-concretes under ponding (bottom) versus reference (top) exposure.

IV.1.1.B. SULFATE INGRESS

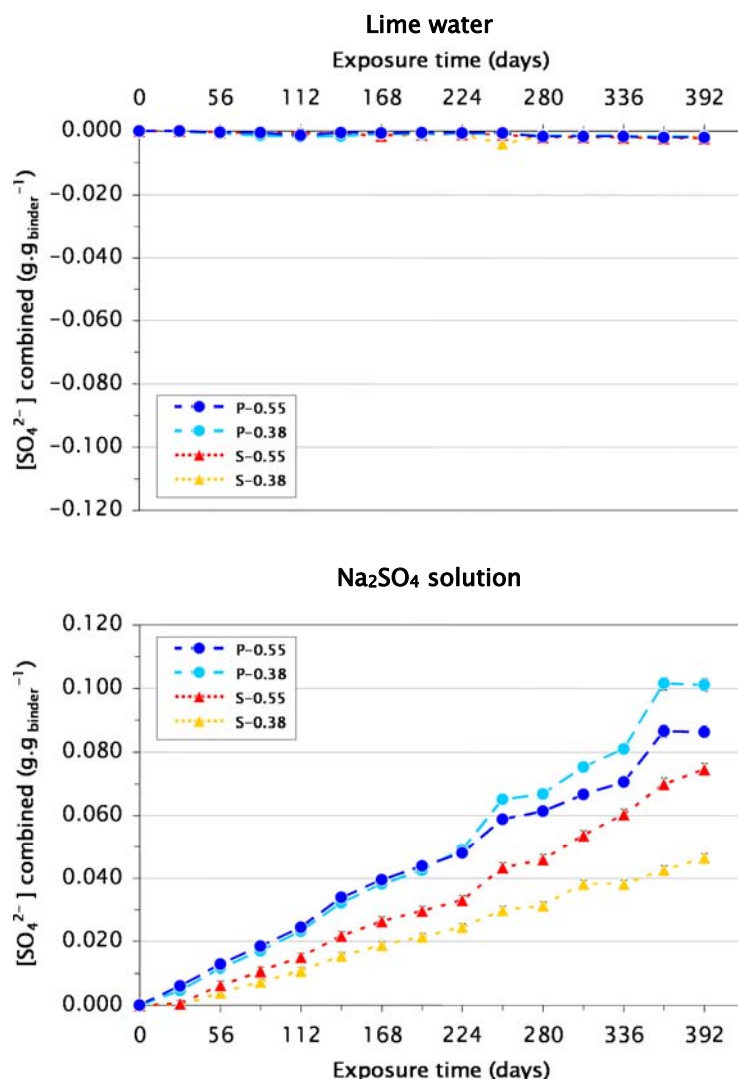


Fig. IV-3. Evolution of sulfate combination from exposure solution to the laboratory micro-concretes under ponding (bottom) versus reference exposure (top).

Sulfate ingress from the surrounding solution can be followed by measuring monthly the SO_4^{2-} concentration in the exposure solution (Fig. IV-3). This revealed a slight leaching of sulfate from the reference samples stored in the saturated lime water and a strong ingress of sulfate into the samples stored in Na_2SO_4 solution. The sulfate ingress appears roughly linear. Nevertheless, the form of the curve indicates that sulfate ingress in concrete is not a pure diffusive process and must imply interaction with the cementitious system.

As with calcium leaching, sulfate combination appears not to be very sensitive to the w/c-ratio of the Portland blends up to 224 days of exposure. This would indicate that sulfate ingress is not simply controlled by the usual parameters of permeability. However there seems to be some dependence on the w/b-ratio for the slag blends.

IV.1.2. PHYSICAL CHANGES

IV.1.2.A. MASS CHANGE

The reference micro-concretes stored in lime water show a slight mass increase (Fig. IV-4): all mixes gained mass in the order of 0.2-0.4 % within the first 70 days after the start of exposure. This can be attributed to an uptake of water maybe to compensate the chemical shrinkage from continued hydration.

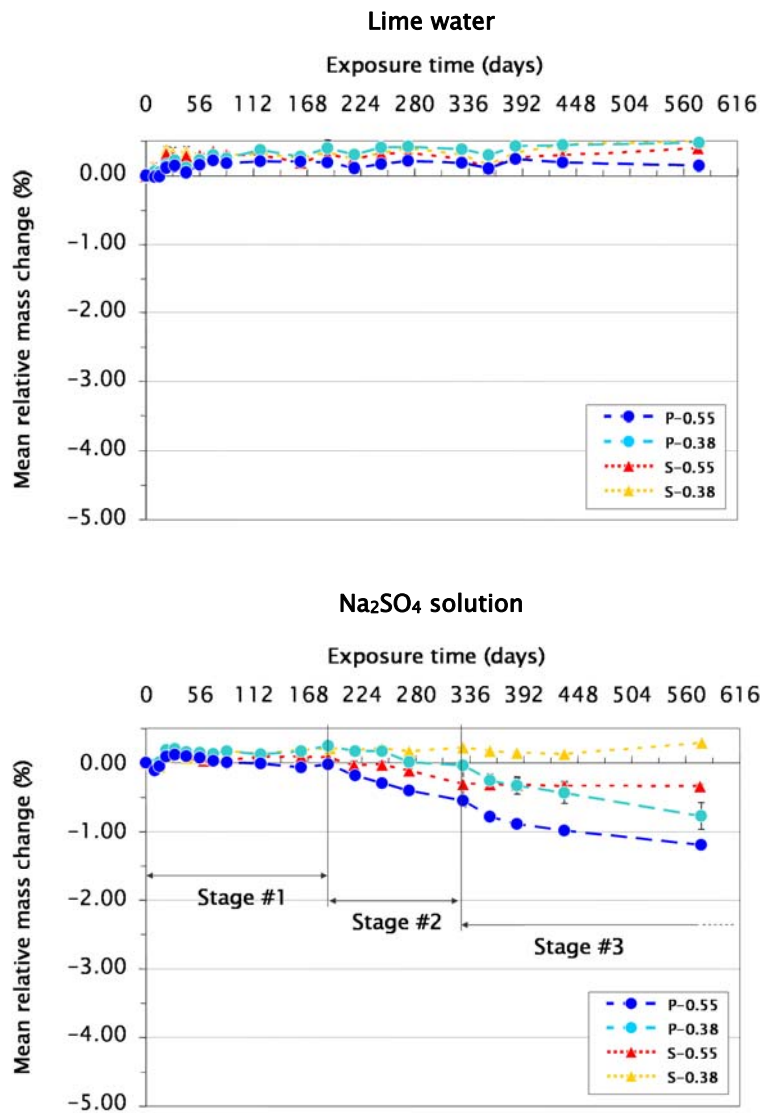


Fig. IV-4. Mass evolution of the laboratory micro-concretes under ponding versus reference exposure.

In Na_2SO_4 solution, all mixes except S-0.38 started losing mass after 189 days of exposure (Fig. IV-4). After this time the water uptake would be outweighed by sulfate induced mass loss. Particularly interesting is the mass loss trend of P-0.55, which shows a three-stage behaviour. The different stages could be described as follow:

- stage #1 – negligible mass loss;
- stage #2 – linear mass loss;
- stage #3 – reduced mass loss.

The other two mixes P-0.38 and S-0.55 show similar patterns of mass loss. Interestingly, stage #2 starts and ends at the same times of exposure for the three mixes. It is worth noting that the only two mixes showing a stage #3 with measurable mass loss are the two PCs P-0.55 and P-0.38, which tends to confirm that the most deteriorated sample after P-0.55 is P-0.38.

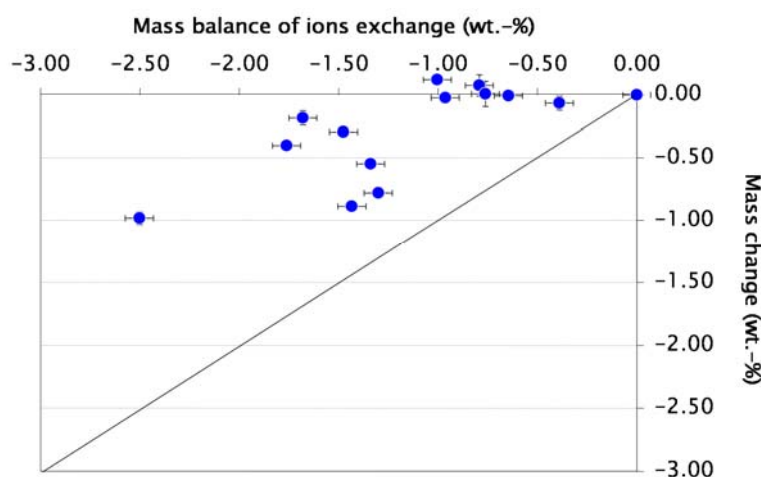


Fig. IV-5. Relationship between mass balance of ions exchange and mass changes of P-0.55 under ponding versus reference exposure.

The mass balance of the ions exchange was calculated based on the measurements of the remaining sulfate and sodium in the exposure solution and on the dissolved calcium and hydroxide (deduced from pH measurement) in the exposure solution. For P-0.55 in Na_2SO_4 solution, the mass loss recorded for P-0.55 seems to be somehow related to or at least in the range of the mass balance of ions exchange (Fig. IV-5). It appears that after a negative mass balance of the ions exchange exceeding 1.00 wt.-%, during which the ion mass loss may be compensated by water ingress, material loss is recordable. Such a link between the two measurements was not observed for the other samples, nor in the case of the other exposure settings.

IV.1.2.B. EXPANSION

A slight length change is observed within the first 84 days of exposure even for the reference samples in lime water, which if not in the range of deleterious expansion, remains positive (Fig. IV-6). This would be in agreement with the slight mass increase observed attributed to continued hydration.

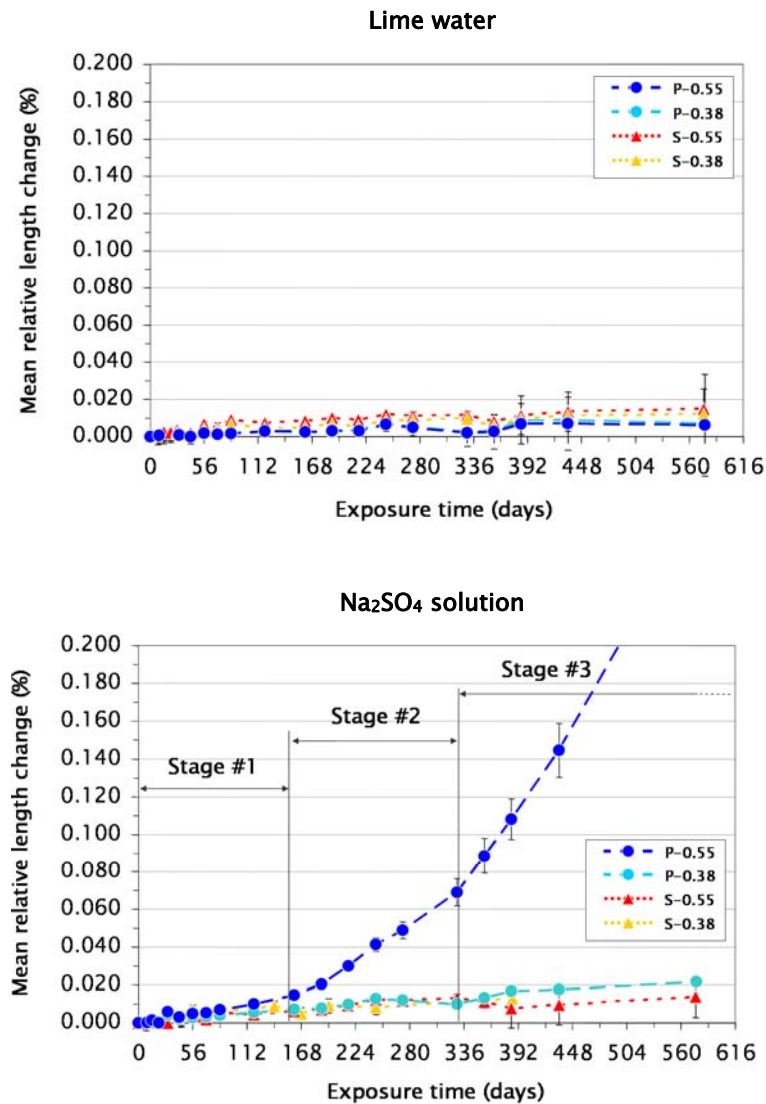


Fig. IV-6. Length evolution of the laboratory micro-concretes under ponding versus reference exposure.

Many laboratory tests fix the expansion criterion at 0.02 %, which is not passed in samples when sulfate is not present. From the test in Na_2SO_4 solution conducted over 560 days, only P-0.55 micro-concrete shows expansion in excess of 0.02 % (Fig. IV-6).

The expansion of P-0.55 follows a three-stage process, described as follow:

- stage #1 – *low expansion comparable to reference*;
- stage #2 – *stable expansion*;
- stage #3 – *unlimited expansion*.

Studies in the literature generally refer to a two-stage expansion process [3] corresponding to the low expansion described as the stage #1 here and to an expansive regime corresponding to the combination of the stages #2 and #3 here. A slight increase in length is nevertheless observable for all the other mixes in Na₂SO₄ solution, which could be a sign of preliminary expansion. This is largest for S-0.38, starting after 168 days and evolving linearly up to more than 560 days of exposure. It can be noted that the second highest expansion after P-0.55 is obtained from the other PC P-0.38, but this has to be taken with caution considering the dispersion of measurements.

IV.1.2.C. COMPRESSIVE STRENGTH

The asymptotical increasing strength of the reference samples stored in lime water (Fig. IV-7) is characteristic of normal microstructural development and space filling due to hydration. The decrease observed between 357 and 576 days of exposure could be attributed to measurement error or to later leaching. This decrease is especially significant for the PCs which contain more portlandite than the slag blends, which tends to confirm the second hypothesis of leaching effect.

In the case of exposure to Na₂SO₄ solution, hydration and deterioration due to sulfate ingress are in competition. The two PCs samples P-0.55 and P-0.38 reveal a decrease in compressive strength, while the two slag blended micro-concretes appeared to maintain their mechanical properties in compression compared to the reference samples in lime water (Fig. IV-7).

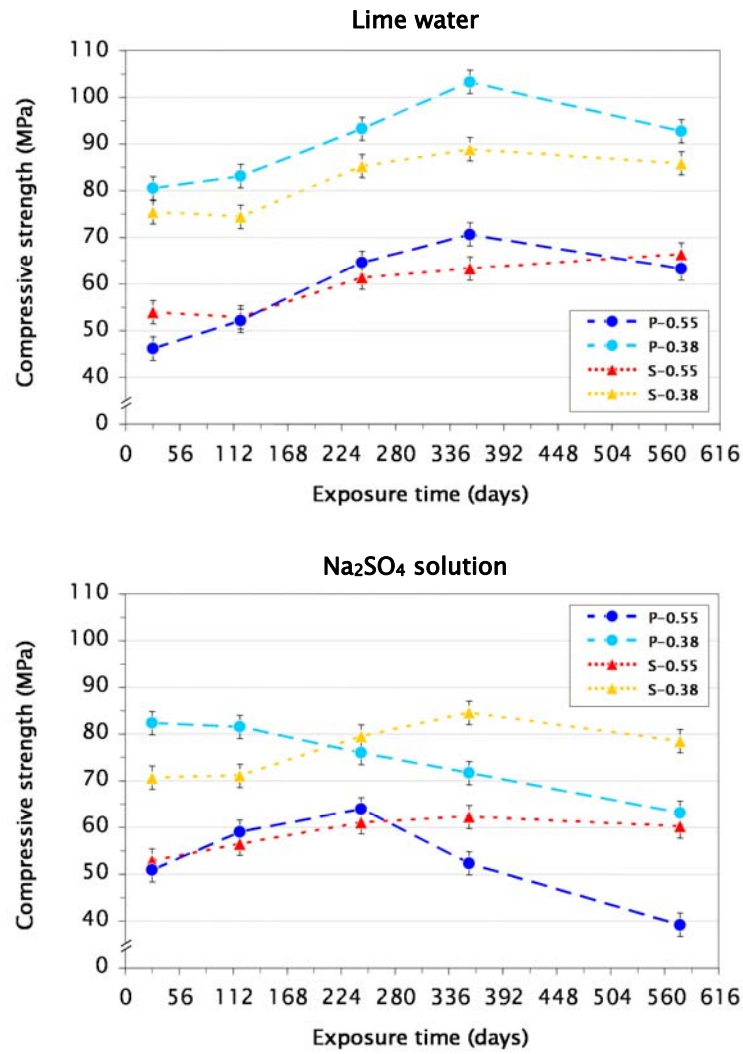


Fig. IV-7. Compressive strength evolution of the laboratory micro-concretes under ponding versus reference exposure.

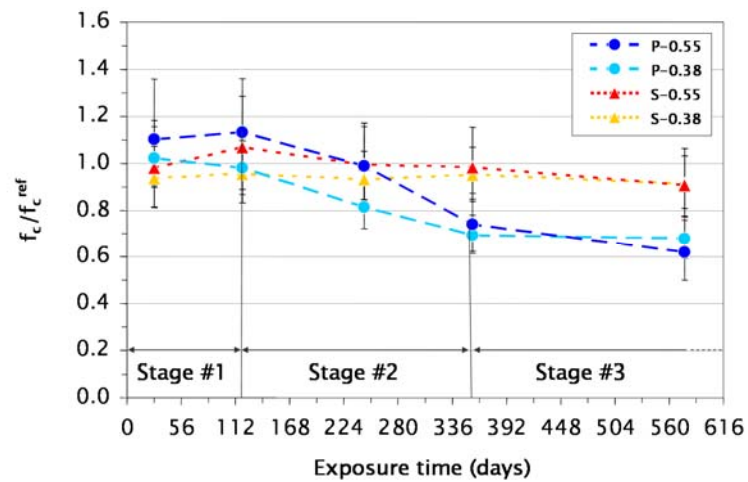


Fig. IV-8. Normalised compressive strength evolution of the laboratory micro-concretes under ponding.

In order to better isolate the effect of sulfate from the hydration influence, the compressive strengths measured on samples in ponding exposure were normalised by the compressive strengths measured on samples in lime water (Fig. IV-8). This clearly shows that the strengths of the PCs binders are diminished (30 % over 576 days) while the strength of the slag blends remains fairly constant (within 10 % over 576 days). P-0.55 and P-0.38 clearly show the three-stage behaviour identified earlier for mass loss and expansion. The different stages could be described as follow:

- stage #1 – *preserved sound strength*;
- stage #2 – *linear strength loss*;
- stage #3 – *limited strength loss*.

The compressive strength is representative of the state of the bulk of the material while mass loss is more representative of the state of the surface material. Furthermore, the mass loss encountered by the micro-concretes would lead to loss of the material over a few mm. The reduced section of the samples could not lead to the range of strength loss observed. P-0.38, S-0.55 and S-0.38 showed a comparable behaviour regarding their mass-loss. However, the good compressive strength of the slag blends indicates that they do not suffer much internal damage compared to the PCs and especially compared to P-0.38. Additionally, P-0.38 shows almost the same strength loss as P-0.55 even with much less expansion. This indicates that the stresses developed in P-0.38 do not cause expansion but still lead to an important loss of mechanical properties. This underlines the complexity of the sulfate attack phenomenon and indicates that monitoring of expansion as the sole criterion of degradation may be misleading.

IV.1.2.D. ELASTIC MODULUS

The flexural dynamic elastic modulus appears to be the most sensitive to microstructural changes due to hydration or sulfate ingress compared to longitudinal elastic modulus and torsion shear modulus (Fig. IV-9). This slight anisotropy of the elastic behaviour might be due to the geometric asymmetry of the prisms facilitating displacement ability in flexion. In all measurement modes the elastic behaviour of the references is characterised by a first period during which properties increase. This period is of same length (about 161 days) for all mixes. This increase in elastic properties can be attributed to continued hydration. This period is comparable to the one observed for compressive strength increase considering the lower frequency of measurement in the later case.

As for compressive strength, when samples are fully immersed in a $3 \text{ g.l}^{-1} \text{ Na}_2\text{SO}_4$ solution, deterioration due to sulfate ingress competes with changes due to hydration. The tendencies observed for deterioration of mechanical properties of the two PCs P-0.55 and P-0.38 are confirmed, while a loss of properties is additionally identified for S-0.55 and to a smaller extend for S-0.38 although these slag blends did not show any loss of compressive strength.

As for compressive strength, in order to separate the impact of sulfate the results for the samples ponded in Na_2SO_4 solution are plotted relative to the references (Fig. IV-10). This representation underlines the fact that in addition to the PC binders the two slag blends show some loss of their elastic properties. P-0.55 performs the worst, loosing 25 % of its properties, then P-0.38 (15 %), followed by S-0.55 (10 %) and finally S-0.38 (less than 5 %). Again a three-stage behaviour can be seen for the PCs blends:

- stage #1 – *preserved sound elastic properties*;
- stage #2 – *linear loss of elastic properties*;
- stage #3 – *accelerated loss of elastic properties*.

Finally, the normalised dynamic elastic and shear moduli have the advantage of better discriminating between samples compared to the other degradation criteria (e.g.; expansion, mass and strength loss).

The relationship between normalised dynamic elastic or shear moduli and expansion (Fig. IV-11) is linear for P-0.55 and tends to be linear for the other samples but with a different slope. This emphasises the reliability of dynamic elastic and shear moduli for sulfate attack damage evaluation

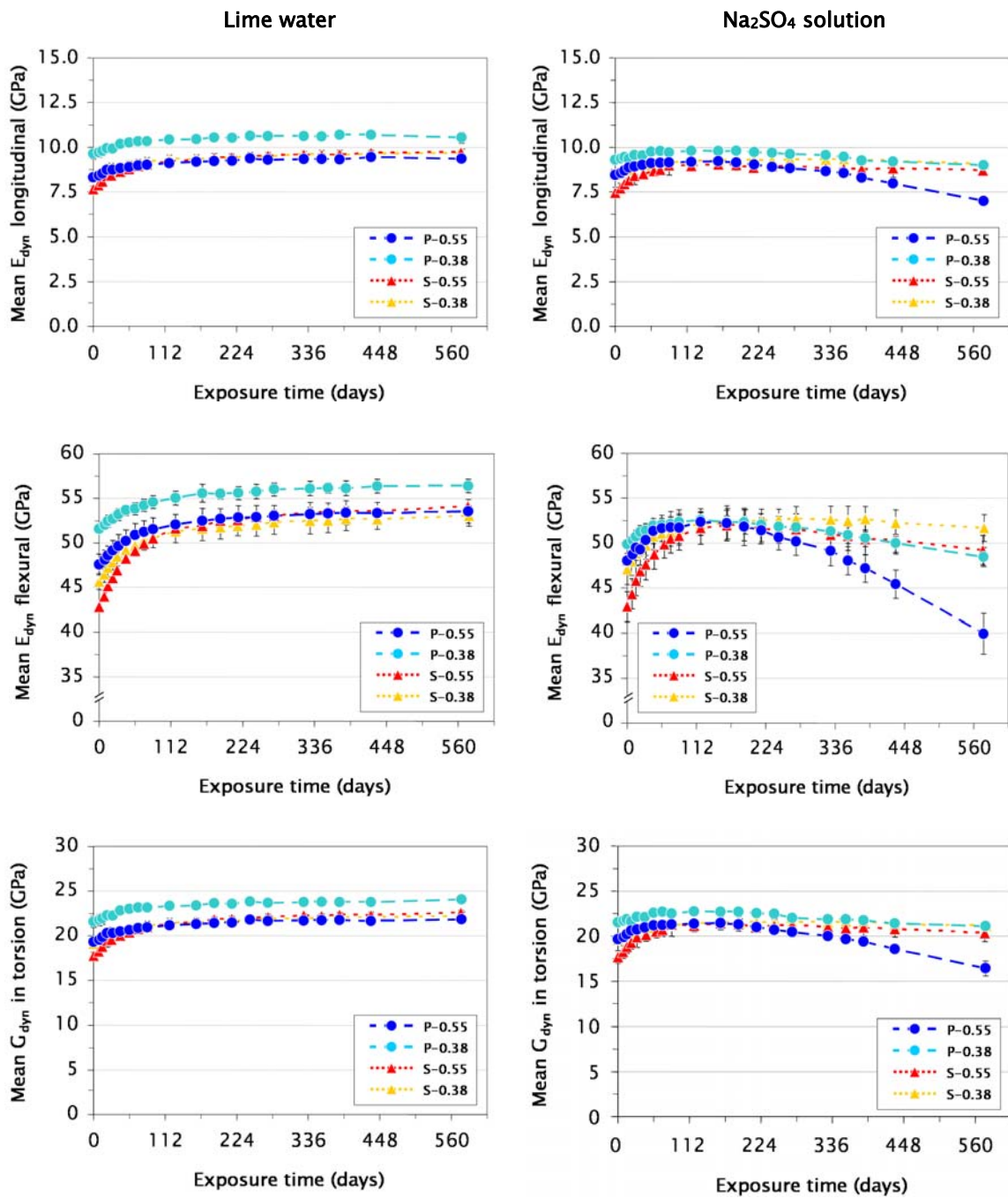


Fig. IV-9. Dynamic elastic and shear modulus evolution of the laboratory micro-concretes under ponding versus reference exposure.

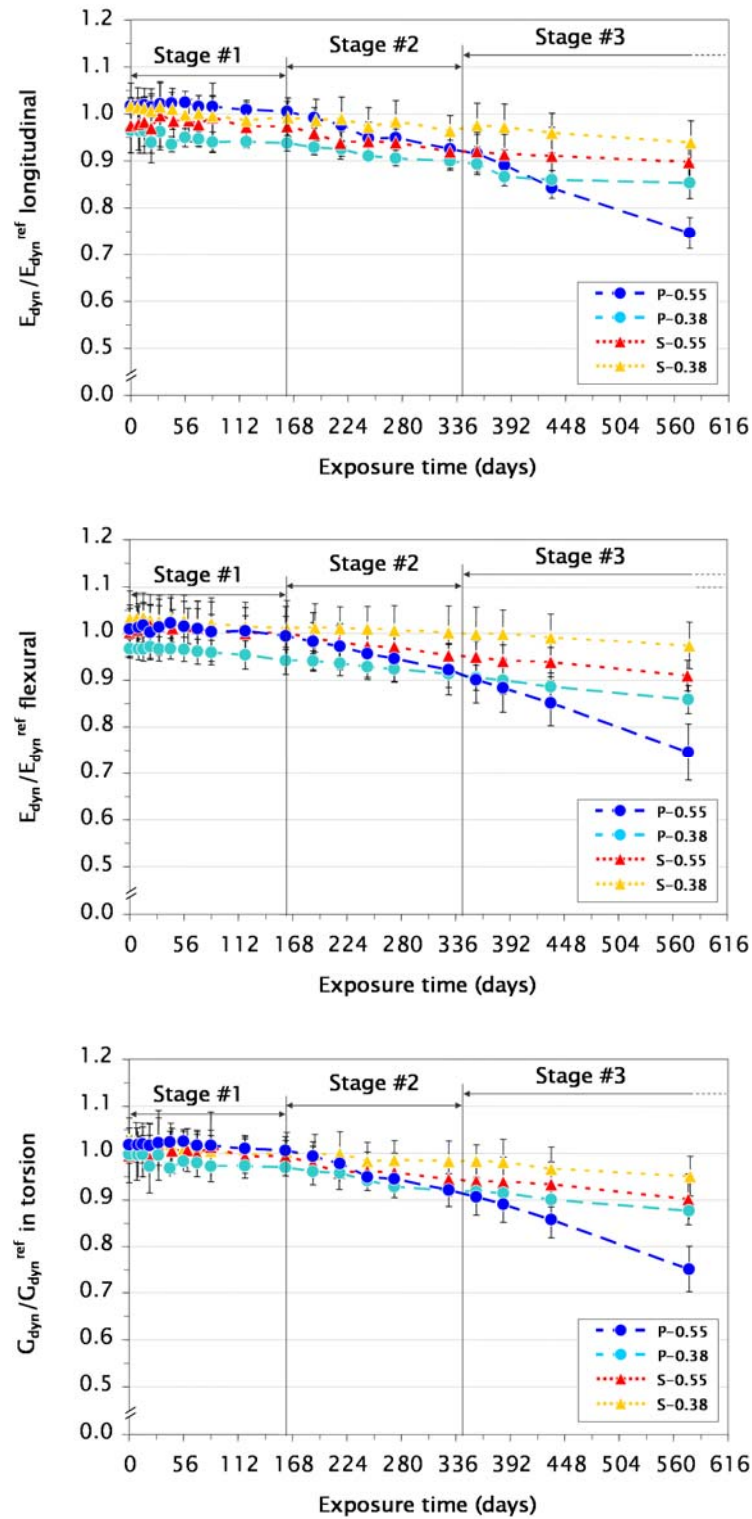


Fig. IV-10. Normalised dynamic elastic and shear modulus evolution of the laboratory micro-concretes under ponding exposure.

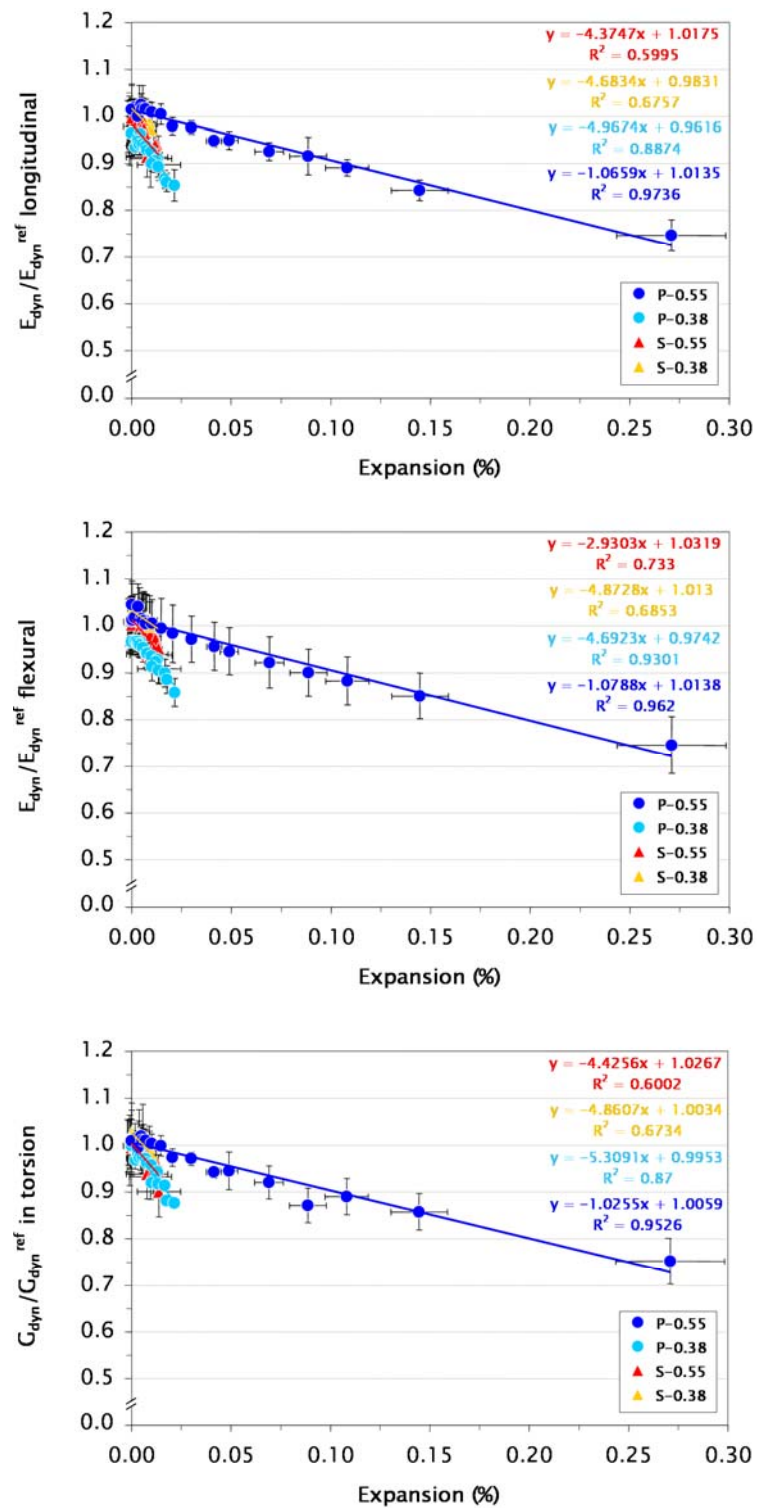


Fig. IV-11. Relationships between the normalised dynamic elastic or shear moduli and the expansion of the laboratory micro-concretes under ponding.

IV.1.3. EXTERNAL APPEARANCE

Carbonation of the micro-concretes was checked with phenolphthalein. No significant carbonation could be identified and photographs are reported in appendix (Appendix B).

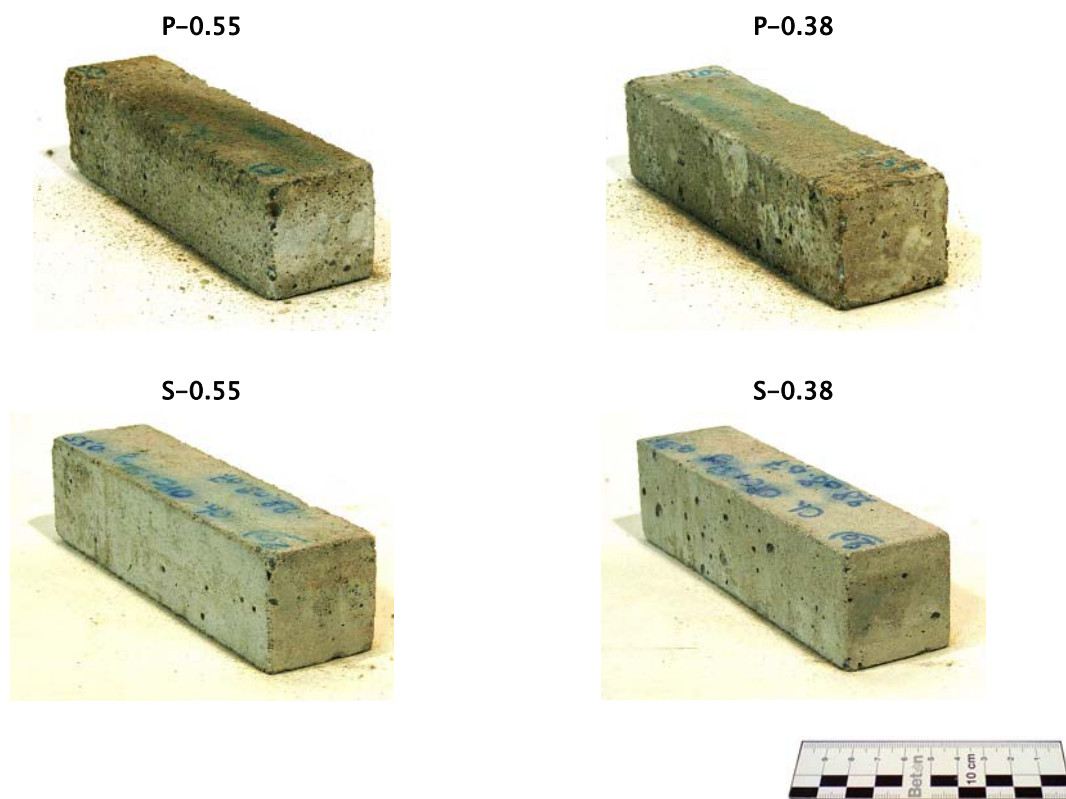


Fig. IV-12. Visual appearance of the laboratory micro-concretes after 575 days of exposure in ponding.

From visual examination of the micro-concretes after 576 days of exposure in ponding (Fig. IV-12) the two PCs P-0.55 and P-0.38 show a high disintegration of the surface: sand grains and tiny cementitious matrix pieces of size in the range of sand grains were easily removed from the surface of the PCs samples, P-0.55 being slightly more affected than P-0.38. The two slag blends S-0.55 and S-0.38 appear little affected. However, sand grains were exposed on the edges. The first signs of disintegration were recorded for the PCs micro-concretes from 329 days of exposure, which corresponds to the start of the second stage of expansion, mass loss, strength and loss of elastic properties. The first visual sign of cementitious matrix weakness were observed much later for the slag blends, after 441 days of exposure. Samples do not appear to be cracked at this level of observation: they reveal a softening type of damage characterised by surface disintegration and decohesion.

IV.1.4. SUMMARY

IV.1.4.A. A THREE-STAGE PROCESS (P-0.55)

The physical changes due to sulfate attack on P-0.55 appeared to follow a three-stage behaviour (Table IV-1).

Table IV-1. Characteristics of the three-stage behaviour of the physical changes of P-0.55 under ponding exposure;

	Expansion	Mass change	Compressive strength	Dynamic elastic modulus	
Stage #1	insignificant	slight gain	slight gain	slight gain	0
Stage #2	slow	slow loss	slow loss	slow loss	6
Stage #3	quick	very slow loss	very slow loss	quick loss	13

Exposure time (months)

The relationship between mass and length changes for P-0.55 in Na₂SO₄ solution (Fig. IV-13) is linear during stage #2, after which expansion dominates (stage #3) probably involving stresses too deep inside the material to be responsible for surface mass loss.

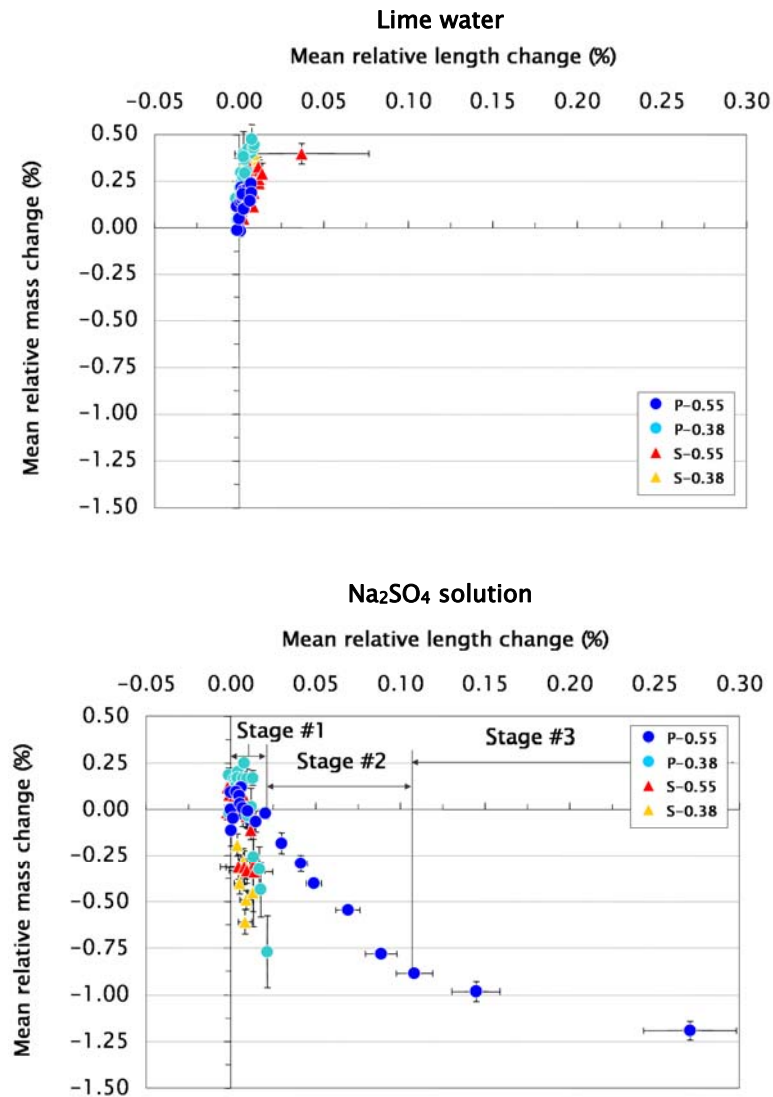


Fig. IV-13. Relationship between length and mass changes of the laboratory micro-concretes under ponding versus reference exposure.

A first understanding of the three-stage behaviour observed for P-0.55 in Na₂SO₄ solution can therefore be the following:

- stage #1 – *induction* – slight water uptake without any significant expansion;
- stage #2 – *surface damage* – slow expansion with surface concrete loss;
- stage #3 – *bulk damage* – quick expansion attributed to bulk damage.

This macroscopic evaluation needs however to be completed by looking inside the material at the microstructure damage and changes encountered.

IV.1.4.B. EFFECT OF REDUCTION OF W/C-RATIO (P-0.38)

The ionic transports involved in the ponded concretes in a low sodium sulfate solution couple leaching and sulfate ingress. Both phenomena progress in the Portland micro-concretes at constant rate independent of the w/c-ratio. Calcium leaching and sulfate ingress are hence not diffusion controlled and limited by chemical uptake or depletion of the solution. For comparable level of ion transport, P-0.55 and P-0.38 do not show the same state of physical properties (e.g.; expansion), which could indicate that the mechanical properties of the material and/or the repartition of the ions inside the materials can play a major role in the damage process.

A tendency towards linear relationship between mass loss and expansion is observed for P-0.38 as in stage #2 for P-0.55. But considering the low expansion of P-0.38, the damage would be dominated by mass loss. Moreover, the plot of mass change against length change points out the performance ranking of the samples: P-0.55 is the worst performing followed by the other PC P-0.38.

IV.1.4.C. EFFECT OF SLAG ADDITION (S-0.55 AND S-0.38)

The ion exchange in the slag blends is reduced compared to that in the pure Portland blends.

Before exposure, the Ca/Si and Ca/(Si + Al) ratios of the outer C-S-H are 1.98 and 1.75 for P-0.55 and 1.44 and 1.26 for S-0.55. This indicates that the availability of calcium from C-S-H in P-0.55 is 1.4 times higher than in S-0.55. This ratio of reacted calcium availability is slightly below the ratio of leaching between the two mixes (1.7). Additionally, the leaching from the pure PCs starts as soon as exposure starts while slag blends leaching starts with a delay of 28 days after exposure start. Such differences in the leaching level and rate might be due to the lower connectivity of capillary porosity of the slag blends compared to the pure Portland blends.

Slag addition seems to control somehow the sulfate ingress. The sulfate combination rate for the pure PCs is 1.4 times higher than that for the slag blends. This is close to the ratio between the calcium leaching rate of the PCs and of the slag blends. As for calcium leaching, the fact that the sulfate combination rate is not directly proportional to the amount of Portland cement contained in the binder indicates that sulfate combination is

not limited to the Portland hydrates but involves also the slag hydration products. Slag addition provides additional source of alumina in the cementitious matrix. The slag blends contain 9.935 wt.-% Al_2O_3 while the PCs have half as much with 4.626 wt.-%. All the alumina in the slag blend is not available for reaction since there is a large amount in the unhydrated slag grains that react very slowly. Nevertheless, a correlation can be seen between the sulfate combination and the C-S-H chemistry characterised by the $\text{Ca}/(\text{Si} + \text{Al})$ ratio: as detailed in the previous section on leaching, $\text{Ca}/(\text{Si} + \text{Al})$ ratio of the outer C-S-H is 1.4 times higher in the PCs than in the slag blends (Al/Ca ratio of 0.06 for the PCs and 0.14 for the slag blends) which can be directly related to the 1.3 factor between the sulfate combination in the PCs compared to the slag blends. Sulfate ions are known to adsorb on the C-S-H [54]. Aluminium is known to be found in substitution in the C-S-H structure occurring on bridging tetrahedral and in the interlayer and perhaps on particle surfaces [55]. In slag blends typically, the outer C-S-H is found to be enriched in aluminium which is assumed to be substituted in the C-S-H [56]. Therefore, an increase aluminium amount in the C-S-H, as observed in the slag blends compared to the PC blends, might reduce the sulfate adsorption while increasing the C-S-H steric hindrance, especially in case of aluminium substitution in the interlayer or on particle surfaces. Sulfate combination for the pure PCs starts as soon as exposure starts, while sulfate combination for the slag blends starts with a delay of 28 days after the start of exposure. As for calcium leaching, this might be related to the lower connectivity of capillary porosity of the blends compared to the pure Portland blends.

As for P-0.38, a tendency towards linear relationship between mass loss and expansion is observed for the two slag blends S-0.55 and S-0.38 revealing damage dominated by mass loss. The two slag blends seem to perform better than the PCs. Their relative performance can nevertheless not be split from this macroscopic point of view.

IV.2. DAMAGE PROCESS AND LINK TO PHASE ASSEMBLAGE

In order to link the macroscopic observations to the changes in the microstructure, a detailed examination was made by SEM and XRD. These changes are presented first for the P-0.55 which undergoes the most extensive deterioration and then for the less deteriorated samples.

IV.2.1. P-0.55

IV.2.1.A. MICRO-CRACKING

The crack patterns of P-0.55 ponded in Na_2SO_4 solution were examined by SEM-BSE (Fig. IV-14). The first 0.5 mm was characterised by a low density zone with darker grey levels compared to the bulk. This is characteristic of a leached zone. The transition between the dark grey level of the leached surface and the brighter sound bulk paste is progressive for this micro-concrete.

Cracks in P-0.55 (Fig. IV-14) progress from the surface of the sample towards the bulk, following the direction of the sulfate ingress. As seen, especially from the crack pattern after 357 days of exposure, and from the corresponding sulfur mapping, former cracks in the surface region are filled due to sulfate ingress. This later point could explain the fact that mass loss rate decreases after 357 days of exposure: the surface of the sample is densified due to the precipitation of sulfate-bearing phases in open spaces. This might also explain the reduced loss in compressive strength observed after 357 days of exposure. Furthermore, cracks at the surface of the sample will more likely cause decohesion and therefore mass loss than cracks propagating deeper inside the sample. The cracks propagate in the cementitious matrix of the sample and around aggregates (gaps at the interface aggregate-paste). This propagation pattern is characteristic for expansion of the cementitious matrix [50].

Thus, the hypothesis made after observing the three-stage expansion behaviour in the previous section is verified: stage #2 of expansion at lower rate is characterised by surface cracking, while stage #3 at higher rate involves bulk cracking of the cementitious matrix.

These micrographs also point out the surface mass loss from which the samples suffer: aggregates become exposed on the surface because the surrounding cement paste disintegrates. Due to this feature there is some uncertainty in the following analyses concerning the depth from the original contact surface.

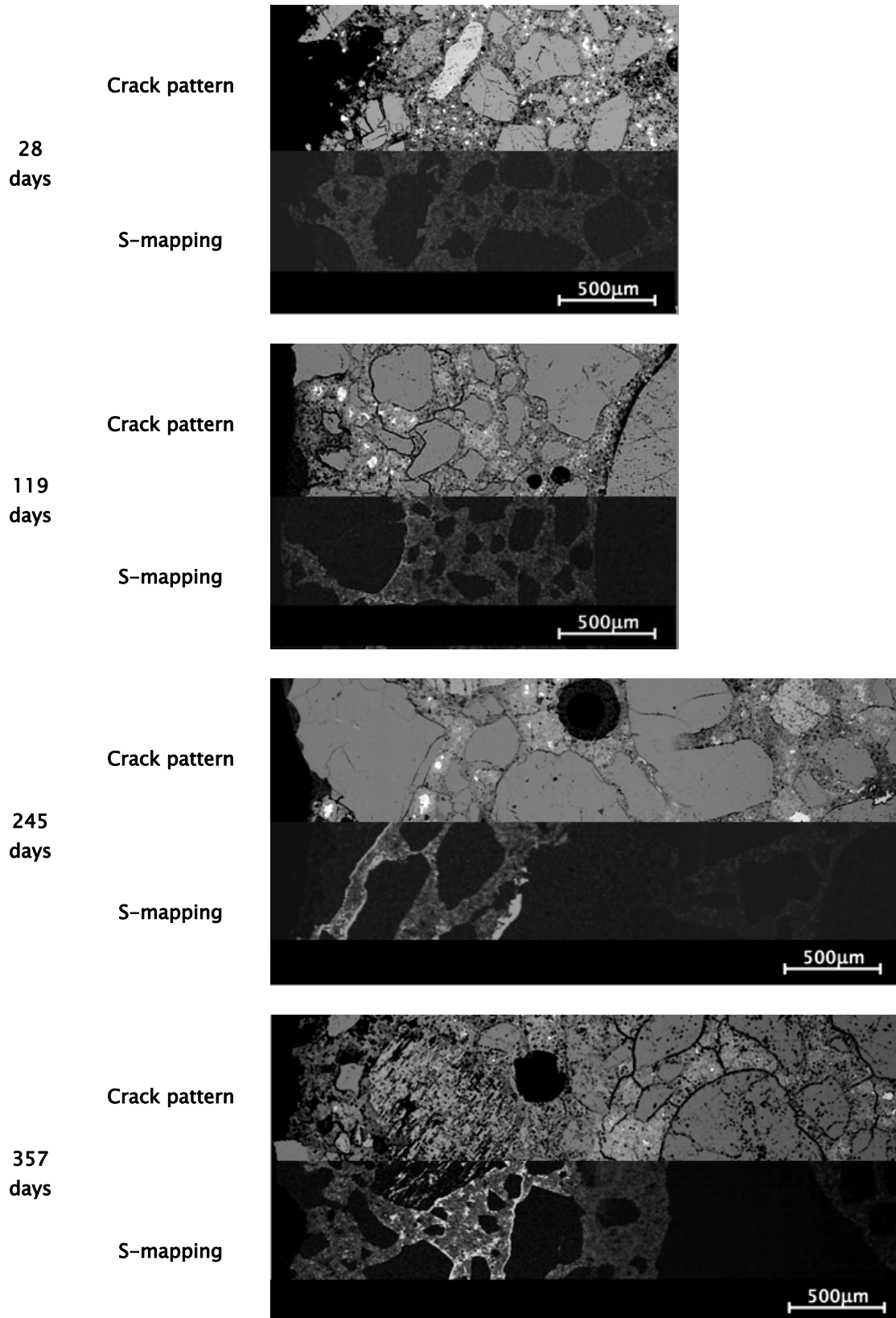


Fig. IV-14. Crack patterns from BSE micrographs with corresponding quantified S-mapping of P-0.55 under ponding in Na_2SO_4 solution.

IV.2.1.B. IONIC PROFILE

Quantitative calcium profiles and sulfur profiles were calculated by image analysis from qualitative SEM-mappings for P-0.55 after 28, 119, 245 and 357 days under ponding in Na_2SO_4 solution (Fig. IV-15).

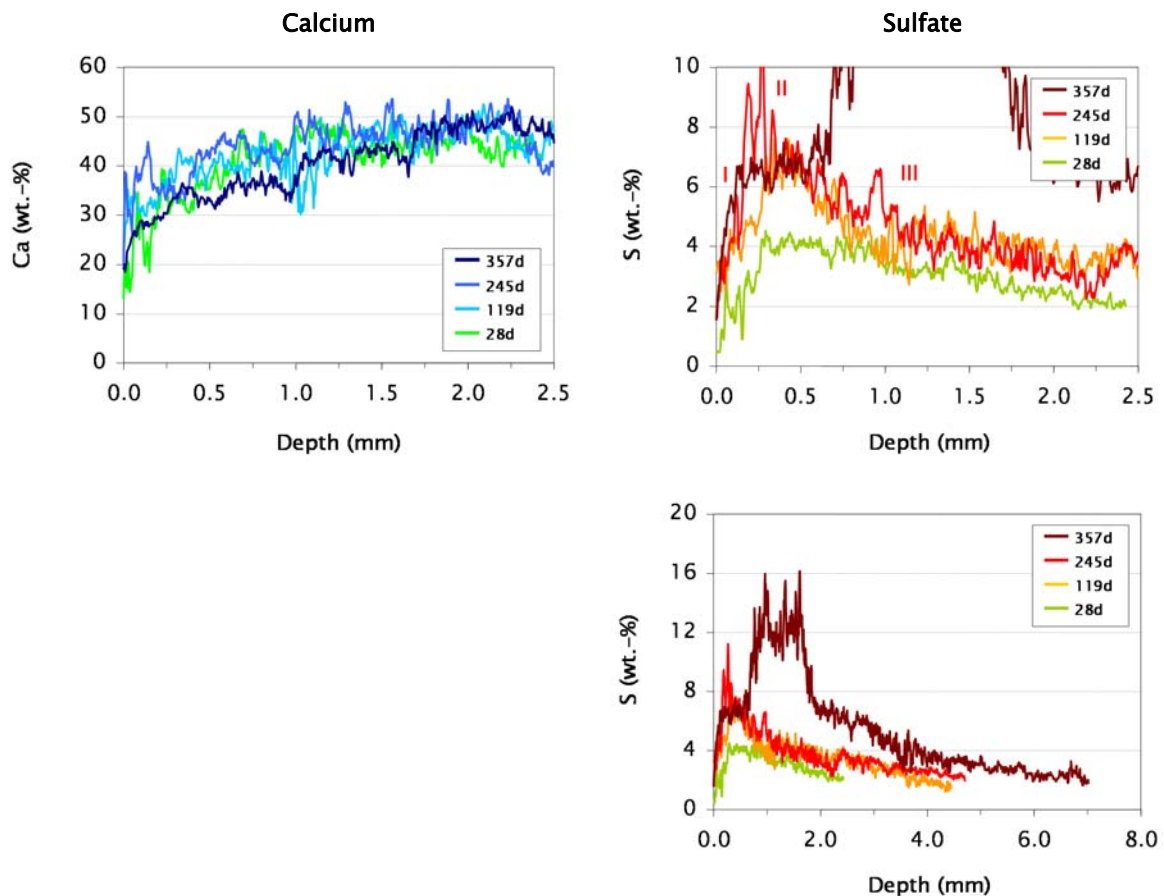


Fig. IV-15. Evolution of calcium (left) and sulfur (right) profiles of the cementitious matrix of P-0.55 under ponding in Na_2SO_4 solution.

The progressive leaching of calcium in P-0.55 indicated by the SEM-BSE micrographs observations is verified.

The sulfur ingress profile appears to have a shape in three parts (reported on the graph for the sulfur profile after 245 days of exposure):

- I: reduced amount at the contact surface;
- II: maximum below the surface and at edge of the calcium leaching zone;
- III: continuous decrease down to the bulk content of 2-3 wt.-%.

The first region closest to the surface where sulfate content is reduced corresponds to a part of the leaching zone. The pH might be too low to stabilize sulfate-bearing phases such as gypsum or ettringite, which would explain that the sulfate ingress is not highest at the contact surface. However, the leaching zone has an increased porosity due to material loss. This makes place for other phases and especially for sulfate-bearing phases to precipitate. The calcium released in this zone (from portlandite dissolution and in some instance from C-S-H decalcification) is free to precipitate as gypsum and ettringite in presence of alumina, which could explain that the maximum of the sulfate ingress is found at edge of the calcium leaching zone.

The four exposure times at which the analysis were done can be related to the three stages observed from the study of the macroscopic behaviour:

- 28-119 days – stage #1 – *continuous quick ingress of sulfate*;
- 119-245 days - stage #2 – *reduced ingress of sulfate*;
- 357 days – stage #3 – *massive ingress of sulfate*.

The sulfur ingress profile reaches 10 wt.-% after 119 days and shows a peak up to 15 wt.-% after 357 days of exposure. Interestingly, 10 wt.-% and 20 wt.-% sulfur correspond to the sulfur content in ettringite and gypsum respectively. A cementitious matrix rich in ettringite with a zone of high gypsum content between 1 and 2 mm depth is therefore expected for after 357 d of exposure, while ettringite should dominate at 0.5 mm depth after 119 days.

IV.2.1.C. PHASE ASSEMBLAGE ZONATION

Coarse approach: XRD

Qualitative XRD patterns were acquired mm by mm from the contact surface after 28, 119, 245 and 357 days of ponding in Na₂SO₄ solution down to the depth at which formation of ettringite could no longer be detected (Fig. IV-16). The patterns clearly revealed the effect of leaching on portlandite dissolution. Additionally, the precipitation of sulfate-bearing crystalline phases was identified. Ettringite precipitates along the sulfate profile, and is already detected at the surface up to 1 mm depth after 28 days of exposure. Gypsum is present at the surface of the micro-concrete, already after 28 days of exposure, but also deeper in the material after 357 days of exposure. This could be linked with previous observations of increased amount of sulfate penetrated between 1 and 2 mm. Gypsum was identified by XRD in massive amounts between 2 and 3 mm. Nevertheless, the method used to collect the powder for XRD analysis gives a rather coarse spatial resolution. Therefore, XRD phase assemblages were refined making statistical SEM-EDS analysis at specific depths to better situate the zones of phase formation.

A “double ettringite peak” was observable at $2\theta \sim 9^\circ$ (Fig. IV-17). The peak position corresponds to the U-phase which is a Na-AFm stable in environment enriched in alkaline [57]. However, this peak was also observed in the reference samples stored in lime water. Therefore, the hypothesis of a structural change of ettringite is preferred. The hypothesis of the shift of the ettringite peak towards lower angles would imply an increase in the *d*-spacing of ettringite. This could be achieved by 1°/ substitution of Al³⁺ by a bigger cation (e.g.; Fe³⁺), 2°/ integration of elements in the structure of ettringite (e.g.; Ti, Cr, Cl), 3°/ solid solution with thaumasite and 4°/ OH-ettringite formation. No composition changes could be confirmed by SEM-EDS analysis. The case of solid solution with thaumasite is unlikely to happen in the conditions applied where carbonation has been limited. The last hypothesis of OH-ettringite would be the most probable could not be verified.

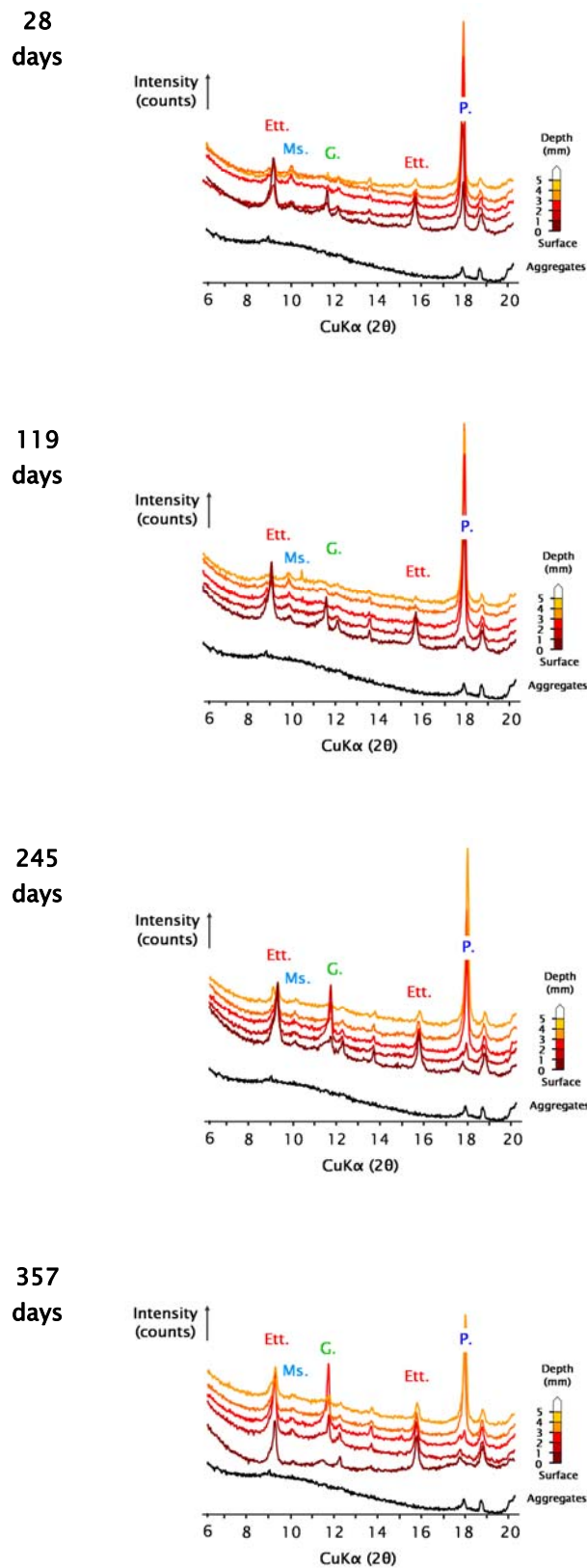


Fig. IV-16. XRD patterns at low angles of the first millimetres of P-0.55 after 28, 119, 245 and 357 days under ponding in Na_2SO_4 solution; Ett.: ettringite, G.: gypsum, Ms.: monosulfoaluminate, P.: portlandite.

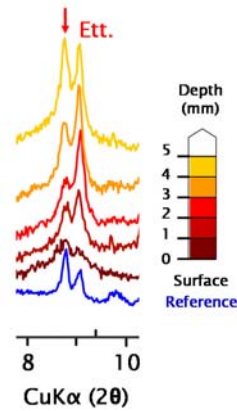


Fig. IV-17. Typical double ettringite peak observable in some samples exposed to sulfate and in the reference samples exposed to lime water; Ett.: ettringite.

Fine approach: SEM-EDS

In order to locate where sulfate-bearing phases are formed (e.g.; gypsum and ettringite), EDS quantitative analyses were carried out in the regions of outer and inner C-S-H after the different exposure times 28, 119, 245 and 357 days (Fig. IV-18).

Gypsum was found to form in the outer C-S-H at 1 mm depth after 357 days of exposure, which confirms the first observations of the sulfur profile. Gypsum seems to be finely intermixed to the outer C-S-H and not only precipitated as coarse crystals in cracks as could have been thought from the sulfur SEM-mappings. This fine intermixing could be a sign that gypsum has formed partly from the calcium of the C-S-H. In addition to the fact that gypsum is only to be seen at the surface of the samples, this could explain the surface softening of P-0.55 by a loss of the cohesive properties of C-S-H due to its increased decalcification.

The destabilisation of monosulfoaluminate to form ettringite is observable in both C-S-H regions.

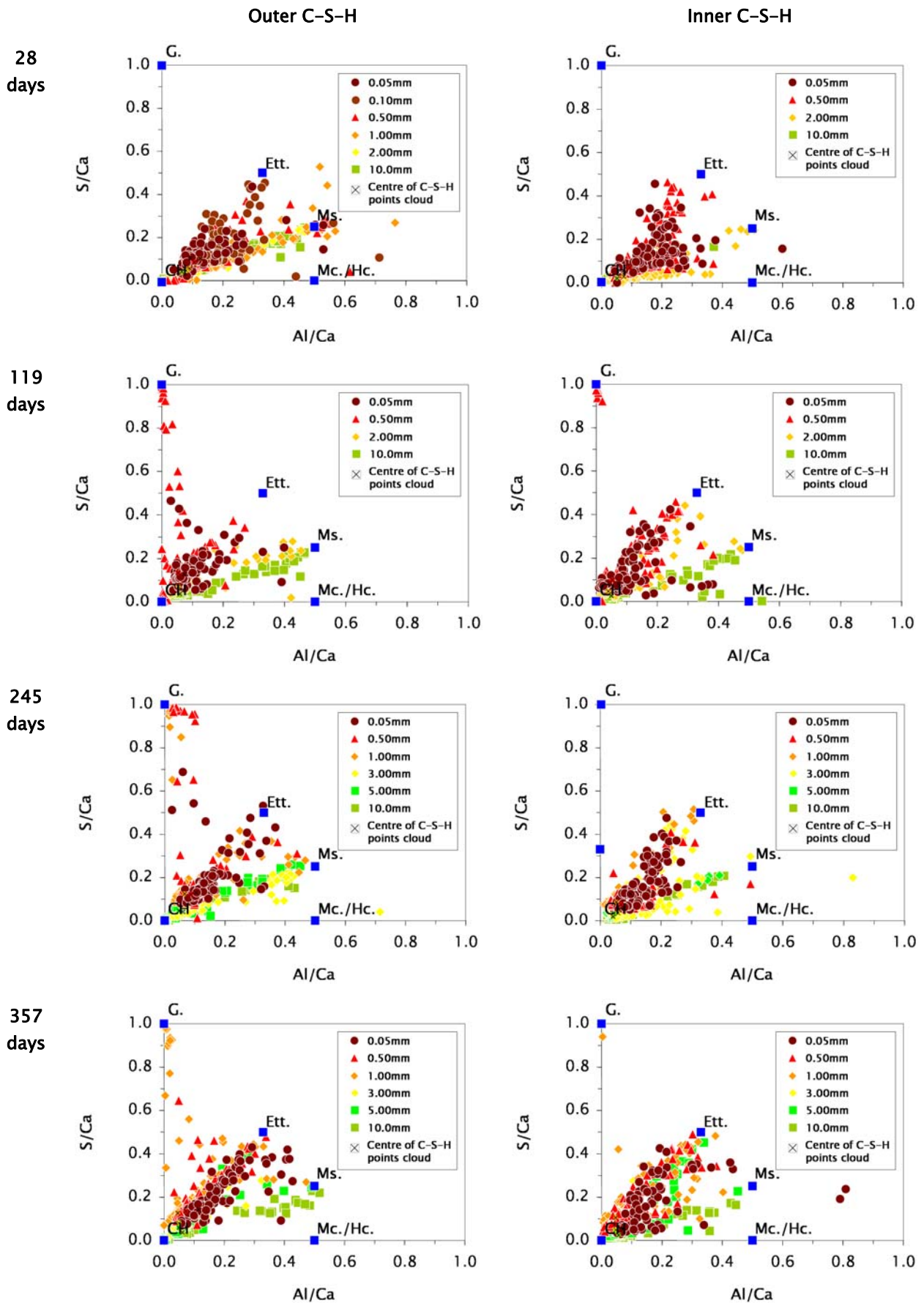


Fig. IV-18. SEM-EDS plots of S/Ca versus Al/Ca atomic ratios from the outer (left) and inner C-S-H (right) of P-0.55 under ponding in Na_2SO_4 solution; Ett.: ettringite, G.: gypsum, Mc./Hc.: mono- or hemicarboaluminate, Ms.: monosulfoaluminate.

Phase assemblages

Combining the results from XRD and SEM-EDS analysis, schematic graphs of the phases with the sulfate penetration depth and at the different exposure times were constructed (Fig. IV-19).

The carbonation degree seems constant, with a slight formation of monocarboaluminate after 357 days of exposure.

Progressive portlandite leaching is observable as well as a progressive decalcification of the C-S-H (C-S-H_d). It is worth noting that gypsum forms in the leaching zone where portlandite is less available. This indicates that gypsum may form from the calcium of C-S-H. This supports the previous hypothesis that gypsum could be responsible for the surface softening of the samples due to C-S-H decalcification.

The phase assemblages after 119 and 245 days of exposure are similar, which confirms the similar sulfur profiles previously observed. Between 28 and 119 days, no significant change in the depth of formation of ettringite could be seen. Deeper ettringite formation was observed only after 245 and 357 days, when expansion was already initiated. Therefore, the depth of ettringite formation does not seem to play a significant role in the expansion initiation. Between 119 and 245 days, expansion was recorded (stage #2). This points out that expansion cannot be so easily related to the phases formed. Further microstructural study is therefore required to better correlate the mineralogical and microstructural changes to macroscopic expansion.

After 119 days of exposure, prior to expansion, P-0.55 reveals a substantial formation of ettringite in the inner C-S-H compared to the outer C-S-H (Fig. IV-18). This could indicate that, apart from sulfate combination, ettringite precipitation in the inner C-S-H could play a role at the origin of expansion. Nevertheless, the availability of Al₂O₃ from the ferrite phase in the inner C-S-H could better stabilise ettringite in this C-S-H region rather than in the outer.

Nevertheless, as pointed out by the crystal growth theory [16], the size of the crystals formed would be a major parameter in their ability to cause stresses high enough for expansion to occur. The size of a crystal cannot be directly assessed in this study but considering the statistical EDS measurements the relative size of the crystals can be approached. The larger the crystal is, the closer to its theoretical stoichiometry the EDS analysis will be: the points will be close to the theoretical plot of the concerned crystal. If

the crystal is small, the EDS analysis will contain influences of its surrounding: the points will be between the different phases analysed theoretical plots.

Hence, the plots for the outer C-S-H of P-0.55 after 119 days of exposure could result from small ettringite crystals intermixed in the outer C-S-H. The plots for the inner C-S-H would reveal the presence of both relative large and small ettringite crystals in the inner C-S-H. Nevertheless, for a same size of ettringite crystals formed, the effects of the stresses developed in the inner C-S-H might be higher due to its the density of this C-S-H region. The outer C-S-H is surrounded by a capillary porosity network in which phases may crystallise without causing any deleterious stresses.

Results after 357 days of exposure in ponding revealed a finer and deeper ettringite formation in the outer C-S-H than in the inner C-S-H for P-0.55. Nevertheless, fine ettringite is present in comparable amount in the inner and in the outer C-S-H of P-0.55 after 119 days of exposure. It seems that the fine ettringite in the inner C-S-H of P-0.55 present after 119 days of exposure has recrystallised in coarser ettringite in free spaces of the inner C-S-H after 357 days of exposure.

A first refinement of the statistical SEM-EDS analysis to the cloud of points of the C-S-H phases (Fig. IV-20) indicates that ettringite may be finely intermixed to the outer but also to the inner C-S-H..

Moreover, the centre of the cloud of points of the outer and inner C-S-H seems to move towards higher values of S/Ca, which could be an indication of the sulfate combination to both C-S-H phases.

The plots of the outer C-S-H of P-0.55 after 28 days of exposure under ponding are characteristic of a microstructure dominated by C-S-H and monosulfoaluminate. However, the centre of the C-S-H points cloud seems to move towards higher S/Ca atomic ratios within the first 0.50 mm of the sample. After 119 days, the centre of the C-S-H points cloud has moved further towards higher S/Ca atomic ratios within the first 2 mm of the sample. At this stage of exposure, the microstructure seems to undergo some precipitation of ettringite finely intermixed to the C-S-H, which is accompanied by a reduced amount of monosulfoaluminate. At further times of exposure (245 and 357 days) the outer C-S-H does not seem to continue loading in sulfate while ettringite does continue precipitating.

In parallel, the inner C-S-H seems to load in sulfate and ettringite becomes quickly stable to the detriment of monosulfoaluminate.

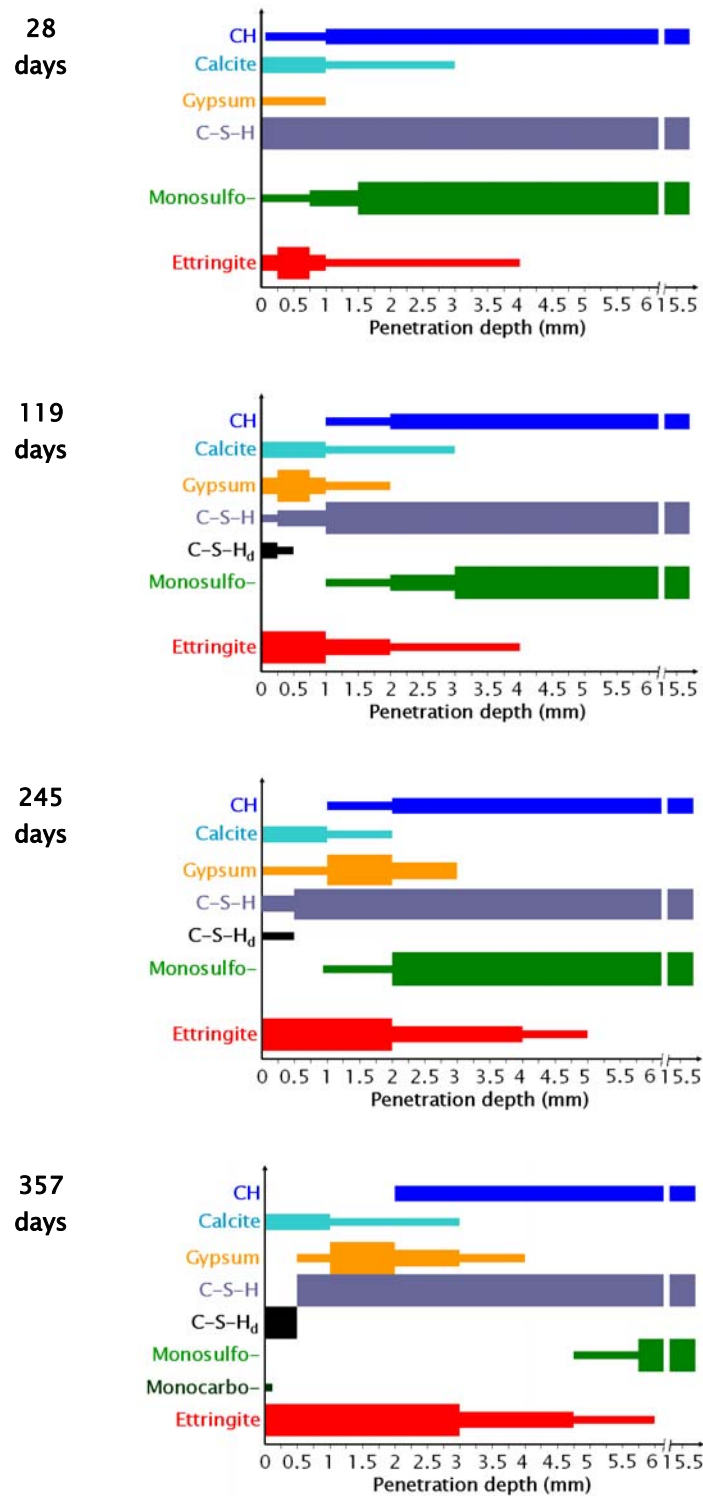


Fig. IV-19. Evolution in depth of phase assemblage in the binder of P-0.55 after various exposure times under ponding in Na_2SO_4 solution.

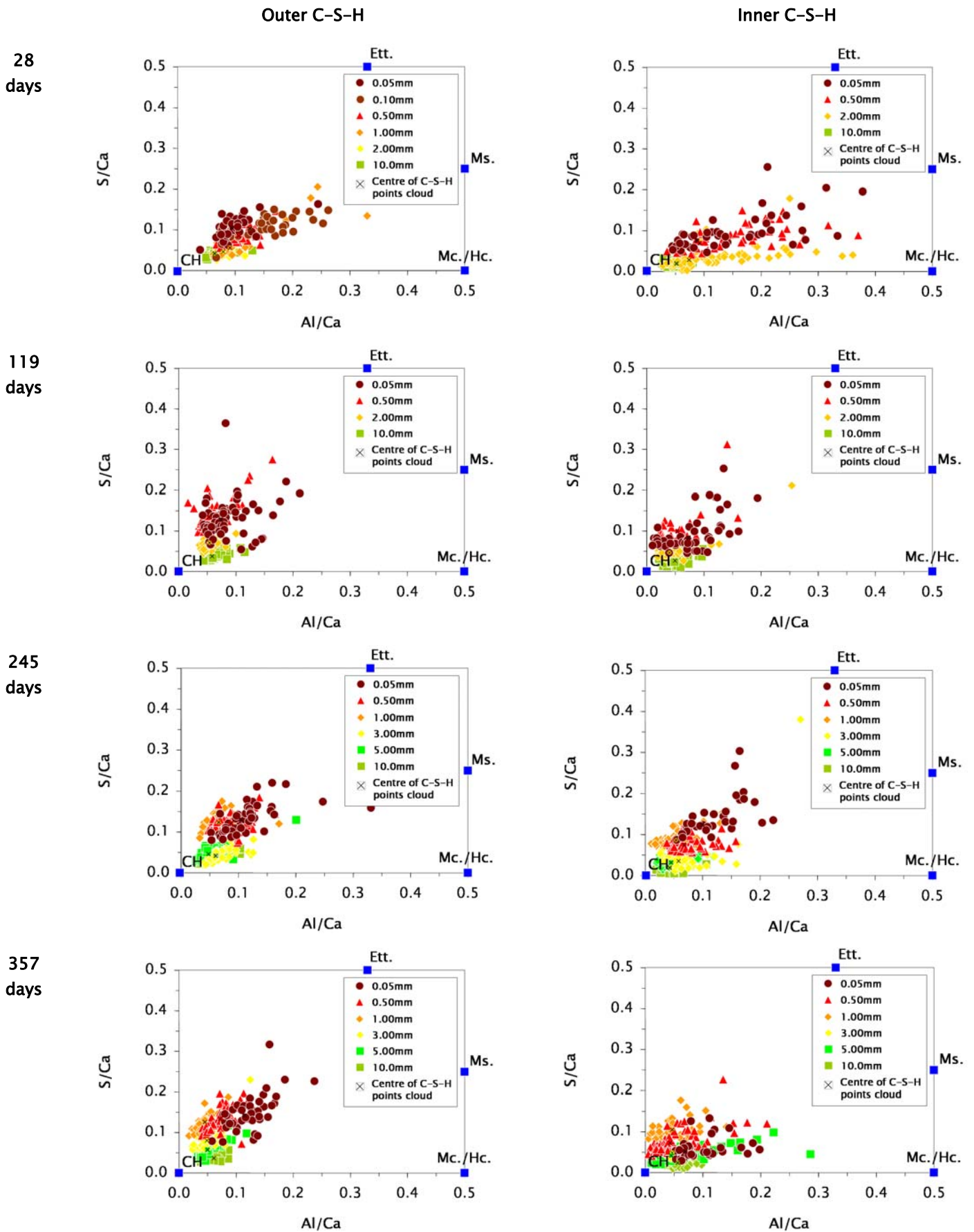


Fig. IV-20. SEM-EDS plots of S/Ca versus Al/Ca atomic ratios from the outer (left) and inner C-S-H (right) after refinement of P-0.55 under ponding in Na₂SO₄ solution; Ett.: ettringite, G.: gypsum, Mc./Hc.: mono- or hemicarboaluminate, Ms.: monosulfoaluminate.

IV.2.1.D. SUMMARY

From observations made on P-0.55, it appeared that under ponding exposure sulfate attack follows a three-stage process:

- stage #1 – *induction* –
 - continued hydration predominates resulting in an increase in strength and elastic properties;
 - the associated chemical shrinkage causes a slight solution uptake;
 - the continuous sulfate ingress is accompanied by ettringite formation and associated to surface micro-cracking;
 - gypsum is formed at the surface of the micro-concrete.

- stage #2 – *surface damage* –
 - sulfate ingress starts to dominate the behaviour resulting in a loss of the strength and elastic properties and is sufficient to start and maintain a slow expansion characterised by micro-cracking development.
 - the increased leaching causes material loss at the surface;

- stage #3 – *bulk damage* –
 - the increased sulfate combination in the binder results in an accelerated expansion and loss of the elastic properties;
 - the developed cracks penetrate deeper in the material and promote increased ion transport (calcium leaching and sulfate ingress with massive gypsum precipitation) through the opened microstructure;
 - the sulfate-bearing products precipitating in the cracks may cause a relative increase in strength resulting in a slow down of the strength loss.

Nevertheless, it has been brought into light that the outer and inner C-S-H phases could load in sulfate prior to ettringite precipitation. A more detailed observation and analysis of the microstructure is required to fix such aspects and their potential influence on the damage process. This is the object of the next section (§ IV.3.).

IV.2.2. EFFECT OF REDUCTION OF W/C-RATIO (P-0.38)

IV.2.2.A. MICRO-CRACKING

P-0.38 revealed the same kind of softening damage at the surface at the macro-scale without either micro-cracking or expansion and does not show any sign of particularly high sulfate intrusion after 357 days fully immersed in Na_2SO_4 solution (Fig. IV-21) despite a comparable ingress measured from the exposure solutions compositions. Neither leaching is observable at this stage of the study.

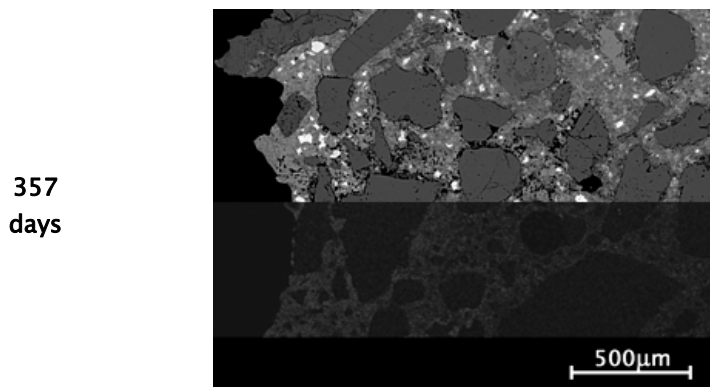


Fig. IV-21. Crack patterns from BSE micrographs with corresponding quantified S-mapping of P-0.38 after 357 days of exposure under ponding in Na_2SO_4 solution.

IV.2.2.B. IONIC PROFILE

Reduction of the w/b-ratio reduces the depth of leaching, making the front more abrupt (Fig. IV-22). Nevertheless, the profiles only inform about the global leaching process. Local fluctuations may be envisaged and could be at the origin of the fact that for a same leaching rate (§ IV.1.1.A) the leaching profiles are different.

As for calcium leaching, reduction of the w/b-ratio reduces the apparent depth of sulfate penetration that could be directly related to the fact that P-0.38 does not expand on the contrary to P-0.55. This supports the previous remarks concerning the effect of the ion repartition and especially the ion penetration depth on the damage process (§ IV.1.4.B). P-0.38 shows lower sulfate ingress than P-0.55 while it revealed the same sulfate absorption from the exposure solution (§ IV.1.1.B). The two results are not necessary contradictory and may indicate that the all sulfate diffused in solution through the porous network (measured from the exposure solution) is not fixed in the hardened binder (assessed by the sulfur profiles). Hence, the cementitious matrix of P-0.55 would more easily fix sulfate than that of P-0.38 for the same level of available sulfate. Whether this is due to a chemical or a physical effect is however not clear. Nevertheless, the very narrow

sulfur profile of P-0.38 compared to that of P-0.55 tends to indicate that, if the same amount of sulfate went into P-0.38 as into P-0.55, the entire sulfate might have concentrated at the surface of the sample without reaching a critical depth that would cause macroscopic bulk damage. The surface of P-0.38 is eroded and this related to the lower sulfur profile measured after 357 days than after 245 days of exposure might support the idea that damage on P-0.38 occurs step by step, concentrated at the surface of the material, without affecting the bulk.

The sulfur profile is again characterised by a shape in three parts as described for P-0.55 (leaching, accumulation and transport to the bulk of the material).

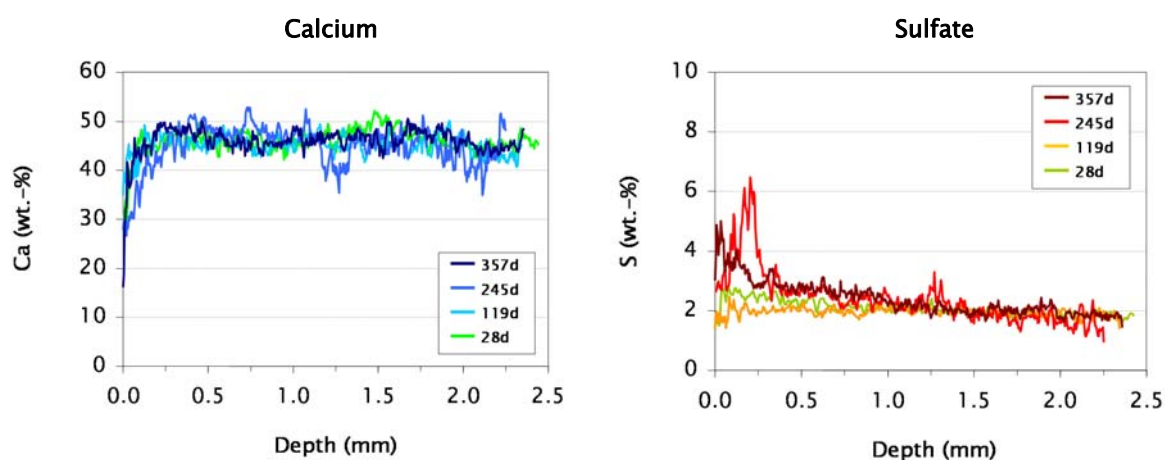


Fig. IV-22. Evolution of calcium (left) and sulfur (right) profiles of the cementitious matrix of P-0.38 under ponding in Na_2SO_4 solution.

IV.2.2.C. PHASE ASSEMBLAGE ZONATION

The phase assemblage of P-0.38 after 357 days of exposure (Fig. IV-23) follows the same pattern observed for P-0.55 but with reduced depths (especially for ettringite formation). Gypsum is formed at the surface of the sample, which suffers also from softening as P-0.55.

Portlandite has been largely dissolved for the samples with w/b of 0.55 up to 3 mm depth while for their homologues with w/b of 0.38 portlandite dissolution only concerns less than 1 mm at the surface. This is in agreement with the previous observations on C-S-H leaching from the SEM-BSE micrographs.

The depth of reaction might be a critical parameter for damage to occur. Again, a finer microstructure study is required to understand such influences especially relative to the interactions of the C-S-H with sulfate ions.

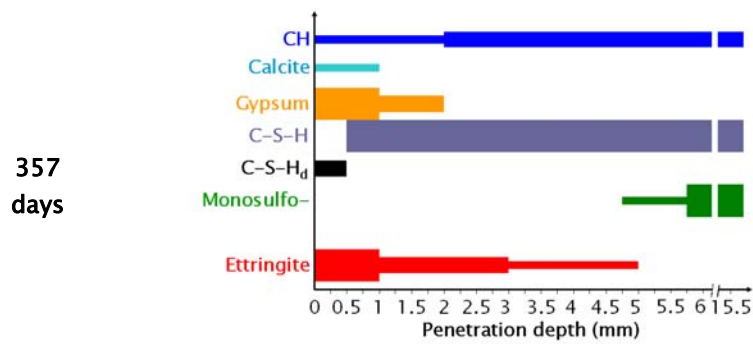


Fig. IV-23. Phase assemblage in the binder of P-0.38 after 357 days under ponding in Na_2SO_4 solution.

IV.2.3. EFFECT OF SLAG ADDITION (S-0.55 AND S-0.38)

IV.2.3.A. MICRO-CRACKING

Neither the cracking nor the sulfate ingress of the slag blends is significant after 357 days under ponding exposure (Fig. IV-24). The surface of S-0.55 is characterised by a very abrupt change in grey level characteristic for leaching, which differs from the progressive leaching behaviour observed for P-0.55.

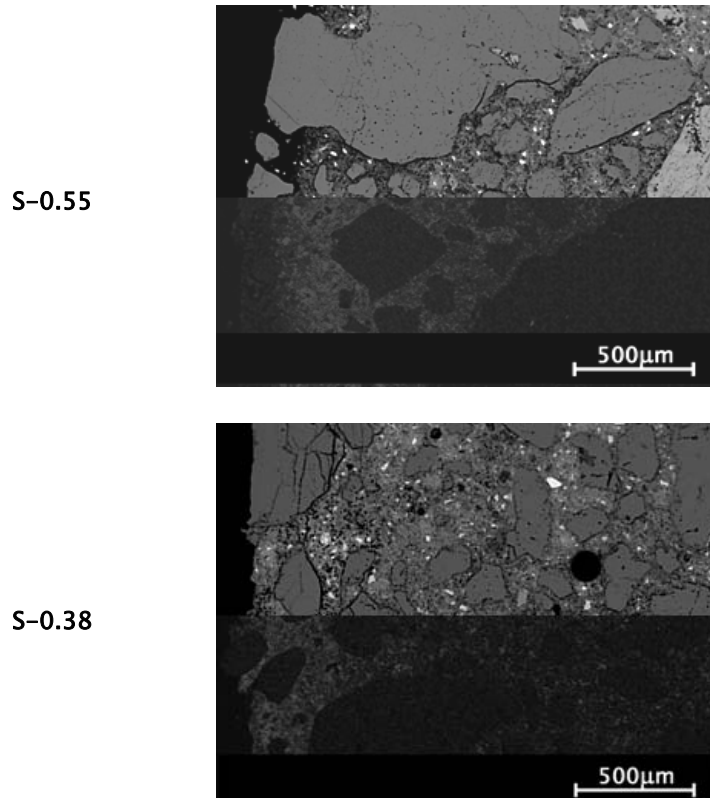


Fig. IV-24. Crack patterns from BSE micrographs with corresponding quantified S-mapping of S-0.55 and S-0.38 after 357 days of exposure under ponding in Na_2SO_4 solution.

IV.2.3.B. IONIC PROFILE

The decrease in capillary porosity connectivity due to slag addition ensures a reduced penetration of the surrounding solution into the sample which consequently reduces the leached zone and the amount of sulfate penetrated (Fig. IV-25). Reduction of the leaching depth implies none complete decalcification before further penetration can occur leading to an abrupt leaching front as seen for S-0.55 compared to P-0.55, with material loss characterised by the rise of aggregates at the surface of the material. Reduction of the w/b-ratio reduces the depth of leaching for the slag blends but it does not influence as much the sulfur profiles in terms of penetration depth as it did in the case of the PCs.

Again, as for the PCs, the sulfur profiles are characterised by a shape in three parts (leaching, accumulation and transport to the bulk of the material).

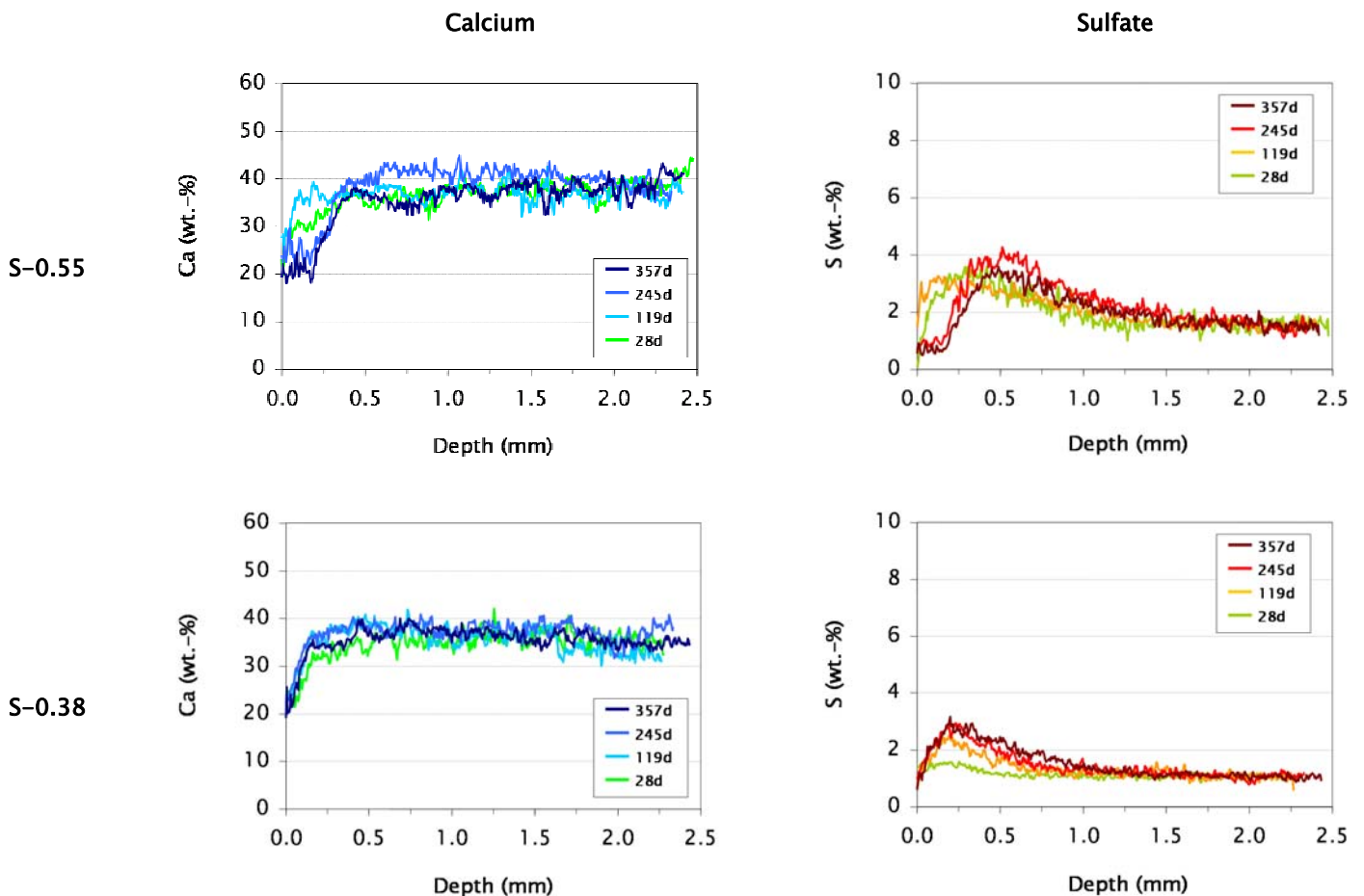


Fig. IV-25. Evolution of calcium (left) and sulfur (right) profiles of the cementitious matrix of S-0.55 and S-0.38 under ponding in Na_2SO_4 solution.

IV.2.3.C. PHASE ASSEMBLAGE ZONATION

S-0.55 suffers from more leaching compared to S-0.38 characterised by portlandite dissolution and C-S-H decalcification (Fig. IV-26), which matches the differences observed in the calcium profiles.

Only traces of gypsum and ettringite could be identified in S-0.55 after 357 days of exposure. Compared to P-0.55 those sulfate-bearing products seem to be present in minor quantities.

Slag addition appears to stabilise monocarboaluminate. However, as seen in the next section (§ IV.3.), slag blends revealed a reduced sulfate combination to the C-S-H phases compare to their plain Portland homologues (Fig. IV-39 and Fig. IV-40 compared to Fig. IV-36 and Fig. IV-37). Both features go in the sense that the overall microstructure of slag blends is depleted of sulfate compared to the plain Portland blends microstructures.

The phase identified in the phase assemblages as hydrotalcite, hydrate of the slags, is in fact quintinite, which is hydrotalcite like but with $Mg/Al = 2$ and not 3. Abusively, the term hydrotalcite is used.

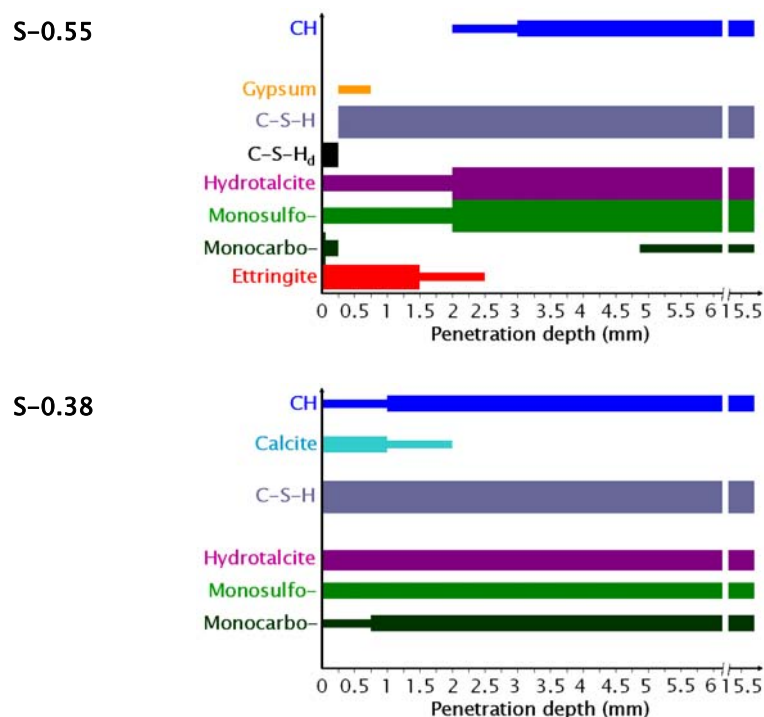


Fig. IV-26. Phase assemblage in the binder of S-0.55 and S-0.38 after 357 days under ponding in Na_2SO_4 solution.

IV.2.4. SUMMARY

IV.2.4.A. SULFATE INGRESS

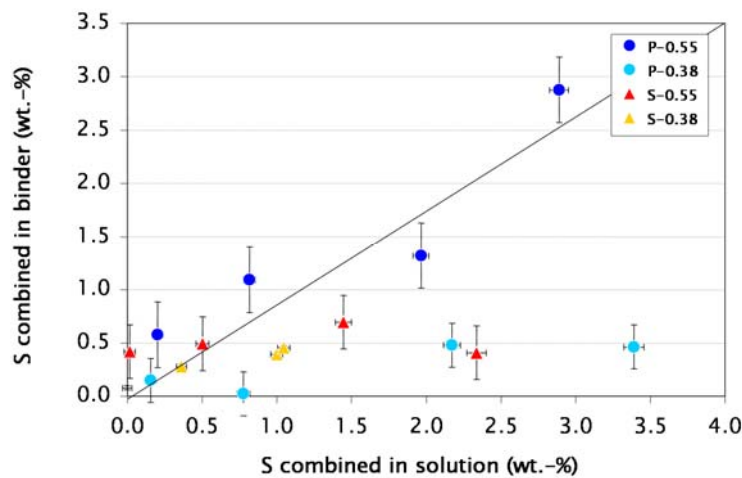


Fig. IV-27. Relationship between the sulfur combined in the solution and the sulfur combined in the binder of the laboratory micro-concretes along exposure time in ponding in Na_2SO_4 solution.

The integration of the quantitative sulfur profiles delivers information on the cumulative sulfur content which, with subtraction of the initial bulk sulfur content from the reference samples after the 28 days curing, can lead to the cumulative sulfur combined in the binder.

The relationship between the sulfur combined in the solution and the sulfur combined in the binder of the micro-concretes in ponding (Fig. IV-27) confirms the previous remark that for P-0.55 the entire sulfate penetrated has been fixed to the binder and has potentially reacted with. For the three other mixes, the sulfate penetrates into the material but does not fully react with or is only partially fixed to it.

This put into light the dual aspect of sulfate attack on concrete that decomposes in physical (diffusion of sulfate in the pore solution of the material) and chemical (fixation of sulfate to the binder) effects.

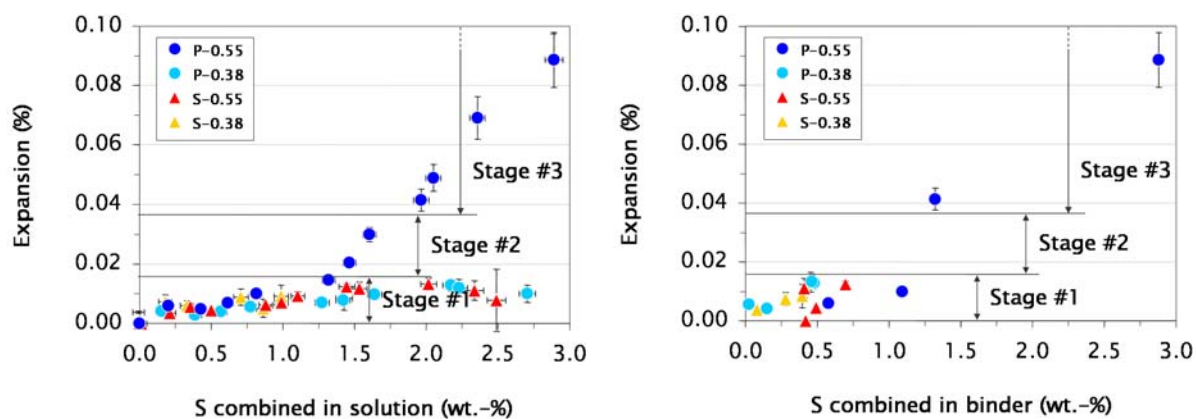


Fig. IV-28. Relationship between the expansion and the sulfur combination in the solution (right) and in the binder (left) of the laboratory micro-concretes under ponding in Na_2SO_4 solution.

Relationships can be drawn between the expansion and the sulfur combination either in solution or in the binder (Fig. IV-28). It appears that expansion is independent of the amount of sulfur combined from the pore solution but starts to be significant after a critical total amount of sulfur combined in the binder in the range of 1.0 wt.-% reached for P-0.55. The three stages pointed out for expansion have been reported on the graph which indicates that the three behaviours identified from the highly discrete data on this figure do match with the three-stage behaviour observed from the close to continuous data of expansion:

- stage #1 is characterised by a low sulfate ingress accompanied by a low expansion;
- stage #2 represents the critical stage where a slight ingress of sulfate is accompanied by extensive expansion;
- stage #3 is characterised by a large sulfate ingress accompanied by an extended expansion. Nevertheless, as noted earlier, stage #3 might also be characterised by sulfate-bearing products precipitation in pre-existing cracks leading to an increased sulfate ingress which is not be directly related to expansion.

IV.2.4.B. GYPSUM FORMATION

Gypsum was only identifiable in the PCs samples P-0.55 and P-0.38 which are precisely the samples suffering softening kind of macro-damage. Gypsum could therefore be at the origin of softening as it has been already reported by several authors. Gypsum precipitates in the leaching zone where ettringite is not stable, after extensive ettringite precipitation in the zone of higher sulfate amount (see quantitative sulfur profiles in previous section) and in locations typical for portlandite precipitation (Fig. IV-29): around the aggregates, in the

interfacial transition zone (ITZ). This leads to the conclusion that, in external sulfate attack, gypsum forms when the system is sulfate dominated directly from portlandite (portlandite dissolution, gypsum precipitation). Considering the structural differences between the two crystals (monoclinic gypsum and hexagonal portlandite), gypsum forms more likely by a through solution mechanism and not by a topochemical mechanism. However, gypsum can also form from the calcium of the C-S-H. The reduced gypsum formation in the slag blends could therefore be attributed to the relative reduced portlandite amount and the lower calcium in C-S-H of such mixes. Gypsum formation seems to be related to the softening of the PCs in ponding exposure.

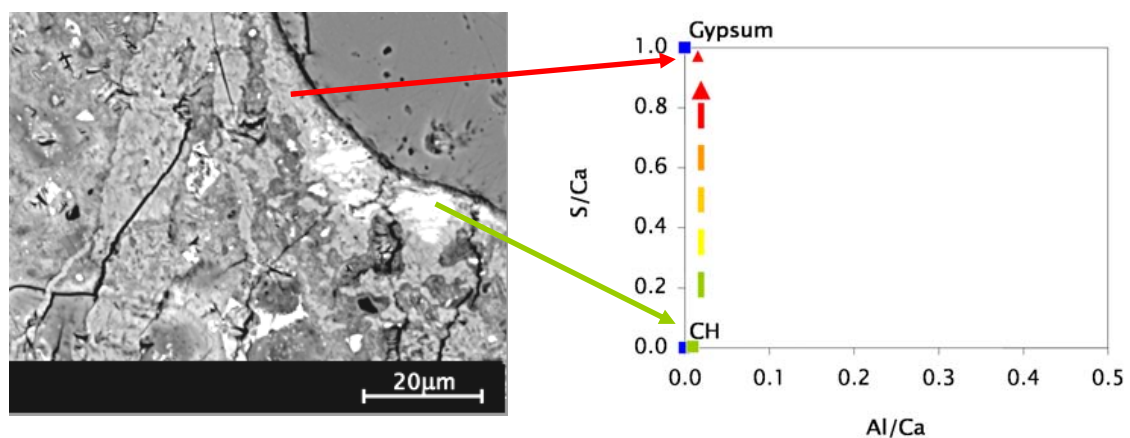


Fig. IV-29. BSE micrographs (left) with corresponding EDS plots of S/Ca versus Al/Ca of P-0.38 at 0.5 mm depth after 357 days under ponding in Na_2SO_4 solution.

IV.2.4.C. ETTRINGITE FORMATION

P-0.55 is characterised by a extensive ettringite formation compared to the other mixes. Since P-0.55 is the only sample in ponding to show significant expansion, ettringite formation could be at the origin of expansion. P-0.38 also showed some ettringite formation after 357 days of exposure comparable in terms of relative amount and depth of formation to P-0.55 after 119 days of exposure while the corresponding expansions were in the same range: respectively 0.013 % and 0.010 %. The influence of the depth of formation of ettringite might therefore play a role in the expansion in addition to the amount of ettringite formed. Owing to this remark, ettringite would lead to expansion when formed beyond the first 1-2 mm in such $4 \times 4 \times 16 \text{ cm}^3$ prisms. Semi-quantification can be done measuring the area under the ettringite peak at $2\theta_{\text{CuK}\alpha} = 15.8$ while subtracting the background. Summing this area up to detection level along the depth the cumulative semi-quantified amount of ettringite formed in a sample can be assessed.

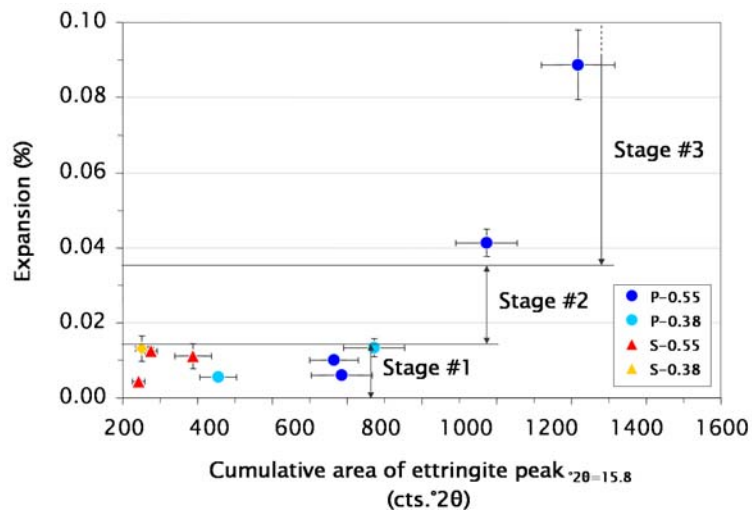


Fig. IV-30. Relationship between the cumulative semi-quantified ettringite from XRD and the expansion of the laboratory micro-concretes under ponding in Na_2SO_4 solution.

Plotting this cumulative ettringite amount against expansion (Fig. IV-30), a relationship can be extracted for the PCs while no clear behaviour is observable for the slag blends. The three stages identified for the expansion of P-0.55 are shown on the graph. Increased ettringite formation is identified for the stages #2 and #3 while the ettringite present in stage #1 is more similar to the background level. Expansion is detected in stages #2 and #3 but initiated in stage #1. The relatively low ettringite formation in stage #1 leads therefore to the conclusion that ettringite formation as precursor to expansion is a doubtful concept in ponding kind of exposure. More likely according to the increased ettringite formation during stages #2 and #3, ettringite precipitation would be a consequence of expansion or feeds late expansion.

The plot for P-0.55 of the ettringite amount formed against the sulfate ingress in the outer and inner C-S-H (Fig. IV-31) indicates the fact that during the initiation stage #1 (28 and 119 days measurements) ettringite does not precipitate in significant amounts while the two C-S-H phases become loaded with sulfate. Expansion could therefore be initiated by sulfate combination to outer and inner C-S-H. Stages #2 and #3 (245 and 357 days measurements) are characterised by a continuous sulfate combination to the outer and inner C-S-H accompanied by a continuous ettringite precipitation.

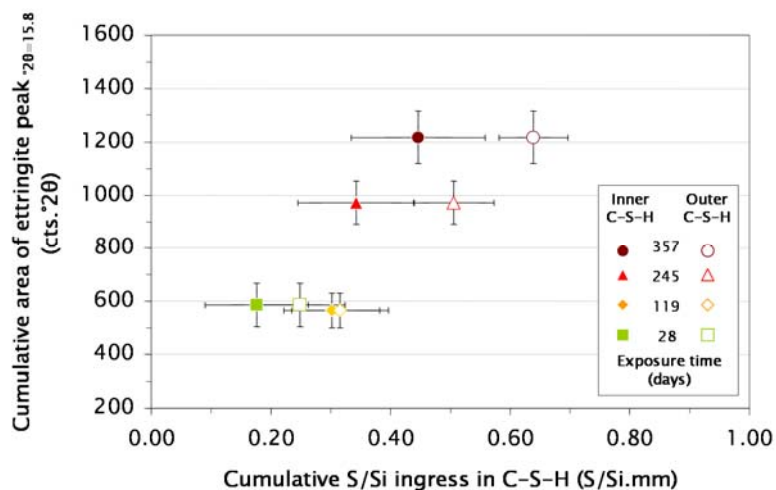
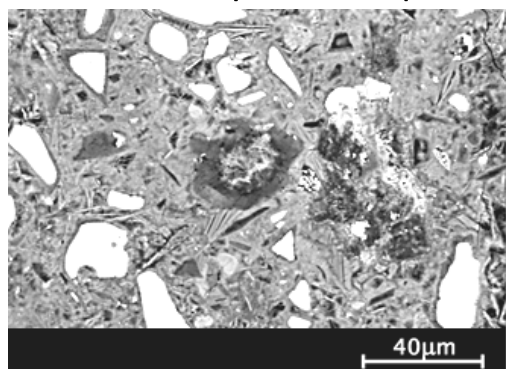


Fig. IV-31. Relationship between the cumulative S/Si atomic ratio of the outer and inner C-S-H and the cumulative semi-quantified ettringite from XRD of P-0.55 under ponding in Na_2SO_4 solution.

In the slag blends matrix the inner C-S-H is characterised by a high calcium leaching. It can be supposed that the calcium went out from the inner C-S-H to activate slag hydration as mentioned in other works [51] leaving therefore a large empty space for ettringite to precipitate extensively without causing any stress high enough to lead to expansion (Fig. IV-32). This can explain why no relationship between ettringite formation and expansion could be seen for the slag blends.

S-0.55 after 357 days - 10 mm depth (bulk)



S-0.55 after 357 days - 0.2 mm depth (surface)

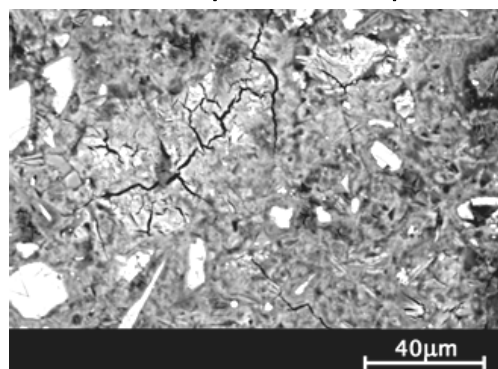


Fig. IV-32. BSE micrographs of the bulk (left) and the surface (right) of S-0.55 after 357 days of exposure in ponding in Na_2SO_4 solution.

Investigation of the microstructure is required to underpin the mechanisms behind sulfate attack process in ponding in Na_2SO_4 solution.

The main question to solve is the repartition of sulfate ingress in the microstructure and how the local microstructural effects can influence the macroscopic damage process.

IV.3. IMPACTS ON THE MICROSTRUCTURE

IV.3.1. LOCAL EFFECTS ON THE MICROSTRUCTURE

IV.3.1.A. LEACHING OF THE HYDRATES

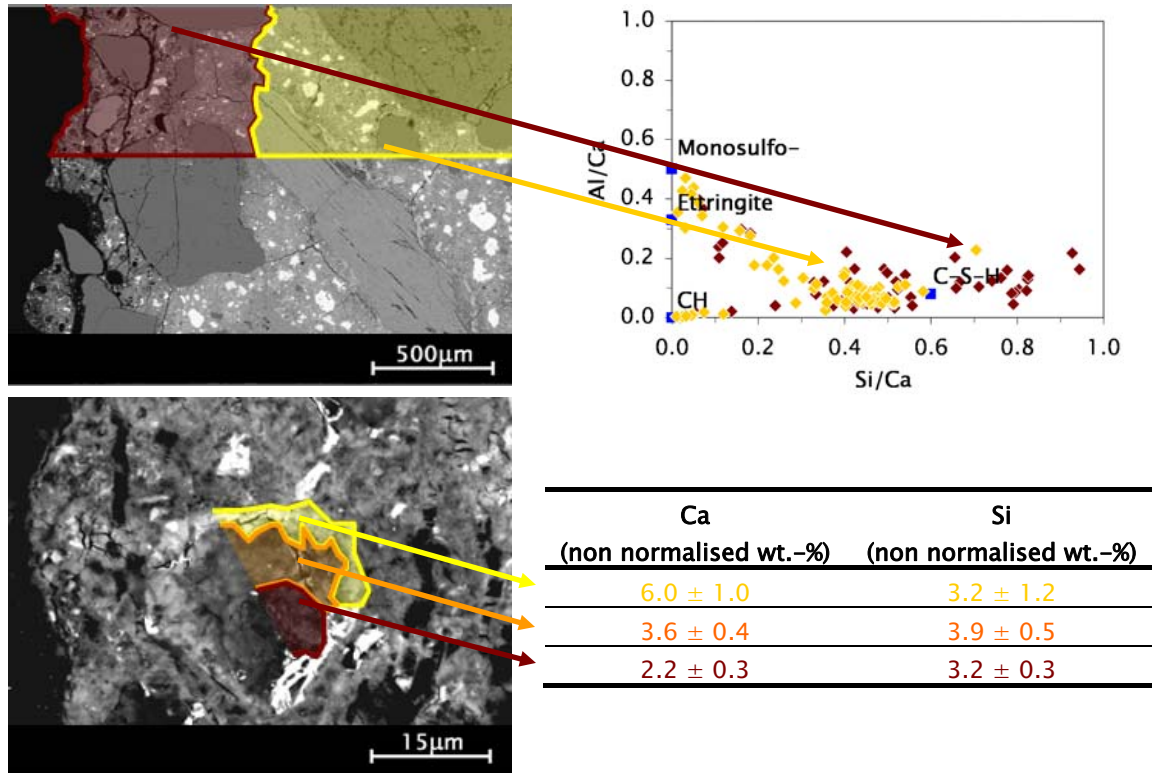


Fig. IV-33. Leaching of the outer (top) and inner C-S-H (bottom); case of P-0.38 after 245 days under ponding in Na₂SO₄ solution.

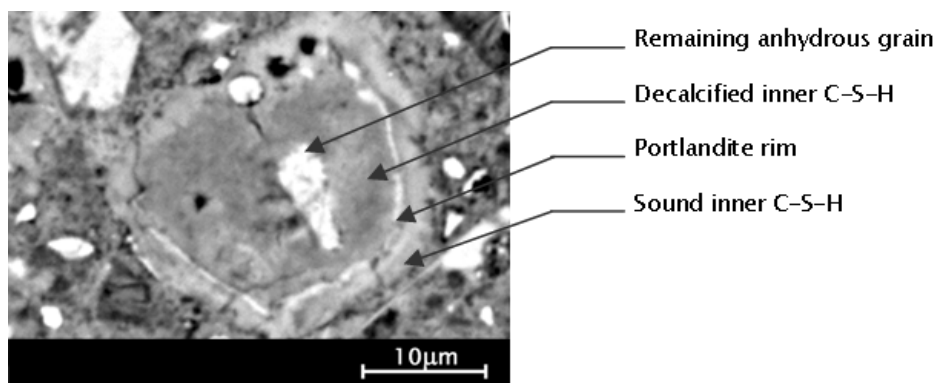


Fig. IV-34. Leaching of the inner C-S-H with precipitation of portlandite rim; case of P-0.38 after 357 days under ponding in Na₂SO₄ solution.

While dissolving portlandite frees Ca²⁺ ions. Furthermore, in case of high leaching up to full dissolution of portlandite, C-S-H can in turn play the role of buffer, freeing OH⁻ and Ca²⁺ ions leaving a silicate skeleton that evolves in silica gel. The leaching phenomenon

concerns both outer and inner C-S-H (Fig. IV-33). The cloud of EDS points of the darker outer C-S-H from the surface zone appears to be deviated towards higher Si/Ca and to a lower extent towards higher Al/Ca compared to the cloud of EDS points of the brighter outer C-S-H from the bulk of the sample. This is a typical sign for a lack in Ca. The gradient in grey levels in the outer C-S-H showing a darker C-S-H zone at the surface of the sample can therefore be identified as due to calcium leaching. However, this gradient in grey levels is also observed inside hydrated grains themselves when situated in the overall darker outer C-S-H surface zone. Since this difference might be caused by a removal of material (leaching), EDS plots analysis has been carried out without normalisation of results in order to better point out which element is in deficit or in excess in the darker zone. The effect of silicon enrichment on the C-S-H points cloud would be the same as a calcium deficit, moving points towards high Si/Ca values. But EDS analyses conducted in the inner C-S-H in wt.-% non normalised revealed a constant amount of Si (3.4 wt.-% \pm 0.7), while the amount of Ca decreased (from 6.0 wt.-% \pm 1.0 to 2.2 wt.-% \pm 0.3) when the corresponding area became darker. Hydrated grains are decalcifying from the inside outwards because anhydrous grains are most reactive. Hence, in relative acid conditions leaching changes the hydration process and can come to competition with hydration mechanisms. In some cases, a rim of portlandite can precipitate at the interface between the decalcified and the sound inner C-S-H (Fig. IV-34 and also pictures in [58]). This phenomenon could be attributed to a local gradient of pH from acid close to the anhydrous grain to basic in the inner sound C-S-H: portlandite becomes stable when in proximity to the sound inner C-S-H. Nevertheless, this can be found in sound cement pastes and is in any case not a sign of strong acid attack.

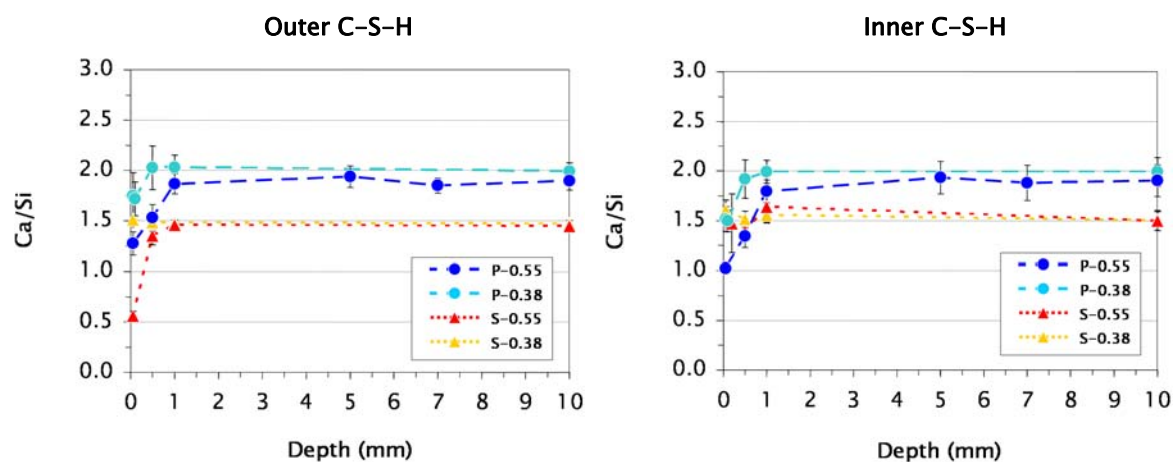


Fig. IV-35. EDS Ca/Si-ratio evolution from the outer (left) and inner C-S-H (right) of the laboratory micro-concretes after 357 days under ponding in Na_2SO_4 solution.

Leaching in the outer and inner C-S-H can be compared based on EDS Ca/Si-ratio evolution in depth in the two kinds of C-S-H phases (Fig. IV-35). In principle outer and inner C-S-H are leached to a comparable degree and depth out for S-0.55 which reveals a large surface leaching of its outer C-S-H while the inner C-S-H remain sound relative to leaching at the surface. The very abrupt superficial leaching zone of S-0.55 is also verified. The continuous gradual leaching of the PCs samples is verified for the outer and the inner C-S-H. The role of w/b is confirmed regarding leaching: samples with w/b of 0.38 reveal a shallower leaching than their respective homologue with w/b of 0.55. Nevertheless, as it was stated for the calcium profiles (§ IV.1.1.A), local fluctuations may be envisaged that could explain the reduced leaching observed for the micro-concretes with lower w/b-ratio while their leaching rates were similar to their homologues with higher w/b-ratio. The higher error bar in the Ca/Si-ratios of P-0.38 compared to those of P-0.55 could be a sign of such local fluctuations. Also, the high concentration of attack at the very top surface of P-0.38, as previously identified, may increase local fluctuations in this region.

IV.3.1.B. SULFATE INGRESS IN THE HYDRATES

It is considered that sulfate ions ingresses through the porous cementitious matrix, which is generally assumed to be the outer C-S-H. Nevertheless sulfate also penetrates in the inner C-S-H and combines significantly up to depths in the same range as that of the outer C-S-H in the case of the PCs (Fig. IV-36 and Fig. IV-37) but also in the case of the slag blends (Fig. IV-39 and Fig. IV-40). A saturation level seems to be reached for P-0.55 after 119 days of exposure, which corresponds to the expansion start. This could mean that sulfate combination to the outer and to the inner C-S-H phases could be able to initiate expansion. A saturation level seems also to be reached for P-0.38 after 245 days of exposure, as well as for S-0.55 and S-0.38. But the depths concerned are clearly reduced compared to that of P-0.55, which could emphasise that the depth of chemical changes must reach a critical value so that damage can occur.

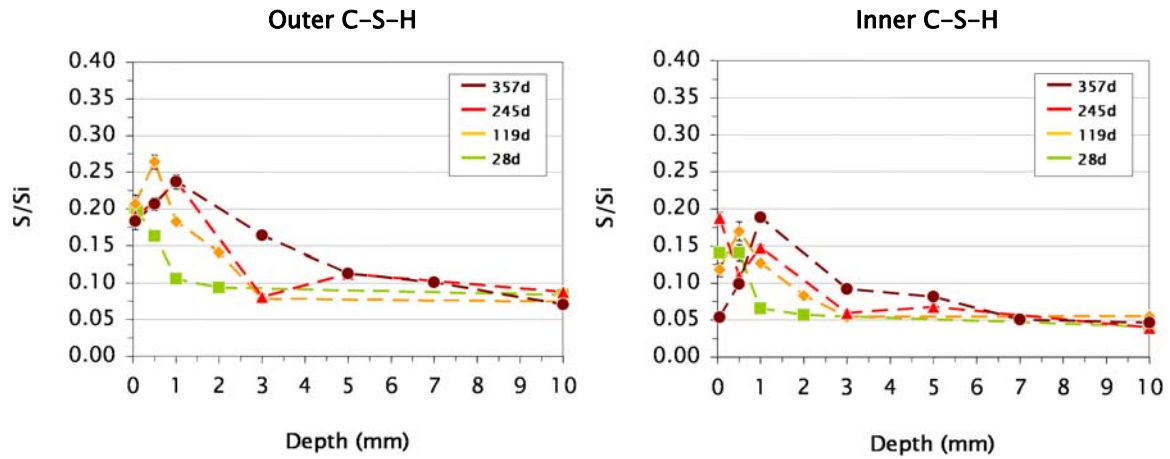


Fig. IV-36. EDS S/Si atomic ratio evolution from the outer (left) and inner C-S-H (right) of P-0.55 under ponding in Na_2SO_4 solution.

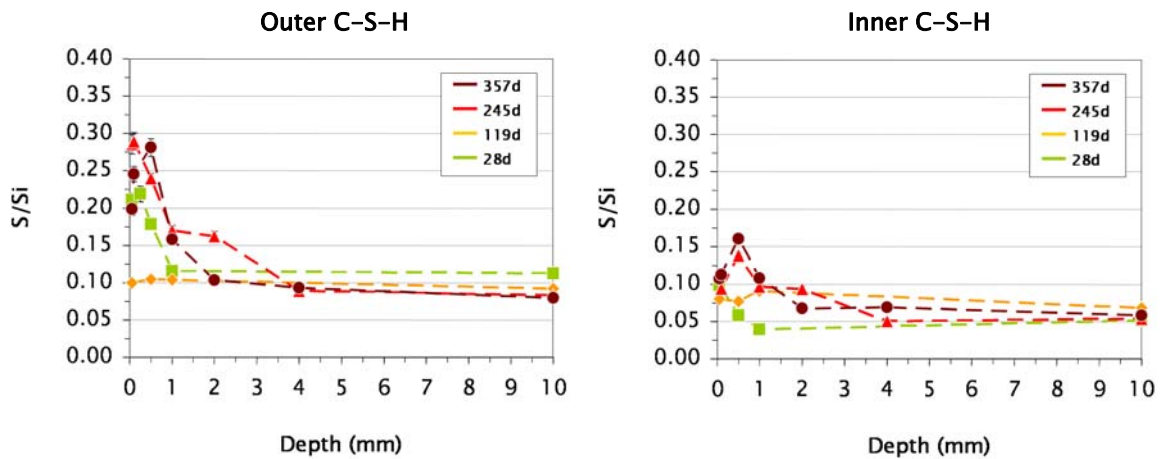


Fig. IV-37. EDS S/Si atomic ratio evolution from the outer (left) and inner C-S-H (right) of P-0.38 under ponding in Na_2SO_4 solution.

Quantitative elemental mappings of reacted grains are acquired for P-0.55 sample after 28, 119, and 357 days of exposure at depths corresponding to the maximal sulfate ingression (Fig. IV-38). If inner C-S-H is assumed to be denser than outer C-S-H, it does not prevent sulfate from penetrating in. After 28 days of exposure sulfate starts to penetrate the inner C-S-H, coming close to the reacting anhydrous grains. The reacting anhydrous grains are highly reactive calcium source for any reaction, including reactions involving sulfate ions. Furthermore, calcium seems to be evacuated from the centre of inner C-S-H through cracks. Also, the anhydrous grain leaves a hole after complete hydration, which is free space for crystals (e.g.; ettringite) precipitation. However, the inner C-S-H would be more rigid than the outer and would therefore less good relax stresses caused by internal strains such as phase growth than the outer C-S-H.

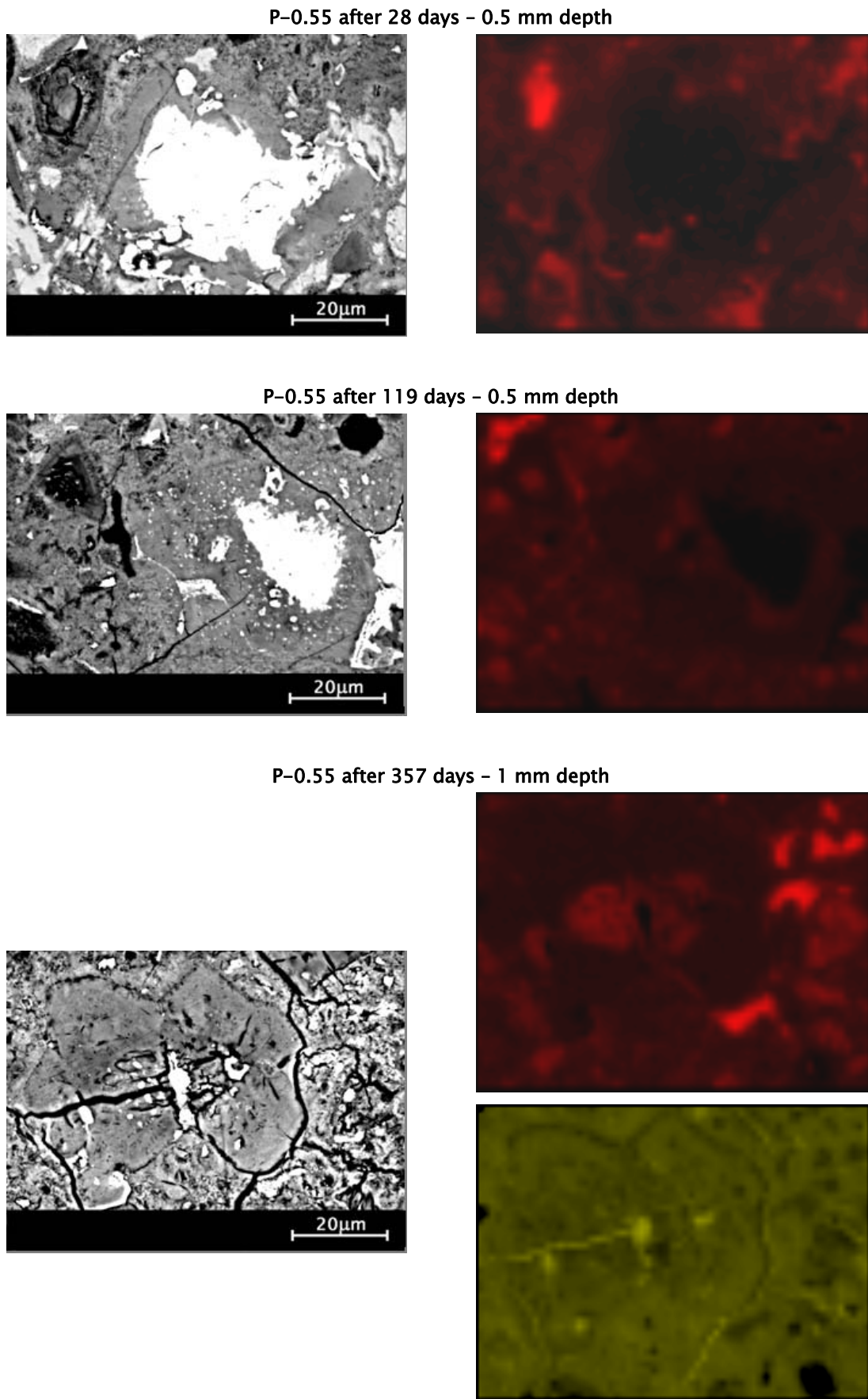


Fig. IV-38. BSE micrograph and corresponding quantified S-and Ca-mappings of inner C-S-H from P-0.55 under ponding in Na_2SO_4 solution at different times of exposure and depths.

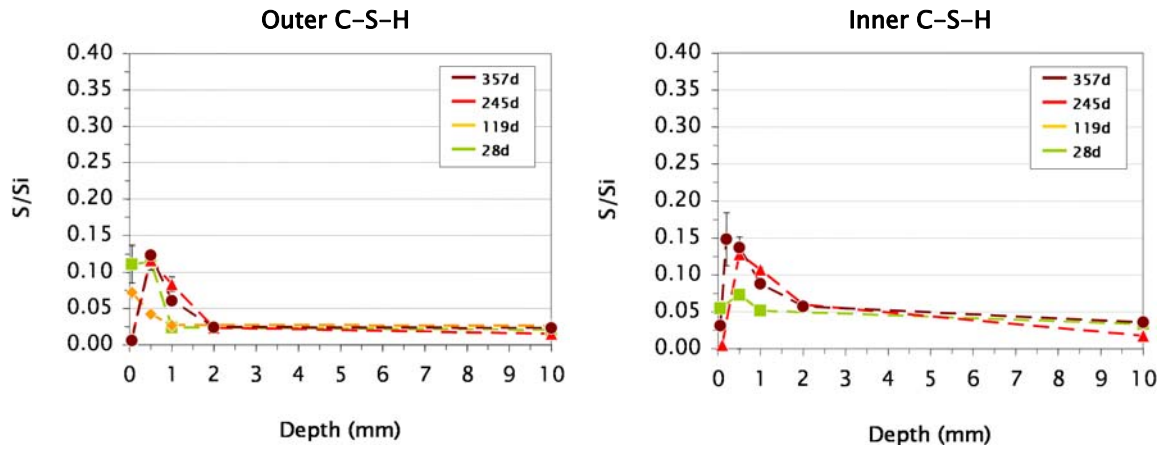


Fig. IV-39. EDS S/Si atomic ratio evolution from the outer (left) and inner C-S-H (right) of S-0.55 under ponding in Na_2SO_4 solution.

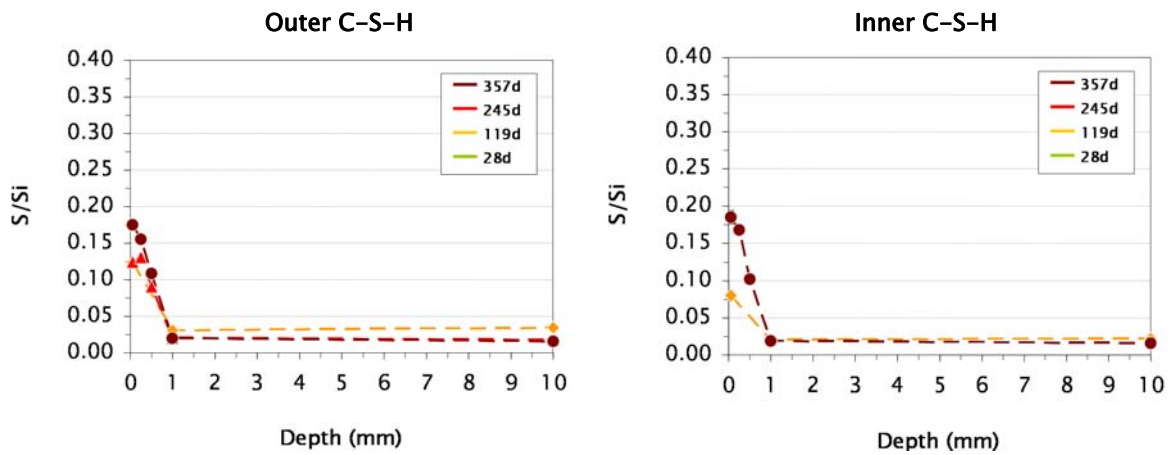


Fig. IV-40. EDS S/Si atomic ratio evolution from the outer (left) and inner C-S-H (right) of S-0.38 under ponding in Na_2SO_4 solution.

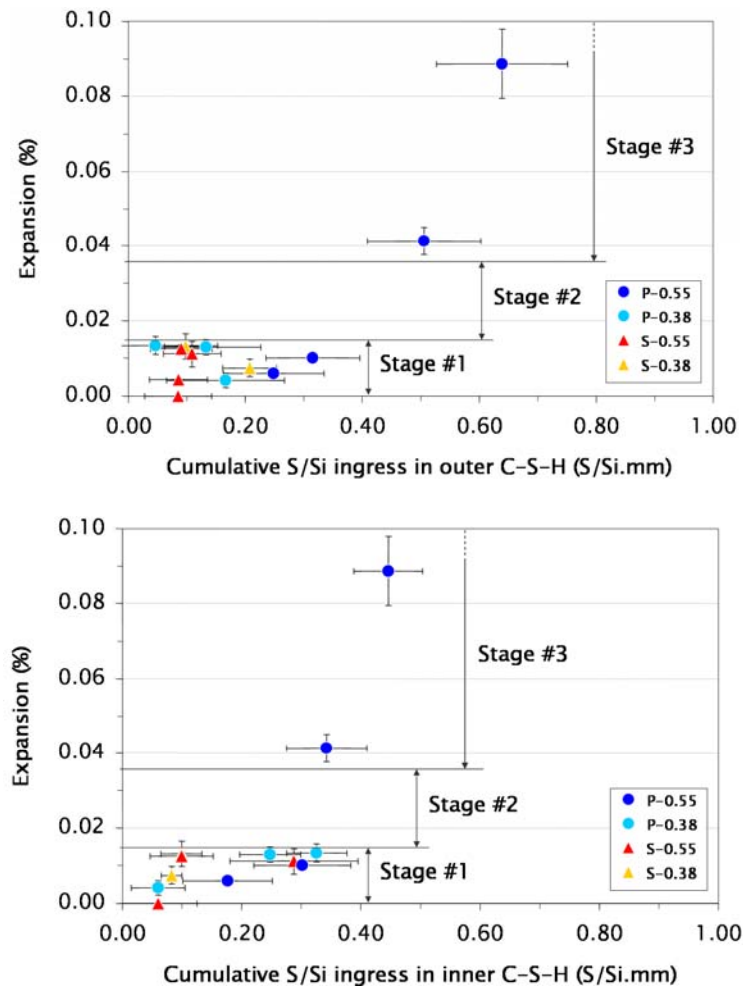


Fig. IV-41. Relationship between the cumulative S/Si atomic ratio of the outer (top) and inner C-S-H (bottom) and the expansion of the laboratory micro-concretes under ponding in Na_2SO_4 solution.

As for the quantitative sulfur profiles, the integration of the quantitative S/Si profiles of the outer and inner C-S-H delivers information on their respective cumulative S/Si content. Subtracting the initial bulk S/Si content of the outer and inner C-S-H from the reference samples after the 28 days cure the cumulative sulfate ingress in the two C-S-H phases can be deduced. A relationship is visible for P-0.55 between the cumulative sulfate ingress and expansion both in the case of the outer and inner C-S-H (Fig. IV-41). The three stages observed for expansion have been reported on the graphs. For the outer C-S-H, this relationship is continuous while for the inner C-S-H it tends to follow the three-stage behaviour of the cumulative sulfate ingress previously observed. The three stages also match the three stages of expansion observed in section IV.1.2.B. For the inner C-S-H, stage #1 is characterised by a significant sulfate ingress accompanied by a low expansion, stage #2 represents the critical stage where a slight ingress of sulfate is accompanied by extensive expansion and stage #3 is characterised by a significant sulfate ingress accompanied by an extended expansion. Regarding the error range, no significant

difference can be identified between stage #2 and stage #3. No influence of massive sulfate-bearing products precipitation can be expected here since the S/Si measured has been reduced to the C-S-H phases themselves, excluding points of measurement with corresponding S/Ca and Al/Ca ratios in the range of ettringite and gypsum. It appears therefore that for P-0.55, expansion does not require any critical sulfate ingress in the outer C-S-H but would require the S/Si in the inner C-S-H to overcome a critical value in the range of 0.30. It might therefore be thought that sulfate combination in the inner C-S-H might play a role in the expansion mechanism in such ponding exposure while sulfate combination in the outer C-S-H could be a side effect.

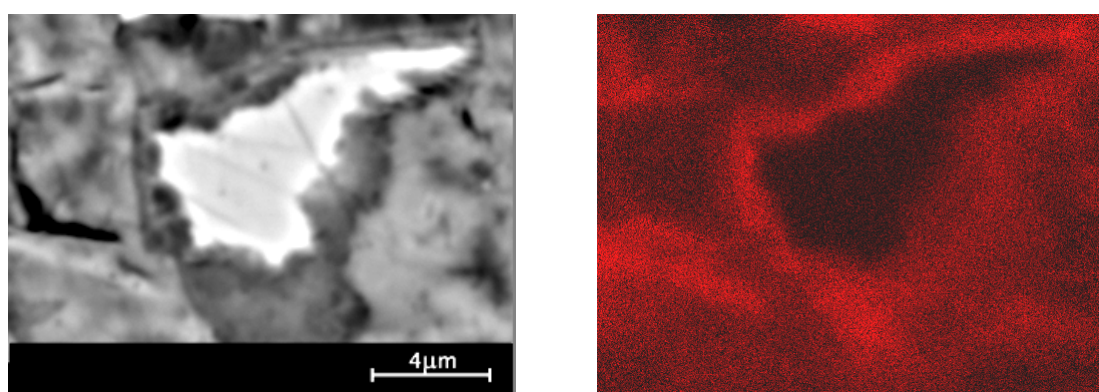


Fig. IV-42. BSE-micrograph (left) and corresponding quantified S-mapping (right) of a slag grain with hydration rim at 0.5 mm depth of S-0.55 after 357 days under ponding in Na₂SO₄ solution.

Table IV-2. EDS S/Si atomic ratio from slag hydration rim of S-0.55 at 0.5 mm depth: evolution along ponding in Na₂SO₄ solution.

Exposure time (days)	S/Si(normalised at.-% ratio)
	S-0.55
28	0.06 ± 0.01
119	0.13 ± 0.01
245	0.19 ± 0.01
357	0.29 ± 0.02

Quantitative elemental mapping of reacted slag acquired for S-0.55 after 357 days of exposure revealed that slag inner hydration product combines sulfate (Fig. IV-42). The morphology of slag inner hydration product does not seem to be affected as was the case for inner Portland C-S-H. The sulfate combination to slag hydrate has been checked measuring the EDS S/Si atomic ratio in the slag hydration rim at different exposure times for S-0.55 and S-0.38 (Table IV-2).

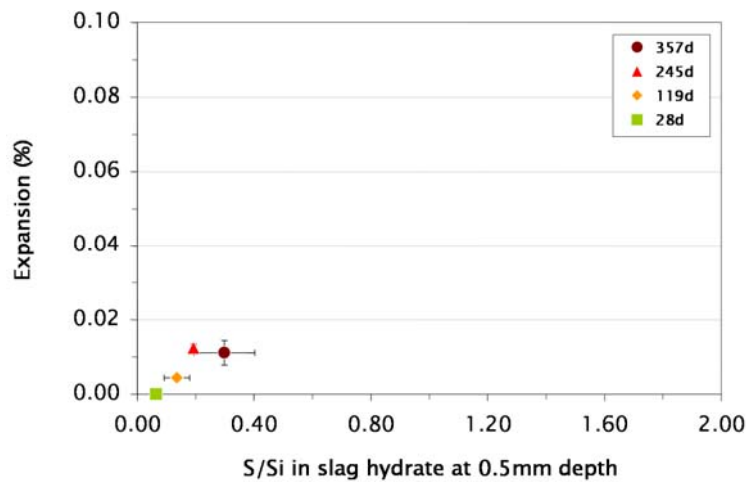


Fig. IV-43. Relationship between the cumulative S/Si atomic ratio of the slag hydration rim and the expansion of S-0.55 and S-0.38 under ponding in Na_2SO_4 solution.

A tendency towards a relationship between the S/Si atomic ratio in the slag hydration rim at 0.5 mm depth (depth of highest sulfate ingress) can be observed for S-0.55 (Fig. IV-43). Even considering the low level of expansion of S-0.55, the sulfate combination of the slag hydrates seem to play a more important role than the sulfate combination of the cement outer and inner C-S-H.

IV.3.1.C. CRACKING OF THE HYDRATES

Observations at high magnification of the polished sections of the expansive P-0.55 sample point out a cracking behaviour at low scale (Fig. IV-44). After 119 days of exposure, cracks start to form in the inner C-S-H. After 357 days of exposure, cracks have developed and are not restricted to the inside of the inner C-S-H but form significantly at the inner/outer C-S-H interface. Cracking at the interface of such phase contrast is characteristic of a difference in mechanical properties between the two phases. A difference in mechanical properties between the outer and the inner C-S-H would lead to a difference in expanding behaviour but it is not obvious which one of the phases would expand more than the other. Nevertheless, the absence of such cracks between the outer C-S-H and portlandite would indicate a common mechanical behaviour regarding sulfate ingress. An expansion of the inner C-S-H as cause for macroscopic expansion would therefore not be excluded. The fact that no cracking is observable in the inner C-S-H at the surface of P-0.55 after 357 days of exposure can be explained by the high calcium leaching level of these inner C-S-Hs which become less dense and can accept large precipitation of ettringite without developing any stress. Cracking between the outer and

the inner C-S-H is also observed for P-0.38 but probably not deep enough inside the sample to cause macroscopic expansion (Fig. IV-45).

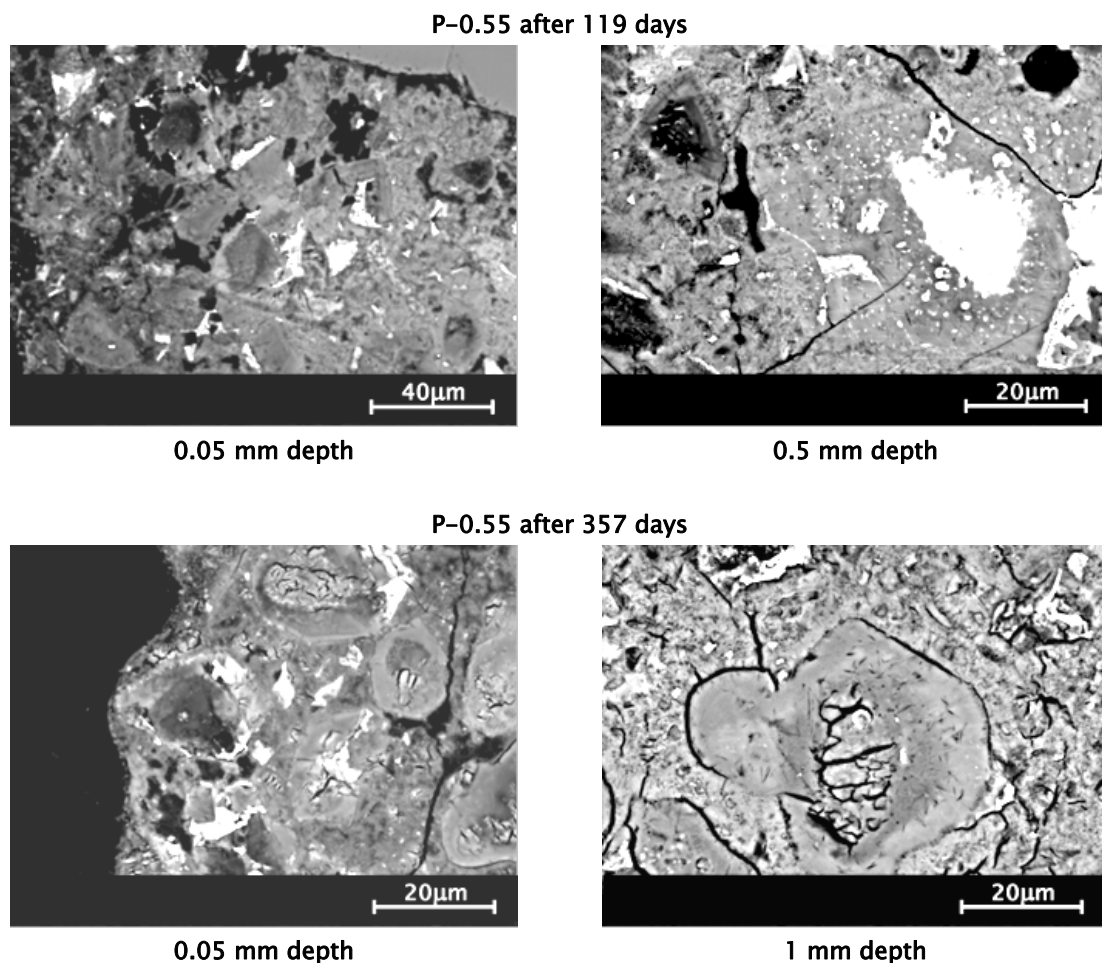


Fig. IV-44. BSE micrographs of inner C-S-H at the surface of P-0.55 after 119 (top) and 357 days (bottom) under ponding in Na_2SO_4 solution.

Such crack patterns observed by SEM-BSE imaging can either have been developed in the material due to stresses or have been initiated by the SEM vacuum. In the later case, this is typically the issue for cracking in ettringite: ettringite has a very high amount of water molecules that dry when under the SEM vacuum resulting in random orientated cracks.

In the case of the cracked C-S-H and especially the cracked inner C-S-H observed here, the cracks generally do not show any radial or orientated pattern. This could rather indicate that they are an artefact of the observation. Nevertheless this would mean that the C-S-H has loaded in water molecules, through ion adsorption for instance, and may therefore have swelled. The cracking of the inner C-S—H observed could be due to a particular swelling of this C-S-H region compared to the outer C-S-H.

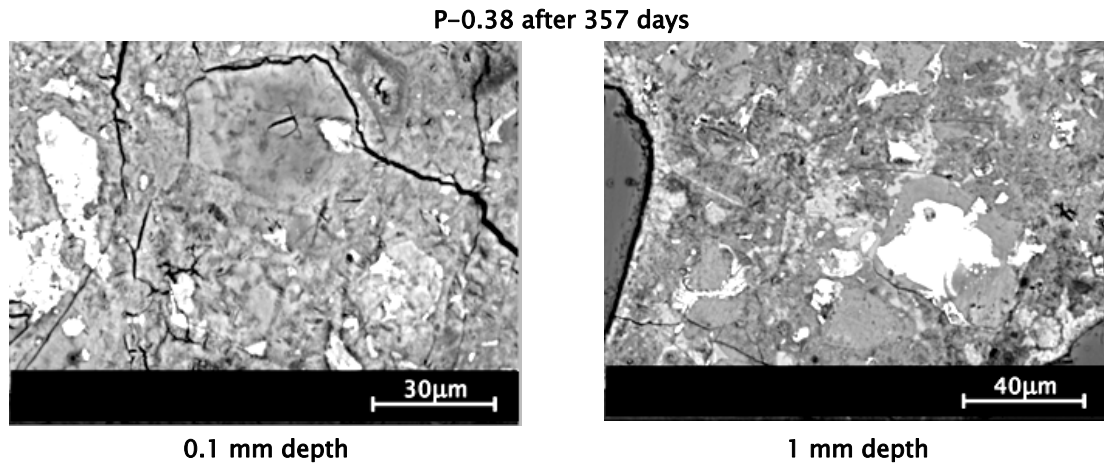


Fig. IV-45. BSE micrographs of inner C-S-H of P-0.38 after 357 days under ponding in Na_2SO_4 solution.

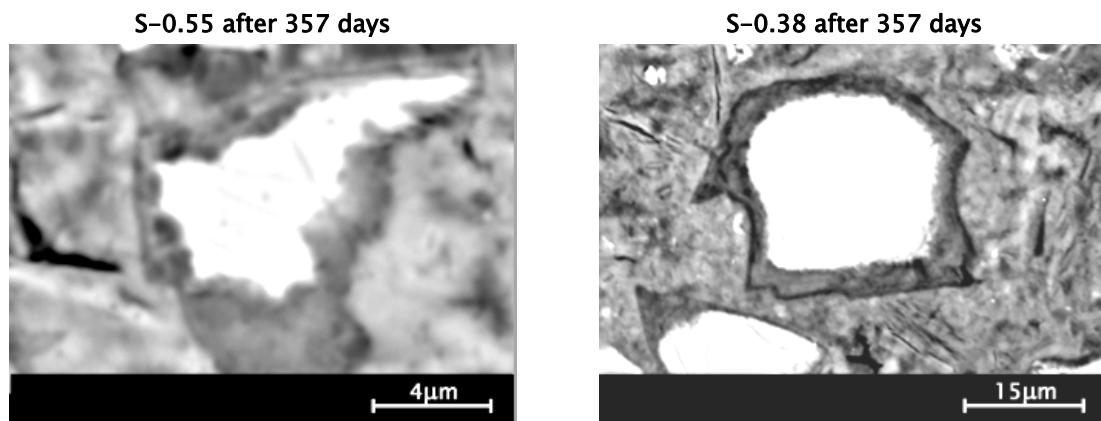


Fig. IV-46. BSE micrographs of slag grain with hydration rim at 0.5 mm depth in S-0.55 (right) and S-0.38 (left) after 357 days under ponding in Na_2SO_4 solution.

The high level of slag replacement (70 wt.-%) in S-0.55 and S-0.38 implies that the mechanical behaviour of the micro-concretes is governed by the properties of the slag and its hydration products. It appears that S-0.55 and S-0.38 slag and its hydration rim do not suffer cracking (Fig. IV-46) on the contrary to the inner C-S-H of P-0.55 for instance. Nevertheless the hydration rim of the slag grains in the surface shows darker zones of lower density that could be a sign for leaching. The absence of macroscopic damage of the slag blends in ponding exposure might be related to the fact that slag inner hydration products are not physically affected by sulfates in ponding exposure as inner C-S-H is.

IV.3.1.D. SUMMARY

Sulfate ingress is not restricted to the outer C-S-H but does concern also the inner hydration products (inner C-S-H and slag hydration rim). Sulfate combination to the hydration products could cause a swelling at the origin of the expansion. Relationships were shown between expansion and sulfate combination to the outer and inner C-S-H for the PCs and to the slag hydration product for the slag blends. This was underlined by micro-cracking observations at the interface of the outer and inner hydrates. It is however not clear which one of the outer or inner hydrates would dominate the expansion.

Nevertheless, sulfate ingress in the hydrates may stabilise some phases that can have a link with expansion.

IV.4. SUMMARY

IV.4.1. RELEVANCE OF TECHNIQUES

It has been emphasized that expansion cannot be taken as sole criterion for damage due to sulfate attack in ponding exposure. Furthermore, the elastic properties have shown a very good reliability for evaluation of damage due to sulfate attack. The normalised dynamic elastic moduli revealed to be a precise tool for the samples ranking in terms of performances against sulfate exposure in ponding.

SEM-EDS quantitative analyses present the advantage over XRD to localize the phase formations in the microstructure. But SEM preparation and acquisition is more time consuming.

IV.4.2. PROPOSED MECHANISM OF DAMAGE

Both C-S-H phases are combining sulfate and both present fine ettringite formation. It remains unclear which one of the C-S-H phases predominates in the expansion process. Nevertheless a mechanism can be proposed based on the observation from P-0.55 in ponding (Fig. IV-47):

- stage #1 – *induction* –
 - sulfate combination to the outer and inner C-S-H causes a swelling of the C-S-H phases;
 - sulfate combination to the outer and inner C-S-H reaches saturation and fine ettringite precipitates accompanied by micro-cracking of the inner C-S-H.

- stage #2 – *surface damage* –
 - coarse ettringite starts to precipitate in the free spaces in the inner C-S-H without causing cracking;
 - sulfate combination to the outer C-S-H becomes predominant;
 - fine ettringite precipitates in the outer C-S-H causing an accelerated expansion with cracking of the cementitious matrix.

- stage #3 – *bulk damage* –
 - coarse ettringite precipitation in the developed cracks;
 - the developed cracks penetrate deeper in the material promoting a large ion transport through the opened microstructure;
 - the massive sulfate intrusion can combine to deeper outer and inner C-S-H up to ettringite saturation feeding the increased expansion.

However, gypsum formation was found to be at the origin of the surface softening of the micro-concretes under ponding exposure.

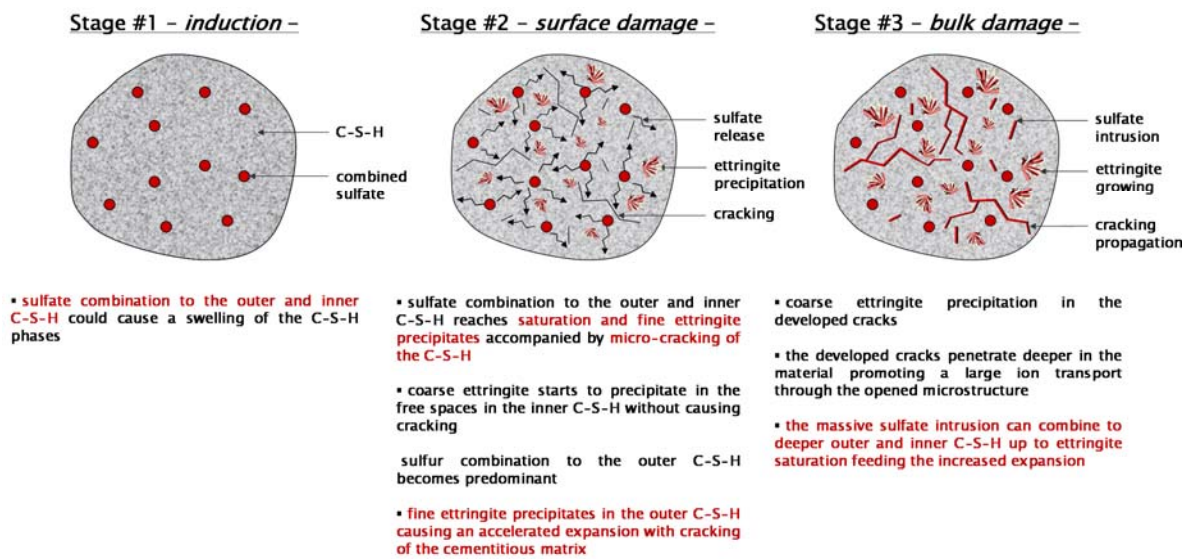


Fig. IV-47. Proposed mechanism of expansion in three stages as depicted for P-0.55 under ponding exposure.

IV.4.3. EFFECT OF W/B-RATIO

The w/b-ratio does not control the transport of the ions through the cementitious matrix.

The w/b-ratio does not affect the phase assemblages qualitatively (same phases formed) but quantitatively. Reduction of the w/b reduces the depth of chemical changes and the phase formation. Microstructures with lower w/b-ratio withstand better chemical and phase transformations maybe due to intrinsic better mechanical resistance.

The importance of the quantity and depth of the phase formed to be able to cause expansion is however underlined

IV.4.4. EFFECT OF SLAG ADDITION

Slag addition reduces the capillary porosity which consequently limits the sulfate ingress. Expansion is therefore prevented.

Slag causes a high decalcification of the inner C-S-H which makes free spaces for phases (e.g.; sulfate-bearing phases) to precipitate without causing any stress high enough to lead to expansion.

However, slag could in principle slow down ettringite formation due to monocarboaluminate stabilisation.



Chapter V – Effect of different testing conditions

This chapter evaluates the influence of different types of exposure conditions on the process of sulfate attack. The specimens were exposed to three types of exposure condition at $20.5\text{ °C} \pm 0.5$ in addition to the ponding described in the last chapter: pH-control, semi-immersion and wet/dry cycles.

The samples were studied with the same array of methods as presented for the case of ponding.

V.1. PH-CONTROL

V.1.1. MACROSCOPIC BEHAVIOUR

V.1.1.A. IONIC TRANSPORT

Leaching

The pH of the exposure solution of the pH-control tests was kept constant in the range of 7.5 compared to the pH in ponding raising 12.5. The normal distribution of the pH values measured in the exposure solutions of the PCs and of the slag blends were found to be respectively in the range of 7.3 ± 0.5 and 7.6 ± 0.4 (Fig. V-1).

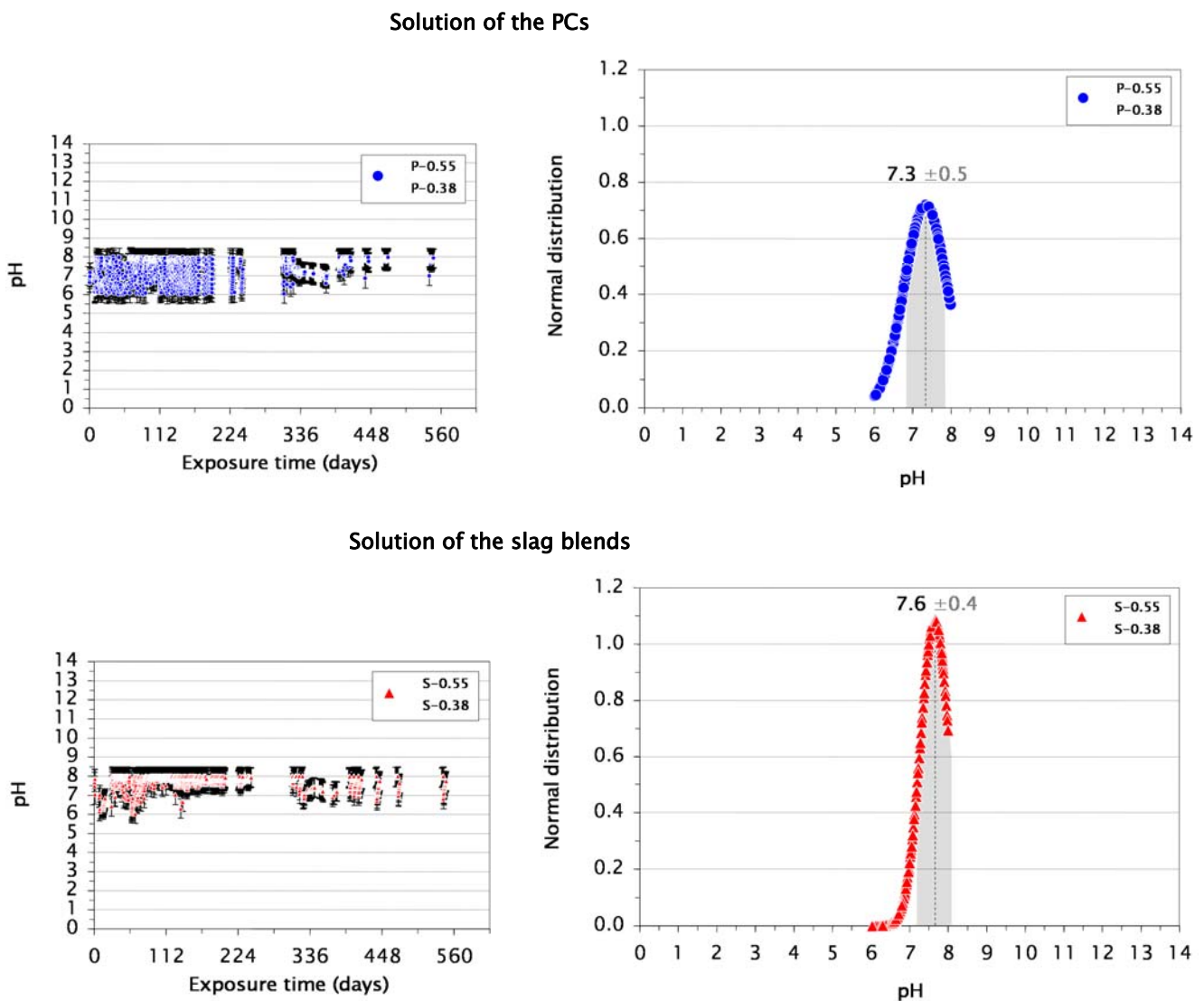


Fig. V-1. pH evolution of the pH-control exposure solutions.

Calcium leaching only occurs within the first 28 days of exposure for all the micro-concretes under pH-control (Fig. V-2). The calcium leached from the binders reaches $0.005 \text{ g.g}_{\text{binder}}^{-1} \pm 0.001$. The fact that the solution of the pH-control test is not renewed limits the portlandite dissolution to its solubility level.

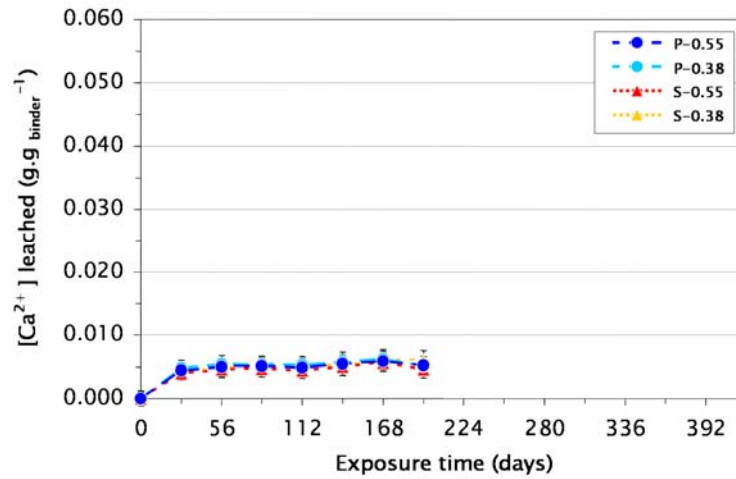


Fig. V-2. Evolution of calcium leaching from the laboratory micro-concretes under pH-control.

Sulfate ingress

The pH-control test has a pH titration system with a solution at 0.2 M of H_2SO_4 to influence as little as possible the initial sulfate concentration, which is of 2.017 g.l^{-1} for the 3 g.l^{-1} Na_2SO_4 solution employed for the exposure. The fluctuations of the sulfate concentration is slightly higher in the case of pH-control compared to ponding within one month and one year of exposure but values remain close to the initial concentration to an acceptable range (Table V-1). As a consequence, the sulfate concentration in the exposure solution is kept constant and cannot be of any indication on the sulfate combination in the micro-concretes.

Table V-1. Sulfate concentration evolution of the solutions of the ponding and pH-control tests.

Setting	Exposed sample	[SO ₄ ²⁻] (g.l ⁻¹)			Δ [SO ₄ ²⁻] (g.l ⁻¹)	
		Before exposure	After 28 days of exposure	After 392 days of exposure	After 28 days of exposure	After 392 days of exposure
Ponding	P-0.55	2.017	1.741	2.028	±0.138	±0.005
	P-0.38	2.017	1.822	2.034	±0.098	±0.008
	S-0.55	2.017	1.998	1.897	±0.009	±0.060
	S-0.38	2.017	2.023	1.873	±0.003	±0.072
pH-control	P-0.55	2.017	1.856	1.928	±0.080	±0.044
	P-0.38	2.017	1.844	1.967	±0.087	±0.025
	S-0.55	2.017	1.847	1.956	±0.085	±0.030
	S-0.38	2.017	2.024	1.816	±0.004	±0.100

V.1.1.B. PHYSICAL CHANGES

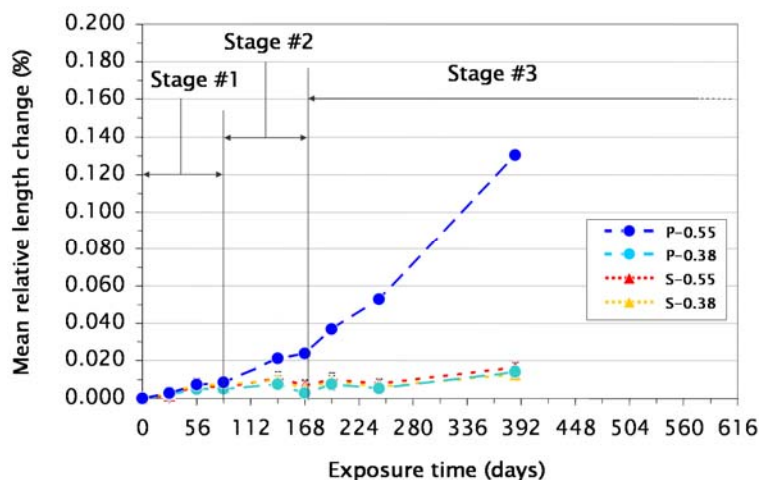
Expansion

Fig. V-3. Length evolution of the laboratory micro-concretes under pH-control exposure.

During the 392 days of exposure in pH-control, only P-0.55 showed significant expansion, as was the case for ponding exposure over 560 days of exposure (Fig. V-3). Moreover, as its homologue in ponding, P-0.55 in pH-control revealed a three-stage expansion behaviour characterised by: a first induction period prior to significant expansion, then a first linear increase in length of rate $2.0 \cdot 10^{-4} \text{ \%} \cdot \text{days}^{-1}$ starting after 84 days and up to 168 days, followed by a second quicker linear stage with a higher rate of $3.3 \cdot 10^{-4} \text{ \%} \cdot \text{days}^{-1}$ takes place. The ratio in expansion rates is close to two (1.7) but not so

high as encountered for ponding. Due to the reduced exposure time for this test there is a lack of data concerning the expansion behaviour between 386 and 560 days needed to be fully comparable with ponding exposure. Nevertheless, it appears clearly that pH-control accelerates the expansion of P-0.55 which expands in the same manner as in ponding but with an advance in the range of 84 and 56 days respectively for stage #2 and stage #3. From 273 days of exposure the three other mixes seem to start to expand as well, which corresponds to an advance in the range of 56 days compared to their homologues in ponding.

Plotting the expansion under pH-control against the expansion under ponding (Fig. V-4), it appears more clearly that expansion of P-0.55 in pH-control is of the same kind that in ponding but with an advance in time.

The exposure pH of 7.5 is relatively acid for concrete. This is below the range of stability for cementitious phases. Nevertheless, the lower stability of ettringite tends to contradict the hypothesis that ettringite alone is at the origin of expansion.

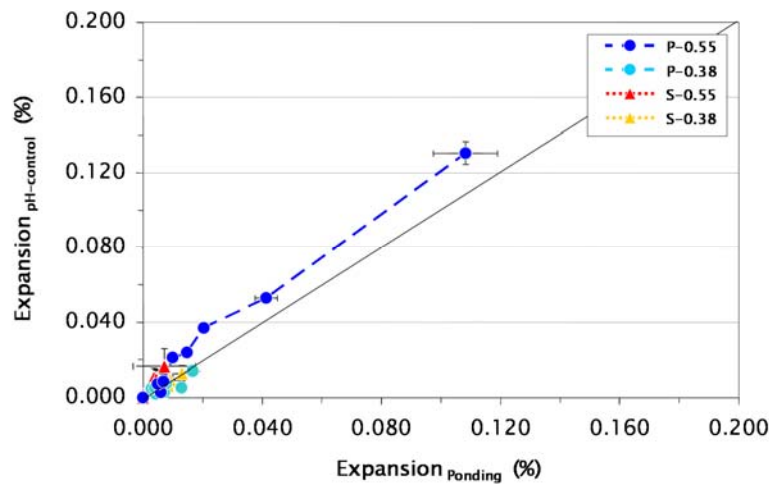


Fig. V-4. Expansion under pH-control versus expansion under ponding for the laboratory micro-concretes.

Mass change

The mass loss of the micro-concretes under pH-control is not significant (Fig. V-5) and is far from the three-stage behaviour encountered for the micro-concretes under ponding. This might be related to the reduced leaching under pH-control compared to ponding.

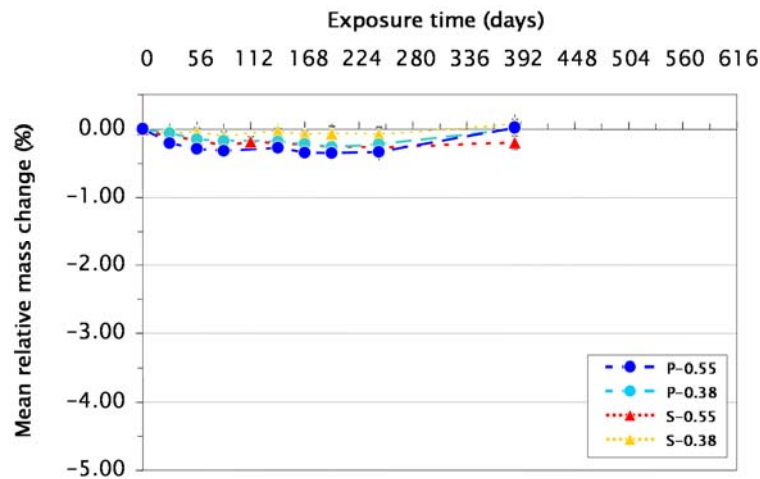


Fig. V-5. Mass evolution of the laboratory micro-concretes under pH-control.

Compressive strength

The normalised compressive strength evolution of the samples under pH-control revealed a significant decrease in mechanical properties only for P-0.55 (Fig. V-6). This decrease is in the range of the one observed for the same sample in ponding. The lack of measurement points does not allow any stages to be distinguished as seen for the expansion results. In principle, the same kind of behaviour as explained for ponding would be expected for pH-control at this stage of the exposure: P-0.55 suffers internal stresses due to expansion that damage the bulk of the sample without causing any surface damage. The other three mixes do not present internal stresses high enough to affect their bulk mechanical properties nor their surface cohesion.

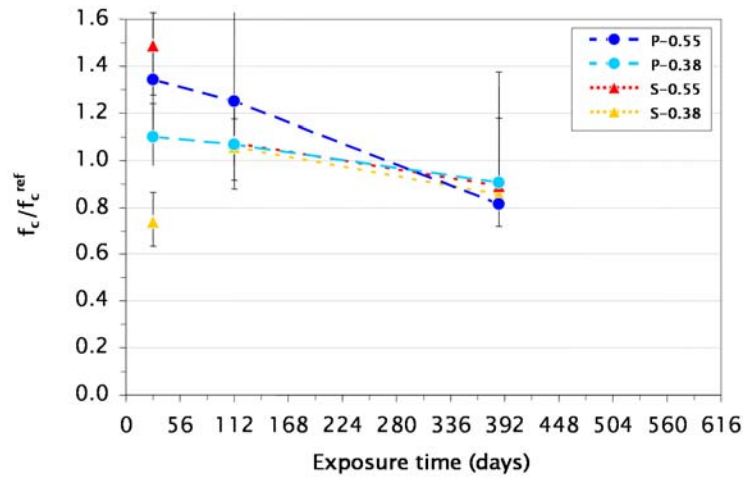


Fig. V-6. Normalised compressive strength evolution of the laboratory micro-concretes under pH-control.

Dynamic elastic modulus

From the normalised flexural dynamic elastic modulus evolution of the micro-concretes under pH-control, it appeared that only the two PCs revealed significant loss in properties (Fig. V-7) in contrast to ponding where the slag blends also showed a decrease of elastic and shear moduli. This is surprising since it has been already pointed out that pH-control exposure seems to accelerate the damage process compared to ponding exposure. Nevertheless, it could be a sign that slag and slag hydrates withstand better low pH conditions than cement and its hydrates.

No three-stage behaviour is identifiable as for expansion for P-0.55. Nevertheless, the relationships between normalised flexural dynamic elastic modulus and expansion (Fig. V-8) is linear for P-0.55 and tends to be linear for the other samples as seen for ponding exposure but with a lower correlation (R^2 lower). This emphasises that the same kind of damage processes might be involved in the samples subjected to pH-control than in the samples subjected to ponding.

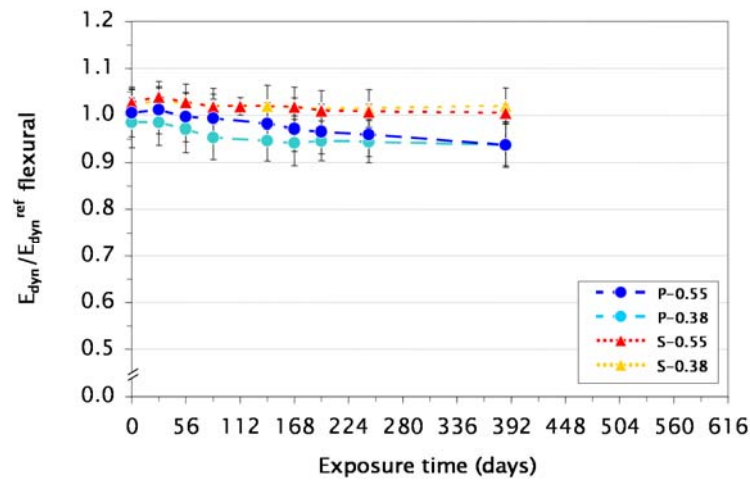


Fig. V-7. Normalised flexural dynamic elastic modulus evolution of the laboratory micro-concretes under pH-control.

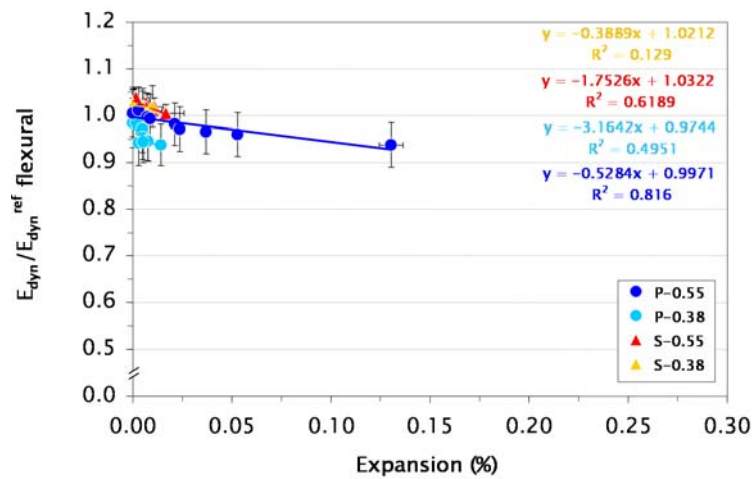


Fig. V-8. Relationship between the normalised flexural dynamic elastic modulus and the expansion of the laboratory micro-concretes under pH-control.

V.1.2. DAMAGE AND CRACKING

V.1.2.A. EXTERNAL APPEARANCE



Fig. V-9. Visual appearance of P-0.55 after 386 days of exposure under pH-control.

In appearance, only P-0.55 was macroscopically affected by the exposure, showing a slight surface disintegration (Fig. V-9) comparable to that observed in ponding.

V.1.2.B. MICRO-CRACKING

The laboratory micro-concretes under pH-control present the same kind of microstructure state than the one in ponding (Fig. V-10). P-0.55 seems to undergo comparable cracking of its cement paste with gaps around aggregates. The two PCs show signs of surface material loss. After 112 days of exposure in pH-control, the two slag blends reveal a marked leaching zone of depth comparable to that observed on the slag blends after 357 days in ponding. This leaching zone is already observed on the slag blends after 28 days of exposure, which may be a sign that leaching occurs very quickly in pH-control but does not develop over exposure time.

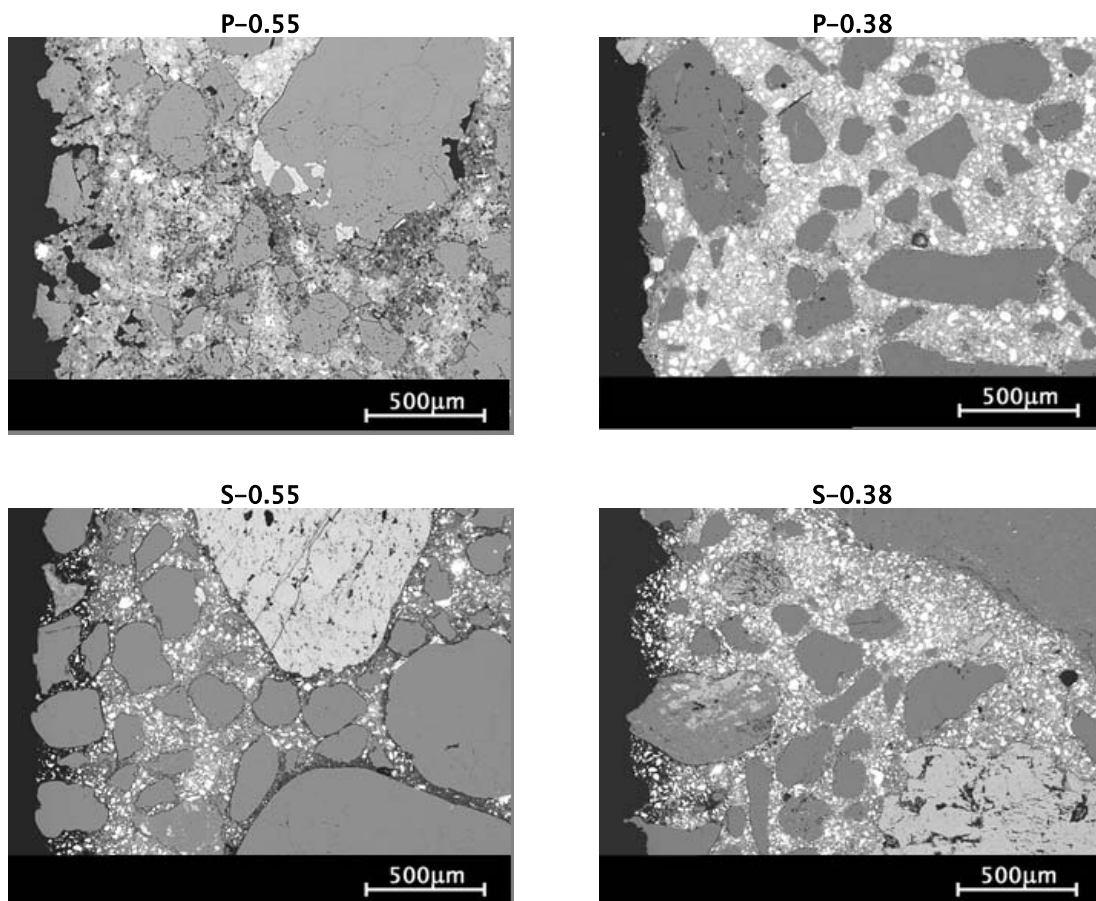


Fig. V-10. Crack patterns from BSE micrographs of the laboratory micro-concretes after 112 days of exposure under pH-control.

V.1.3. STUDY OF THE MICROSTRUCTURE

V.1.3.A. IONIC PROFILE

Leaching

The calcium profiles of the micro-concretes under pH-control exposure (Fig. V-11) reveal the same kind of leaching behaviours as observed in ponding. The PCs are characterised by a progressive leaching while the slag blends present a step by step leaching.

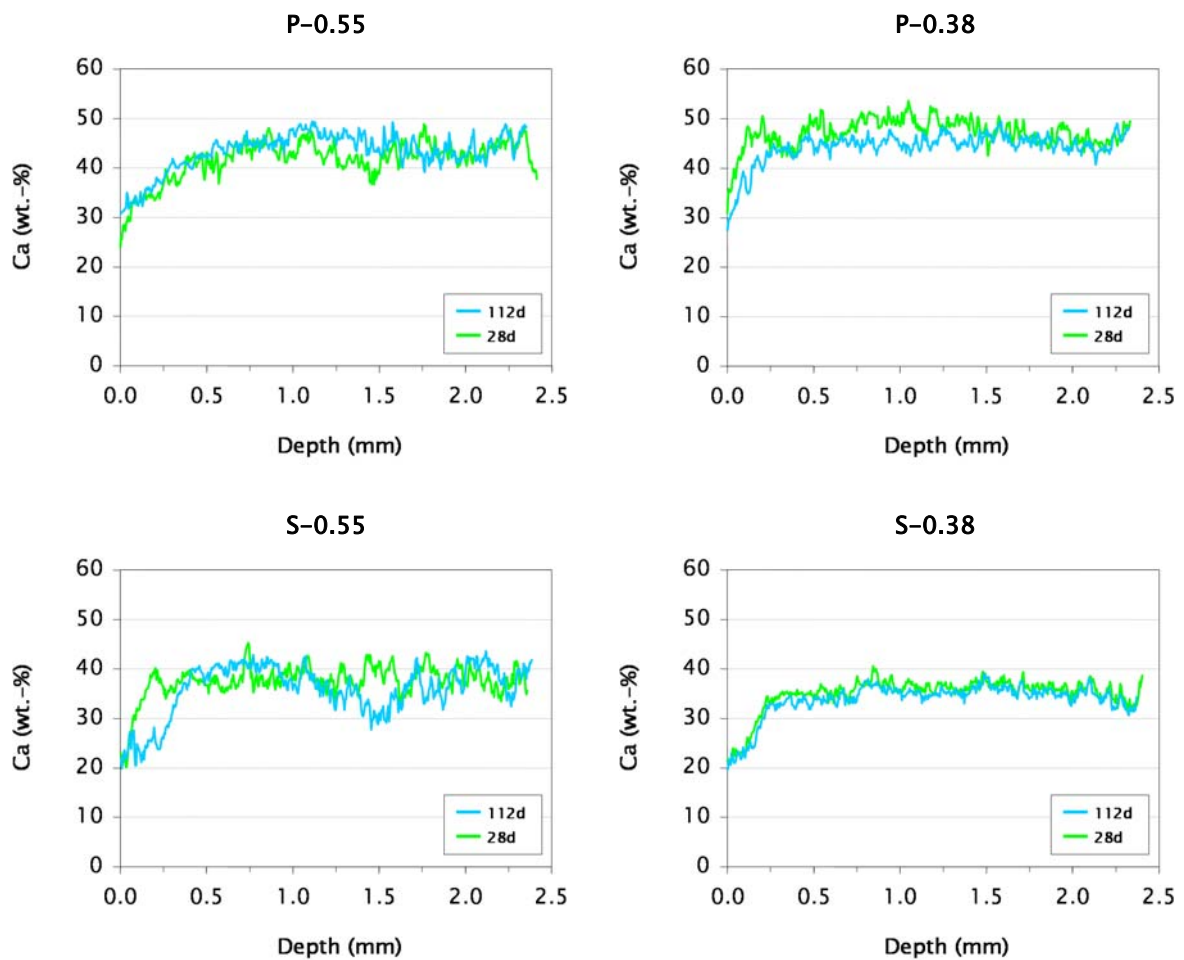


Fig. V-11. Evolution of calcium leaching from the cementitious matrix of the laboratory micro-concretes under pH-control.

Sulfate ingress

The pH-control condition enhances sulfate ingress in the micro-concretes compared to ponding (Fig. V-12). This is particularly true for the PCs while the slag blends seem not to be much sensitive to the low pH. This could be due to the fact that in the pH-control exposure no depletion of sulfate occurs on the contrary to the other tests. Slag addition seems to reduce sulfate ingress as was observed in ponding. It is worth noting that the sulfur profile of P-0.38 is much narrower than that of P-0.55, which confirms previous statements, made in the case of exposure under ponding, that the reduced w/c-ratio limits the ingress of sulfate to the very top surface of the material.

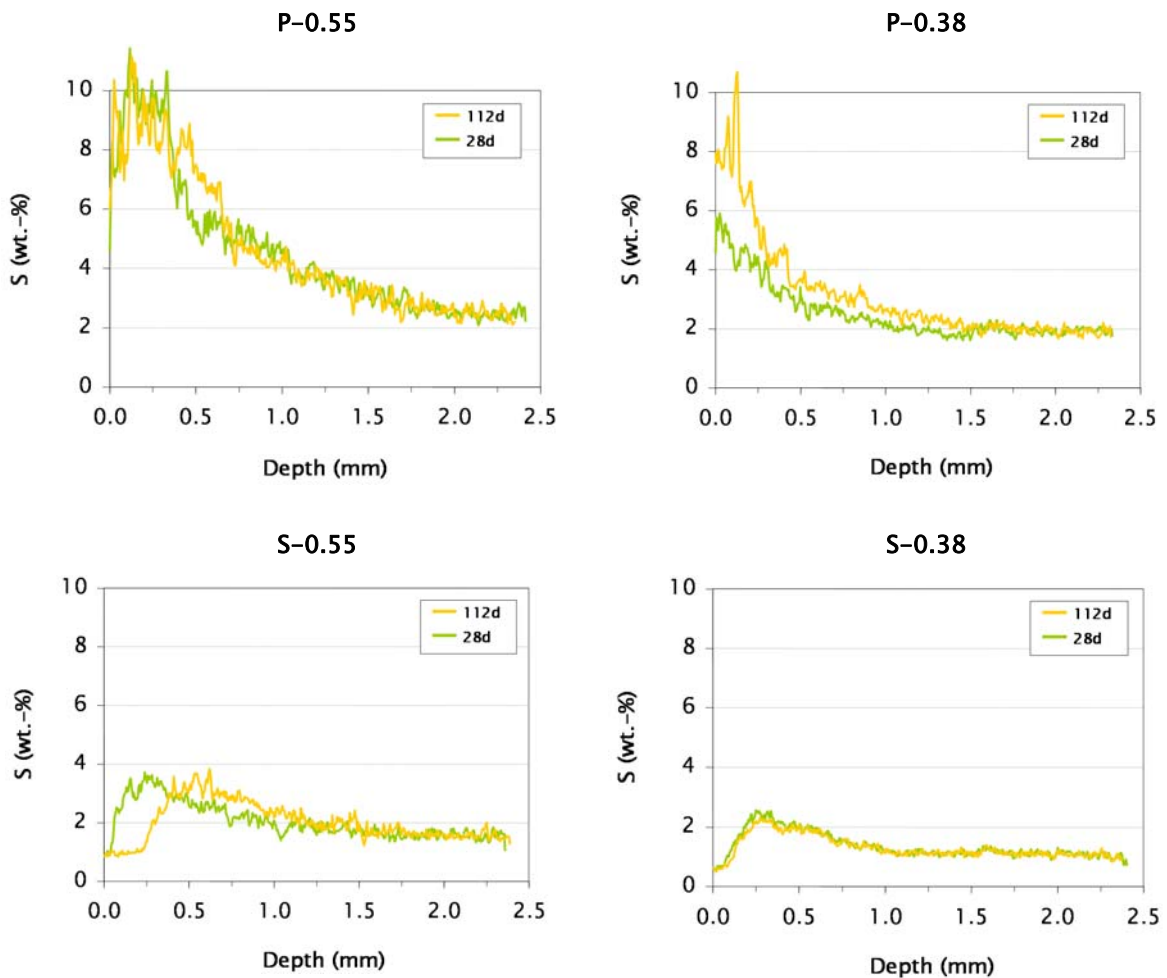


Fig. V-12. Evolution of sulfate ingress in the cementitious matrix of the laboratory micro-concretes under pH-control.

V.1.3.B. PHASE ASSEMBLAGE ZONATION AND IMPACTS ON THE MICROSTRUCTURE

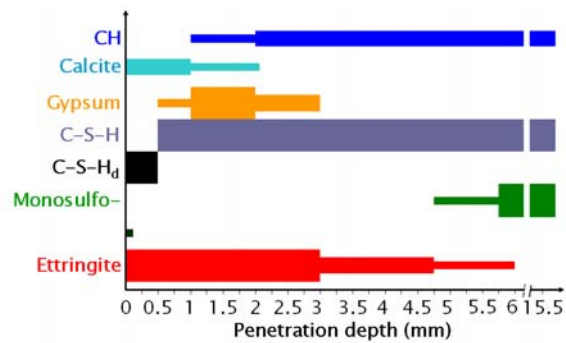


Fig. V-13. Phase assemblage zonation of P-0.55 after 386 days of exposure under pH-control.

After one year of exposure, the phase assemblage of P-0.55 under pH-control is pretty similar, in terms of phases in presence and their depths of formation, to that developed under ponding after the same time of exposure. This tends to indicate that the start of the exposure is accelerated in the case of pH-control but not the entire exposure.

In addition, the S/Si atomic ratio in the outer and the inner C-S-H of P-0.55 under pH-control reaches after 112 days of exposure the same saturation value as observed after 119 days under ponding in the range of respectively 0.27 ± 0.01 for the outer and 0.21 ± 0.01 for the inner.

The damage encountered under pH-control must be comparable to that encountered under ponding.

V.2. SEMI-IMMERSION

V.2.1. MACROSCOPIC BEHAVIOUR

V.2.1.A. IONIC TRANSPORT

Leaching

The pH of the solution of the semi-immersion test followed a cyclic evolution according to the monthly solution renewal frequency, as observed for the ponding test in the previous chapter (§ IV.1.1.A).

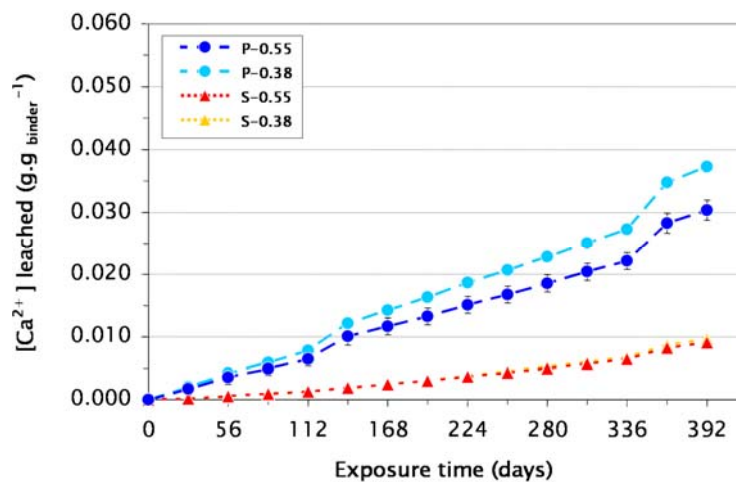


Fig. V-14. Evolution of calcium leaching from the laboratory micro-concretes under semi-immersion.

The calcium leaching evolution deduced from regular exposure solution measurements has been calculated taking into account only the submerged part of the micro-concretes (Fig. V-14). A direct comparison with the ponding case can be done since the same ratio between the volume of solution and the volume of prisms submerged in the solution was maintained. It appears that for all the samples the values remained below that calculated for ponding. This indicates that the calcium leaching has been reduced in the semi-immersion setting. The contact with the air in this setting let the samples carbonate both in the air exposed part and in the submerged part (§ AAppendix B). The calcite formed due to carbonation might be too stable so that further calcium leaching is limited. Apparently the air exposed part does not play any role in the calcium leaching process.

Sulfate ingress

On the same principle as for calcium leaching, the sulfate combination to the samples in semi-immersion has been calculated taking into account only the submerged part of the prisms (Fig.V-15). It appears that the sulfate combination is stronger for the Portland blends in semi-immersion than in ponding. This might be understood as the air exposed part of the prisms may play a role in the ion exchange and combine sulfate. Considering the slag blends, the sulfate combination appeared reduced compared to the ponding case. Their air exposed part might not be affected in such by ion transport. Capillary suction is therefore only expected for the Portland blends and not for the slag blends.

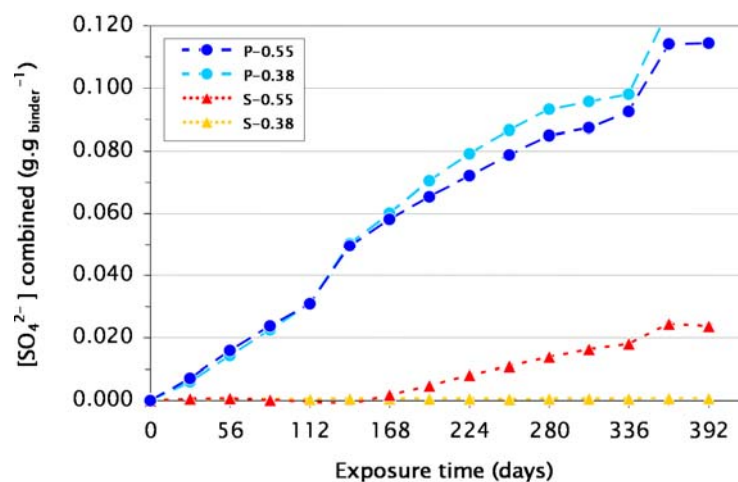


Fig.V-15. Evolution of sulfate combination from exposure solution to the laboratory micro-concretes under semi-immersion.

V.2.1.B. PHYSICAL CHANGES

Expansion

The measurements of the length change of the samples in semi-immersion revealed a shrinkage within the first 56 days of exposure without further large expansion (Fig. V-16). A slight increase in length can be seen after 161 days of exposure for the PCs micro-concretes but this is not large enough to confirm deleterious expansion. The two slag blends remain stable regarding their length after the first stage of shrinkage. This shrinkage behaviour has been verified by a repeat series of semi-immersion tests. This shrinkage behaviour can be explained by the water evaporation from the half of the samples that is in the air. The samples have been fully immersed in a lime saturated

solution during 28 days of curing prior to exposure and are therefore saturated at the start of semi-immersion exposure. The half of the prisms in the air losses its capillary water during the first 56 days of exposure.

As in ponding, only the two PCs seem to show any sign of expansion while the two slag blends show no signs of expansion. The expansions observed in semi-immersion are nevertheless less than half than the ones observed in ponding. Semi-immersion cannot be seen as a semi-ponding in terms of expansion behaviour. This relative reduced expansion may be influenced by carbonation of the surface of the samples in their submerged part that creates a barrier for sulfate to ingress. Indeed, on the contrary to the other test settings where contact with the air is limited, the semi-immersion test implies a large air contact surface and CO_2 from the air can dissolve in the exposure solution and carbonate the submerged surface of the samples.

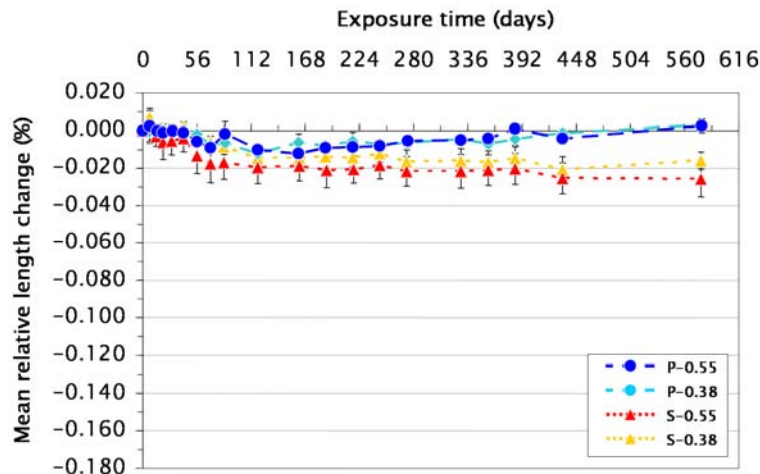


Fig. V-16. Length evolution of the laboratory micro-concretes under semi-immersion.

Mass change

The mass loss of the micro-concretes in semi-immersion is not very significant (Fig. V-17). Nevertheless, the samples present the particularity to start losing mass after 56 days of exposure. This is comparable to the time during which the air exposed part of the samples is desaturating as seen from shrinkage behaviour occurring during these first 56 days of exposure. The fact that no mass loss before 56 days of exposure is to be seen may be explained looking at the reference samples stored in lime water that showed mass gain within the first 70 days after the start of exposure that had been attributed to an uptake of water to compensate the continued hydration. The drying and the water uptake

effect would therefore be in competition during the first part of exposure where water uptake would be the strongest and after which the desaturation effect would become observable.

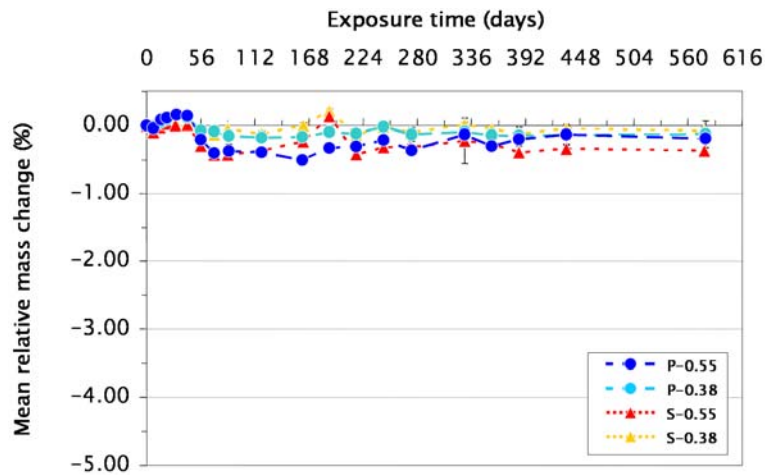


Fig. V-17. Mass evolution of the laboratory micro-concretes under semi-immersion.

Compressive strength

Compressive strengths of the samples in semi-immersion were not measured considering the non-symmetry of the sulfate attack phenomenon and the fact that those measurements were only done on remaining material after sampling for SEM analysis; sampling of semi-immersion exposed samples necessitates cutting the prism transversally.

Dynamic elastic modulus

In semi-immersion all the four mixes seemed to lose some of their elastic properties within the first 56 days of exposure after which they remain stable (Fig. V-18). This is to be correlated to the shrinkage due to drying of the air exposed part of the samples occurring within the first 56 days of exposure. This loss in properties due to drying is particularly clear for S-0.55, which is in accordance with following observations made in the case of wet/dry cycles exposure where S-0.55 appeared to be the mix to perform the worst against drying cycles.

As will be seen subsequently this confirms the vulnerability of slag blends to drying.

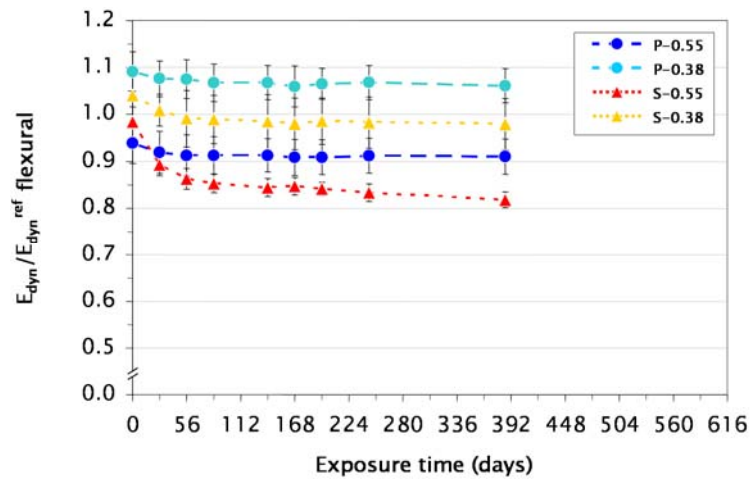


Fig. V-18. Normalised flexural dynamic elastic modulus evolution of the laboratory micro-concretes under semi-immersion.

V.2.2. DAMAGE AND CRACKING

V.2.2.A. EXTERNAL APPEARANCE

Semi-immersion



Fig. V-19. Typical visual appearance of the laboratory micro-concretes after 175 days of exposure in semi-immersion.

The samples in semi-immersion typically show a crystal efflorescence in the capillary suction zone (Fig. V-19). The crystal formed has been identified as thenardite by XRD. Repeated crystallisation of thenardite and mirabilite in such semi-immersion exposure due to local changes in the RH are known to be harmful for the material. There was however no sign of such damage in the semi-immersion samples.

V.2.2.B. MICRO-CRACKING

Microstructure state of the immersed part of the samples in semi-immersion is comparable to that observed in ponding with reduced cracking and leaching.

The crack patterns shown have been taken from the exposure zone where capillary suction phenomena take place, just above the solution line (Fig. V-20). The zone has been identified owing to sulfur mappings carried along the exposed surface (§ V.2.3.A). It seems that the slag blends suffer of stronger surface erosion than the PCs. Slight cracking of the microstructure of the PCs is nevertheless observable.

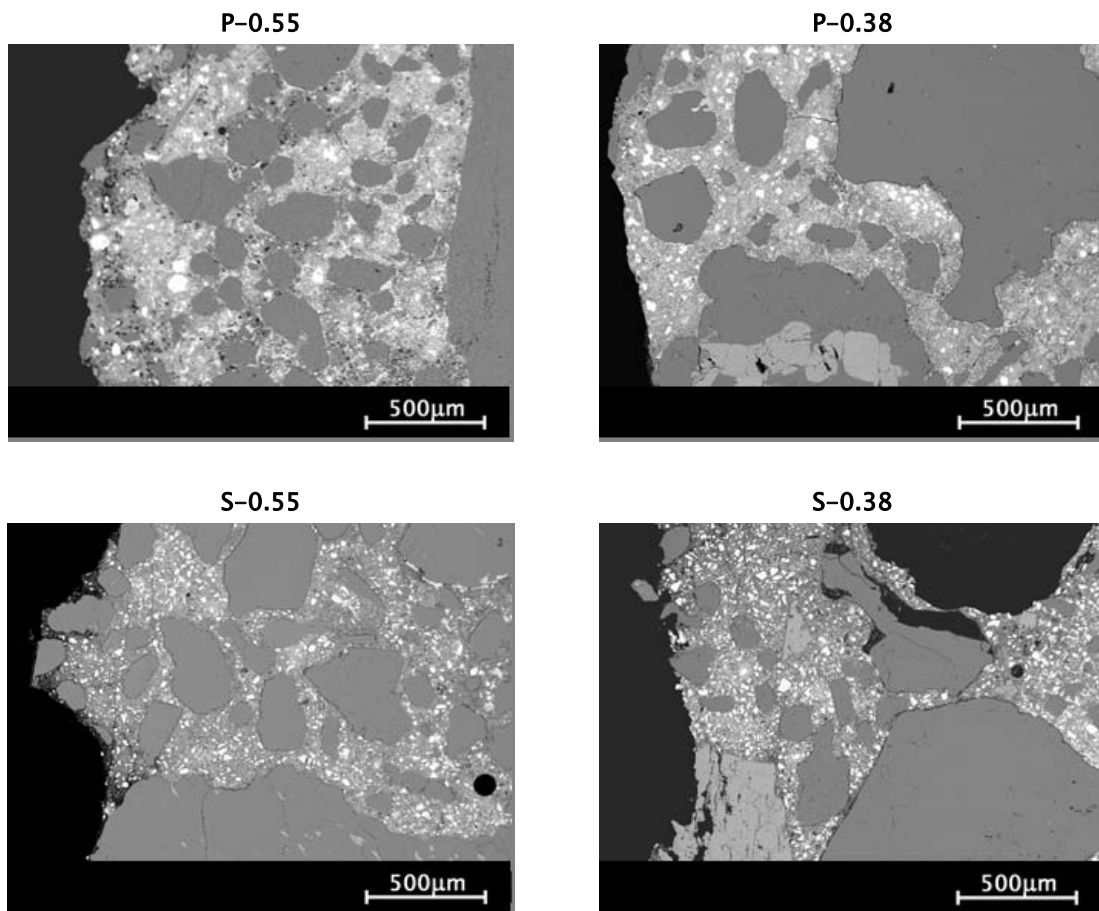


Fig. V-20. Crack patterns from BSE micrographs of the laboratory micro-concretes after 357 days of exposure under semi-immersion.

V.2.3. STUDY OF THE MICROSTRUCTURE

V.2.3.A. IONIC PROFILE

Leaching

Leaching in the submerged part of the micro-concretes in semi-immersion is similar to that occurring in ponding exposure (Fig. V-21). The emerged part shows also some leaching.

Sulfate ingress

The different sulfate ingress behaviours occurring in the submerged and in the emerged part of the micro-concretes in semi-immersion is observable matching the qualitative SEM sulfur mappings transversally to the exposure (Fig. V-22). The sulfur profiles calculated in the submerged and in the emerged part of the samples (Fig. V-37) confirm that capillary suction occurs in the air exposed part of the samples leading to sulfate suction in the zone above the immersion level without much leaching effect. The behaviour in the immersed zone is comparable to that in ponding exposure. In both parts of the samples the sulfate ingress was found to be more pronounced in the PCs than in the slag blends as suggested by the sulfate combination calculation (Fig.V-15) and as verified by the sulfur profiles (Fig. V-23).

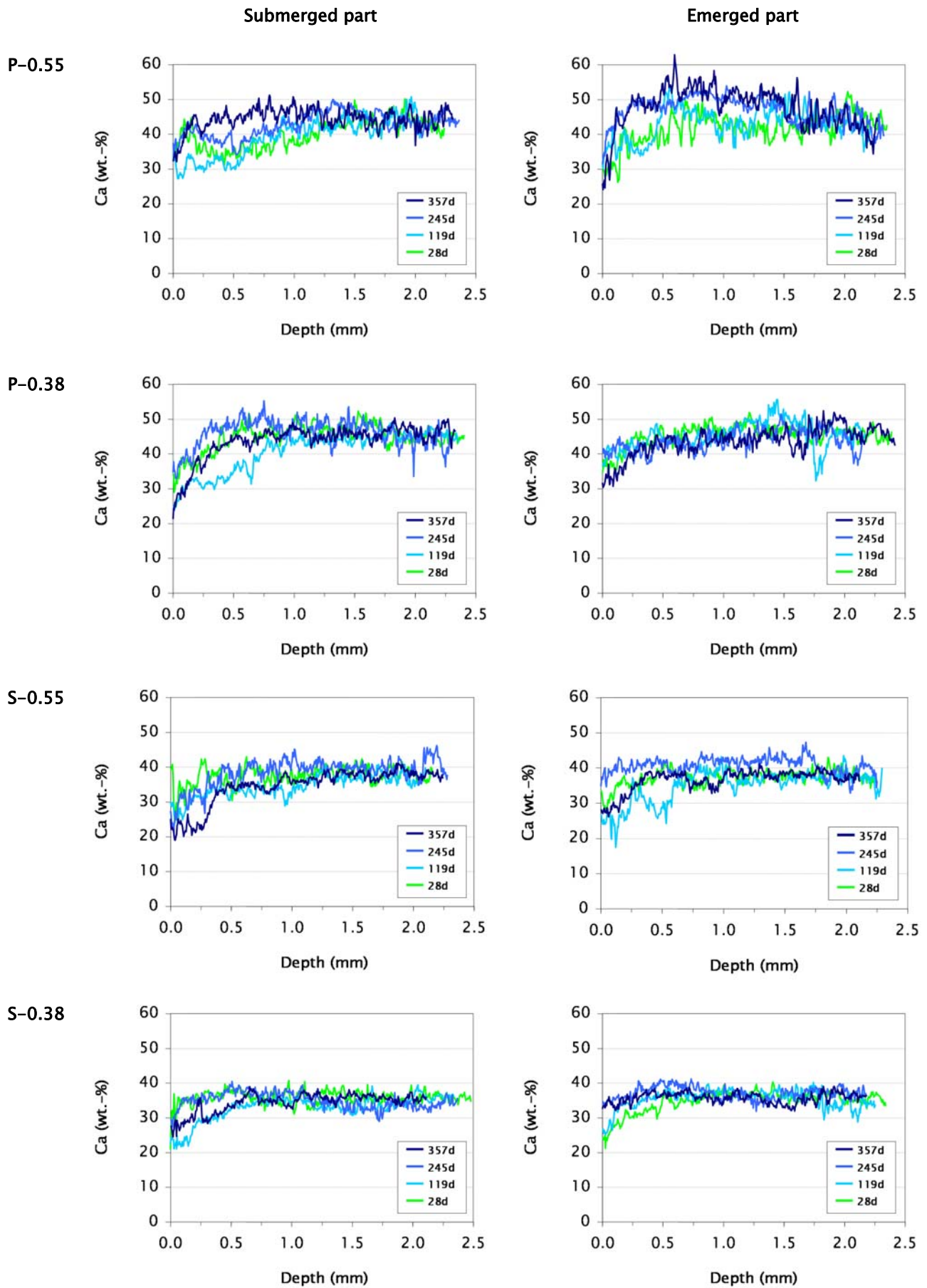


Fig. V-21. Evolution of calcium leaching from the cementitious matrix of the laboratory micro-concretes under semi-immersion exposure; submerged part (left) and emerged part (right).

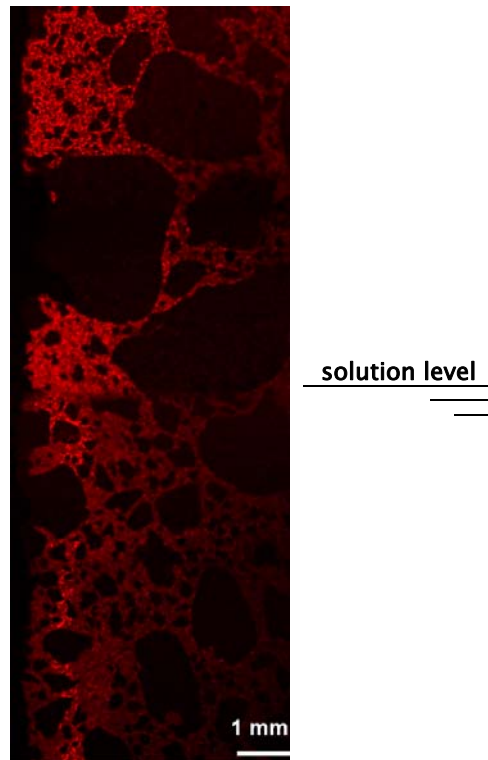


Fig. V-22. Qualitative SEM sulfur mapping of P-0.55 in semi-immersion.

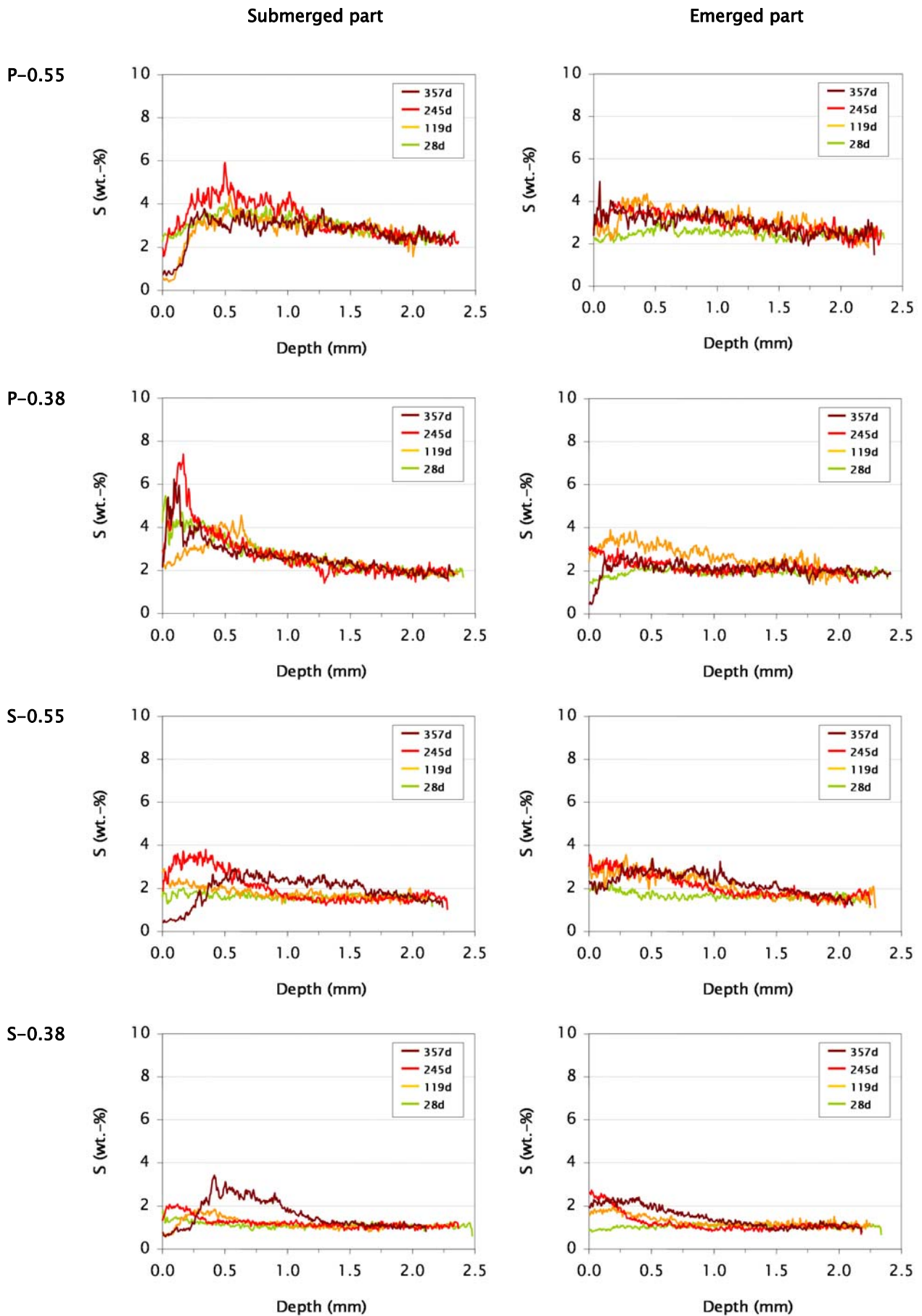


Fig. V-23. Evolution of sulfur profiles in the cementitious matrix of the laboratory micro-concretes under semi-immersion; submerged part (left) and emerged part (right).

V.2.3.B. PHASE ASSEMBLAGE ZONATION AND IMPACTS ON THE MICROSTRUCTURE

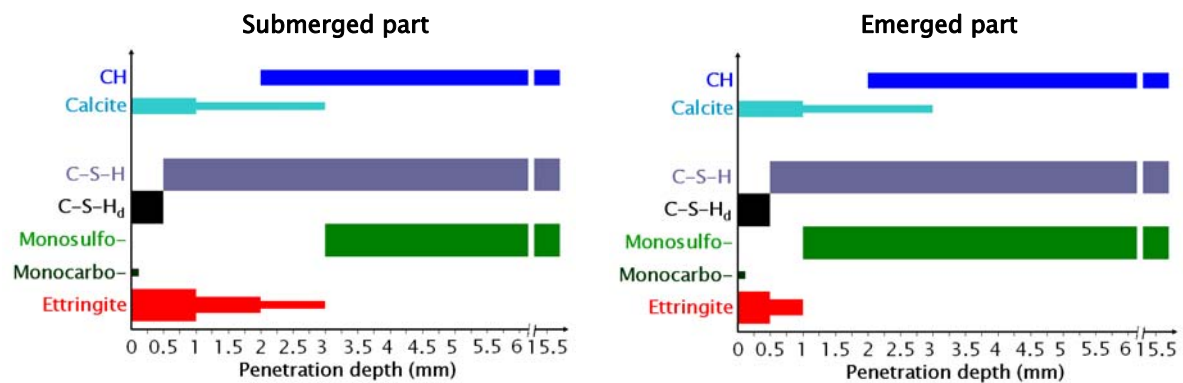


Fig. V-24. Phase assemblage zonation of the submerged part (left) and the air emerged (right) of P-0.55 after 357 days under semi-immersion; submerged part (left) and emerged part (right).

The phase assemblage in the immersed part seems close to that observed in ponding (Fig. V-24) with less deep ettringite formation probably due to carbonation that may prevent sulfate from penetrating. The air exposed part looks similar to the immersed part in terms of phase assemblage but with a much reduced and less deep ettringite formation. This is however particularly interesting that the sulfate penetrated by capillary suction in the emerged part of the samples may be enough to stabilise ettringite formation above the solution level.

In addition, the levels of sulfate combination to the C-S-H of P-0.55 reaches comparable values as observed in ponding, both in the submerged and emerged parts. After 245 days of exposure in semi-immersion, the S/Si atomic ratio of the outer C-S-H is brought in the submerged part to 0.23 ± 0.01 at 1 mm depth and goes down back to 0.12 ± 0.005 at 3 mm depth, while in the emerged part it is brought to 0.27 ± 0.01 at 0.05 mm depth and goes down back to 0.17 ± 0.005 at 1 mm depth. The saturation level of the CSH in sulfate seems to be reached both in the submerged and emerged parts but less deep inside the sample in the emerged part. The depth of sulfate combination into the C-S-H in the submerged part of P-0.55 in semi-immersion is comparable to that of P-0.55 in ponding after the same time of exposure. This may be a sign that expansion is indeed being initiated for P-0.55 in semi-immersion. The damage might not be visible due to a less deep change in the phase assemblage (i.e.; a less deep ettringite formation).

V.3. WET/DRY CYCLES

V.3.1. MACROSCOPIC BEHAVIOUR

V.3.1.A. IONIC TRANSPORT

Leaching

The pH of the solution of the wet/dry cycles test followed a cyclic evolution according to the monthly solution renewal frequency, as observed for the ponding test in the previous chapter (§ IV.1.1.A).

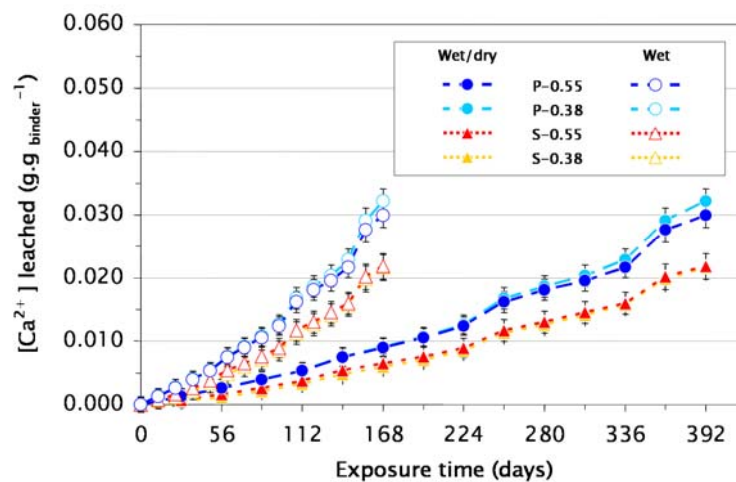


Fig. V-25. Evolution of calcium leaching from the laboratory micro-concretes under wet/dry cycles exposure.

The wet/dry cycles exposure is characterised by the alternation of wetting and drying cycles of respectively 3 and 4 days a week. One can consider the wetting and drying cycles in the whole and deduce from the calcium leaching evolution along exposure (Fig. V-25) that the wet/dry cycles setting reduces calcium leaching compared to the ponding exposure. This is appropriate in terms of prediction of structure service life. Nevertheless, one can consider the effective time in exposure to the solution during the wet phase of the wet/dry cycles and conclude that the wet/dry cycles setting enhances calcium leaching compared to the ponding exposure. This approach allows evaluating the effect of wet/dry cycles compared to ponding in terms of damage mechanism, which is the aim of the study.

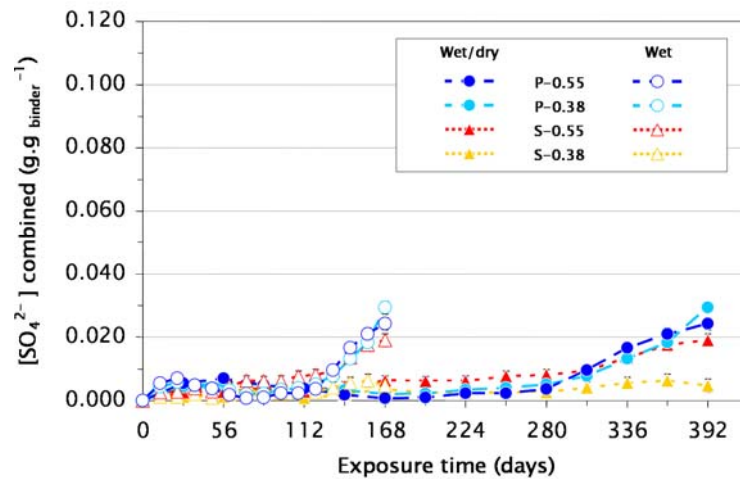
Sulfate ingress

Fig. V-26. Evolution of sulfate combination from exposure solution to the laboratory micro-concretes under wet/dry cycles exposure.

As exposed for calcium leaching, two approaches can be considered face to the wet/dry cycles exposure and its effect on sulfate combination (Fig. V-26). In terms of service life (overall time), the wet/dry cycles appear to delay the sulfate combination without having much effect on its rate. But in terms of mechanism (wet time), the wet/dry cycles do increase the rate of onset of sulfate combination. It is worth to note that S-0.55 combines sulfate in the same range than the two PCs P-0.55 and P-0.38, while the other slag blend S-0.38 does not seem to combine much sulfate. The delay observed before sulfate combination is characterised by a first slight sulfate combination followed by an almost complete release of the combined sulfate. In a first time, the sulfate might have penetrated the micro-concretes and crystallised in it, while the precipitated crystals might have dissolved in a second time. Admitting a progressive degradation of the micro-concretes, the available surface area may increase over exposure time and enable higher sulfate combination.

V.3.1.B. PHYSICAL CHANGES

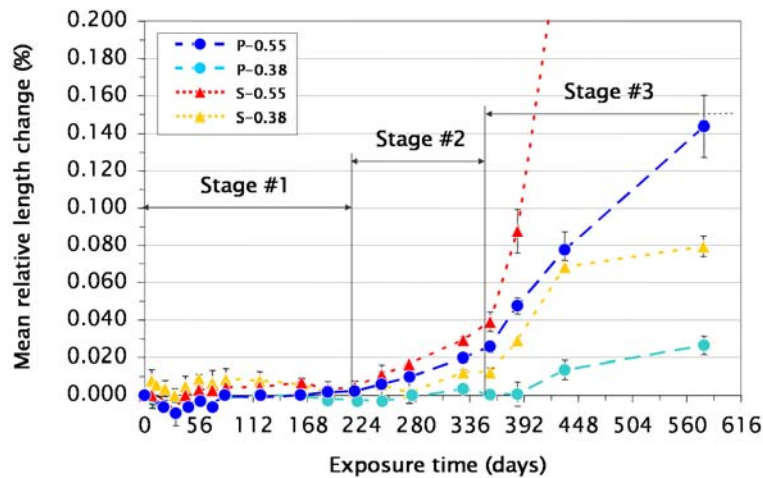
Expansion

Fig. V-27. Length evolution of the laboratory micro-concretes under wet/dry cycles.

Under wet/dry cycles the PCs showed expansion, in a comparable range as for ponding and faster if only wet time considered, but interestingly the slag blends appeared to be very sensitive to wet/dry cycles regarding expansion (Fig. V-27). The expansion of P-0.55 and S-0.55 seems to show a three-stage behaviour with the same start and end times: induction stage #1 up to 217 days, slow expansion stage #2 from 217 to 357 days and quick expansion stage #3 after 357 days. The times of the start of the different stages are similar as for ponding but with a delay of 56 days for stage #2 and 28 days for stage #3. These delays could be explained by the fact that the samples in wet/dry cycles are in contact with the exposure solution for less of the time than in ponding. Indeed, the micro-concretes are 1.75 times less in immersion to the exposure solution under wet/dry cycles than under ponding. The start of the expansion of P-0.55 under wet/dry cycles occurs after 217 days of exposure corresponding to 124 days after effective exposure to the solution, which is in the range of expansion start of P-0.55 after 161 days under ponding. Additionally, slight fluctuations are to be seen for all samples during the first stage where the induction period prior to expansion probably alternates with shrinkage due to drying. The rates of expansion of P-0.55 and S-0.55 are respectively of $1.7 \cdot 10^{-4} \text{ \%} \cdot \text{days}^{-1}$ and $2.6 \cdot 10^{-4} \text{ \%} \cdot \text{days}^{-1}$ during stage #2 and of $5.3 \cdot 10^{-4} \text{ \%} \cdot \text{days}^{-1}$ and $2.9 \cdot 10^{-3} \text{ \%} \cdot \text{days}^{-1}$ during stage #3. The ratios between the expansion rates in the two different stages are in the range of three for P-0.55 (comparable to the ratio of two and half for P-0.55 in ponding) and eleven for S-0.55. P-0.38 seems to enter stage #2 after 385 days of exposure (220 wet days), which is delayed compared to the start of expansion

detected after 168 days in ponding. Similarly to S-0.55 compared to P-0.55 behaviour in wet/dry cycles, S-0.38 show a higher degree of expansion than P-0.38. S-0.38 seems to enter stage #2 after 357 days of exposure, which is in the same range as P-0.38. S-0.38 seems however to enter a stage #3 of expansion after 434 days of exposure where expansion seems to stop. This later stage #3 seems to be representative of the material behaviour regarding the low scatter of the measurements but would need to be checked by further study. It is difficult to conclude in the case of P-0.38 concerning such a stage #3 since a reduced rate of expansion after 434 days of exposure is not clearly evident.

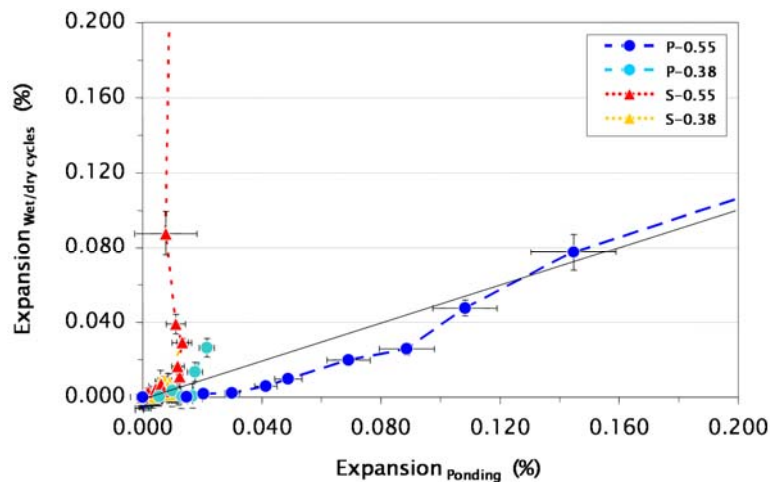


Fig. V-28. Expansion under wet/dry cycles versus expansion under ponding for the laboratory micro-concretes.

In conclusion, the slag blends are highly sensitive to wet/dry cycles with respect to expansion, while the behaviour of the PCs is comparable to their behaviour in ponding (Fig. V-28). This is particularly true for the samples with w/b of 0.55 (P-0.55 and S-0.55) since sorption would be more rapid due to the higher connectivity of the capillary pore network. The relationship between the expansions of P-0.55 in ponding and wet/dry cycles follows the $x = 1.75 \cdot y$ regression line, that takes into account the reduced exposure time in wet/dry cycles compared to ponding, especially after cracking occurs.

Considering the high slag replacement level (70 wt.-%), the behaviour of the slag blends is expected to be dominated by slag and its hydrates. It seems that the microstructure of the slag blends has a poor behaviour under wet/dry cycles. Thus, slag and slag hydrate must stand bad against drying and their microstructure might be irreversibly affected.

Mass change

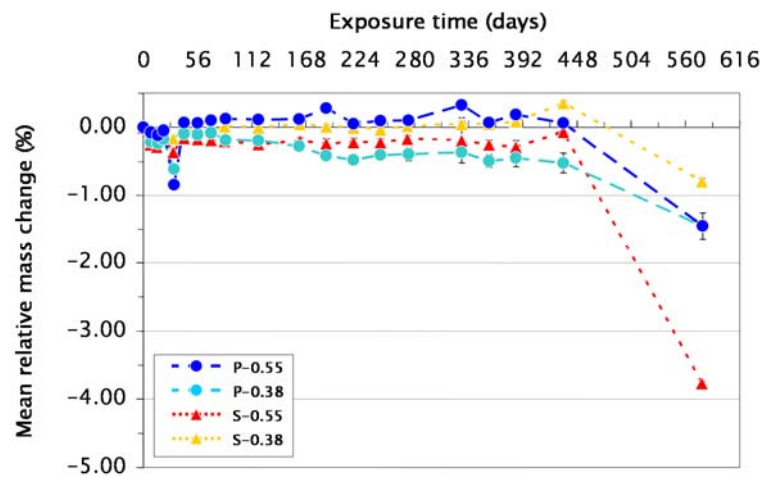


Fig. V-29. Mass evolution of the laboratory micro-concretes under wet/dry cycles.

Under wet/dry cycles, all samples show similar behaviour with respect to mass change: no significant loss during the first 434 days of exposure followed by a sudden abrupt decrease in mass (Fig. V-29). This mass loss reaches 3.8 % for S-0.55 after 577 days of exposure and is therefore likely to be related to material loss due to extensive cracking from the high expansion rather than to leaching as was the case for P-0.55 in ponding. This is supported by the macroscopic appearance of the samples which shows spalling, especially of S-0.55, rather than surface softening as observed in ponding particularly for P-0.55. For the two PCs P-0.55 and P-0.38, the mass loss remains in the range of 1 % as observed in ponding after 578 days of exposure and could therefore be related to leaching as well as to material loss. The abrupt mass loss is particularly surprising for S-0.38 since it revealed a stop in expansion precisely after 434 days of exposure. This might nevertheless indicate that stresses developed by expansion created a massive cracking that caused the abrupt mass loss and release the expansive stresses preventing the sample from further expansion. The representation of the mass loss against expansion (Fig. V-30) underlines the discontinuous behaviour for the slag blends while the behaviour of the PCs remain more similar to the continuous one observed in ponding. The microstructure of the slag blends is clearly damaged by the wet/dry cycles.

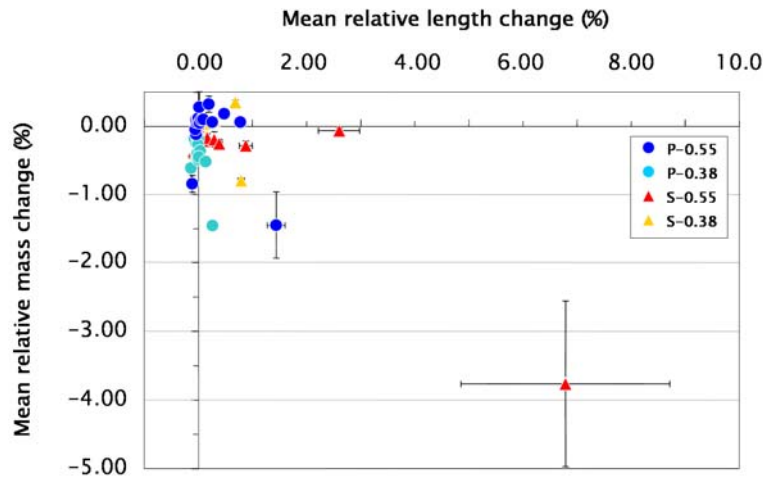


Fig. V-30. Relationship between length and mass changes of the laboratory micro-concretes under wet/dry cycles.

Compressive strength

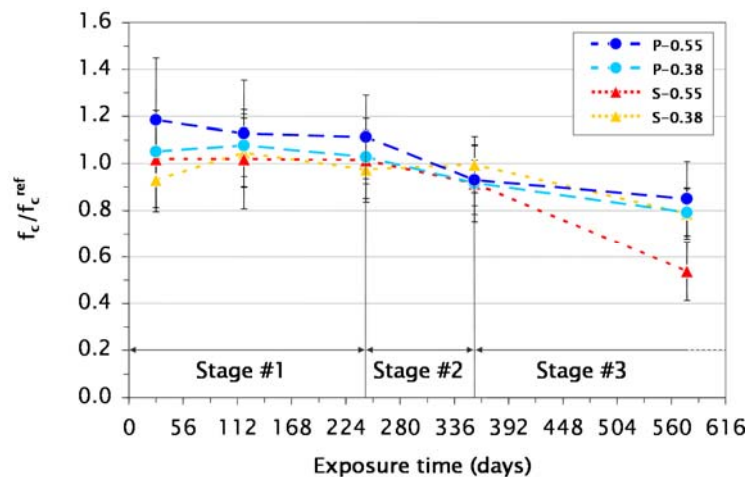


Fig. V-31. Normalised compressive strength evolution of the laboratory micro-concretes under wet/dry cycles.

The compressive strengths evolution of the samples under wet/dry cycles revealed the fact that damage in the four samples does not occur abruptly as seen from mass loss but develops progressively during exposure (Fig. V-31). This underlines the fact that stresses during expansion were high enough at any stage of the expansion to damage the bulk of the samples. S-0.55 encountered the highest loss in mechanical performance but no three-stage behaviour can be identified as for expansion. Nevertheless, the rate of strength loss seems to increase with time. The three other mixes evolve in the same range of compressive strength loss which points out that to different expansion behaviours correspond the same kind of mechanical properties loss. A three-stage behaviour is identifiable for P-0.55 similarly to what has been observed in ponding with start and end

times of the stages corresponding to the one observed for the expansion of P-0.55 in wet/dry cycles. This would indicate that the PCs suffer similar kind of damage in wet/dry cycles and in ponding while the slag blends suffer a specific damage process when placed under wet/dry cycles.

Dynamic elastic modulus

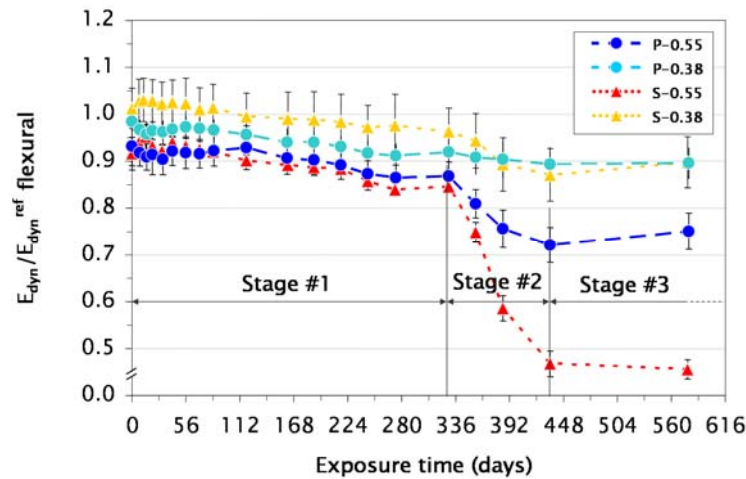


Fig. V-32. Normalised flexural dynamic elastic modulus evolution of the laboratory micro-concretes under wet/dry cycles.

Results from normalised flexural elastic modulus evolution of the laboratory micro-concretes under wet/dry cycles clearly revealed a particular behaviour specific to this exposure condition (Fig. V-32). All the four samples showed a linear decrease of their elastic properties from the start of exposure up to 357 days, the time of the start of stage #3 for the expansion of S-0.55, P-0.55 and S-0.38 and start of stage #2 for the expansion of P-0.38. Then a high reduction of the elastic properties is observable for all the samples up to 434 days after which the performance remains constant corresponding to the reduced expansion observed for all the samples. The clear delineation of behaviour again shows the usefulness of this technique in following the damage behaviour and in ranking the samples. The abrupt changes in the behaviour of the elastic properties is in agreement with the sudden expansion and mass loss previously observed. The last stage where no change in elastic properties is observed (and there is no further expansion) occurs exactly at the time when abrupt mass loss is measured. This supports the hypothesis that stresses developed during expansion are relaxed by the mass loss and the remaining stresses in the material are not sufficient to continue expansion.

Relationship between normalised flexural dynamic elastic modulus and expansion of the micro-concretes underlines this different damage mechanism observed in wet/dry cycles compared to ponding (Fig. V-33). Also the ranking of the samples exposed to wet/dry cycles is clear: S-0.55 performs the worst, followed by P-0.55, then S-0.38 and finally P-0.38. This ranking highlights the vulnerability of slag blends to changes in humidity.

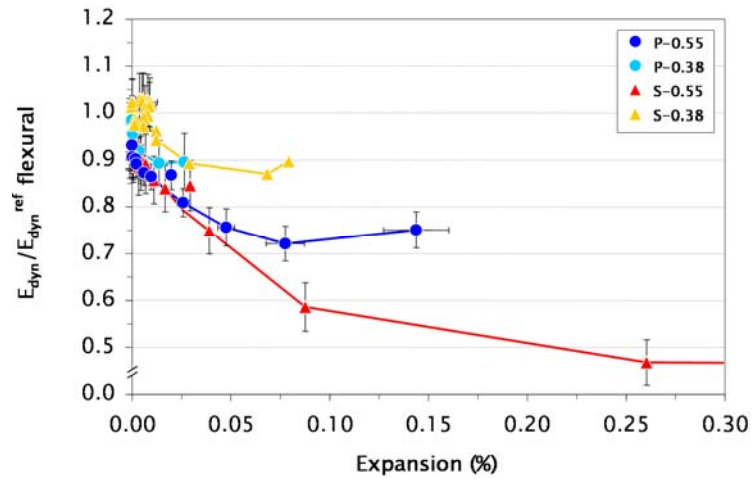


Fig. V-33. Relationship between the normalised flexural dynamic elastic modulus and the expansion of the laboratory micro-concretes under wet/dry cycles.

V.3.2. DAMAGE AND CRACKING

V.3.2.A. EXTERNAL APPEARANCE

All the samples exposed to wet/dry cycles revealed some signs of macroscopic damage (Fig. V-34). The PCs edges appeared eroded. S-0.55 showed severe surface cracking and loss of corners while the other slag blend S-0.38 did not show much damage.

As for ponding test, carbonation of the micro-concretes has been checked with phenolphthalein. No significant carbonation could be identified and photographs are reported in appendix (Appendix B).

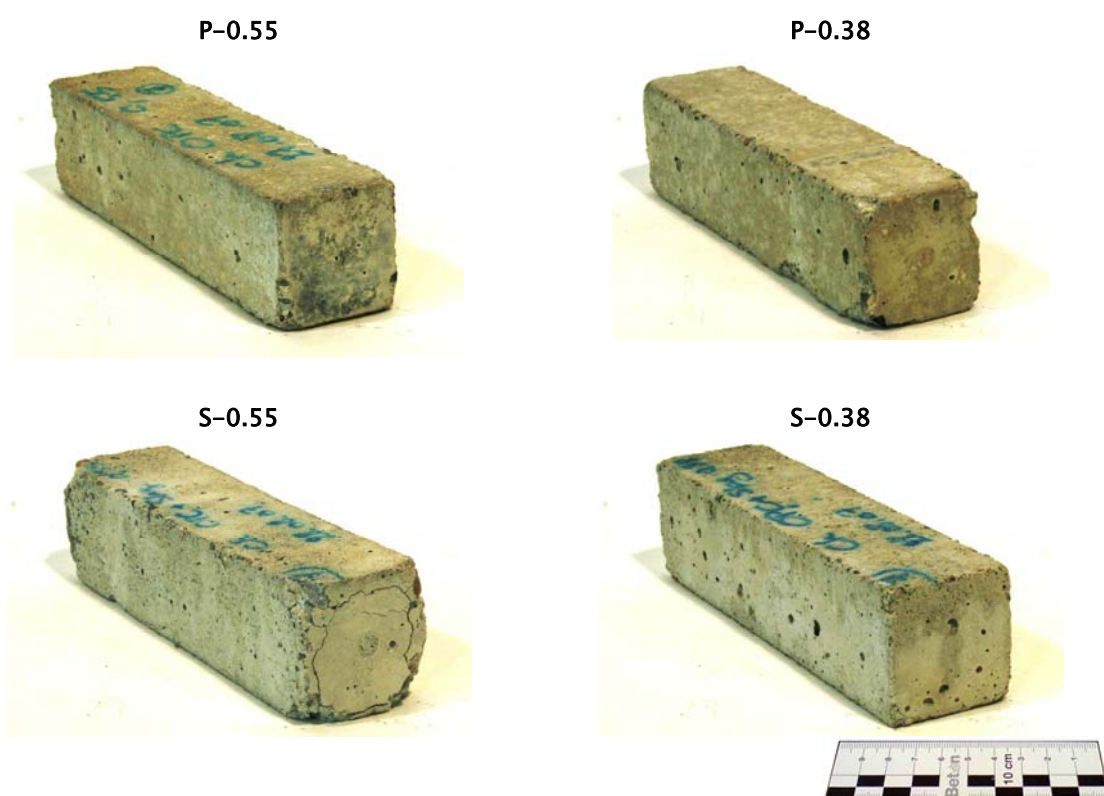


Fig. V-34. Visual appearance of the laboratory micro-concretes after 577 days of exposure in wet/dry cycles.

V.3.2.B. MICRO-CRACKING

In the wet/dry cycles, P-0.55 and S-0.55 show the most severe damage characterised by a progressive leaching with dense cracking developing at late stage (Fig. V-35). The start of the cracking seems to correspond to the start of expansion. Cracking appears particularly pronounced for S-0.55 which is also the one to expand the most. S-0.38 revealed similar damage with less cracking while P-0.38 only started to show slight cracking around the aggregates after 357 days of exposure.

P-0.55

S-0.55

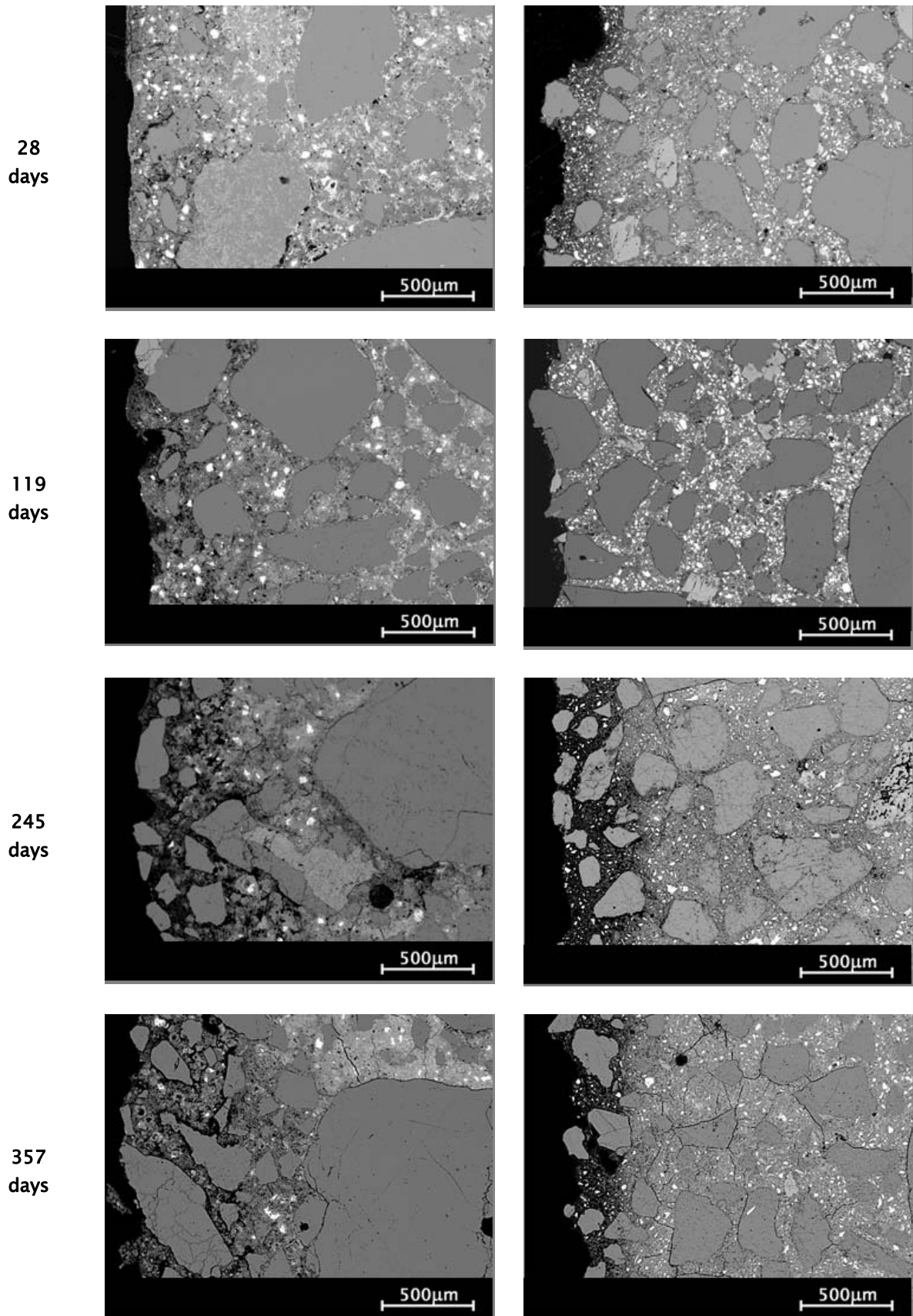


Fig. V-35. Crack patterns from BSE micrographs of P-0.55 and S-0.55 after 28, 119, 245 and 357 days of exposure in wet-dry cycles

V.3.3. STUDY OF THE MICROSTRUCTURE

V.3.3.A. IONIC PROFILE

Leaching

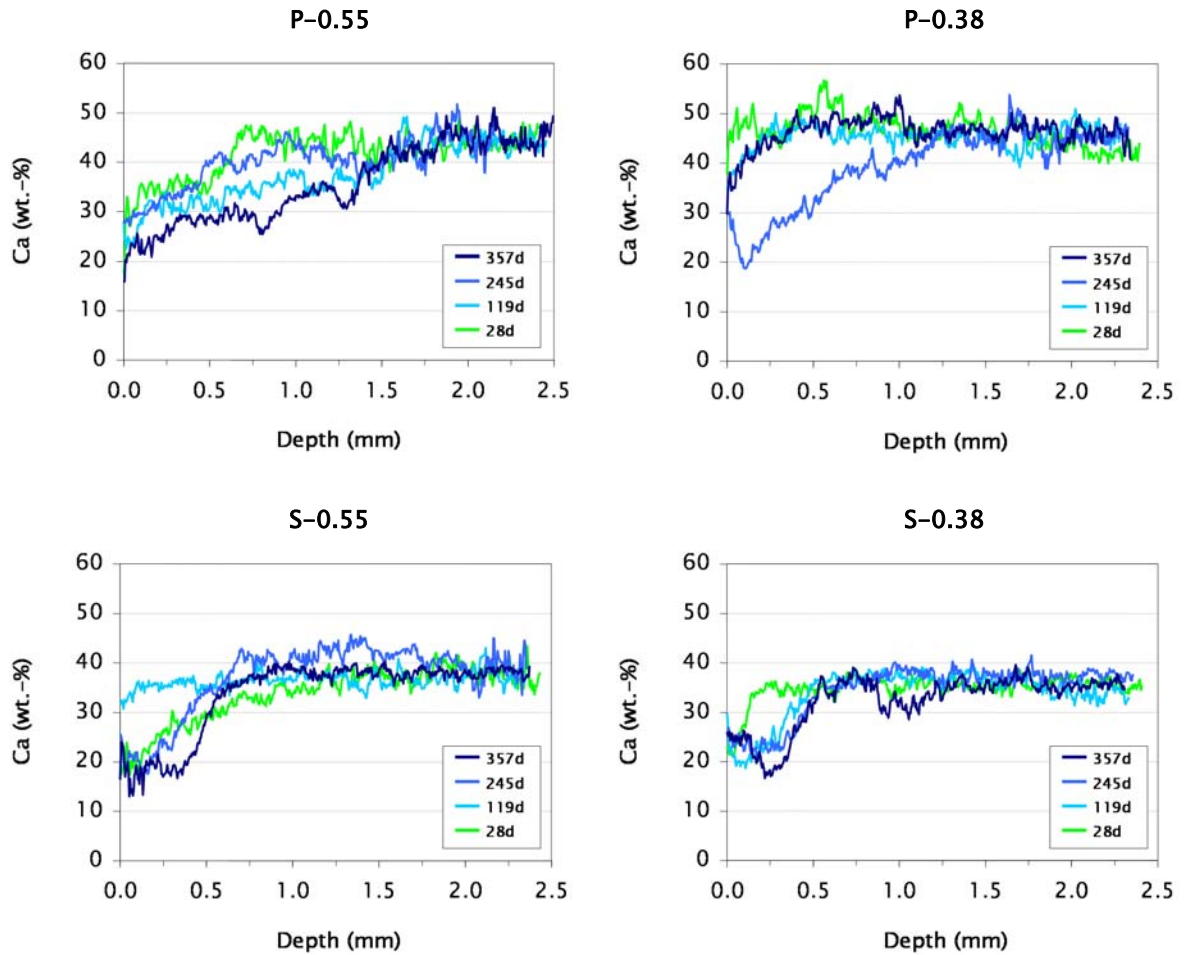


Fig. V-36. Evolution of calcium leaching from the cementitious matrix of the laboratory micro-concretes under wet/dry exposure.

Calcium leaching of the micro-concretes is enhanced under wet/dry cycles compared to ponding (Fig. V-36).

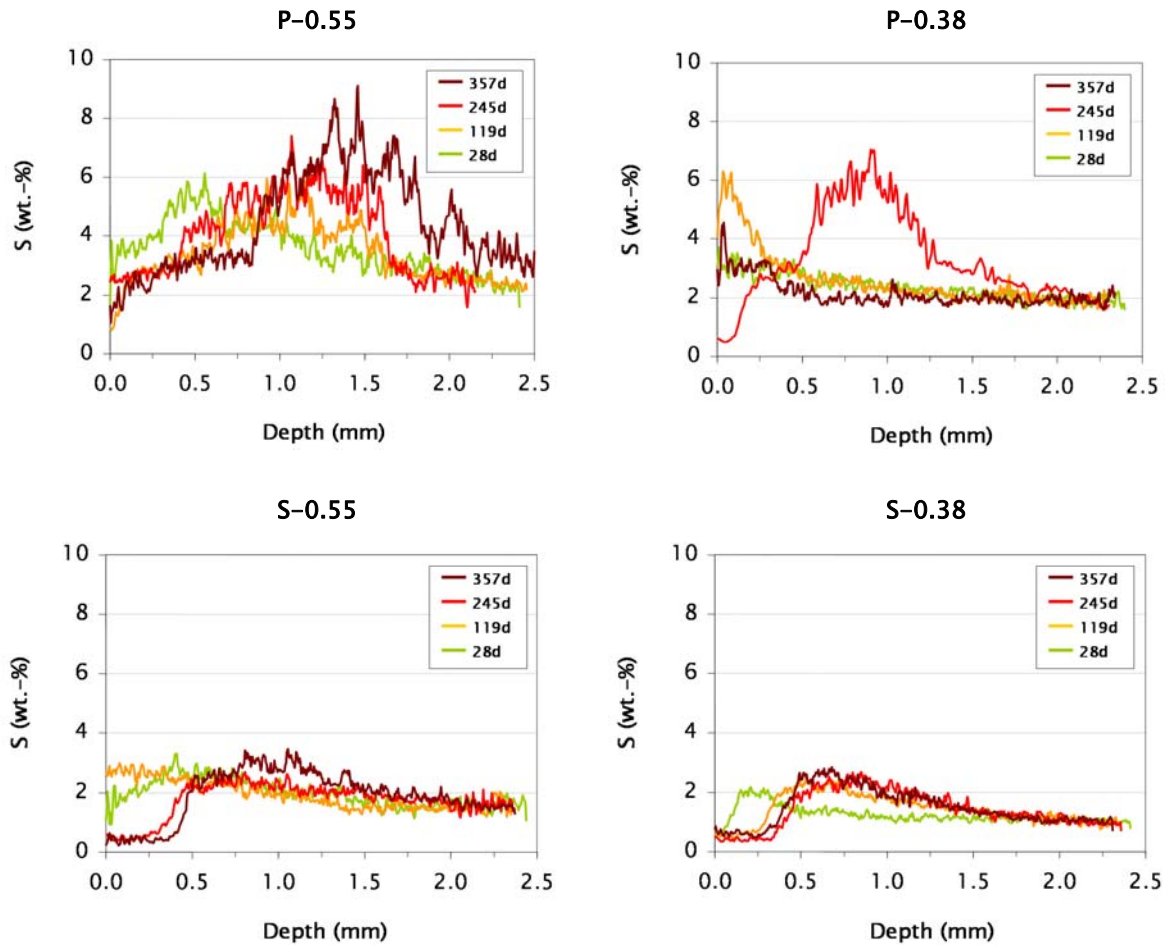
Sulfate ingress

Fig. V-37. Evolution of sulfur profiles in the cementitious matrix of the laboratory micro-concretes under wet/dry cycles.

The sulfur profiles of the micro-concretes under wet/dry cycles (Fig. V-37) reveal a reduced sulfate ingress for P-0.55 while the other samples and especially the slag blends show comparable profiles as observed in ponding. Nevertheless, sulfate penetrate deeper with the wet/dry cycles. It is worth noting that the previous observation made for ponding that the slag blends showed reduced sulfate ingress is verified in the case of the wet/dry cycles.

V.3.3.B. PHASE ASSEMBLAGE ZONATION

The phase assemblage zonations of the binder of micro-concretes under wet/dry cycles as determined from the combination of XRD and SEM-EDS analysis (Fig. V-38 and Fig. V-39) confirm some observations from the ponding exposure. Gypsum is found only in the Portland systems. The slag blends seem to stabilize monocarboaluminate over monosulfoaluminate. The samples present the characteristics of leaching with depletion of portlandite and decalcification of C-S-H at the surface. Carbonation identified by the calcite formation appears enhanced and deeper in the wet/dry cycles compared to ponding.

Ettringite formation in P-0.55, P-0.38 and S-0.55 seems to be comparable in terms of relative amount and depth to that found in the ponding exposed samples. Additionally, ettringite has been found in S-0.38, which tends to indicate that cracking is accompanied by extensive ettringite formation. This is supported by the relationship clearly observed for P-0.55 and S-0.55 between the expansion and the total amount of ettringite formed (Fig. V-40). Nevertheless, this does not mean that ettringite is at the origin of the expansion since the large cracking of the micro-concretes under wet/dry cycles may promote sulfate ingress and extensive ettringite precipitation in the opened free spaces (i.e.; in the cracks).

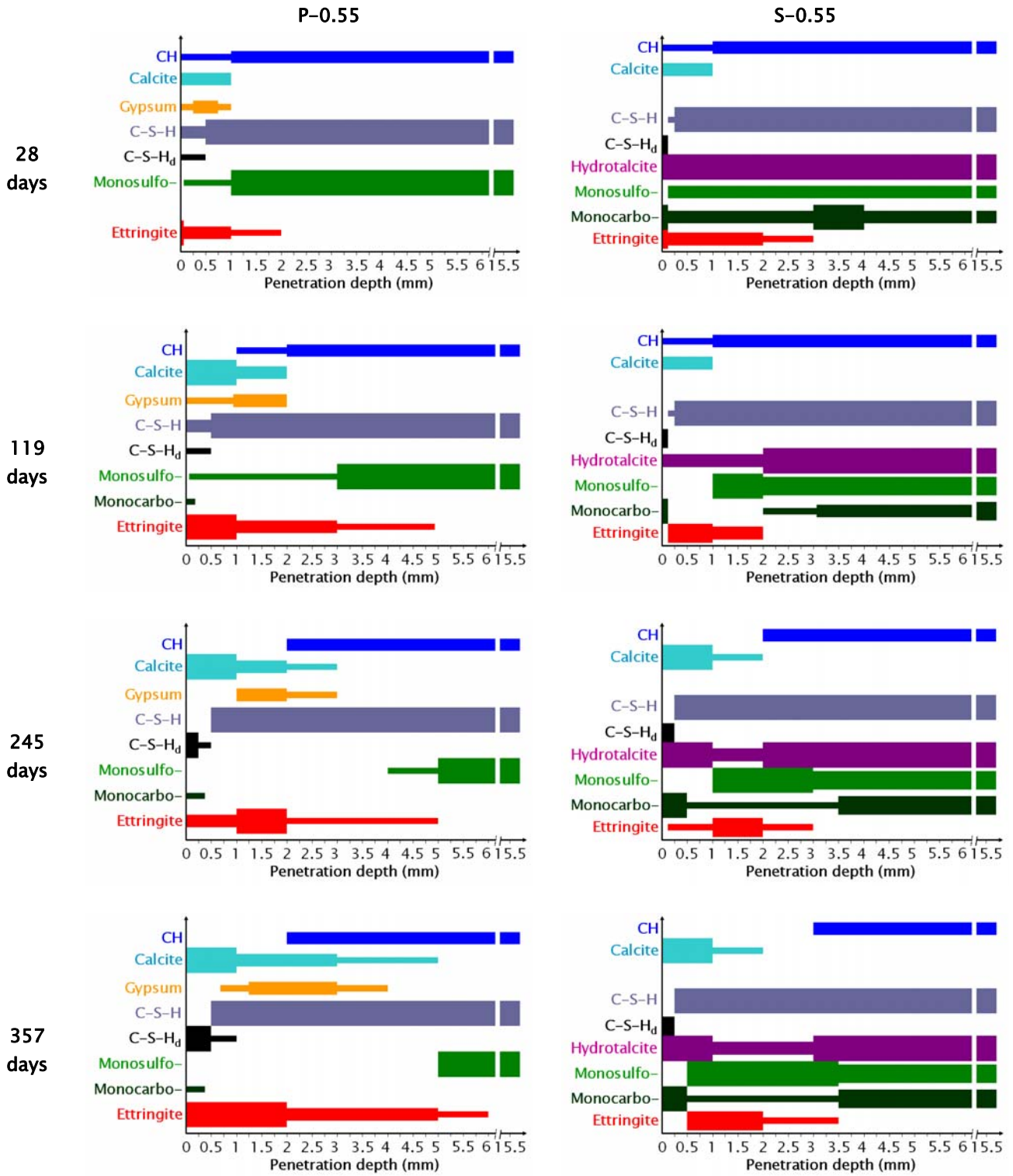


Fig. V-38. Evolution in depth of phase assemblage in the binder of P-0.55 and S-0.55 after various exposure times under wet/dry cycles.

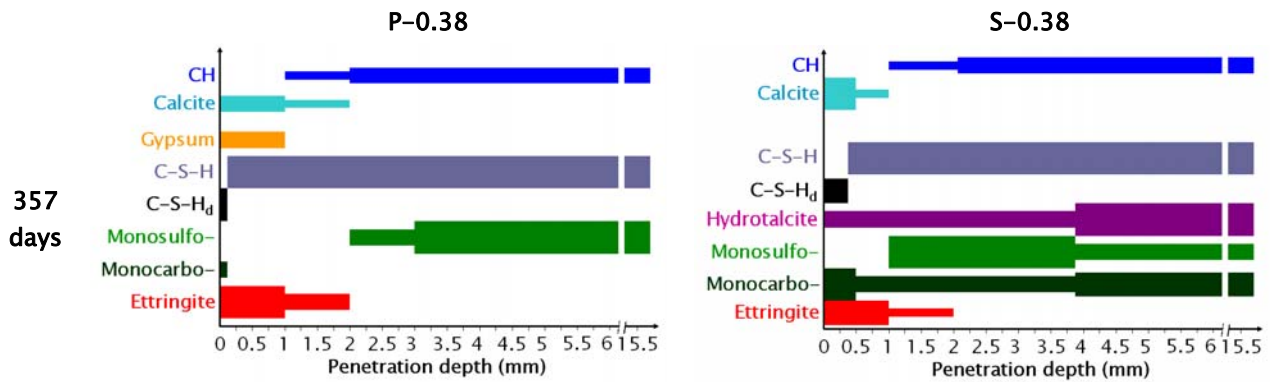


Fig. V-39. Evolution in depth of phase assemblage in the binder of P-0.38 and S-0.38 after 357 days of exposure under wet/dry cycles.

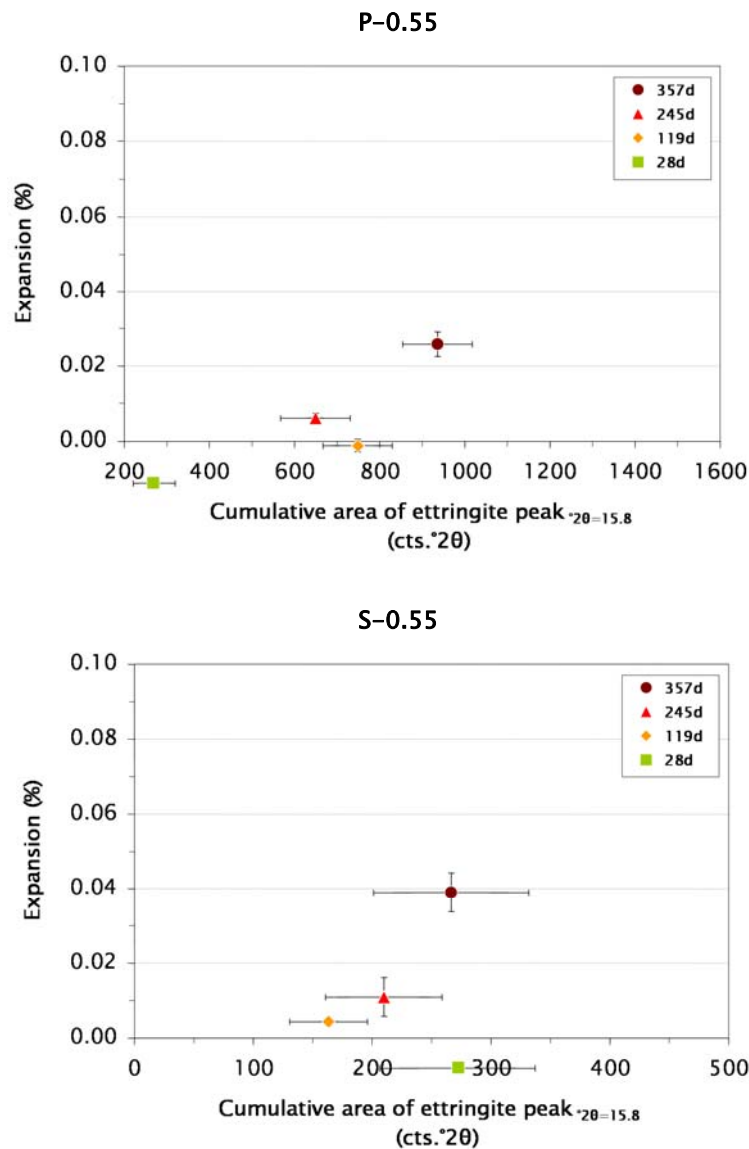


Fig. V-40. Relationship between expansion and ettringite formation in P-0.55 and S-0.55 under wet/dry cycles.

Gypsum seems to form in comparable amounts and depths in the Portland micro-concretes exposed to wet/dry cycles as for ponding. Nevertheless, the pattern of deterioration is different: the samples subjected to wet/dry cycles are characterised by cracking while the samples exposed to ponding showed surface decohesion that was attributed to the gypsum formation. In the case of the wet/dry cycles, the gypsum formed does not seem to lead to any decohesion of the samples. However, gypsum has been found to be finely intermixed to the C-S-H of P-0.55 in the case of ponding exposure while it appears more separate in wet/dry cycles (Fig. V-41). This might indicate that gypsum formed partly from the C-S-H in ponding exposure and probably only from portlandite in wet/dry cycles. The formation of gypsum from the C-S-H causes a decalcification of the C-S-H that can explain the decohesion of the micro-concretes surface. The formation of gypsum from portlandite in turn would not be so harmful since one phase is replaced by another and both do not intercede in the overall performance of cement. This could explain why the micro-concretes subjected to wet/dry cycles do not show any decohesion of their surface despite the formation of gypsum.

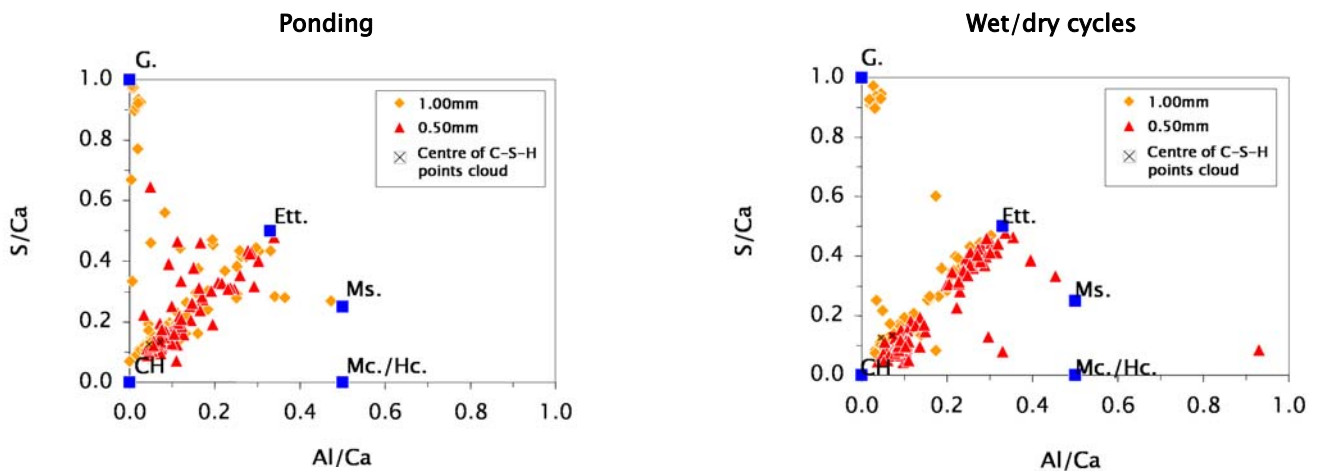


Fig. V-41. SEM-EDS plots of S/Ca versus Al/Ca atomic ratios from the outer C-S-H of P-0.55 after 357 days under ponding (left) and wet/dry cycles (right); Ett.: ettringite, G.: gypsum, Mc./Hc.: mono- or hemicarboaluminate, Ms.: monosulfoaluminate..

These observations underline the fact that consideration of the phase assemblage alone does not give a definitive indication about the damage mechanisms: the local microstructure needs to be investigated.

V.3.3.C. IMPACTS ON THE MICROSTRUCTURE

Ion transport and phase formation

On the contrary to the case of the ponding exposure, P-0.55 expansion may not so easily be linked to the sulfate combination to the outer but also to the inner C-S-H (Fig. V-42). S-0.55 reveals in turn a linear relationship between its expansion and the sulfate combination to the inner C-S-H.

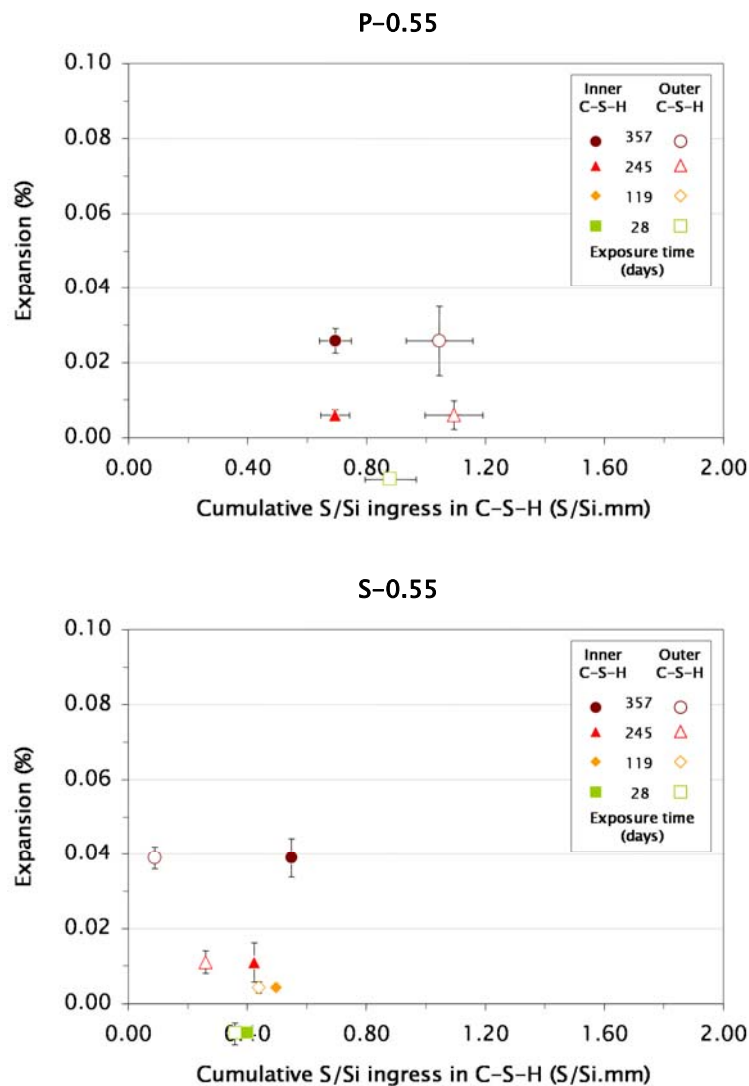


Fig. V-42. Relationship between the cumulative S/Si atomic ratio of the outer and inner C-S-H and the expansion of P-0.55 (top) and S-0.55 (bottom) under wet/dry cycles.

However, as already mentioned, the high slag replacement level of 70 wt.-% could have the consequence that the material properties would be more controlled by the slag and he slag hydrates than by the cement and its hydrates. As found in the case of the ponding exposure, it appears that under wet/dry cycles slag hydrates can combine sulfate (Fig. V-43).

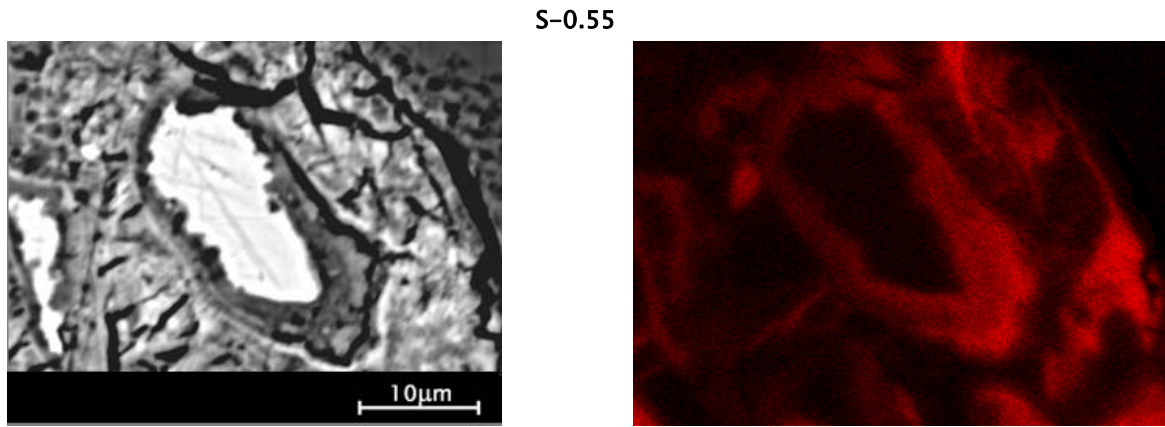


Fig. V-43. SEM-BSE micrograph (left) and corresponding quantified S-mapping (right) of a slag grain with hydration rim at 0.5 mm depth of S-0.55 after 357 days under ponding.

The sulfur level in the slag hydrate was found to reach $4.53\% \pm 1.34$ at 0.5mm and $1.22\% \pm 0.22$ at 1.0mm. The slag hydrate enriched in sulfur showed cracking while the one with lower sulfur content appeared sound. This compared with the very low levels of sulfur found in the slag hydrate of the ponded samples leads to the conclusion that sulfate combination to the slag hydrate could be link with the macroscopic damage.

A tendency towards relationship between the expansion of S-0.55 under wet/dry cycles and the combination of sulfate to the slag hydrates could be drawn (Fig. V-44).

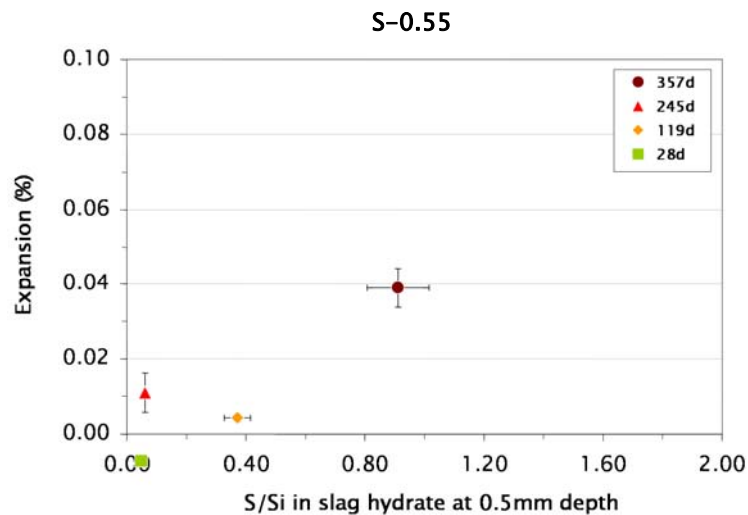


Fig. V-44. Relationship between the cumulative S/Si atomic ratio of the slag hydration rim and the expansion of S-0.55 under wet/dry cycles.

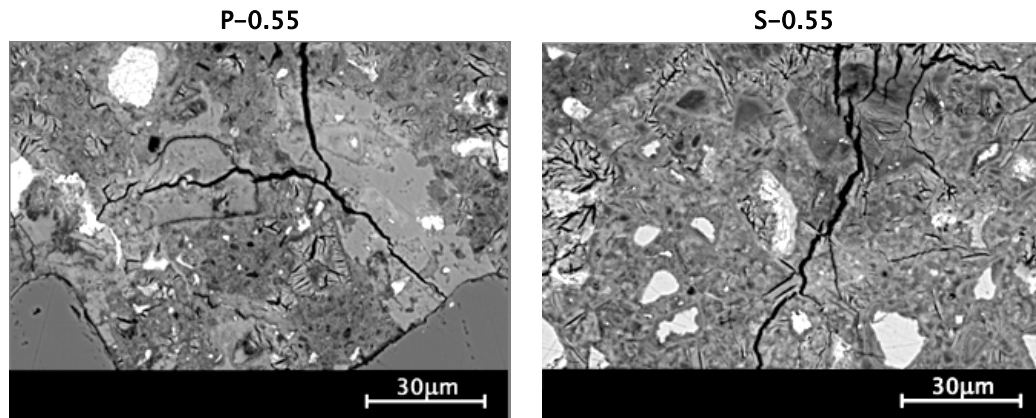
Cracking of the hydrates

Fig. V-45. SEM-BSE micrographs of the inner C-S-H of the micro-concretes after 357 days under wet/dry cycles exposure.

Looking closer at the cracking behaviour of P-0.55 and S-0.55 under wet/dry cycles (Fig. V-45), it appears that cracking goes through the outer C-S-H, around aggregates and through the inner C-S-H and at the interface between the inner and the outer C-S-H. Also important to note is the large formation of ettringite in the inner C-S-H of S-0.55 as observed in the case of ponding.

Considering S-0.55, the slag hydration rims seemed to undergo specific damage of their microstructure when put under wet/dry cycles, showing crack development at the close interface with the outer products (Fig. V-46).

It is however difficult to conclude whether expansion comes from the inner hydration products or from the outer ones. Nevertheless, drying as conducted in the wet/dry cycles tests might not be without consequence regarding the hydrates. Jennings [59] showed that drying from 20 to 0 % RH is accompanied by loss of interlayer water causing irreversible collapse in the structure. The RH was measured in the micro-concretes exposed to wet/dry cycles. After the wet period, the RH inside the micro-concretes was of 91.4 %, while after the dry period, the RH appeared to be lowered down to 21.0 %, which is in the critical range mentioned by Jennings. The slag hydrates may be more sensitive to such drying and stronger collapse than the cement hydrates.

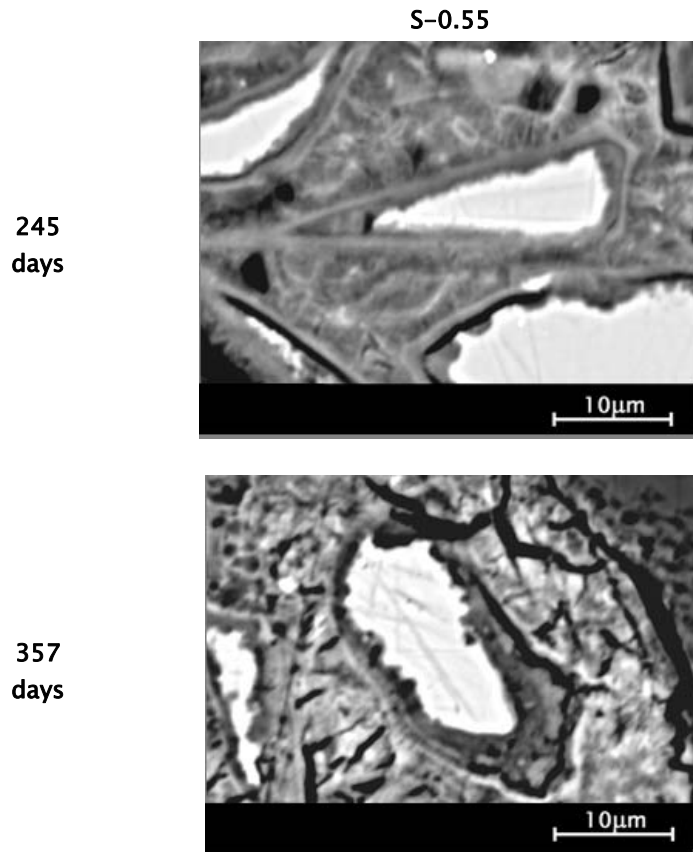


Fig. V-46. SEM-BSE micrographs of the slag with hydration rim at 0.5 mm depth for S-0.55 and S-0.38 after 357 days under wet/dry cycles exposure.

V.4. SUMMARY

The pH-control test appeared to be comparable to the ponding case with the difference that the non-renewal of the solution reduced the leaching.

The semi-immersion test seems to involve similar mechanisms of ion transport to the ponding test. The capillary suction might nevertheless contribute to sulfate combination for the Portland blends while it is not observable in the case of the slag blends.

The wet/dry cycles seem to induce a mechanical fatigue with discontinuous and abrupt loss of performance. The wet/dry cycles applied imply an oscillation in relative humidity in the microstructure. Sulfate-bearing phase precipitation and stability is highly dependant on the relative humidity. This may explain in a first approach the delay observed in sulfate combination. However, this test points out the ability of slag blends to combine sulfate at a comparable level than the PCs. The slag hydrates seem to be very sensitive to the drying operated.



Chapter VI – Field exposures

The field concretes selected for detailed study come from two different locations involving various exposure chemistries and settings. The first series most comparable to the laboratory samples were exposed in a sulfate enriched ground in Argentina for 19 years. The muddy soil had a sulfate content of 0.97 wt.-%, corresponding to an equivalent Na_2SO_4 solution of 14.34 g.l^{-1} . The pH was in the range of 7-8. The samples were partially submerged so that their upper layer was subjected to weathering with a wet/dry cycles frequency of 15-20 cycles.year⁻¹. The temperatures were in the range of 0-34 °C. The study focuses on a CEM I P-0.53 and on a CEM III/B with high level slag replacement (80 wt.-%) S-0.53.

The field samples were studied following the same methodology developed for the laboratory specimens, with the difference that only data at a single exposure time t could be assessed.

VI.1. PARTIAL IMMERSION IN SULFATE ENRICHED GROUND (ARGENTINA)

VI.1.1. STATE OF DAMAGE

VI.1.1.A. MASS CHANGE

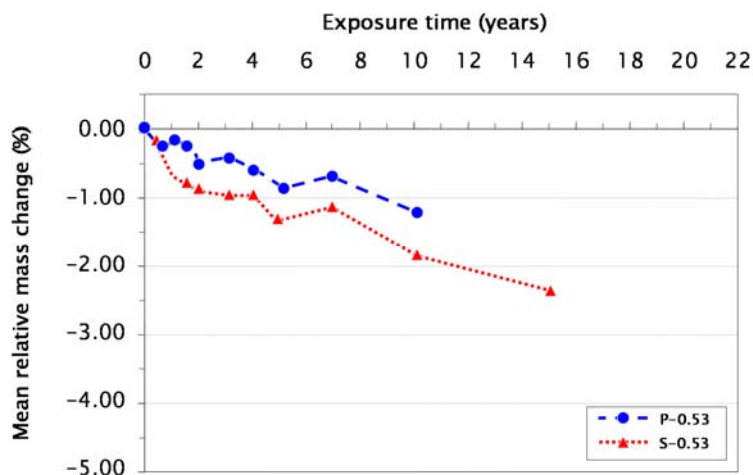


Fig. VI-1. Mass evolution of the field concretes under partial immersion in sulfate enriched ground, after Irassar.

The mass change of the concrete specimens was regularly recorded and results have been provided by Irassar (Fig. VI-1). The concretes appear to lose mass progressively under the Argentinean exposure conditions. The CEM I P-0.53 shows a reduced mass loss rate relative to the blended concretes that could be comparable to that observed for the laboratory micro-concrete P-0.55 under the ponding exposure in terms of range of values and behaviour (§ IV.1.2.A).

The ranking of the samples is closer to that observed in the laboratory tests under wet/dry cycles with the Portland specimens having a reduced mass loss compared to the slag blends (§ V.3.1.B).

VI.1.1.B. DYNAMIC ELASTIC MODULUS

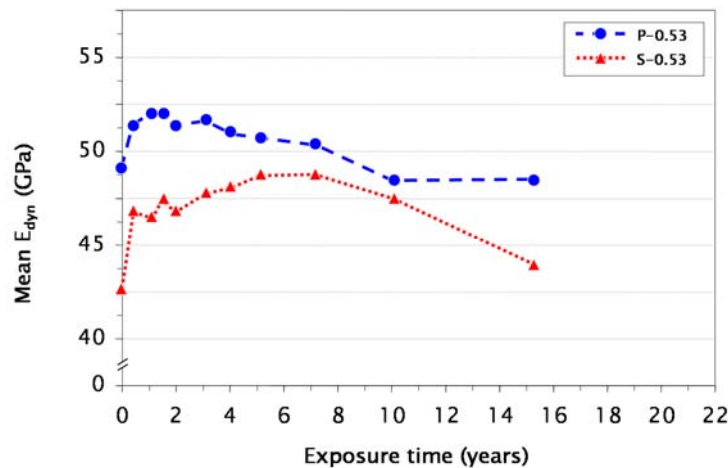


Fig. VI-2. Dynamic elastic and shear modulus evolution of the field concretes under partial immersion in sulfate enriched ground, after Irassar.

The dynamic elastic modulus data supplied by Irassar (Fig. VI-2) indicate values after 15 years of exposure for P-0.53 and S-0.53 of respectively 48 GPa and 44 GPa. The values are in the range of that measured in the flexural mode on the laboratory micro-concretes. The slag blend would perform worst than the plain Portland, as observed in the case of the laboratory micro-concretes under wet/dry cycles exposure (§ V.3.1.B). But in order to evaluate accurately the ranking of the specimens, the dynamic elastic modulus measurements should be normalised by values of reference specimens not exposed to sulfate. Such values are not available. However, the evolution of the dynamic elastic modulus of P-0.53 characterised by a loss of properties followed by a plateau correlates with that observed in the case of the wet/dry cycles exposure from the laboratory tests undertaken (§ V.3.1.B). The evolution of the blended concrete would more likely correlate with that observed in the case of the ponding exposure (§ IV.1.2.D) unless the last plateau has not occurred yet.

VI.1.1.C. VISUAL APPEARANCE

The visual appearance of the Argentinean field concretes (Fig. VI-3) reveals broken corners of the Portland blend, which might not be very significant since such parts are very fragile and may have broken during the transport of the samples. The slag blend shows significant erosion, with aggregates rising the surface, on its top side exposed to weathering.

This confirms observations made by Irassar on other specimens in semi-immersion in such a sulfate soil [21]. Irassar pointed out that especially high slag additions in concrete would have a negative effect on sulfate resistance when wet/dry cycles and salt crystallisation are concerned (Fig. VI-4). This would tend to confirm the observation from the laboratory study that slag blends with high slag replacement level do not withstand well wet/dry cycles exposure.

However, the bottom side fully submerged of both samples seems to be in good state.



Fig. VI-3. Visual appearance of the field concretes after 19 years under partial immersion (submerged part: bottom of the concrete blocks – exposed part: top of the concrete blocks) in sulfate enriched ground.

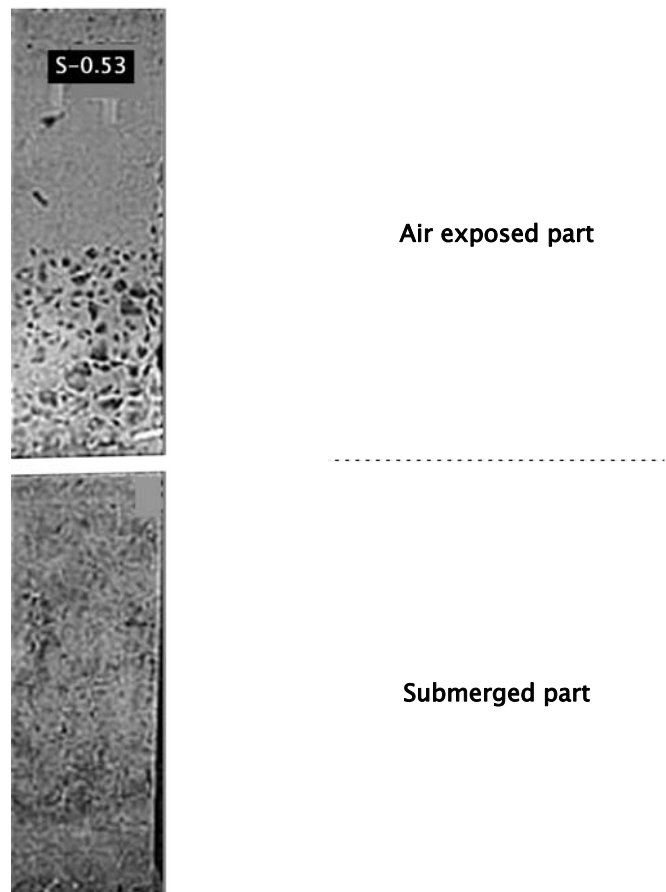


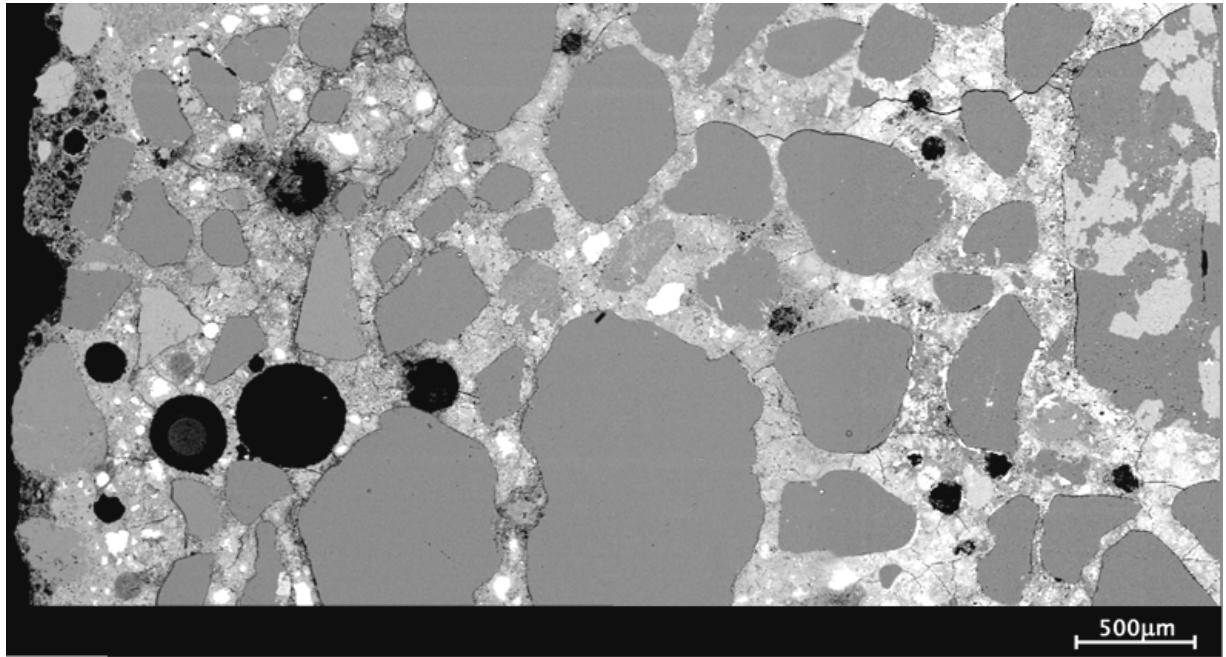
Fig. VI-4. Visual appearance of the field blended concretes after 15 years under semi- immersion in sulfate enriched ground, after Irassar.

VI.1.1.D. MICRO-CRACKING

Looking closer to the microstructure, it appears that the Portland blend shows cracking in its submerged surface while the slag blend remains in relative good state (Fig. VI-5). P-0.53 crack pattern can be directly related to that observed in the laboratory for P-0.55 under ponding.

Submerged part

P-0.53



S-0.53

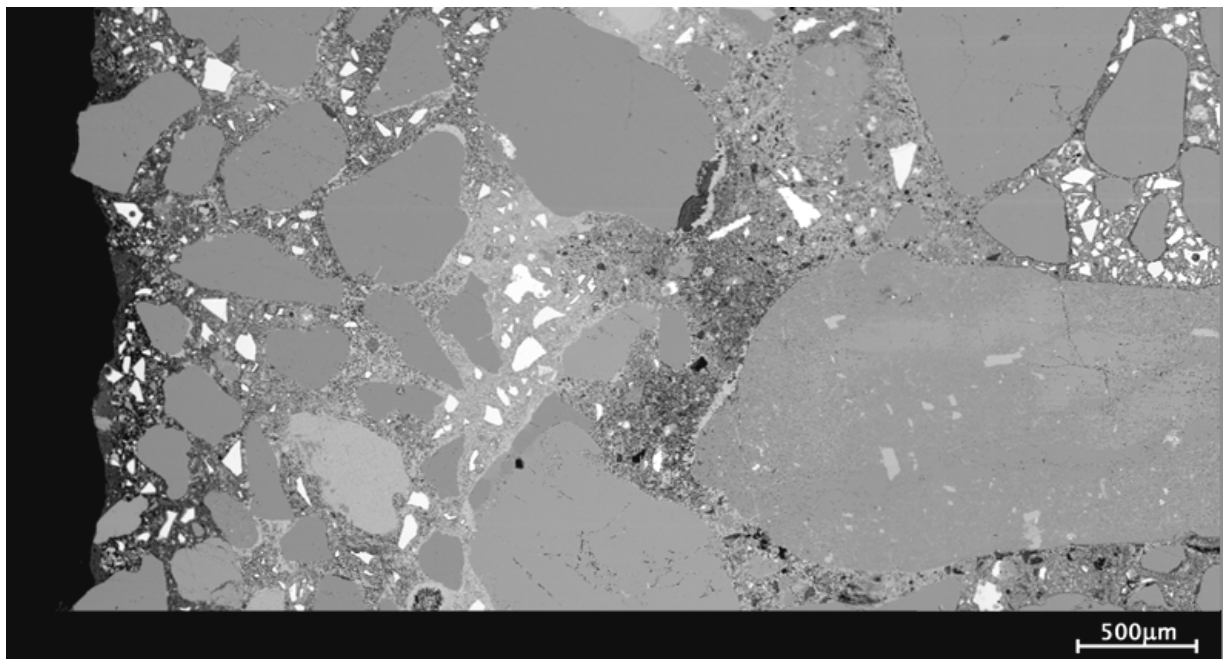


Fig. VI-5. Crack patterns from BSE micrographs of the field concretes after 19 years under full immersion in sulfate enriched ground.

VI.1.2. STUDY OF THE MICROSTRUCTURE

VI.1.2.A. IONIC PROFILE

Leaching

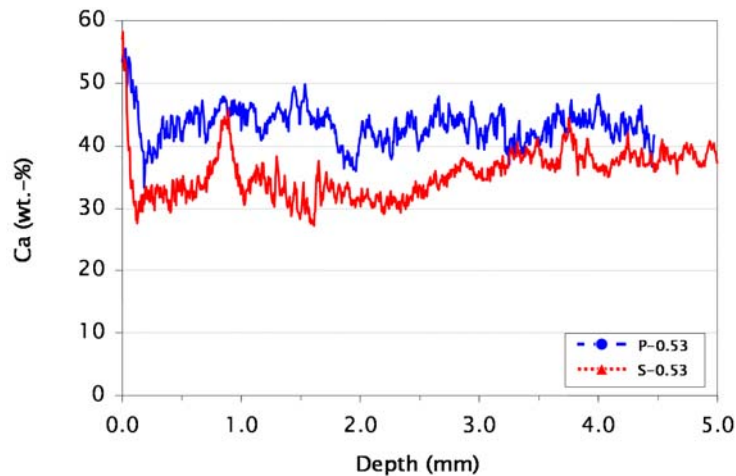


Fig. VI-6. Calcium profiles of the cementitious matrix of the field concretes after 19 years under partial immersion in sulfate enriched ground; submerged part.

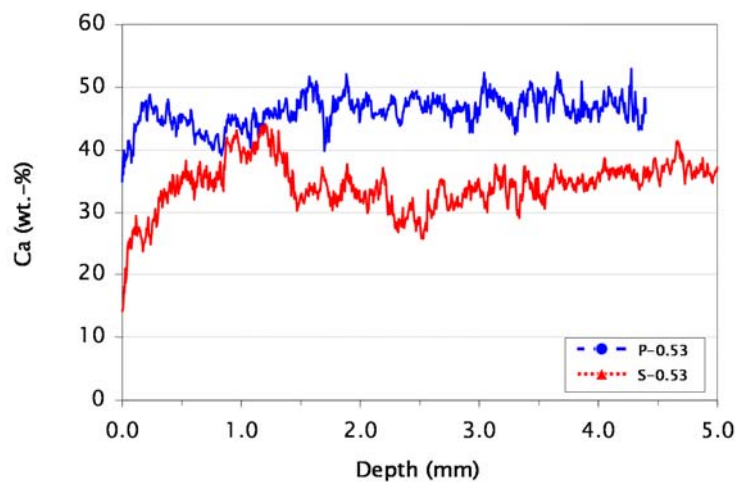


Fig. VI-7. Calcium profiles of the cementitious matrix of the field concretes after 19 years under partial immersion in sulfate enriched ground; exposed part.

The calcium profiles (Fig. VI-6 and Fig. VI-7) confirm the presence of leaching both in the fully submerged and exposed parts of the concretes, the phenomenon being increased in the exposed part. This supports previous observation from the laboratory owing to which wet/dry cycles appeared to increase leaching.

The irregular leaching behaviour is probably due to the heterogeneous compaction of the cement pastes. However, the increased calcium content on the surface of the concretes must be a sign of surface carbonation.

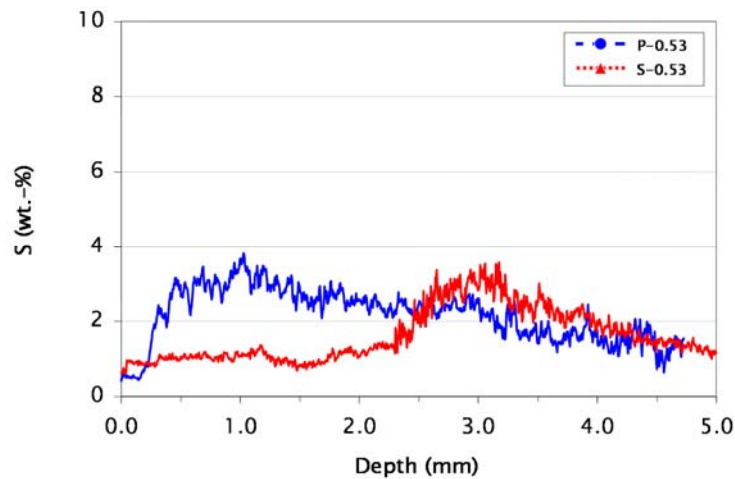
Sulfate ingress

Fig. VI-8. Sulfate profiles of the cementitious matrix of the field concretes after 19 years under partial immersion in sulfate enriched ground; submerged part.

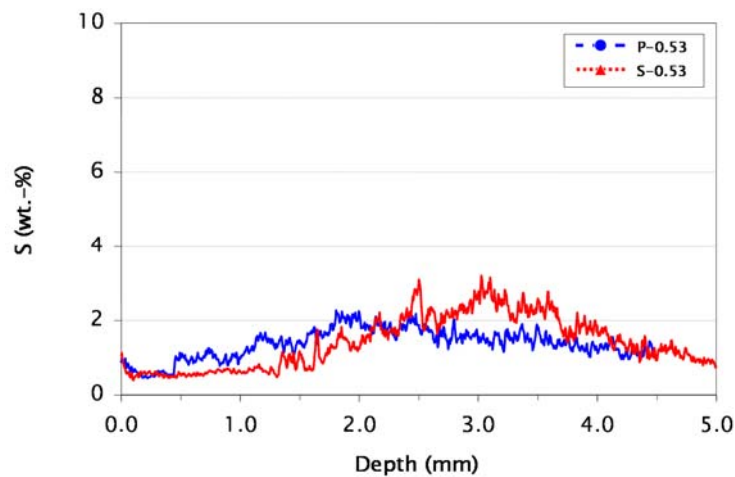


Fig. VI-9. Sulfate profiles of the cementitious matrix of the field concretes after 19 years under partial immersion in sulfate enriched ground; exposed part.

The sulfate ingress is also subjected to leaching effects in the full and to lesser extend in the exposed part of the concretes (Fig. VI-8 and Fig. VI-9). Interestingly, the levels of ingress are comparable in both exposure types as was also observed in the laboratory micro-concretes. The reduced sulfate ingress observed for the laboratory samples in the slag blend compared to the pure Portland is nevertheless not confirmed here, where the sulfate ingress seems to reach lower values than observed in the laboratory. This might be related to the fact that the exposure surrounding is not liquid but solid (mud) making a reduced connection between the pore network and the environment in terms of ion transport

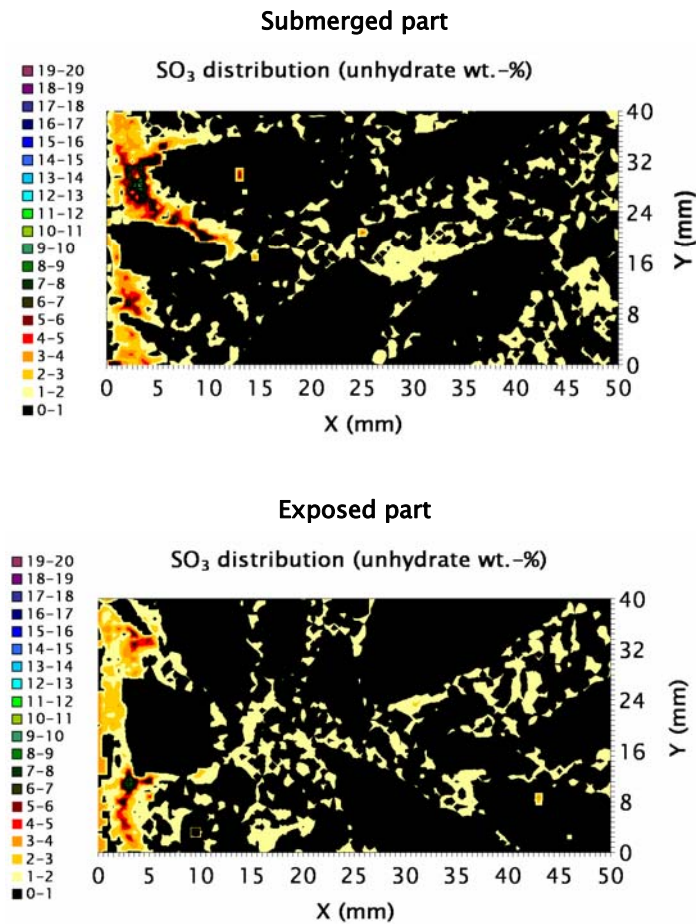


Fig. VI-10. Micro-XRF quantitative sulfate mapping of S-0.53 after 19 years under partial immersion; submerged part (top) and exposed part (bottom).

Micro-XRF measurements of the quantitative sulfate mapping in the submerged and exposed parts of S-0.53 (Fig. VI-10) reveal similar ingress behaviour as depicted by the SEM sulfur-mapping image analysis method. The SO₃ values ranging from 0 to 8-9 wt.-% do correspond to values of sulfur from 0 to 3-3.5 wt.-% as deduced by the calculation of the sulfur profiles from SEM sulfur-mapping image analysis.

Both techniques are validated. The micro-XRF requires poor sample preparation (minutes) but long acquisition time (days) and the SEM-based method long sample preparation (days) and short acquisition and analysis time (minutes).

VI.1.2.B. PHASE ASSEMBLAGE ZONATION

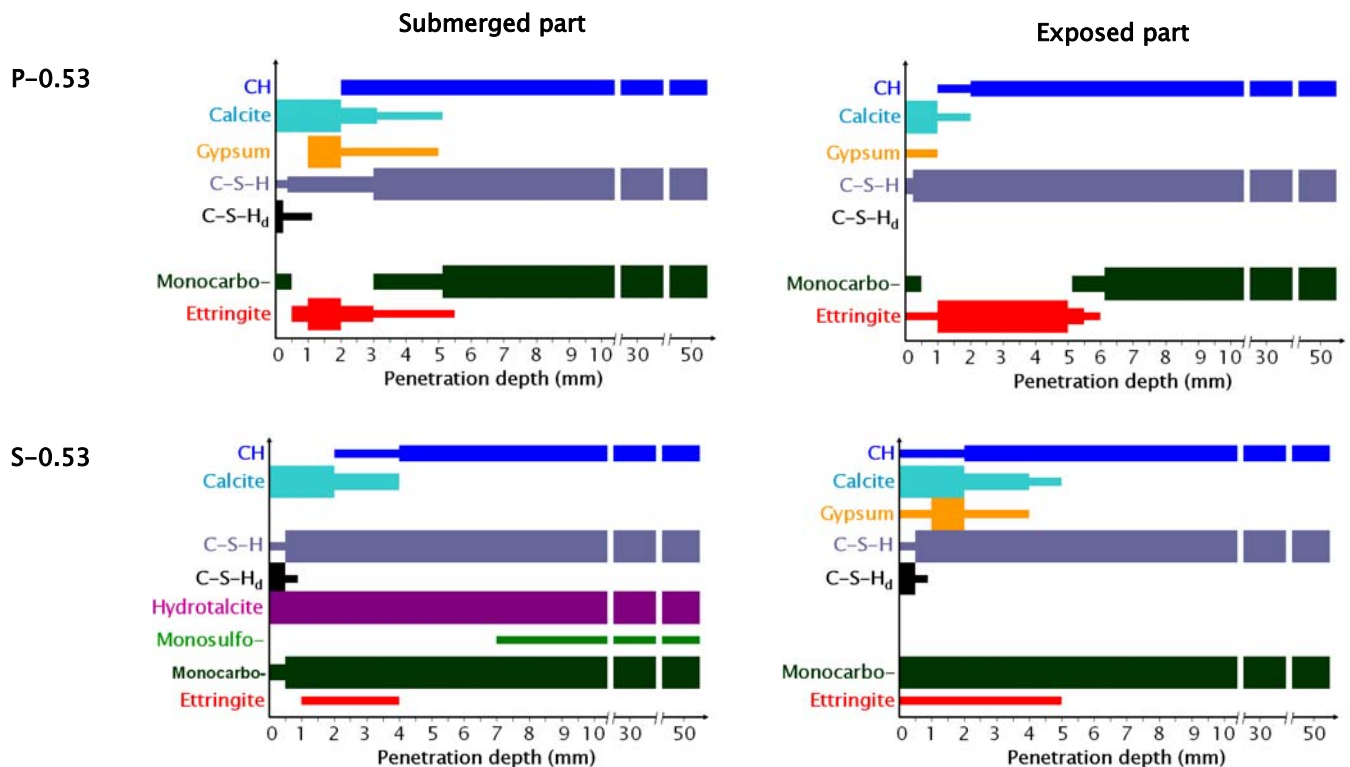


Fig. VI-11. Phase assemblage zonations as determined from XRD and SEM-EDS analyses of the field concretes after 19 years under partial immersion in sulfate enriched ground (submerged part: left – exposed part: right).

The qualitative phase assemblage zonations (Fig. VI-11) reveal comparable phase assemblages for P-0.53 under full and exposed immersion, confirming the laboratory observations of P-0.55 under ponding and wet/dry cycles. The major difference is found for the slag blend S-0.53 for which ettringite is found to form deeper in the exposed part compared to the submerged part. This confirms again the observations from the laboratory micro-concrete S-0.55 that presented deeper ettringite precipitation when exposed to wet/dry cycles compared to ponding. Also gypsum formation was detected in the exposed part of the S-0.53 but not in the submerged part. The difficulty to detect hydrotalcite in the exposed part of the slag blend while it was easily detected in the submerged part indicates that the slag hydrates may undergo some deterioration from the exposed conditions.

It is worth noting that gypsum formation was found in these field concretes in contrast to what is often claimed. Nevertheless, the particularly high sulfate content of the soil might be at the origin of gypsum stabilization, which should not be taken as representative of real field cases.

Monocarboaluminate is found to be more important in the field concretes over monosulfoaluminate which is the main AFm phase present in the laboratory samples.

VI.1.2.C. LOCAL EFFECTS ON THE MICROSTRUCTURE

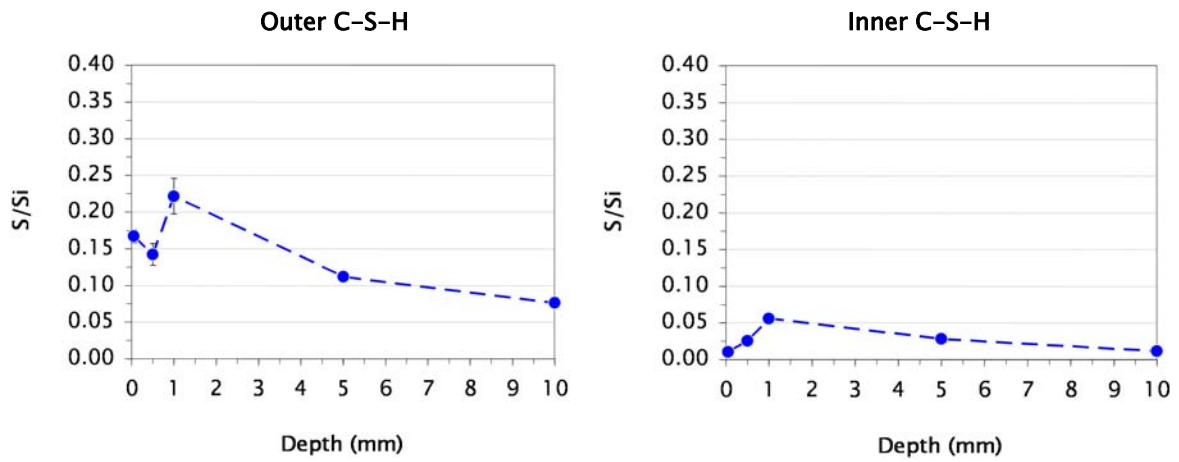
Sulfate combination to the hydrates

Fig. VI-12. EDS S/Si atomic ratio of the outer (left) and inner C-S-H (right) of P-0.53 after 19 years under partial immersion in sulfate enriched ground; submerged part.

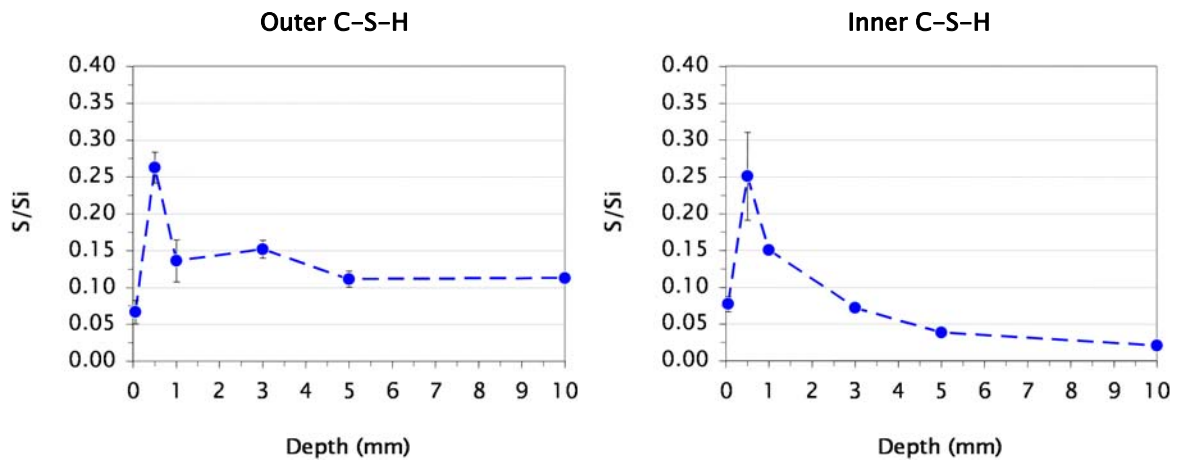


Fig. VI-13. EDS S/Si atomic ratio from the outer (left) and inner C-S-H (right) of P-0.53 after 19 years under partial immersion in sulfate enriched ground; exposed part.

The sulfate combinations to the outer C-S-H of P-0.53 under full and exposed immersion (Fig. VI-12 and Fig. VI-13) reach comparable values to that of P-0.55 under respectively ponding and wet/dry cycles with a maximum of S/Si atomic ratio of 0.25. The sulfate combination to the inner C-S-H in turn seems to be reduced for the submerged part of the field concrete compared to the laboratory micro-concrete under ponding but increased for the exposed part of the field concrete compared to the laboratory micro-concrete under wet/dry cycles. Nevertheless, the sulfate combination to the inner C-S-H of P-0.55 was found to be higher in the case of wet/dry cycles exposure than in the case of the ponding exposure. The field concrete P-0.53 follows the same tendency comparing the sulfate combination to its inner C-S-H in the submerged and exposed parts.

Cracking of the hydrates

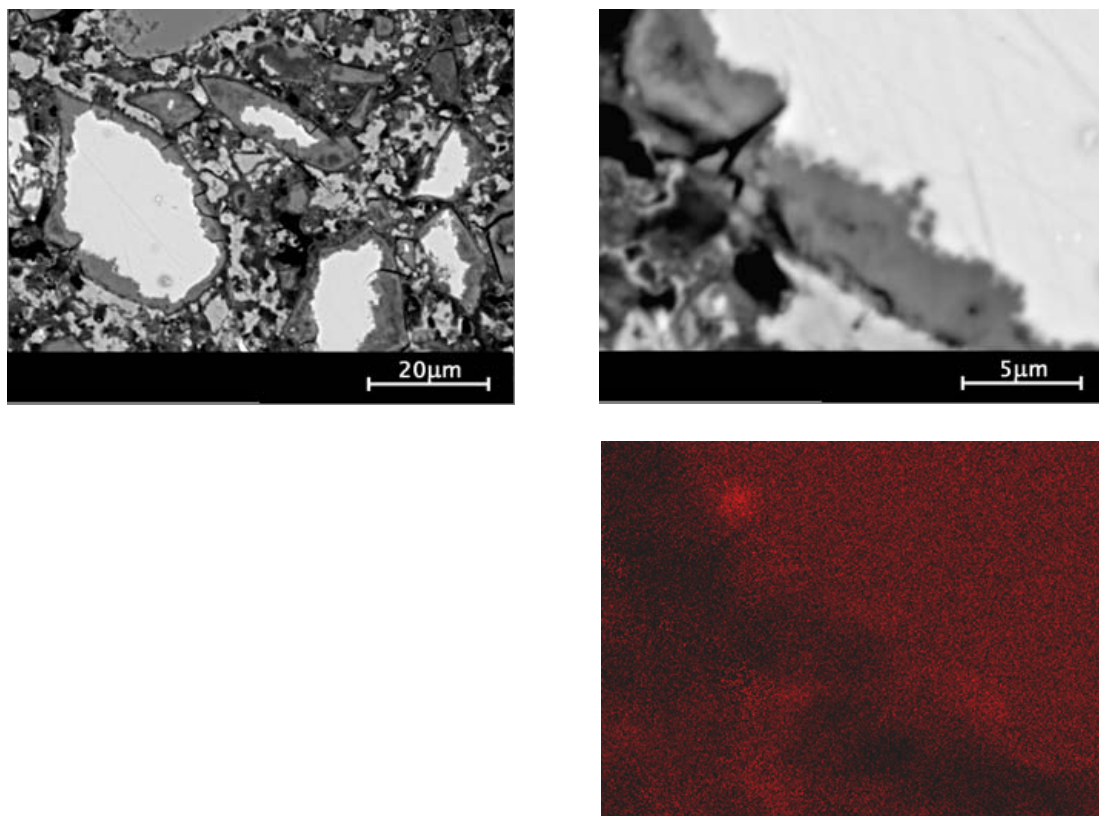


Fig. VI-14. SEM-BSE micrograph of a slag with hydration rim with corresponding quantitative S-mapping for S-0.53 after 19 years under partial immersion in sulfate enriched ground; submerged part.

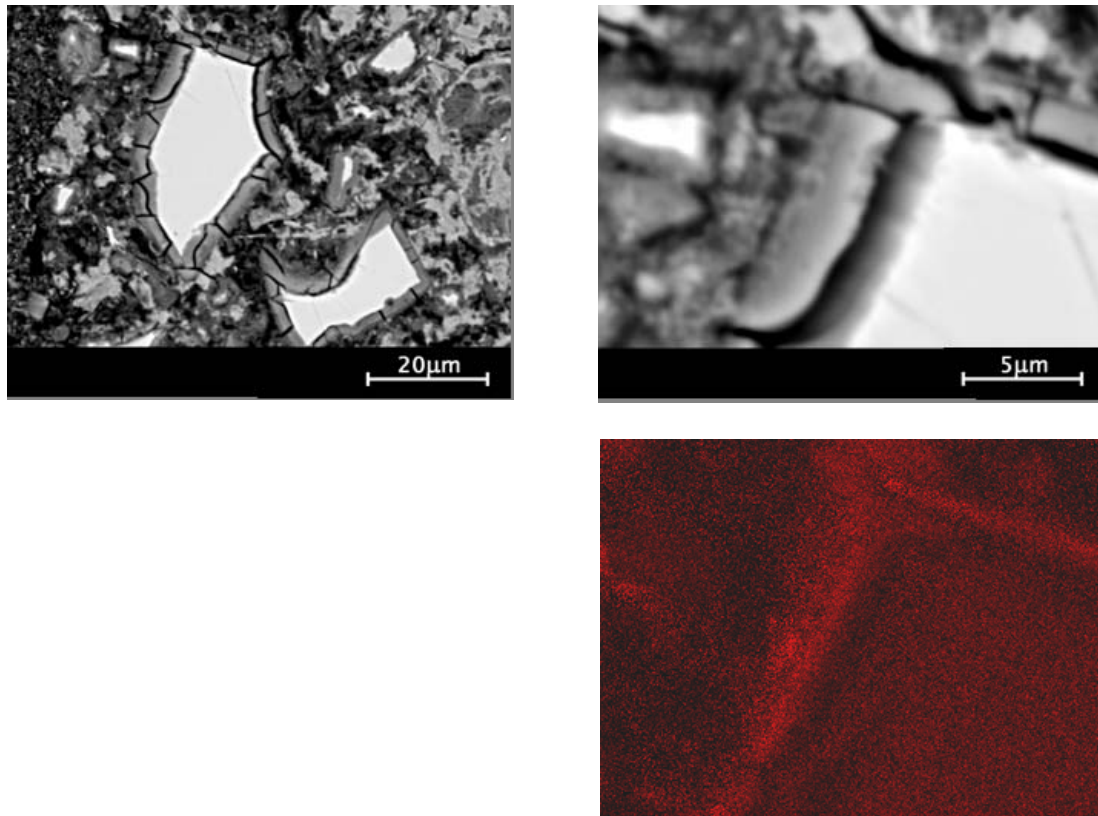


Fig. VI-15. SEM-BSE micrograph of a slag with hydration rim with corresponding quantitative S-mapping for S-0.53 after 19 years under partial immersion in sulfate enriched ground; exposed part.

The slag hydration rims of S-0.53 under exposed immersion showed severe cracking compared to that from the full immersion part (Fig. VI-15 and Fig. VI-15). The cracking of the slag hydration rims seems to be associated with a higher sulfur combination. This would tend to confirm observations made from the S-0.55 laboratory micro-concrete after 357 days of exposure under wet/dry cycles where cracked slag hydration rims revealed sulfur content up to 4 at.-%.

However, the fact that hydrotalcite could be hardly identified by XRD neither by SEM analysis on S-0.53 subjected to exposed immersion indicates that the slag hydrates have encountered some deterioration.

Note that, as it was the case for the laboratory samples, the hydrotalcite like phase consists in fact of quintinite, usually related to hydrotalcite with Mg/Al atomic ratio of 2 and not 3 as in typical hydrotalcite.

VI.2. COMPARISON BETWEEN FIELD AND LABORATORY

The Argentinean concretes were exposed for 19 years in partial immersion. The partial immersion exposure comprises submerged and exposed parts.

The physical changes of the concretes could be related to that observed for the laboratory specimens stored for 1 year under wet/dry cycles. Slag blend with high slag replacement level appeared to perform worst under such partial immersion, in particular concerning the exposed part of the samples despite the lower sulfate ingress. This was also observed in the laboratory for the slag blends under wet/dry cycles.

Nevertheless, no evident relationship between the state of damage and the ettringite formation could be observed.

Sulfate has been found to combine to the outer and inner C-S-H phases of the Portland blend on a comparable manner as observed from the laboratory samples. The slag hydration rim appeared to combine sulfate, especially in the exposed regime where it appeared cracked. Such a cracking of the slag hydration rim could be related to the cracking observed for the slag laboratory blends under wet/dry exposure and might either be a sign of swelling of the hydrates or cracking under local stresses.



Chapter VII – Discussion, conclusions and perspectives

The thesis has been divided into three main steps:

- elaboration of representative and repeatable laboratory tests for sulfate resistance (at BAM – Bundesanstalt für Materialforschung und -prüfung – Germany);
- procurement and selection of sulfate exposed field samples, started before the project (at BAM);
- parallel study at macro and micro level of the laboratory and field specimens (at BAM and EPFL – Ecole Polytechnique Fédérale de Lausanne – Switzerland).

The originality of the thesis is the parallel study of laboratory and field specimens by the same methodology sound track. The laboratory micro-concretes have been designed to be as close as possible to typical field concretes. The laboratory exposure conditions have been adjusted to be as representative as possible to usual field exposures.

The laboratory samples allow a chronological study while the field samples deliver instantaneous state of the damage. The large panel of methods implemented allows correlating the physical changes to the microscopic phenomena.

VII.1. MAIN RESULTS

VII.1.1. IMPROVEMENTS OF UNDERSTANDING OF DAMAGE UNDER PONDING EXPOSURE

VII.1.1.A. DAMAGE PROCESS

The expansion process has been found to follow a three-stage behaviour. The common two-stage expansion process encountered in the literature would in fact have its second stage split into two stages of increasing rate. This three-stage process has been verified for other physical measurements such as mass loss and elastic properties loss. The damage process of concrete under ponding exposure would thus follow a three-stage behaviour characterised by:

- stage #1 – *induction* –
 - dominated by the loading of the outer and inner C-S-H regions in sulfate;
 - accompanied by the precipitation of fine ettringite especially in the inner C-S-H after reaching a saturation level of sulfate combination;
- stage #2 – *surface damage* –
 - dominated by sulfate combination to the outer C-S-H with fine ettringite precipitation that accelerates the cracking of the cementitious matrix;
 - accompanied by coarse ettringite precipitation in empty spaces in the inner C-S-H without causing stress;
- stage #3 – *bulk damage* –
 - dominated by large ion transport through the opened microstructure whose higher available surface area increases the reaction potential with sulfate;
 - accompanied by coarse ettringite and gypsum precipitation in the developed cracks.

The expansion process would thus be driven by the capability of the C-S-H regions to combine sulfate. Two theories for the expansion initiation may be pointed out: swelling of the C-S-H due to sulfate combination or stresses developed in the C-S-H by fine ettringite precipitation due to local supersaturation in sulfate. The saturation of the C-S-H in sulfate seems to be a necessary criterion for expansion, which would be related to the crystal growth pressure theory of expansion for which supersaturation is the driving force [16].

Gypsum precipitation was found to correlate with the surface softening of the samples. Nevertheless it is not explained why gypsum forms in such conditions with so low sulfate concentration.

The sulfate ion penetration in solution through the pore network of the micro-concretes is independent of the w/c or w/b-ratio (i.e.; to the usual parameters of permeability) and cannot therefore be considered as a diffusion controlled process.

VII.1.1.B. INFLUENCE OF W/C-RATIO

The damage process exposed was only encountered by the pure Portland micro-concrete with w/c-ratio of 0.55. Its homologue with w/c-ratio of 0.38 presented comparable microstructural characteristics with the difference that sulfate ingress, sulfate-bearing phase formation and sulfate combination to the hydrates were recorded less deep into the material. The reduced w/c-ratio would thus reduce the transport phenomena and therefore reduce the depth of physico-chemical changes in the material. The absence of significant physical damage for samples with such reduced w/c-ratio may indicate that the depth of reaction between the sulfate ions and the cementitious matrix can play a role in the intensity of the damage process, as also emphasised by Schmidt [30]. However, it might be thought that a reduced w/c-ratio allows a better mechanical resistance against the developed local stresses.

VII.1.1.C. INFLUENCE OF SLAG ADDITION

The slag blends did not reveal much physical damage. Slag addition causes a decalcification of the inner C-S-H from which the calcium is assumed to feed the slag hydration as also mentioned by Kocaba [51]. The empty spaces left allow phase precipitation without causing any stress. Nevertheless, slag hydration product seemed to be sensitive to sulfate ingress as it was found to be able to fix sulfate.

VII.1.2. INFLUENCE OF THE TYPE OF EXPOSURE

VII.1.2.A. pH-CONTROL

Maintaining the pH at 7.5 ± 0.5 did not influence much the process of damage by external sulfate ions compared to the ponding exposure, driven by the combination and saturation of sulfate in the outer and inner C-S-H regions, which appeared to be in the same level range for P-0.55 under pH-control and ponding.

The continuous supply of sulfate ions increased the physico-chemical changes of the micro-concretes.

The non-renewal of the solution caused a reduction of the leaching process.

VII.1.2.B. SEMI-IMMERSION

The submerged part of the micro-concretes under semi-immersion has been found to follow the same microstructural changes than that ones in ponding. The effects were however observed with a delay attributed to a surface carbonation of the samples in semi-immersion. The physico-chemical changes were reduced compared to ponding but, according to the sulfate saturation level of the C-S-H, P-0.55 seemed to undergo the initiation period of the expansion process along the year of observation. It might be expected a later expansion take of for this sample, accompanied by deeper fine ettringite formation.

The air exposed part of the samples was found to contribute in the ion exchange through capillary suction leading to significant physico-chemical changes in this area of the samples. Such effects (e.g.; sulfate penetration and ettringite precipitation) were nevertheless observed at reduced depths, for the given exposure times, to be thought to contribute significantly to the overall damage.

Thenardite efflorescence has been identified at the surface of the samples in the above solution level area but without any sign of damage.

VII.1.2.C. WET/DRY CYCLES

The pure Portland micro-concretes and especially the one with w/c-ratio of 0.55 followed similar physical changes than under ponding. However, a relationship could not be clearly drawn between the sulfate combination to the C-S-H and the expansion of P-0.55, letting think that another kind of damage process is concerned under wet/dry cycles compared to ponding.

The slag blends and especially that with w/b-ratio of 0.55 revealed a different behaviour than in ponding and was found to be particularly sensitive to the drying cycles. The damage process for such samples appeared to occur in three stages, characteristic for mechanical fatigue: induction, cracking and collapse. The damage was accompanied with ettringite formation and could be related to the sulfate combination to the slag hydrate in the case of the slag blend with w/c-ratio of 0.55. The collapse was associated to a cracking of the slag hydrate.

The applied drying was found to reduce the relative humidity inside the concrete down to critical values (20 %) that may cause irreversible collapse of the cementitious hydrates [59] and apparently especially of the slag hydrates.

The wet/dry cycles exposure appeared to enhance leaching and increase the rate of sulfate ingress.

VII.2. DISCUSSION

VII.2.1. COMPARISON BETWEEN LABORATORY AND FIELD

The degradation process in the laboratory and in the field was found to follow the same kind of zoning with different kinetics. The field cases in full immersion were found to be comparable in terms of physical and microstructural state to the laboratory results in ponding. The applied wet/dry cycles in the laboratory appeared representative of the weathering exposed conditions studied in Argentina.

The pure Portland matrix seems to be especially vulnerable to ponding exposure. The cracking (i.e.; expansion) could not be only related to the ettringite formation. The sulfate combination to the outer and inner C-S-H regions appeared to play a major role in the damage process. The sulfate combination in the C-S-H showed comparable saturation levels in the laboratory and field microstructures that seemed to be of key criterion for the expansion initiation. The pure Portland matrix revealed much better resistance towards exposure involving wet/dry cycles.

The slag blended concretes were found to be especially sensitive to exposure involving wet/dry cycles both in terms of physical and chemical resistance of the hydrates characterised respectively by a cracking of the slag hydration rims in the zone of highest sulfate ingress and by a hardly identifiable hydrotalcite phase. Additionally, the slag hydration rim showed comparable sulfate combination levels in the laboratory and in the field microstructures. The expansion of the laboratory specimens was found to be accompanied by an increased sulfate combination to the slag hydrates. The drying might cause a particular strong physical change of the slag hydrates compared to the Portland hydrates characterised by a quicker irreversible collapse of the microstructure. The resulting cracking might enhance the sulfate penetration and thus combination to the slag hydrates up to reaching a critical level after which the expansion increases. The slag blended matrix was found to be sulfate resistant in ponding type of exposure.

The representativity of the laboratory specimens compared to the field cases might nevertheless be questionable in terms of geometry: the surface over volume ratio of a $4 \times 4 \times 16 \text{ cm}^3$ is higher compared to that of a real structure and the consequences of few millimetres of damaged zone consequently overestimated.

Gypsum formation in the laboratory micro-concretes was found to be overrepresented compared to that occurred in the field concretes despite the low sulfate concentration applied. This is especially surprising as it appeared also overestimated compared to the thermodynamic predictions [30]. This might be due to local enrichment in sulfate either from chemical effects (sulfate combination to the hydrates) or physical characteristics (tortuosity of the pore network) that are different in the laboratory from the field and might be underestimated or occulted in thermodynamic calculations.

VII.2.2. EVALUATION OF THE DEVELOPED TESTS

The ponding test seems to be in fact a good way to represent most field cases. As just pointed out in the previous paragraph, gypsum seems nevertheless to be still overrepresented even at low sulfate concentrations, which is not well understood yet.

It might be interesting to include monthly renewal of the solution in the pH-control test in order to enhance the leaching but also to better compare the ion exchange with the other tests.

The semi-immersion test would be worth to carry under noncarbonated atmosphere (N_2 for instance) to prevent from carbonation that seems to be a barrier towards sulfate ingress.

The representativity of the wet/dry cycles test developed may be questionable: does the test be representative of very specific field conditions or does it have any legitimacy in terms of wide representativity of possible field cases?

Nevertheless, other methods for drying could be envisaged such as solvent exchange (if reversible) and regular control of the relative humidity after the drying period should be done.

VII.2.3. RELEVANCE OF THE TECHNIQUES INVOLVED

The dynamic elastic modulus appeared to be a reliable and useful technique to monitor the degradation of concrete when exposed to sulfate and should be more implemented.

The analysis of the ions in the exposure solution has been found to provide information on the physical effects of sulfate attack, but not on the chemical effects.

From the different methods applied for estimation of the ion profiles (Appendix C) the quantitative micro-XRF and the image analysis of qualitative SEM-mapping were found to be the most powerful tools. First of all, both techniques lead to quantitative results. Micro-XRF quantitative mapping are done on cut surfaces, which presents the advantage of not requiring any special preparation of the sample but the measurements last 56 hours. The image analysis from SEM-mapping supposes fine prepared polished section, which is time consuming. However, the mapping itself only last 15 min and quantification using image analysis is immediate.

It has been shown that XRD can inform on the phase assemblage of the binder of concrete samples and even on field concrete samples, while many authors claim that the aggregate diffraction pattern overlap that one of the hydrates, which is true but not in the 6-20 2θ range. Additionally, the aggregates could simply be separated from the paste to check their diffraction pattern. SEM-EDS quantitative analyses present the advantage over XRD to localize the phase formations in the microstructure. But SEM preparation and acquisition is more time consuming.

VII.3. PERSPECTIVES

VII.3.1. INPUTS FOR MODELLING

The data issued from this thesis can be implemented in chemical/thermodynamic modelling. This is already in progress for the ponding and the pH-control exposures (Idiart).

Mechanical modelling should follow (Idiart and Dunant). Mechanical modelling of fracture mechanisms could be a tool to check the damage mechanisms. For example, hypothesis could be made that the combination of sulfate in the outer or in the inner C-S-H is at the origin of the expansion of one or the other phase promoting the overall expansion of the cementitious matrix. The calculated damage especially in terms of loss of elastic properties could be compared to the experimental results to evaluate the validity of the assumption made.

It also in question whether more complex systems in terms of exposure setting and chemistry could be modelled, knowing that different durability problems could hence overlap and compete each others (ASR, carbonation, chloride penetration, ...).

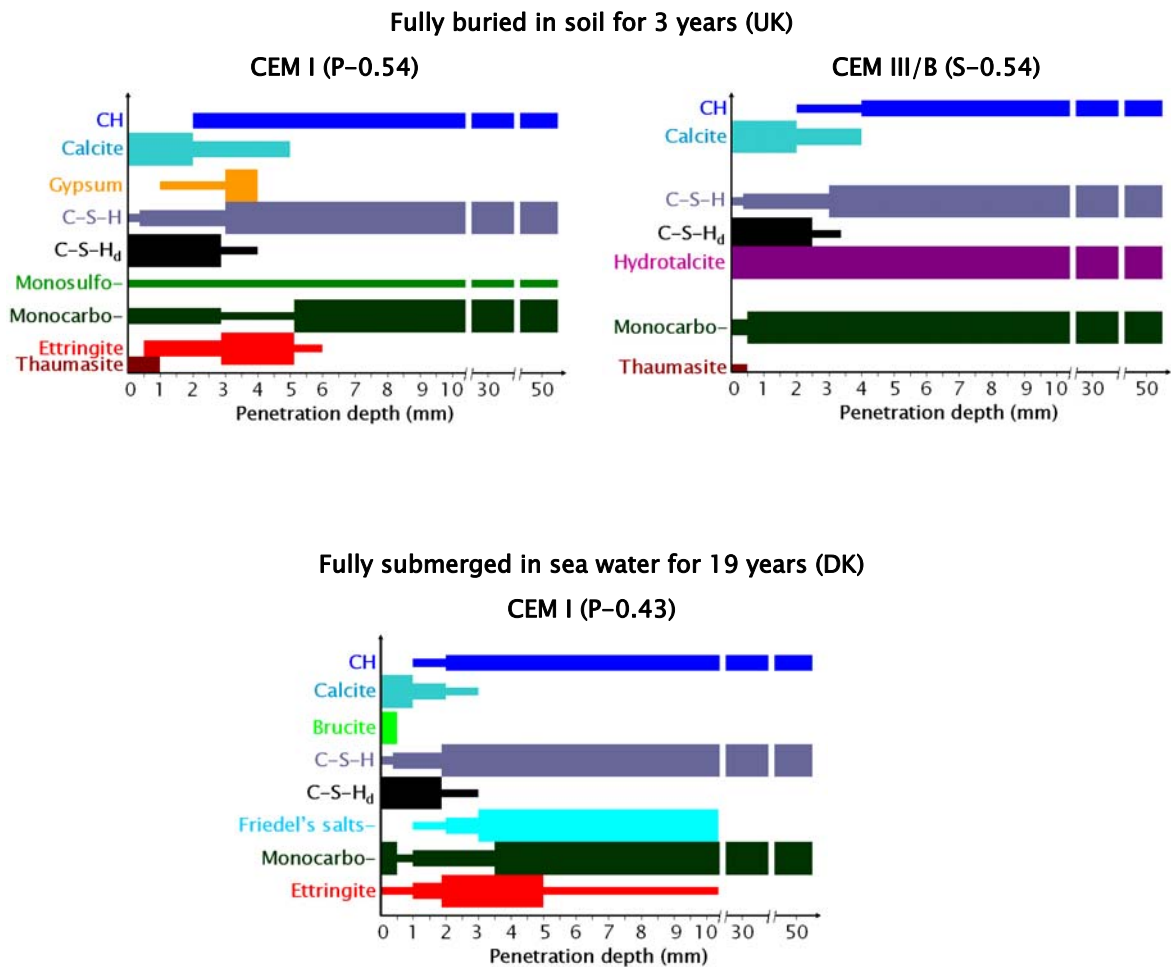
VII.3.2. RECOMMENDATIONS FOR FUTURE RESEARCH

The tests developed are continuing in BAM location.

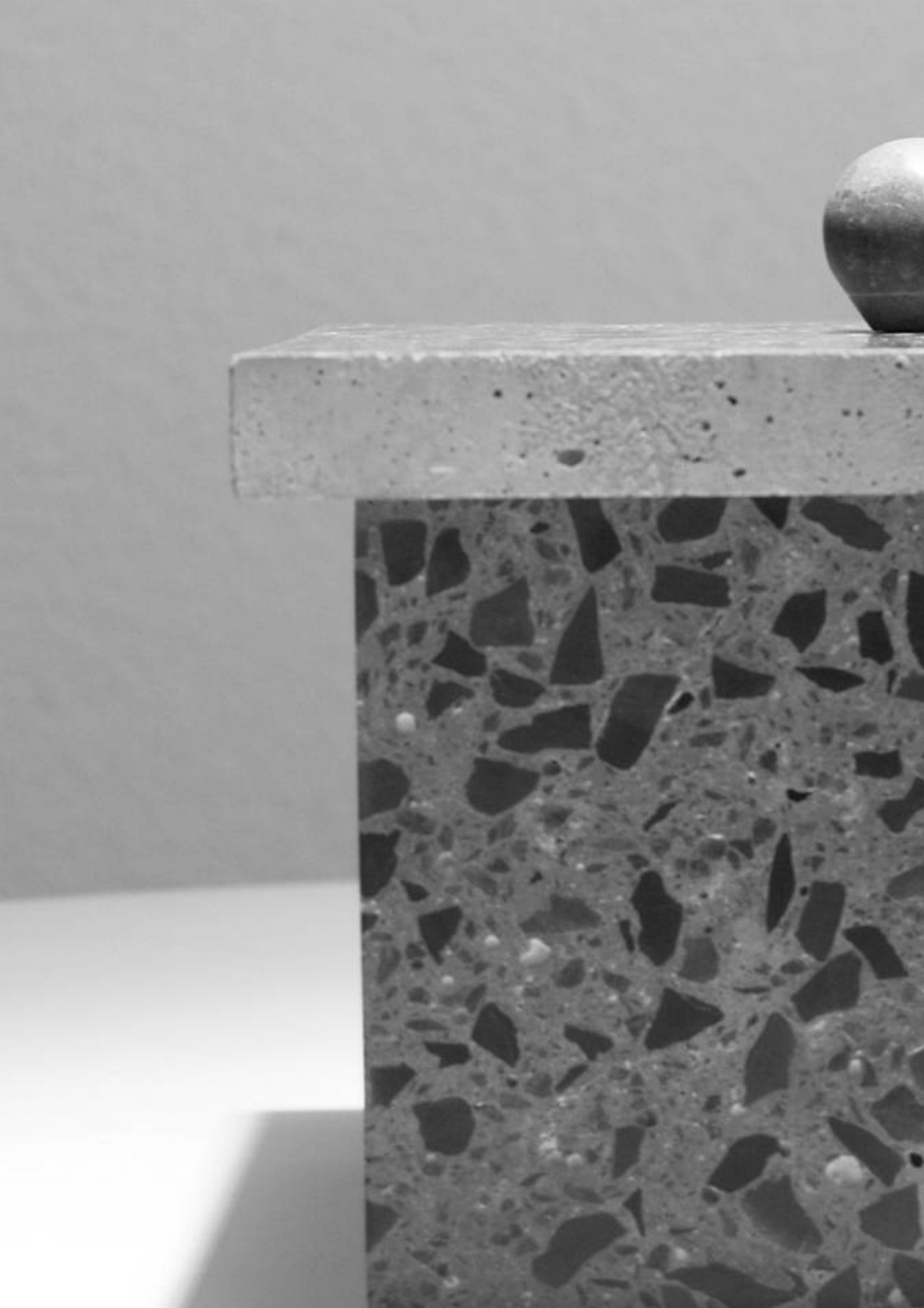
The next step in the understanding of the sulfate attack phenomena would be the quantification of the phase assemblages. This might be done by XRD the problem being the extraction of the aggregate signal. Maybe physical extraction of the aggregate in each slice prior to measurement could be envisaged.

However, more fundamental and more focused studies on specific mechanisms/exposure types would be necessary to confirm/infirm the proposed mechanisms of damage.

Further studies on field samples must be carried out to better adjust the laboratory work. More complex exposures such as sea water were briefly studied during the thesis and would require more interest. They make the object of papers in writing process. The different ions in presence might stabilise other phases: thaumasite is stabilised in presence of carbonate, brucite in presence of magnesium, AFm may transform to Friedel's salts in presence of chloride.



The study of field samples is valuable also for other durability problems such as carbonation or ASR.



Appendices

Appendix A – Thin and Polished Sections Preparation

THIN SECTIONS

Thin section preparation follows five main steps: vacuum resin impregnation, cutting and slight abrasion, glue on a matted glass slide, sawing off of the sample block, thin grinding and polishing of the remaining sample plate. Each one of these steps is conducted so that the end result presents the right optical properties when placed under polarising light and avoiding contact with water to prevent from further hydration and/or dissolution of species (generally use of petrol as lubricant). In-between-steps washings are carried out with petrol intensive brushing and in ultrasonic petrol bath. At the end of the process, the sample itself has a thickness of 25 μ m on its overall surface. This thickness is decisive for further optical properties and especially for refraction index value of the crystalline phases when observed in cross-polar position under a polarizing microscope.

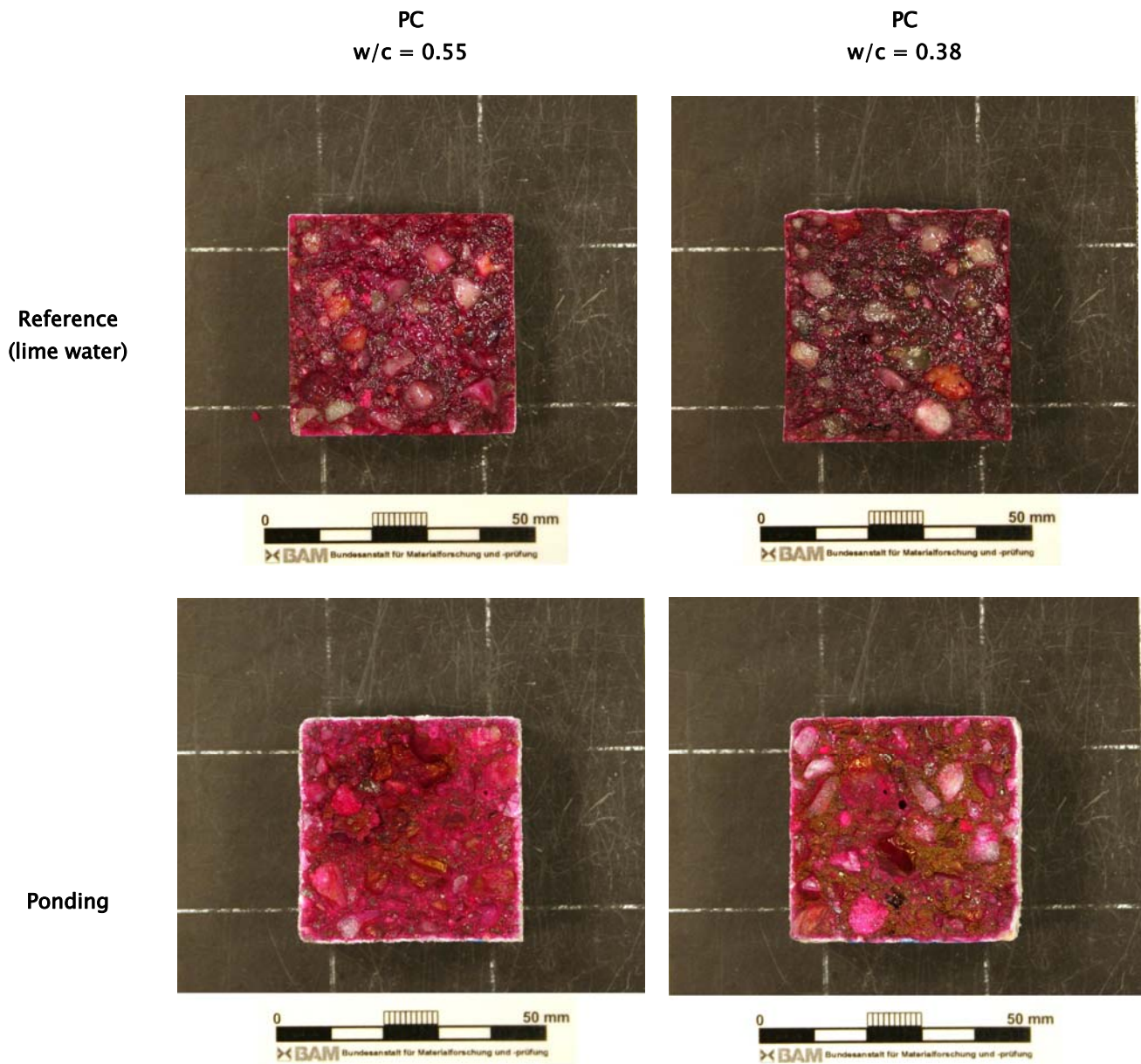
POLISHED SECTIONS

Hydration of the samples is stopped by decreasing the relative humidity into capillary pores below the critical level of 80 % through solvent exchange; isopropanol is used due to its boundary surface tension lower enough than the one of water and due to its inert character towards cement. A minimum of four days is required for full completion of hydration stopping.

Polishing consists in abrasion sequences. The samples must first be epoxy impregnated under low vacuum (10^{-2} mbar). Then the impregnated samples are subjected to polishing sequences with decreasing grades of diamond crystallite suspensions of 9, 3 and 1 μ m, each sequence lasting between 3 and 6 hours. The lubricant employed is petrol and rotation speed fixed at 150 rpm. Mirror polished samples are then coated with carbon by evaporation at 10^{-2} mbar to be conductive and observable under the SEM.

Appendix B – Carbonation of the laboratory samples

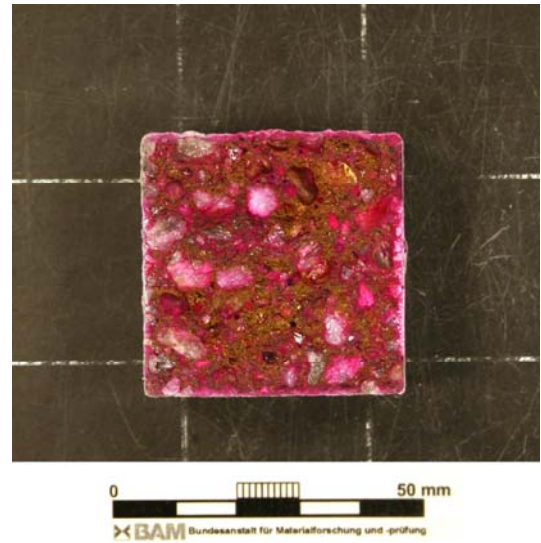
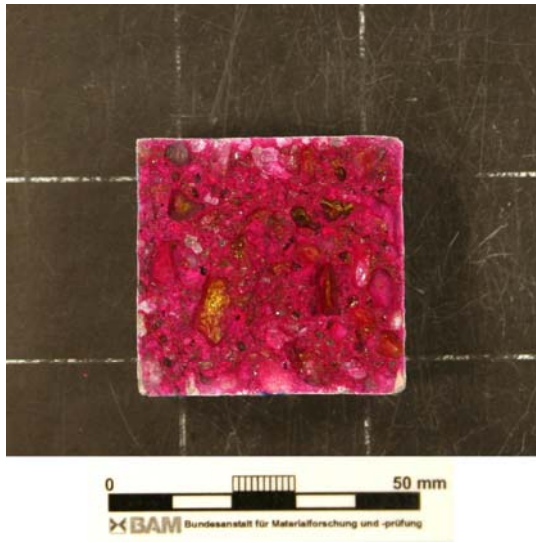
The carbonation of the laboratory specimens has been controlled using a phenolphthalein solution of 1% in an ethanol solvent. Carbonated concrete is characterised by a pH in the below 9 and phenolphthalein has a colour transition in the range of pH of 8.3-10.0; carbonated concrete appears colourless while sound concrete (pH in the range of 12.5-13) appears red. Pictures show the carbonation state after 1 year of exposure.



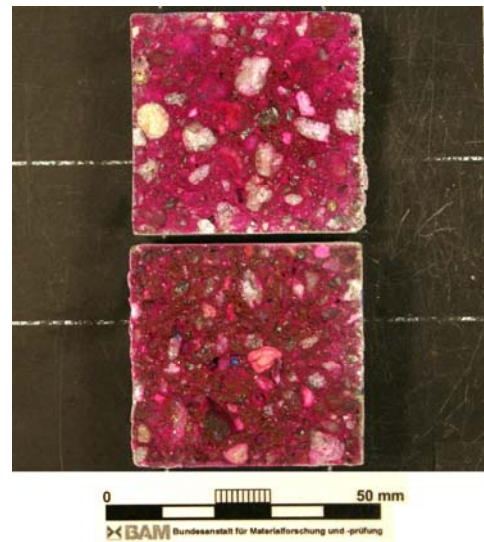
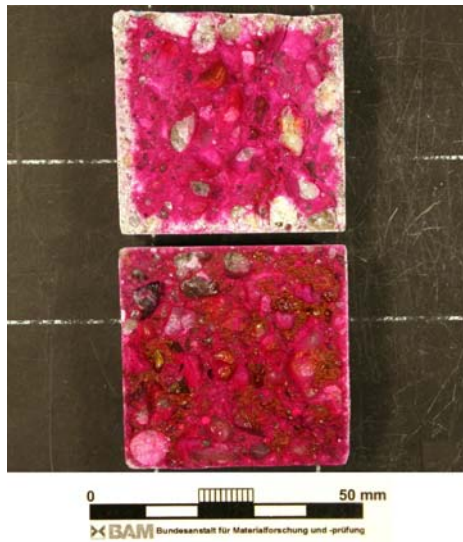
PC
w/c = 0.55

PC
w/c = 0.38

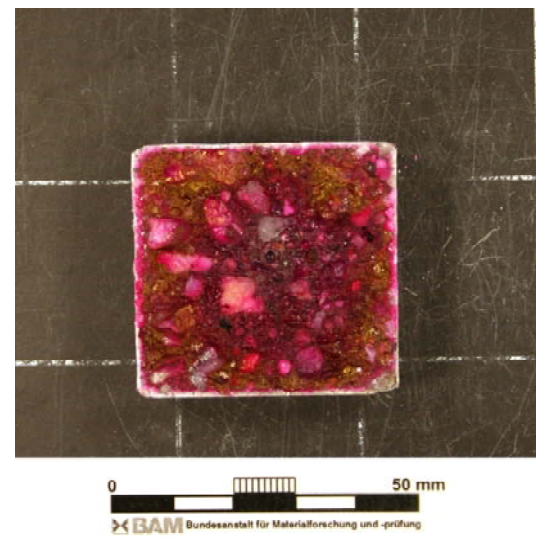
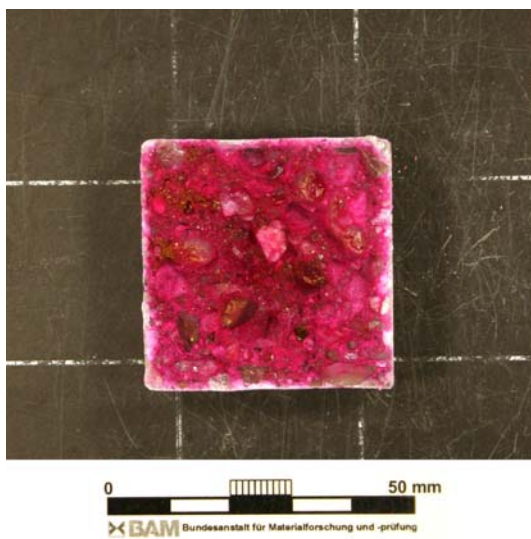
pH-control



Semi-immersion



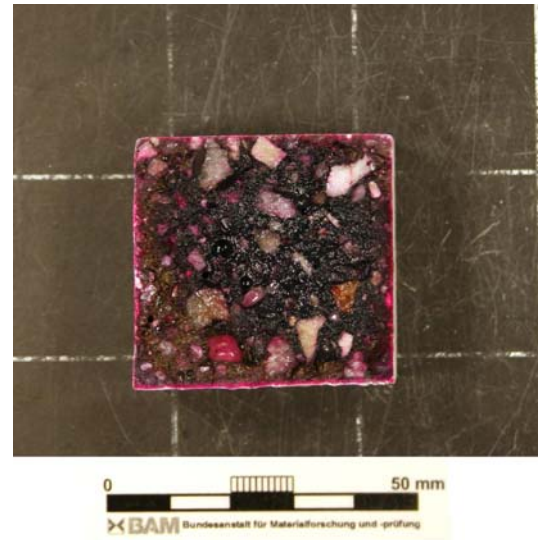
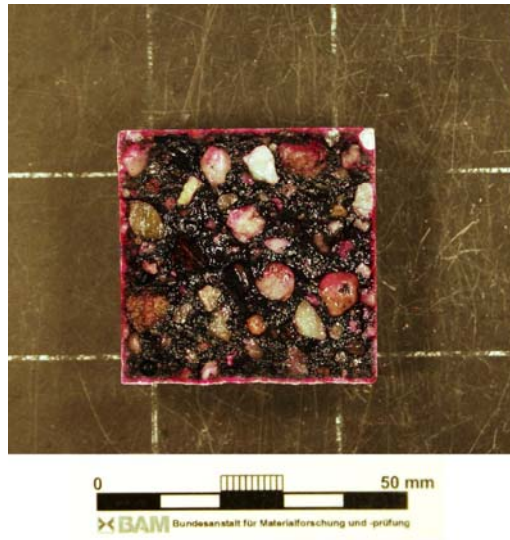
Wet/dry cycles



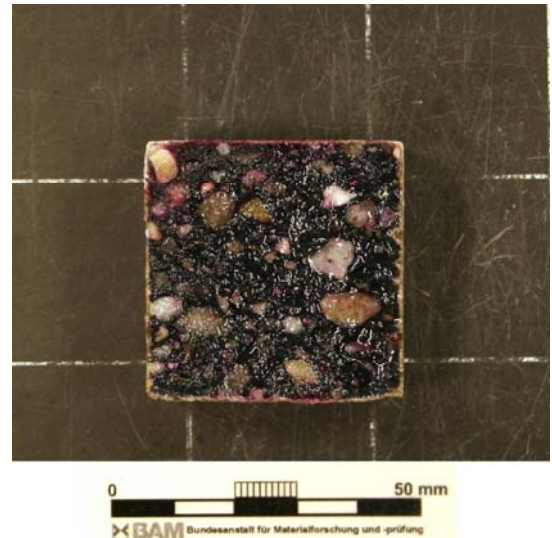
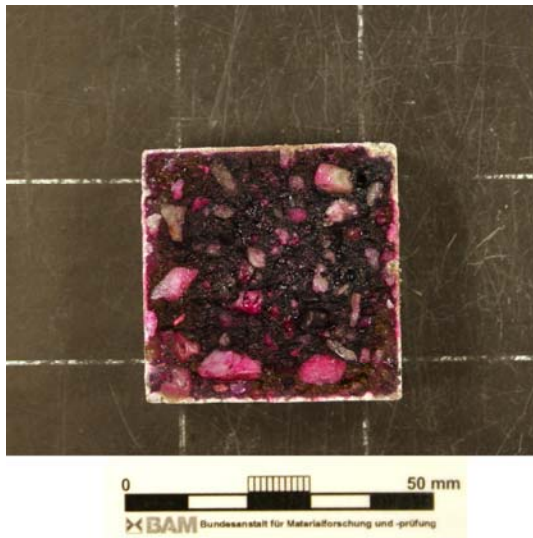
PC+slag
w/c = 0.55

PC+slag
w/c = 0.38

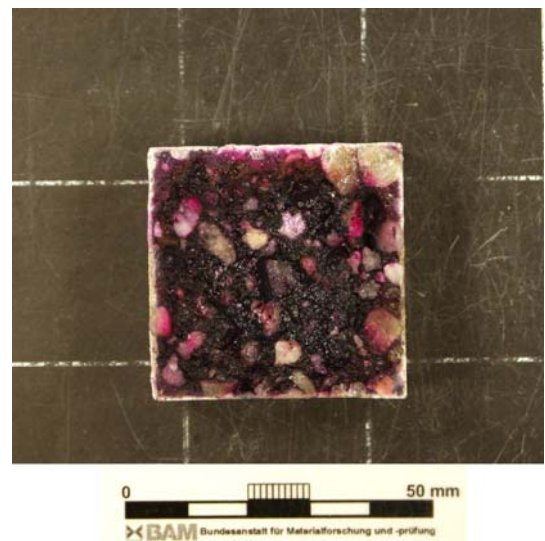
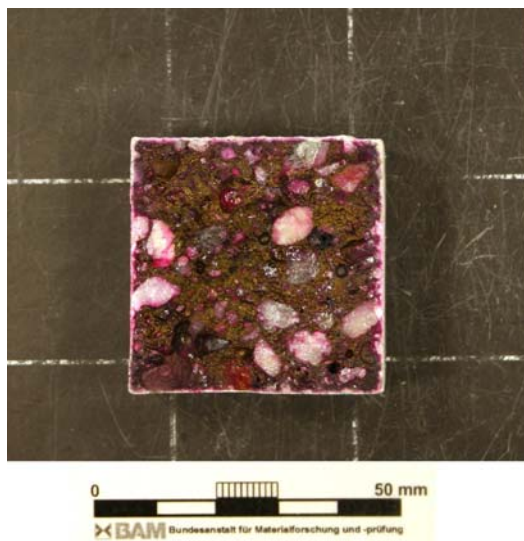
Reference
(lime water)



Ponding



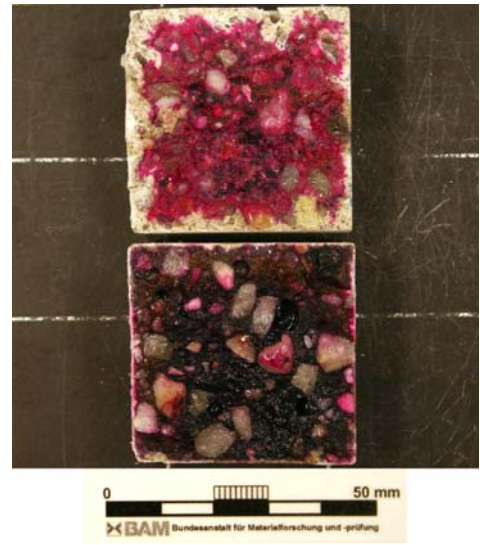
pH-control



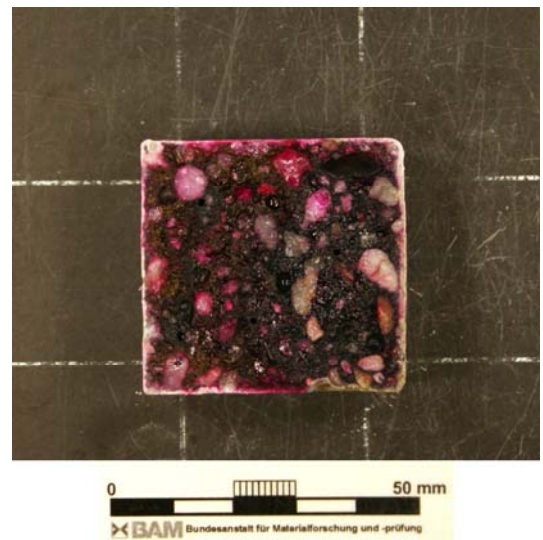
PC+slag
w/c = 0.55

PC+slag
w/c = 0.38

Semi-immersion



Wet/dry cycles



Appendix C – Comparison of Methods for Ion Profiling

Two methods in addition to SEM-mapping image analysis and quantitative micro-XRF were implemented for the ionic profiling: PIXE and Coulometric titration.

PIXE

Proton induced X-ray emission (PIXE) is based on the same principle than SEM-EDS or micro-XRF at the difference that the X-rays are generated from proton-mater interaction. ^1H are used for bombarding the samples and X-ray fluorescence was collected with an Si(Li) semi-conductor detector. The whole diameter of the scanned area is 3 mm in about 215 pixels. The results are expressed in normalised counts as counts.pixel^{-2} or counts.mm^{-2} . In consequence, results can be compared to each others by plotting the elemental ratios, typically S/Ca for sulfur profile.

The obtained ions profiles are discontinuous and semi-quantitative.

Such measurements have been carried out on some field samples, as comparative method to the quantification of the profiles from SEM mappings.

The main disadvantages of the technique over SEM mapping are its low resolution that avoid good discrimination between the cementitious matrix and the aggregates.

COULOMETRIC TITRATION

Coulometric titration goes in three steps: 1°/ vaporisation of the element to measure by burning of a powdered sample, 2°/ precipitation of the element to measure under the form of a component in a solution of which it modifies the pH and 3°/ measurement of the quantity of electrical charge (electrons) required to convert a sample of an analyte quantitatively to a different oxidation state to back-titrate the pH. The amount of material required is in the range of 15 g and concrete slices of 1 mm width should be cut and ground to be analysed.

Sulfur and carbon profiles have been determined on some field samples.

Sulfur and carbon evaporation temperatures are respectively of 1100 and 1400 °C.

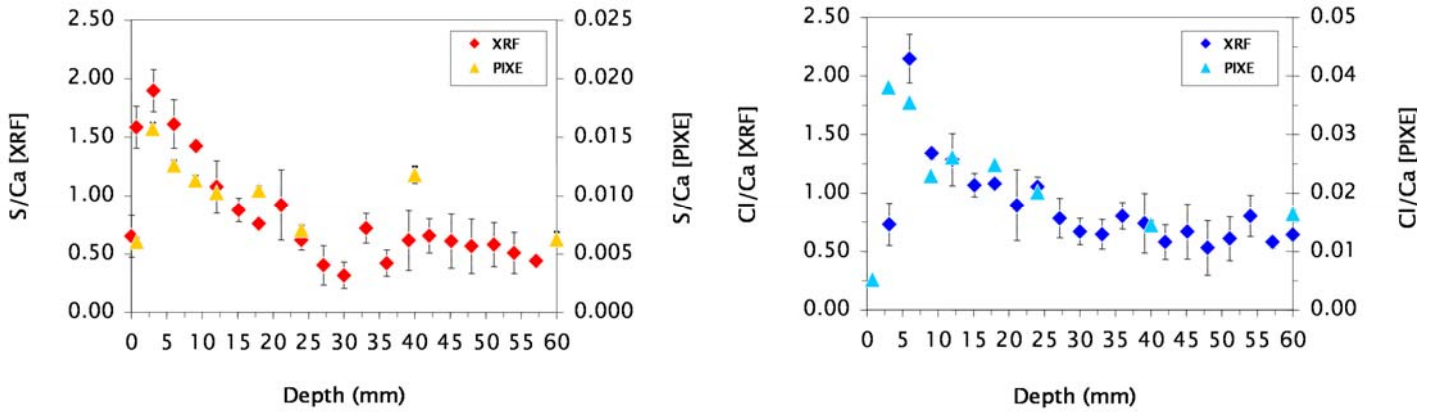
The Coulometric titration system used is a behr C 30 DT/S 30 HT/CS 30 HT from behr Labor-Technik. SO₂ entered a solution of Na₂SO₄;H₂O₂ of which it reduced the pH forming H₂SO₄. The back-titration has been carried out with a ZnO anode. CO₂ entered a solution of Ba(ClO₄)₂ and decreased the pH while precipitating in BaCO₃. The back-titration has been carried out with a BaCO₃ anode.

For chloride measurement, 2 g of powdered material was dissolved in an HNO₃ solution. Ammoniac was then added to precipitate the trioxides and then filtered. To increase the sensitivity regarding the electrode, acetone was added and then a known amount of NaCl. A known amount of AgNO₃ was added to the mix (to precipitate AgCl) whose conductivity was measured by a silver electrode. The relationship between the AgNO₃ added and the conductivity measured allows to come back to the initial chloride content. Out of being a comparative method to the quantification of the sulfur profiles from SEM mappings, this method is particularly interesting for the carbon profiles. Carbon is a too light element to be determined by X-ray fluorescence methods.

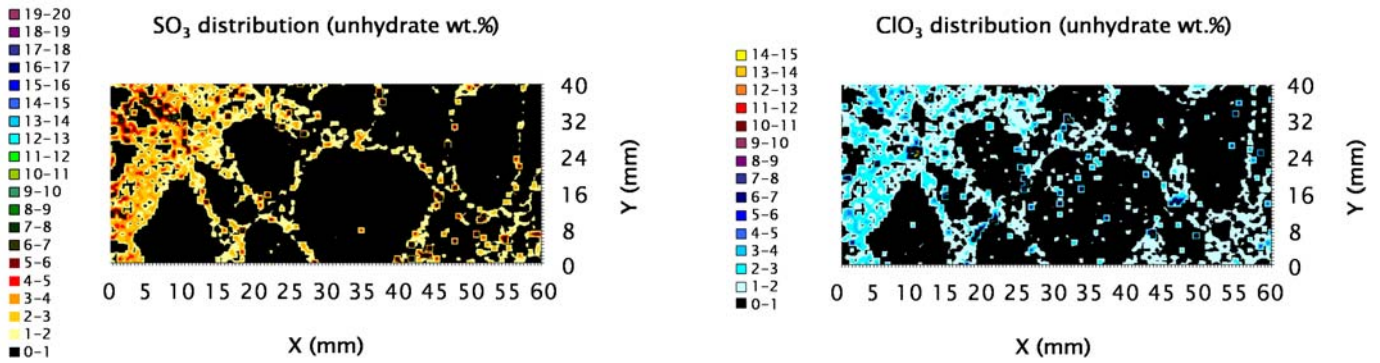
This rapid and quantitative analysis presents the disadvantage over SEM of being highly subjected to the aggregate amount present in each powder. Extraction of the aggregates could not be done, which implies a high dispersion of the results. Moreover, the spatial resolution of the extracted profiles is limited. Additionally, the burned samples cannot be re-used for other measurements on the contrary to the X-rays methods (SEM, micro-XRF and PIXE) where the polished sections can be re-used for further SEM analyses and the cut surfaces for other any analyses.

The following example concerns sulfate and chloride profiles determination by PIXE, micro-XRF and Coulometric titration on a field concretes of type CEM I (P-0.43) fully immersed for 24 years in the sea water in Denmark.

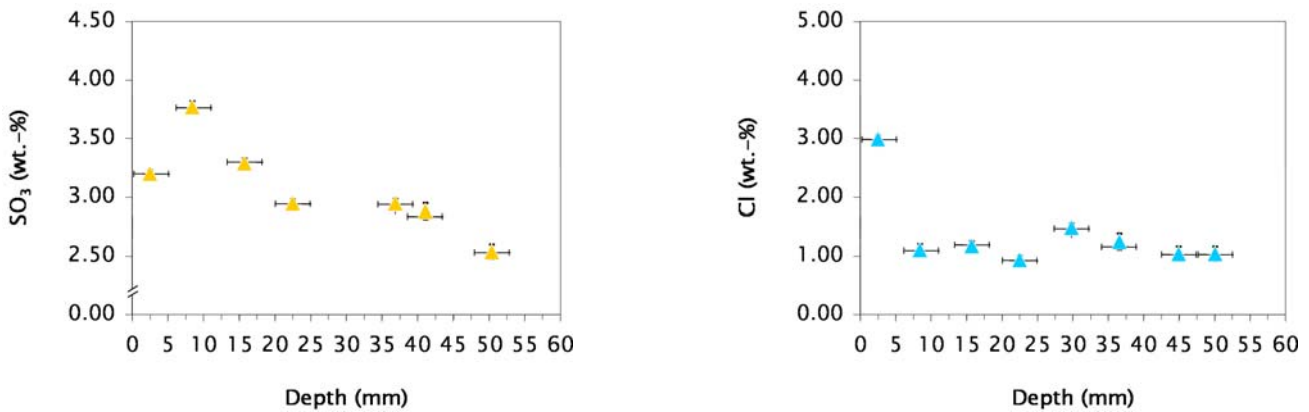
PIXE (proton induced X-ray emission)



Micro-XRF



Coulometric titration



References

- [1] Novak GA, Colville AA. Efflorescent mineral assemblages associated with cracked and degraded residential concrete foundations in Southern California. *Cement and Concrete Research*. 1989;19(1):1-6.
- [2] Peukert S, Garbacik A, Chladzynski S. Cement sulfate resistance evaluation by the draft European standard of direct testing method. In: Dhir RK, Dyer TD, eds. *Modern concrete materials: binders, additions and admixtures* 1999.
- [3] Santhanam M, Cohen MD, Olek J. Effects of gypsum formation on the performance of cement mortars during external sulfate attack. *Cement and Concrete Research*. 2003;33(3):325-32.
- [4] Taylor HFW. *Cement chemistry*: Academic Press 1997.
- [5] Matschei T, Lothenbach B, Glasser FP. Thermodynamic properties of Portland cement hydrates in the system CaO-Al₂O₃-SiO₂-CaSO₄-CaCO₃-H₂O. *Cement and Concrete Research*. 2007;37(10):1379-410.
- [6] Matschei T, Skapa R, Lothenbach B, Glasser FP. The distribution of sulfate in hydrated Portland cement paste. *12th International Congress on the Chemistry of Cement*. Montréal 2007.
- [7] Matschei T, Lothenbach B, Glasser FP. The AFm phase in Portland cement. *Cement and Concrete Research*. 2007;37(2):118-30.
- [8] Juel I, Herfort D, Gollop R, Konnerup-Madsen J, Jakobsen HJ, Skibsted J. A thermodynamic model for predicting the stability of thaumasite. *Cement and Concrete Composites*. 2003;25(8):867-72.
- [9] Juel I. Mineralogical and thermodynamic processes by sulfate and seawater attack of Danish concrete: University of Copenhagen.
- [10] Bonen D, Cohen MD. Magnesium sulfate attack on portland cement paste - II. Chemical and mineralogical analyses. *Cement and Concrete Research*. 1992;22(4):707-18.
- [11] Bonen D, Cohen MD. Magnesium sulfate attack on portland cement paste - I. Microstructural analysis. *Cement and Concrete Research*. 1992;22(1):169-80.
- [12] Kamali S, Moranville M, Leclercq S. Material and environmental parameter effects on the leaching of cement pastes: Experiments and modelling. *Cement and Concrete Research*. 2008;38(4):575-85.
- [13] Kamali S, Gérard B, Moranville M. Modelling the leaching kinetics of cement-based materials--influence of materials and environment. *Cement and Concrete Composites*. 2003/7//;25(4-5):451-8.

- [14] Gollop RS, Taylor HFW. Microstructural and microanalytical studies of sulfate attack. I. Ordinary portland cement paste. *Cement and Concrete Research*. 1992;22(6):1027-38.
- [15] Tsui N, Flatt RJ, Scherer GW. Crystallization damage by sodium sulfate. *Journal of Cultural Heritage*. 2003;4(2):109-15.
- [16] Scherer GW. Stress from crystallization of salt. *Cement and Concrete Research*. 2004;34(9):1613-24.
- [17] Powers TC, Brownyard TL. *Studies of the physical properties of hardened Portland cement paste*. Chicago; 1948.
- [18] Monteiro PJM, Kurtis KE. Time to failure for concrete exposed to severe sulfate attack. *Cement and Concrete Research*. 2003;33(7):987-93.
- [19] González MA, Irassar EF. Ettringite formation in low C3A Portland cement exposed to sodium sulfate solution. *Cement and Concrete Research*. 1997;27(7):1061-72.
- [20] Irassar EF, Di Maio A, Batic OR. Sulfate attack on concrete with mineral admixtures. *Cement and Concrete Research*. 1996;26(1):113-23.
- [21] Irassar EF, Batic OR, Di Maio A, Ponce JM. Sulfate performance of concrete containing high volume of mineral admixtures. In: 234 ASP, editor. 7th CANMET/ACI Int Conf on Durability of Concrete; 2006; Farmington Hills, MI, USA; 2006. p. 589-606.
- [22] Gollop RS, Taylor HFW. Microstructural and microanalytical studies of sulfate attack. V. Comparison of different slag blends. *Cement and Concrete Research*. 1996;26(7):1029-44.
- [23] Gollop RS, Taylor HFW. Microstructural and microanalytical studies of sulfate attack III. Sulfate-resisting portland cement: Reactions with sodium and magnesium sulfate solutions. *Cement and Concrete Research*. 1995;25(7):1581-90.
- [24] CEN/TC 51 N 865 rev, *Sulfate resistance testing - State-of-the-Art*. Bruxelles: Institut belge de normalisation; 2006.
- [25] Damidot D, Glasser FP. Thermodynamic investigation of the CaO---Al₂O₃---CaSO₄---H₂O system at 25°C and the influence of Na₂O. *Cement and Concrete Research*. 1993;23(1):221-38.
- [26] Irassar EF, Bonavetti VL, González M. Microstructural study of sulfate attack on ordinary and limestone Portland cements at ambient temperature. *Cement and Concrete Research*. 2003;33(1):31-41.
- [27] Bellmann F, Möser B, Stark J. Influence of sulfate solution concentration on the formation of gypsum in sulfate resistance test specimen. *Cement and Concrete Research*. 2006;36(2):358-63.
- [28] Damidot D, Glasser FP. Thermodynamic investigation of the CaO---Al₂O₃---CaSO₄---K₂O---H₂O system at 25°C. *Cement and Concrete Research*. 1993;23(5):1195-204.

- [29] Damidot D, Glasser FP. Thermodynamic investigation of the CaO---Al₂O₃---CaSO₄---H₂O system at 50°C and 85°C. *Cement and Concrete Research*. 1992;22(6):1179-91.
- [30] Schmidt T, Lothenbach B, Romer M, Neuenschwander J, Scrivener K. Physical and microstructural aspects of sulfate attack on ordinary and limestone blended Portland cements. *Cement and Concrete Research*. 2009;39(12):1111-21.
- [31] Santhanam M, Cohen M, Olek J. Differentiating seawater and groundwater sulfate attack in Portland cement mortars. *Cement and Concrete Research*. 2006;36(12):2132-7.
- [32] Nielsen EP, Geiker MR. Chloride diffusion in partially saturated cementitious material. *Cement and Concrete Research*. 2003;33(1):133-8.
- [33] Yu P, Kirkpatrick RJ. ³⁵Cl NMR relaxation study of cement hydrate suspensions. *Cement and Concrete Research*. 2001;31(10):1479-85.
- [34] Nielsen EP, Herfort D, Geiker MR. Binding of chloride and alkalis in Portland cement systems. *Cement and Concrete Research*. 2005;35(1):117-23.
- [35] Matschei T. Thermodynamics of cement hydration: University of Aberdeen; 2007.
- [36] Irassar EF, Bonavetti VL, Trezza MA, González MA. Thaumasite formation in limestone filler cements exposed to sodium sulphate solution at 20 °C. *Cement and Concrete Composites*. 2005;27(1):77-84.
- [37] Crumbie AK. Characterisation of the microstructure of concrete: University of London; 1994.
- [38] Scrivener KL, Crumbie AK, Laugesen P. The Interfacial Transition Zone (ITZ) between cement paste and aggregate in concrete. *Interface Science*. 2004;12(4):411-21.
- [39] Taylor HYW. Sulfate attack. In: Telford T, ed. *Cement chemistry*. 2 ed: Academic Press 1997:368-84.
- [40] Tian B, Cohen MD. Does gypsum formation during sulfate attack on concrete lead to expansion? *Cement and Concrete Research*. 2000;30(1):117-23.
- [41] Brown PW, Taylor HFW. The role of ettringite in external sulfate attack. In: Marchand J, Skalny J, eds. *Materials Science of Concrete Special Volume: Sulfate Attack Mechanisms*. Westerville: The American Ceramic Society 1999:73-98.
- [42] Taylor HFW. Sulfate reactions in concrete-microstructural and chemical aspects *Ceramic Transactions*. 1994;40:61-78.
- [43] Lafuma H. Théorie de l'expansion des liants hydrauliques. *La revue de matériaux de construction et de travaux publics*. 1930;Part 1 and Part 2(243 and 244):441-4 and 4-8.
- [44] Mehta PK. Mechanism of expansion associated with ettringite formation. *Cement and Concrete Research*. 1973;3(1):1-6.
- [45] Scherer GW. Crystallization in pores. *Cement and Concrete Research*. 1999;29(8):1347-58.

- [46] Perruchot C, Chehimi MM, Vaulay M-J, Benzarti K. Characterisation of the surface thermodynamic properties of cement components by inverse gas chromatography at infinite dilution. *Cement and Concrete Research*. 2006;36(2):305-19.
- [47] Taylor HFW. In: Telford T, ed. *Cement chemistry*: Academic Press 1997:118-9 and 26-28.
- [48] Schmidt T. Sulfate attack and the role of internal carbonate on the formation of thaumasite: Ecole Polytechnique Fédérale de Lausanne; 2007.
- [49] Hobbs DW, Taylor MG. Nature of the thaumasite sulfate attack mechanism in field concrete. *Cement and Concrete Research*. 2000;30(4):529-33.
- [50] Taylor HFW, Famy C, Scrivener KL. Delayed ettringite formation. *Cement and Concrete Research*. 2001;31(5):683-93.
- [51] Kocaba V. Development and evaluation of methods to follow microstructural development of cementitious systems including slags: Ecole Polytechnique Fédérale de Lausanne; 2009.
- [52] Krautkrämer J, Krautkrämer H. Ultrasonic testing of materials. Berlin Heidelberg New York London Paris Tokyo Hong Kong Barcelona: Springer-Verlag 1990.
- [53] Scrivener KL. Backscattered electron imaging of cementitious microstructures: understanding and quantification. *Cement and Concrete Composites*. 2004;26(8):935-45.
- [54] Fu Y, Xie P, Gu P, Beaudoin JJ. Effect of temperature on sulphate adsorption/desorption by tricalcium silicate hydrates. *Cement and Concrete Research*. 1994;24(8):1428-32.
- [55] Sun GK, Young JF, Kirkpatrick RJ. The role of Al in C-S-H: NMR, XRD, and compositional results for precipitated samples. *Cement and Concrete Research*. 2006;36(1):18-29.
- [56] Richardson IG, Cabrera JG. The nature of C---S---H in model slag-cements. *Cement and Concrete Composites*. 2000;22(4):259-66.
- [57] Li G, Le Bescop P, Moranville M. The U phase formation in cement-based systems containing high amounts of Na₂SO₄. *Cement and Concrete Research*. 1996;26(1):27-33.
- [58] Famy C, Scrivener KL, Crumbie AK. What causes differences of C-S-H gel grey levels in backscattered electron images? *Cement and Concrete Research*. 2002;32(9):1465-71.
- [59] Jennings HM. A model for the microstructure of calcium silicate hydrate in cement paste. *Cement and Concrete Research*. 2000;30(1):101-16.

Curriculum vitae



Aude Chabrelie
 French
 26 years old / Single
 Driving license



Avenue de Préfaully, 54
 CH-1020 Renens / Suisse



0041 78 314 31 82



aude.chabrelie@yahoo.fr

EDUCATION

- | | |
|---|--|
| <p>2006–2009 PhD. Thesis in Materials Science
 " Mechanisms of degradation of concrete by external sulfate ions under laboratory and field conditions "
 Network – Nanocem: Industrial–Academic EU–Research Network on Cement & Concrete
 Funding – Marie–Curie Actions: Mobility of Young EU–Researchers</p> | <p>EPFL – LMC
 Ecole Polytechnique Fédérale de Lausanne – Laboratoire des Matériaux de Construction
 <i>Lausanne – Switzerland</i>
 BAM
 Bundesanstalt für Materialforschung und –prüfung
 <i>Berlin – Germany</i></p> |
| <p>2003–2006 Master of Science / Engineering degree in Materials Science</p> | <p>INP – EEIGM
 Institut National Polytechnique – Ecole Européenne d’Ingénieurs en Génie des Matériaux
 <i>Nancy – France</i></p> |
| <p>2006
 6 months Diploma Project
 " Cement substitutes – Microstructural characterization "</p> | <p>EPFL – LMC
 <i>Lausanne – Switzerland</i></p> |
| <p>2005
 6 months Master Project
 " Ion implantation assisted magnetron sputtering of hard tribological coatings "</p> | <p>MISA
 Moscow State Institute for Steel and Alloys
 <i>Moscow – Russia</i></p> |
| <p>2005
 6 months Specialization Semester in Materials Characterization Methods</p> | <p>Universität des Saarlandes
 <i>Saarbrücken – Germany</i></p> |
| <p>2003–2005 Background in Materials Science
 English – German – Spanish</p> | <p>INP – EEIGM
 <i>Nancy – France</i></p> |
| <p>2001–2003 Bachelor of Science / Classes Préparatoires in Mathematics – Physics – Chemistry
 English – German – French – Communication
 High–level intensive course to prepare for entering French INP engineering schools</p> | <p>INP – CPP
 Institut National Polytechnique
 Cycle Préparatoire Polytechnique
 <i>Grenoble – France</i></p> |
| <p>2001 A’level of Science / Baccalauréat scientifique in Mathematics, Physics & Chemistry
 Emphasis on German – English
 With honours (15/20 : Mention Bien)</p> | <p>LGM
 Lycée du Grésivaudan Meylan
 <i>Meylan – France</i></p> |

PROFESSIONAL EXPERIENCE

2005–2009	Research assistant and trainee	EPFL – LMC <i>Lausanne – Switzerland</i>
	▪ Teaching	BAM <i>Berlin – Germany</i>
	▪ Master Student Supervision	VDZ Verein Deutscher Zementindustrie <i>Düsseldorf – Germany</i>
	▪ Project Management	University of Surrey <i>Guildford – United Kingdom</i>
	▪ Networking	MISA <i>Moscow – Russia</i>
	▪ Industrial & Academia Inter-working	
	▪ Handling of High Technical Instruments	
	▪ Laboratory Experimental Work	
	▪ English Scientific Writing	
	▪ Scientific Articles Reviewer (Cement and Concrete Research)	
2000–2004	Production Internship	Schneider Electric <i>France</i>
1 month½	▪ Surface Treatment	
	Summer Jobs	Le Provençal Restaurant <i>Germany</i>
1 month	▪ Waitress	Camping du Botza Association <i>Switzerland</i>
1 month	▪ Swimming Supervision and Teaching	<i>Lithuania</i>
1 month	▪ French Teaching	UNAREC <i>Rumania</i>

SKILLS

Techniques	▪ Scanning Electron Microscopy (SEM)	▪ Synchrotron X-Ray Radiation
	▪ X-Ray Diffraction (XRD)	▪ Analytical Chemistry
	▪ Micro X-Ray Fluorescence (micro-XRF)	▪ Mechanical Testing
Computer	▪ Office automation software	▪ Finite Element Analysis (Algor/PDEase)
	▪ Programming (Caml, MatLab)	▪ Graphic Programming (LabVIEW)
	▪ Image Analysis (IDL)	
Languages	▪ German – Bilingual / Current & Scientific	▪ Russian – Learning in progress
	ZMP – Zentrale Mittelstufenprüfung – July 2005	▪ Spanish – Understanding
	▪ English – Fluent / Scientific	
	FCE – First Certificate of English – June 2004	

PERSONAL INTERESTS

Sports	▪ Skiing	Arts	▪ Drama
	▪ Windsurfing		▪ Painting/Drawing
	▪ Trekking		▪ Photography/Architecture
